Aerosol Properties and Their Impacts on Climate

U.S. Climate Change Science Program (CCSP)
5-Year Assessment Review

Synthesis and Assessment Product 2.3

Table of Contents

Executive Summary

Authors: L. Remer, NASA GSFC; **M. Chin**, NASA GSFC; **P. L. DeCola**, NASA HQ; **G. Feingold**, NOAA ESRL; **R. N. Halthore**, NASA HQ/NRL; **P. Quinn**, NOAA PMEL; **D. Rind**, NASA GISS; **S. E. Schwartz**, DOE BNL; **D. G. Streets**, DOE ANL; **H. Yu**, NASA GSFC/UMBC.

This report, focusing on the influences of atmospheric aerosols on climate and climate change, is part of the 5-year assessment review of activities and progress of research, conducted by the Climate Change Science Program (CCSP) and mandated by the National Research Council (NRC).

Atmospheric aerosols are a suspension of solid and/or liquid particles in the air, which are ubiquitous and are often observable as dust, smoke, and haze. Both natural and human processes contribute to atmospheric aerosols. On a global basis aerosol mass derives predominantly from natural sources (e.g., sea-salt, and dust). Manmade aerosols, arising mainly from a variety of combustion sources (e.g., "smog"), usually overwhelm the natural ones in areas in and downwind of highly populated and industrialized regions, or areas of intense agricultural burning.

Aerosols affect the Earth's energy budget by scattering and absorbing radiation (direct effect) and by modifying the cloud amount, lifetime, and microphysical and radiative properties (indirect effects). Moreover, the direct absorption of radiant energy by aerosols leads to heating of the troposphere and cooling of the surface, which can change the relative humidity and atmospheric stability thereby influencing the clouds and precipitation (semi-direct effect). The addition of manmade aerosols to the atmosphere may change the radiative fluxes at the top-of-atmosphere (TOA), at the surface, and within the atmospheric column. Such a perturbation of radiative fluxes by anthropogenic aerosols is designated as *aerosol climate forcing*, which is distinguished from the *aerosol radiative effect* of the total aerosol (natural plus anthropogenic). The aerosol climate forcing and radiative effect are characterized by large spatial and temporal heterogeneities due to the wide variety of aerosol sources, the spatial non-uniformity and intermittency of these sources, the short atmospheric lifetime of aerosols (relative to that of the gases), and processing (chemical and microphysical) that occurs in the atmosphere.

On a global average the sum of direct and indirect forcing by anthropogenic aerosols at the TOA is almost certainly negative (cooling) and thus likely offsets the positive forcing (warming) due to anthropogenic greenhouse gases on a global-average basis, and taking into account the sum of longwave and shortwave forcings. However, as the forcings are exerted in different spectral regions and exhibit different magnitudes in different locations the offset cannot be considered to be neutral in terms of effects on Earth's climate.

The Intergovernmental Panel on Climate Change Fourth Assessment Report (IPCC AR4) reported on the results of some 20 participating global climate models. These models can reproduce the observed trend in global mean temperature over the twentieth century due to changes in atmospheric concentrations of greenhouse gases and other forcing agents including aerosols. When anthropogenic aerosol forcings are not included, the models tend to generate too much warming. However the ability of

climate models to reproduce the global mean temperature change over the past 100 years appears to be the result of using a "tuned" aerosol forcing. Although different models exhibit a wide range of climate sensitivity (i.e., the amount of temperature increase due to the increase of CO_2), they yield global temperature change, which is similar to the observed change. Apparently this is because the forcing by aerosols differs between models. For example, the direct cooling effect of sulfate aerosol varies by a factor of 6 among the models, because of different extensive aerosol properties (e.g. sulfate amount) and different intensive properties (e.g. scattering efficiency) used in the models. Greater disparity is found in the model treatment of other aerosol types such as black carbon and organic carbon. Even the choice of which aerosol types and which aerosol forcings are treated in a particular model varies. Some models include only the direct aerosol effect, whereas others include an indirect effect in which the aerosols modify cloud microphysics and hence cloud brightness. In addition, the aerosol indirect effect on cloud brightness varies by up to a factor of 9 among models. This situation is in part a consequence of the large uncertainty in the mechanisms and magnitude of climate forcing by aerosols, and in part due to the differences in cloud amounts between models.

Over the past decade there has been substantial improvement in measurement of the amount, geographical distribution, and physical and chemical properties of atmospheric aerosols, the controlling processes, and the direct and indirect radiative effects of these aerosols. Key research activities have been:

- Execution of intensive field experiments examining aerosol processes and properties in various aerosol regimes around the globe;
- Establishment and enhancement of ground-based networks measuring aerosol properties and radiative effects;
- Development and deployment of new and enhanced instrumentation, importantly aerosol mass spectrometers examining size dependent composition, and;
- Development and implementation of new and enhanced satellite-borne sensors examining aerosol effects on atmospheric radiation.

These efforts are beginning to provide the needed inputs and constraints necessary to improve the accuracy of representation of aerosol effects in climate models. In addition they are allowing for a shift in estimates of aerosol radiative effect and climate forcing from largely model-based to an increasing level of measurement-model synthesis. The new observational capabilities together with dedicated aerosol modeling efforts have led to a better understanding of the aerosol system, and to smaller uncertainties in estimates of aerosol direct radiative effect and climate forcings. The resulting improved understanding and quantification of these aerosol effects have contributed to the finding in the 2007 assessment report of the Intergovernmental Panel on Climate Change that human activities "very likely" have been contributing to the global change that has been observed over the last 100 years.

In short, direct aerosol climate forcing is understood now much better than 10 years ago. However the tools to reduce uncertainties are still urgently needed. The improvement in measurement-based systems is necessary to identify remaining outstanding issues and improve quantification of aerosol effects on climate. Improvement in modeling is necessary to confidently extend estimates of forcing to prior times and to project future emissions. Achieving these capabilities will require a synergistic approach between observational systems and modeling.

1. Measurement of aerosol properties and their evolution

1.1 *In situ and surface remote sensing measurements.*

Over the past two decades, more than a dozen large-scale intensive field experiments have been conducted to study the physical, chemical, and optical properties of aerosol, and the processes that govern aerosol amounts, types and the effects aerosols have on clouds in a variety of aerosol regimes around the world. Ground-based networks including both comprehensive sites with in-situ and remote sensing instrumentation (e.g., NOAA Global Monitoring Division - GMD sites) and simpler ground-based remote sensing networks (e.g., the NASA Aerosol Robotic network - AERONET) provide the long-term context for intensive field campaigns and ground-truth for satellite validation. Widespread application of aerosol mass spectrometers has shown the large contribution of organic substances to total aerosol mass concentration over much of the Northern Hemisphere and the increasing preponderance of secondary organic aerosols with increasing distance from urban source regions. Laboratory studies of aerosol formation and evolution processes provide the fundamental basis for representing aerosols in models.

1.2 *Satellite measurements.*

A measurement-based characterization of aerosols on regional to global scales can be realized only through satellite remote sensing, because of the large spatial and temporal heterogeneities of aerosol distributions. Over the past decade, satellite aerosol retrievals have become increasingly sophisticated. From these observations, retrieved aerosol products include spectral optical depth, particle shape and effective particle size over both ocean and land, as well as more direct measurements of polarization and phase function. Cloud screening is much more robust than before, and onboard calibration is now widely available. Active remote sensing is also making promising progress by collecting essential information about aerosol vertical distributions. These measurements are essential to evaluate the performance of aerosol transport and transformation models used to determine aerosol forcing.

1.3 *Synergy.*

The best strategy for characterizing aerosols has been to integrate measurements from different satellite sensors with airborne and ground-based measurements and models. While we have made much progress toward measurement-based estimates of aerosol effects and forcing, models still provide information lacking in the observations, such as aerosol composition, characteristics, and four-dimensional (4-D) distributions over wide regional areas in situations difficult to observe (i.e., cloudy scenes, complex surface types, different times of day) by satellite or other platforms. Models also provide critical links among different observations, and can simulate the past and project into the future.

1.4 *Looking Forward*

- Long term networks such as the NOAA GMD sites, AERONET and emerging ground-based lidar networks provide essential information on decadal and mulit-decadal trends and on aerosol properties that are vital for satellite validation, model evaluation, and climate change assessment. Progress in aerosol-climate science is dependent on the continuity of these networks.

- Enhancing long term stations to include accurate measurements of spectral aerosol absorption would add an essential characteristic needed for estimates of aerosol forcings, both direct and indirect.
- The modern satellite sensors have a relatively short life time. Global long-term aerosol trends cannot be detected without equivalently-calibrated replacement sensors that at least match current capabilities.
- Current satellite capabilities, while good, still lack accurate information on aerosol size distribution, absorption, type and extinction above clouds. New sensors with enhanced capabilities and different satellite orbit configurations including geostationary and Lagrange points will better constrain models and narrow uncertainties.
- Outstanding questions on aerosol scattering and absorption across the solar spectrum, and on aerosol roles in cloud nucleation will only be answered by development of new measurement techniques applied in the laboratory and during field campaigns.

2. Aerosol representations in models

Aerosol simulations in chemical transport models and climate models have been extensively evaluated using observations. However, comparison of model parameters with observations is problematic because of strong disagreements among the different satellite instruments, between satellite and ground-based sensors, and between remote-sensing and in-situ measurements.

2.1 *General evaluation of aerosol representation in models.*

Differences in simulated aerosol composition between climate models are large. These differences affect calculated aerosol properties and radiative effects. In addition, aerosol models tend to underestimate total aerosol optical depth (AOD) compared with observations, but they are doing better currently than they were a few years ago. The Aerosol Comparisons between Observations and Models (AEROCOM) project report on a set of models that produced global aerosol optical thicknesses at 0.55 μm ranging between 0.11 and 0.15. In comparison the average AOD obtained at a large number of sites comprising the AERONET network is 0.135, and the satellite composite is 0.15. However, even though the models' global mean AOD values are converging, the convergence is obtained despite large differences in aerosol composition, particle size and atmospheric residence times. This implies improvements in model representation of AOD will not translate directly into model improvement of calculated forcing, which depends on AOD as well as other aerosol parameters. An additional concern is that aerosol forcing tends to exhibit large spatial and temporal variability so that global-mean comparisons may not be meaningful.

2.2 *Looking forward*

- Progress requires effort on the observational side to reduce uncertainties and disagreements between different observational data sets.
- Agreement in aerosol optical depth among models and between models and observations can mask large differences that exist in modeled aerosol types and representations of aerosol processes. Comparison of additional aerosol properties (e.g., aerosol chemical composition, spectral variation of optical depth, size parameter, and absorption properties) is expected to

yield information on model differences and begin to constrain representations of the several aerosol component species.

- Better estimates of source strength and location of both primary aerosol particles and precursor gases are needed. Improvements can be achieved by observational techniques including satellite measurements of emissions from biomass burning and improved inversion techniques. However developing emission inventories of primary particles and of aerosol precursor gases is ultimately based on measurements of emission factors for pertinent processes together with detailed inventorying of the intensity of the pertinent activities as a function of location and time.
- Wet/dry removal and transport processes require enhanced understanding by field measurements together with further model evaluation and development. Continued satellite and in situ measurements are needed for model evaluation.

3. Aerosol direct radiative effect and climate forcing

3.1 *Cloud-free aerosol direct radiative effect (DRE).*

Aerosol direct radiative effect denotes the change in radiative flux at top of the atmosphere or at the Earth's surface due to the presence of aerosols. Present measurement capabilities permit determination of the global annual average cloud-free aerosol DRE for solar radiation over oceans as -5.5 ± 0.2 W m^{-2} net flux at the top of the atmosphere (TOA) and -8.8 ± 0.7 W m^{-2} net flux at the surface. Deriving the aerosol direct effect over land from flux measurements such as from CERES is complicated by a large and highly heterogeneous surface reflection. A hybrid of satellite retrievals and model simulations yields a global (land and ocean) cloud-free DRE of solar radiation of -4.9 ± 0.7 W m^{-2} and -11.8±1.9 W m^{-2} at the TOA and surface, respectively. Model simulations result in estimates that are 30-50% weaker (less cooling) than the measurement-based estimates. The model-measurement differences relate to model underestimates of AOD over oceans and tropical land, where dark surfaces allow aerosols to produce big differences in radiative effects.

3.2 *Cloud-free aerosol direct climate forcing (DCF).*

DCF denotes only the effects of *anthropogenic* aerosols. The measurement-based estimate of cloud-free TOA DCF by anthropogenic aerosols ranges from -1.1 to -1.6 W m^{-2} over ocean, stronger than model simulated values of -0.3 to -0.9 W m^{-2}. Including the less certain land component, on global average, the measurement-based estimate of TOA DCF ranges from -1.1 to -1.9 W m^{-2}, again stronger than the model-based estimates of -0.4 to -1.0 W m^{-2}. The range in model estimates is due to having different aerosol components plus different properties for the particular aerosol type. Overall, satellite-based estimates of DCF exhibit much greater uncertainties than estimates of DRE.

3.3 *Total sky aerosol direct radiative effect and climate forcing.*

Aerosols staying above or below clouds can scatter and absorb solar radiation, creating an aerosol effect on the radiation field or a direct climate forcing if the aerosols are anthropogenic. This not an indirect effect when aerosols modify cloud properties. The total sky aerosol direct radiative effect and climate forcing is a sum of cloud-free and cloudy DRE/DCF weighted respectively by cloud-free fraction and

cloud fraction. However the aerosol and its direct radiative effect and climate forcing are difficult to observe in the presence of clouds. As a result, it is only model estimates of the total sky forcing that are generally reported. The total sky aerosol direct climate forcing at the top of the atmosphere shows a wide disparity among models, varying from slight warming (+0.04 W m^{-2}) to cooling (–0.63 W m^{-2}). This is primarily the result of models having different aerosol components plus different properties for the particular aerosol type and relative heights of aerosol and cloud layers.

3.4 *Looking Forward*

- Uncertainties in measurement-based estimates over land can be reduced with more accurate measurements of aerosol absorption and improved understanding of the reflectance from heterogeneous land surfaces.
- Active remote sensing observations can constrain relative heights of aerosol layers and cloud layers in order to estimate the total sky DRE and DCF from measurements. These observations can also constrain the vertical distributions of aerosol absorption in the atmosphere that are essential to understanding how the atmosphere will respond to the aerosol radiative effect.
- Improvements in measurement-based estimates of DCF depend on developing techniques to better determine the anthropogenic component of the aerosol in the measurements. For example, using in situ measurements of composition and optical properties to constrain satellite techniques have not yet been fully explored.
- Ultimately the improvements in measurement-based estimates can be expected to better constrain model results and narrow the range of model estimates of both DRE and DCF.

4. Aerosol indirect effects

4.1 *Observations of aerosol indirect effects*.

Remote sensing estimates of aerosol indirect forcing are still very uncertain. Current estimates of global average aerosol indirect forcing based on remote observations range from -0.6 to -1.7 W m^{-2}. Few observational systems measure cloud liquid water path, even though this quantity is necessary to quantify aerosol indirect forcing. Basic processes still need to be understood on regional and global scales. Uncertainties will likely increase before they decrease as new processes and their feedbacks become known. Remote sensing observations of aerosol-cloud interactions and aerosol indirect forcing are based on simple correlations between variables, from which cause-and-effect are inferred. However, such inferences are not proven. The most difficult aspect of inferring aerosol effects on clouds from the observed relationships is separating aerosol effects from meteorological effects when aerosol loading itself is often correlated with the meteorology. As with the case of direct forcing, the regional nature of indirect forcing is especially important.

4.2 *Representations of aerosol indirect effects in General Circulation Models (GCMs)*.

Most GCMs do not address aerosol indirect effects. Approximately only one-third of the models used for the IPCC 20th century climate change simulations incorporated an aerosol indirect effect. Generally, though not exclusively, this effect was associated with sulfate-only aerosol. The results varied strongly among models. The IPCC estimate of the net radiative forcing associated with the cloud

albedo effect given in the Chapter 2 Executive Summary of the IPCC AR4 ranges from +0.4 to –1.1 W m^{-2}, with a 'best-guess' estimate of –0.7 W m^{-2}. Most models did not incorporate forcing associated with aerosol effects on cloud fraction and amount of condensate. Comparison of the indirect effect in various models showed that differences in cloud dynamics and microphysics play a strong role in inducing differences in the indirect effect(s).

4.3 *Coupling GCMs with cloud resolving models.*

A primary difficulty in representing aerosol cloud interactions in GCMs is that GCMs do not resolve convection on their large grids (order several hundred km), and that their treatment of cloud microphysics is rather crude, as is their representation of aerosols. Until GCMs are able to represent cloud scales, it is questionable what can be obtained by adding microphysical complexity to poorly resolved clouds. Superparametrization efforts (where standard cloud parameterizations in the GCM are replaced by resolving clouds in each grid column of the GCM via a cloud resolving model) could lead the way for the development of more realistic cloud fields. However these are just being incorporated in models that resolve both cloud and aerosols. Global cloud resolving models, with grid sizes on the order of 4 km are in their infancy but represent another possible path forward. They are, however, restricted to shorter integration times. The coupling of aerosol and cloud modules to dynamical models that resolve the large turbulent eddies associated with vertical motion and clouds (large eddy simulations or LES, with grid sizes of ~ 100 m and domains ~ 10 km) has proven to be a powerful tool for representing the details of aerosol-cloud interactions together with feedbacks. Such models, together with observations at similar scales, enable improved understanding of aerosol-cloud processes, and represent a foundation for work at larger scales.

4.4 *Looking forward:*

- All progress in estimating aerosol indirect effects requires a better understanding of the basic processes of aerosol-cloud interaction.
- A methodology for integrating observations (ground-based, airborne and satellite) and models at the range of relevant temporal/spatial scales is crucial, as is separating meteorological effects from aerosol effects on clouds.
- Coupling GCMs with cloud resolving models is the long term solution, but a better overall understanding of the processes must be achieved first.

5. Long term trends of aerosol and radiation

5.1 *Multi-decadal change of solar radiation reaching the surface.*

Systematic changes in observed global solar radiation (a sum of direct and diffuse solar radiation) reaching the surface (so-called dimming or brightening) have been reported in the literature. Speculation suggests that such trends result from multi-decadal changes of aerosol emissions. However, the lack of reliable long-term observations of aerosol trends over both land and ocean during this time period makes it difficult to assess the role aerosols have played in the multi-decadal change of surface solar radiation. Therefore, long-term global aerosol observation in conjunction with high-quality surface radiation measurements is strategically necessary. In addition to the aerosol optical depth,

changes in aerosol composition due to changes in industrial practices, environmental regulations, and biomass burning emissions are required. There are also important ramifications for cloud formation since radiative balance requires that reduced incoming surface radiation results in reduced surface sensible and latent heat fluxes, and therefore weaker convection.

5.2 *Dynamic quality of the aerosol system*.

The global aerosol system is a moving target. Ten years ago the spatial distribution of aerosol production was different than it is today, and ten years from now, it will be different again. This is unlike the observations of the relatively constant increase in greenhouse gases.

5.3 *Looking Forward*:

- Aerosol trend analysis requires long-term consistent data records. Practically this will require multiple sensing systems over decades and careful testing the consistency of the measurements as the record passes from one sensing system to the next. An improved understanding of aerosol indirect and semi-direct effects is particularly needed to make a robust attribution of the observed dimming or brightening to the aerosol changes.
- Simulating long-term aerosol variations with global models can link long-term trends of emissions, aerosol loading, and radiative effects.

6. Climate response to aerosol forcing

6.1 *Aerosol forcing compared with greenhouse gas forcing*.

Although the nature and geographical distribution of forcings by greenhouse gases and aerosols are quite different, it is often assumed that to first approximation the effects of these forcings on global mean surface temperature are additive, and thus that the negative forcing by anthropogenic aerosols has offset the positive forcing by incremental greenhouse gases over the industrial period. The IPCC AR4 estimates the total global average TOA forcing by incremental greenhouse gases (long-lived GHGs, tropospheric and stratospheric ozone, and stratospheric water vapor from methane oxidation) to be 3.0 (2.8 to 3.4) W m^{-2}, where the range in parenthesis is meant to encompass the 5-95% probability that the actual value will be within the indicated range. The corresponding value for aerosol forcing (direct plus enhanced cloud albedo effects only) is –0.6 (0 to -1.8) W m^{-2}. The total forcing, 1.6 (0.6 to 2.4), reflects the offset of GHG forcing by aerosols; the uncertainty in the total forcing is dominated by the uncertainty in aerosol forcing.

6.2 *Implications of aerosol forcing and its uncertainty on GCM calculations of temperature change over the industrial period*.

A key requirement for forcing over the industrial period is as input to GCM calculations, necessary to evaluate the performance of these models in calculating climate change over the industrial period by comparison with observations. In such a comparison Hansen et al. (2007) explicitly took note of the wide range of possible forcings resulting from uncertainty in aerosol forcing and the implications on determining climate model sensitivity, acknowledging that "an equally good match to observations probably could be obtained from a model with larger sensitivity and smaller net forcing, or a model

with smaller sensitivity and larger forcing". This balance between the magnitude of the forcing and the sensitivity of the model thus makes it difficult to determine climate sensitivity. Studies suggest that the climate responses to greenhouse gases and sulfate aerosols are correlated, and separation is possible only occasionally, especially at global scales and during summer when the aerosol effect on solar absorption in the Earth-atmosphere system is likely to be bigger. The conclusions concerning this appear to be model and method-dependent: using time-space distinctions as opposed to trend detection may work differently in different models.

Even distinguishing between the effect of different aerosol types is difficult. Overall, the similarity in response to all these very different forcings is undoubtedly due to the importance of climate feedbacks in amplifying the forcing, regardless of its nature.

6.3 *Absorbing versus reflective aerosol forcing.*

Distinctions in the climate response do appear to arise in the vertical, and these could be used to help quantify aerosol forcing. Absorbing aerosols produce warming that is exhibited throughout the troposphere and into the stratosphere, whereas reflective aerosols cool the troposphere but warm the stratosphere. In the ocean the cooling effect of aerosols extends to greater depths than the warming due to greenhouse gas increases, because of the thermal instability associated with cooling the ocean surface. Hence the temperature response at levels both above and below the surface may provide an additional constraint on the magnitudes of each of these forcings.

6.4 *Looking forward:*

The response of climate models to aerosol forcing is dependent on aerosol forcing in the models. Continued progress in evaluation of climate models will depend on improved estimates of aerosol forcing. There is potential for further improvement by examination of the relative forcing due to absorbing and reflective properties of different aerosols.

7. Aerosol interaction with precipitation and weather

The most important improvement of understanding of aerosols and their role in global change is that the aerosol effect extends much beyond radiative forcing in the Earth's energy budget. Aerosols absorb sunlight and create differential heating within the atmosphere that affects atmospheric circulations and weather at many scales. Aerosol affects clouds by modifying cloud brightness, cloud cover, precipitation and severe weather. Clouds and precipitation, in turn, affect aerosol.

7.1 *Looking forward:*

- Aerosols, clouds, precipitation, weather and climate must be studied as a holistic system, with both observations and models, and with an emphasis on long term monitoring of a system that exhibits a strong degree of regional variability and is continually changing.
- Improved measurement capabilities coupled with more sophisticated treatment of aerosols and clouds in models suggest that more accurate and constrained aerosol forcings are expected to be available for future intercomparisons of general circulation models.

Chapter I. Introduction

Authors:. R. N. Halthore, NASA HQ/NRL; **S. E. Schwartz**, DOE BNL; **D. G. Streets**, DOE ANL; **D. Rind**, NASA GISS; **H. Yu**, NASA GSFC/UMBC; **P. L. DeCola**, NASA HQ

Table of Contents

1.1 Description of atmospheric aerosols

Earth's atmosphere consisting primarily of a mixture of gases also contains particles, such as aerosols and clouds. Aerosols are suspended liquid or solid particles whose typical diameters range over four orders of magnitude (sizes from ~3 nanometers, nm, to a few hundredths of millimeters, mm, generally smaller than cloud droplets) with a wide dynamic range of composition and shape, depending on the their sources and atmospheric processes. It is well known that aerosols can have a variety of important impacts on the environment. Aerosols, also known as particulate matter, have long been recognized as pollutants of concern and may have detrimental effects on human health, such as impairment of pulmonary function. Sulfate and nitrate aerosols are also primarily responsible for acid deposition. Aerosols likewise strongly interact with solar and terrestrial radiation in two different ways. First, they directly scatter and absorb solar (shortwave) radiation (Insets 1 & 2). Second, by acting as cloud condensation nuclei they modify physical and chemical properties of clouds and thus can alter precipitation processes and indirectly affect cloud particle interaction with solar and terrestrial radiation. The net result of these effects is thought to be an enhancement of Earth's shortwave albedo (reflectance) affecting Earth's radiation budget and climate, and also a redistribution of the deposition of radiant and latent heat energy in the atmosphere, with possible effects on atmospheric circulations and precipitation patterns on a variety of length scales.

Major aerosol processes that influence climate are illustrated in **Figure 1.1**. Both natural and man-made processes generate aerosols. Some aerosols are emitted directly to the atmosphere (primary aerosols), while some are formed in the atmosphere from gaseous precursors through photochemical production (secondary aerosols). The amount of aerosols in the atmosphere has greatly increased over the industrial period. The nature of this particulate matter has substantially changed as a consequence of evolving emissions from industrial and residential activities, mainly combustion related. These anthropogenic aerosols are often observable as dust, smoke, haze, and in and downwind of urban environments, as smog. Important classes of natural aerosols are: sulfates - from ocean spray, volcanic emissions, and oxidized sulfides released from the ocean or decomposition of organic matter; sea salt - produced mainly from spray from breaking bubbles of ocean whitecaps; mineral dust; smoke from natural wildfires; and secondary aerosols from gas to particle conversion, mainly of natural hydrocarbons (terpenes, isoprene) emitted by vegetation that is oxidized in the atmosphere to low volatility products which condense to form aerosols. Volcanic eruptions emit large quantities of primary aerosols, which tend to be removed fairly rapidly by dry deposition, and also sulfur dioxide, a source of secondary aerosols; the latter, when injected into the stratosphere by an explosive volcano (e.g., Pinatubo, in the Philippines, in 1991) can form large amounts of sulfuric acid aerosol, which can persist, depending on altitude, for several years.

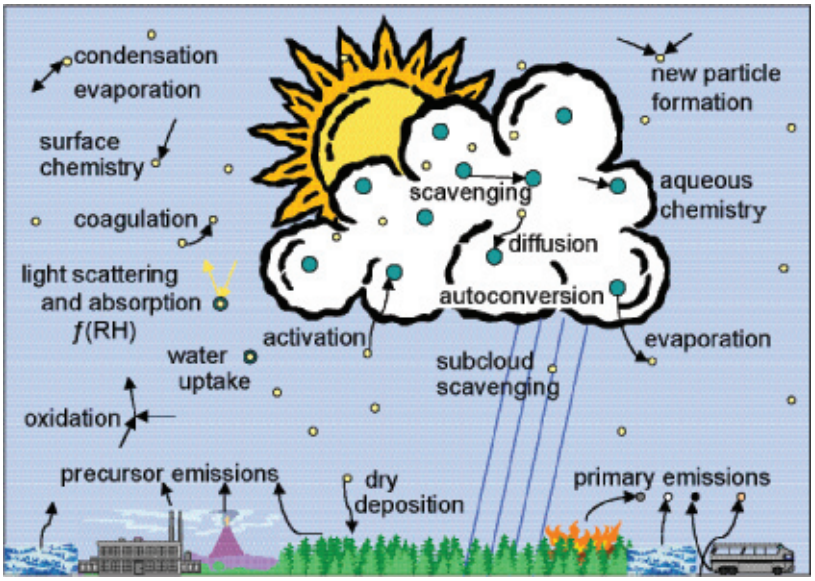

Figure 1.1 Major aerosol processes that influence climate. Aerosol particles are directly emitted as primary particles and are formed secondarily by oxidation of emitted gaseous precursors. The formation of low-volatility materials in this way results in new particle formation and condensation onto existing particles. Aqueous-phase oxidation of gas-phase precursors within cloud droplets accretes additional mass onto existing particles but does not result in new particle formation. Particles age by surface chemistry and coagulation as well as by condensation. With increasing relative humidity particles may accrete water vapor by deliquescence and further hygroscopic growth; with decreasing relative humidity water is lost and ultimately particles may effloresce to the dry state. The uptake of water increases particle size, affecting also the particle optical properties. During cloud formation some fraction of aerosol particles serve as cloud condensation nuclei, by becoming activated, that is, overcoming a free-energy barrier to form cloud droplets. Within clouds interstitial particles can become attached to cloud droplets by diffusion, and activated particles are combined when cloud droplets collide and coalesce. If cloud droplets evaporate the particles are resuspended, but if the cloud precipitates the particles are carried below the cloud and reach the surface, unless the precipitating particles completely evaporate. Aerosol particles below precipitating cloud can also be removed from the atmosphere by impaction by precipitating drops and by dry deposition to the surface. From Ghan and Schwartz (2007).

Aerosol particles are removed from the atmosphere mainly by wet deposition (uptake in cloud droplets followed by removal in precipitation) and to a lesser extent by dry deposition to vegetation, land surface, ocean water (gravitational settling of large particles; impaction of intermediate size particles, diffusion and attachment of small particles). The atmospheric residence time for tropospheric aerosols is typically about a week. As a consequence of the non-uniform distribution of sources and the short atmospheric residence time, the spatial distribution of aerosol particles in the atmosphere is quite non-uniform. For a mean atmospheric transport velocity of 5 m s^{-1}, this residence time of a week corresponds to a transport distance of 3000 km. Likewise at any given location the amount and nature of aerosols can vary substantially as a consequence of variability in atmospheric transport and in aerosol formation processes, driven largely by variability in controlling meteorology, and to some extent by intermittency of sources, e. g., wildfires, agricultural burning, or, in the extreme volcanic eruptions. For most aerosols, whose source is emissions at the surface, concentrations are greatest in the atmospheric boundary layer, decreasing with altitude in the free troposphere.

This report reviews the present state of understanding of the influences of aerosols on Earth's climate system, in particular, their direct and indirect effects for their consequences on climate change.

1.2 Climate effects of aerosols

The recognition, mainly in the past two decades, of the important influences of atmospheric aerosols on climate and climate change has generated a large amount of research. The increase in atmospheric aerosols over the industrial period is thought to have exerted a net cooling influence on Earth's climate relative to the pre-industrial period. The magnitude of this cooling influence, denoted by a negative forcing of climate change (see Inset 3 for a definition of forcing), is thought to be comparable to the warming influence (positive forcing) of enhanced atmospheric concentrations of greenhouse gases (*GHGs*) – mainly carbon dioxide, methane, nitrous oxide, chlorofluorocarbons, and ozone. Aerosol forcing is defined (Inset 3) as the difference in a quantity, such as the outgoing shortwave flux, without and with aerosols present. A negative forcing in the top-of-the-atmosphere flux for example, means that the outgoing flux is greater with aerosols present than without, and therefore represents a cooling effect. In discussions of aerosol effects a sign convention is adopted such that a positive radiative effect at the TOA indicates addition of energy to the earth-atmosphere system (i.e., a warming influence) whereas a negative effect indicates a net loss of energy (i.e., a cooling influence).

However these influences are not yet well quantified, and uncertainties associated with changes in Earth's radiation budget due to anthropogenic aerosols (radiative forcing) are considered to be the greatest contribution to uncertainty in radiative forcing of climate change over the industrial period (IPCC AR4). Much of the difficulty in quantifying aerosol influences arises from the heterogeneity of aerosol loading and properties: spatial, temporal, size, and composition. This multidimensional heterogeneity stands in marked contrast to the uniform distributions and properties of greenhouse gases and makes the characterization of aerosols and quantification of their influences on climate and climate change extremely challenging.

1.2.1. *Direct and indirect effects*

Aerosols participate in the Earth's energy budget (**Figure 1.2**) directly by scattering and absorbing radiation (McCormick and Ludwig, 1967; Charlson and Pilat, 1969; Atwater, 1970; Mitchell, Jr., 1971; Coakley et al., 1983) and indirectly by acting as cloud condensation nuclei (that is by serving as

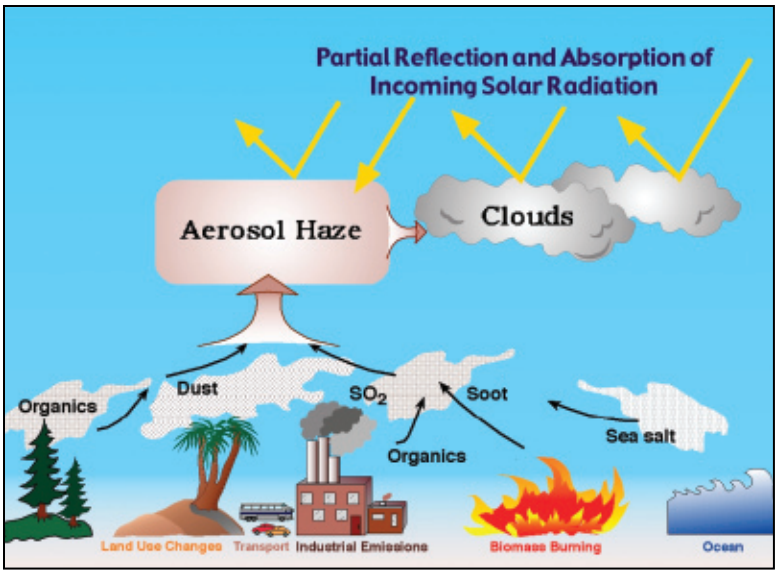

Figure 1.2. Radiative forcing by tropospheric aerosols. Tropospheric aerosols (aerosols in the lower atmosphere) scatter solar radiation; this light scattering exerts a cooling effect on climate by decreasing the absorption of solar radiation. Aerosol particles also increase the brightness and persistence of clouds, exerting a further cooling influence on climate. Increases in aerosols over the industrial period have resulted in a cooling influence on climate change that is opposite to the warming influence of increased concentrations of greenhouse gases.

the particles on which cloud droplets form and grow) and, thereby, affecting cloud microphysical and radiative properties (Gunn and Phillips, 1957; Twomey, 1977; Liou and Ou 1989; Albrecht, 1989). Other things being equal, the greater the number concentration of aerosol particles, the greater the number concentration of cloud drops, and hence the greater the probability of scattering of incident radiation, and hence the brighter the cloud; this effect is commonly referred to as the first aerosol indirect effect, or the Twomey effect. Likewise, other things being equal, the greater the number concentration of cloud drops, the less efficient the formation of precipitation, and hence the greater the persistence of the cloud, and hence the greater the time-average reflectance of solar radiation; this effect is commonly referred to as the second aerosol indirect effect, or Albrecht effect. The direct absorption of radiant energy by aerosols can influence the atmospheric temperature structure and cloud droplet evaporation rate – a phenomenon that has been labeled the "semi-direct effect" (Hansen et al., 1997; Ackerman et al., 2000; Koren et al., 2004).

The potential influences of aerosols on climate were proposed and debated at least several decades ago (Gunn and Philips, 1957; McCormick and Ludwig, 1967; Charlson and Pilat, 1969; Atwater, 1970; Mitchell, 1971; Twomey et al., 1977). However, because of the paucity of aerosol measurements, even the sign of the aerosol effect on global radiation (warming or cooling) was uncertain. Nevertheless, these pioneering studies highlighted the importance of acquiring better information concerning aerosols, and thereby inspired substantial research efforts in the intervening decades.

1.2.2. *Anthropogenic aerosol climate forcing*

Radiative forcing of climate change by anthropogenic aerosols regained scientific attention in the 1990s (Charlson et al., 1990; 1991; 1992; Penner et al., 1992) followed by the assessment of Intergovernmental Panel on Climate Change (IPCC, 1995 and IPCC, 1996) that first identified anthropogenic aerosol as a climate forcing agent. The Third and Fourth IPCC Assessment Reports concluded that on a global average the sum of direct and indirect TOA forcing by anthropogenic aerosols is negative (cooling) and comparable in magnitude to the positive forcing by anthropogenic GHGs of about 2.4 Wm^{-2} (IPCC, 2001; IPCC, 2007, see **Figure 1.3**). These aerosol forcing assessments have been based largely on model calculations, with scientific understanding designated as "Medium - Low" and "Low"

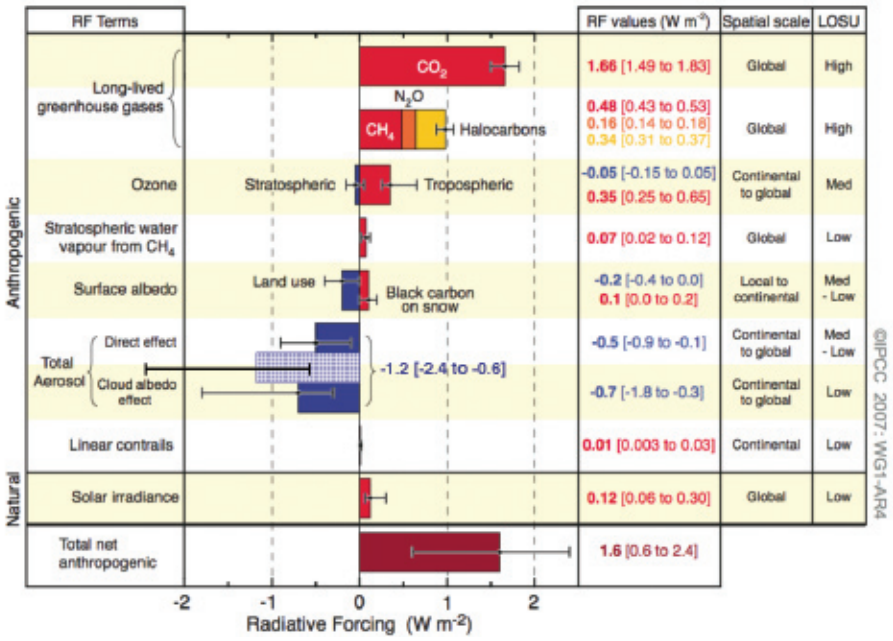

Figure 1.3. Global average radiative forcing (RF) estimates and uncertainty ranges (5-95% confidence interval) in 2005, relative to the pre-industrial climate, for anthropogenic carbon dioxide (CO_2), methane (CH_4), nitrous oxide (N_2O) and aerosols and for other important identified agents and mechanisms, together with the typical geographical extent (spatial scale) of the forcing and the assessed level of scientific understanding (LOSU). Forcings are expressed in units of watts per square meter,W m^{-2}. The total anthropogenic radiative forcing and its associated uncertainty are also shown. The figure is modified from IPCC (2007) by addition of a bar for total aerosol forcing (hatched blue) representing the sum of aerosol direct and indirect forcings, and associated uncertainty.

for the direct and indirect climate forcing, respectively. It is also important to recognize that the global-scale aerosol TOA forcing alone is not an adequate metric for climate change (NRC, 2005). Because of aerosol absorption mainly by soot particles, the aerosol direct radiative forcing at the surface could be much greater than the TOA forcing, and the atmospheric radiative heating rate increases. The aerosol climate forcing and radiative effect are characterized by large spatial and temporal heterogeneities due to the wide variety of aerosol sources, the spatial non-uniformity and intermittency of these sources, the short atmospheric lifetime of aerosols, and processing (chemical and microphysical) that occurs in the atmosphere. Over heavily polluted regions, the aerosol forcing can be much stronger than the global average and be far more of an offset for the GHGs warming effect. By realizing aerosol's climate significance and the challenge of charactering highly variable amount and properties of aerosols, the US Climate Change Research Initiative (*CCRI*) has specifically identified research on atmospheric concentrations and effects of aerosols as a top priority (NRC, 2001).

1.3. Reducing uncertainties in estimating aerosol climate forcing

1.3.1. Synergy between observations and models

Over the past decade, significant progress has been made on one hand in measuring aerosol distributions and properties from satellite, ground-based networks, and in-situ field experiments, and on the other hand in developing/improving chemistry transport models that simulate a suite of atmospheric aerosols. Incorporating aerosol representations in the GCM then allows assessment of aerosol climate

effects. Together, through synthesis and integration, observations can be used to improve and constrain model simulations (e.g., Bates et al., 2006; Yu et al., 2006), while the models are indispensable tools for estimating past aerosol forcing and projecting future climate due to changes in atmospheric aerosols (Schulz et al., 2006).

The key to reducing uncertainty in effects of anthropogenic aerosols on climate change is understanding of, and numerically based description of, the processes that contribute to these effects. The geographical distribution of anthropogenic aerosols and the properties of these aerosols depend on emissions of primary particles and precursor gases, on new particle formation and on gas to particle conversion processes and on aerosol dynamical processes, on removal processes, and on transport. These processes are represented in chemical transport models, which must be evaluated by in-situ measurements and by surface- and space-based remote sensing. The requirement is to accurately model the distribution of aerosol mass concentration and size and composition distribution as a function of location and time. There is a further requirement to model the optical properties (and their relative humidity dependence) and the cloud nucleating properties (CCN concentration as a function of supersaturation, and any kinetic limitations). Reduction in uncertainties in aerosol forcing thus requires a coordinated research strategy that will successfully integrate data from multiple platforms (e.g., ground-based networks, satellite, ship, and aircraft) and techniques (e.g., in-situ measurement, remote sensing, numerical modeling, and data assimilation) (Kaufman et al., 2002; Diner et al., 2004; Anderson et al., 2005). The accuracies of current measurements to describing relations between aerosol composition and optical and cloud nucleating properties are not well established; consequently, aerosol forcing has been estimated mainly using modeled mass concentrations and assumed aerosol properties. Model simulations, in turn, rely on the representation of processes of aerosol formation and evolution in the atmosphere, and in particular the estimates of emissions of primary aerosol particles and of precursor gases, which are subject to large uncertainties.

1.3.2. *Estimates of emissions*

Following earlier attempts to quantify man-made primary emissions of aerosols (Turco et al., 1983; Penner et al., 1993) systematic work was undertaken in the late 1990s to calculate emissions of black carbon (BC) and organic carbon (OC), using fuel-use data and measured emission factors (Liousse et al., 1996; Cooke and Wilson, 1996; Cooke et al., 1999). The work was extended in greater detail and with improved attention to source-specific emission factors in Bond et al. (2004), which provides global inventories of BC and OC for the year 1996, with regional and source-category discrimination that includes contributions from industrial, transportation, residential solid-fuel combustion, vegetation and open biomass burning (forest fires, agricultural waste burning, etc.), and diesel vehicles. Emphasis is on sub-micron sized particles, of greatest relevance to radiative forcing applications.

Emissions of primary aerosols from natural sources—which include wind-blown mineral dust, wildfires, sea salt, and volcanic eruptions—are less well quantified, mainly because of the difficulties of measuring emission rates in the field and the unpredictable nature of the events. Often, emissions must be inferred from ambient observations at some distance from the actual source. As an example, it was concluded (Lewis and Schwartz, 2004) that available information on size dependent sea-salt production rates could only provide order-of-magnitude estimates. One conclusion from this work is that primary emissions, just like the observed aerosol concentrations, can vary dramatically over space and

time. However, again, progress has been made in modeling these inputs and observing some of them from satellite platforms.

With regard to secondary aerosol production, the emissions of their man-made precursors are in some cases quite well known, e.g., SO_2 emissions for sulfate formation and NO_x emissions for nitrate formation; however emissions of cation precursors, such as NH_3, Ca, and Mg, are much less well known. Progress has been made at speciating the primary man-made precursors of secondary organic aerosols such as toluene and xylenes (Streets et al., 2003); however, the natural-source precursors of secondary organic aerosols, such as terpene and isoprene, are known at global scale only to within a factor of two (Guenther et al., 2006) and are poorly defined at a particular time and place. Even some of the fundamental mechanisms of secondary organic aerosol formation are not well understood; identifying these mechanisms and quantifying the aerosol production rate as a function of controlling variables is a subject of active research. Understanding of the secondary organic aerosol formation is, however, rapidly evolving. Recent studies by several groups involving field measurements, laboratory studies, and modeling are showing much greater amounts of secondary organic aerosol than were previously recognized, in some instances an order of magnitude or greater.

The difficulties encountered in quantifying present-day aerosol emissions, are magnified when attempting to develop past or future trends. Information for past years on the source types and strengths and even the world regions that dominate emissions are difficult to obtain, and the historical inventories from pre-industrial time to present had to be based on limited knowledge and database. Several studies on historical emission inventories of BC (e.g., Novakov et al., 2003; Ito and Penner 2005; Junker and Liousse, 2006; Bond et al., 2007), SO_2, and NO_x (van Aardenne et al., 2001; Stern, 2005) have been available in the literature with some similarities and differences among them, but the emission estimates for early times do not have the rigor of the studies for present emissions. One major conclusion from all these studies is that growth of aerosol emissions in the 20th century was not nearly so rapid as the growth in CO_2 emissions. This is because in the late 19th and early 20th centuries, PM emissions were relatively high from the heavy use of biofuels and the lack of particulate controls on coal-burning facilities; however, as economic development continued, traditional biofuel use remained fairly constant and PM emissions were reduced by technological controls. Thus, PM emissions in the 20th century did not grow as fast as CO_2 emissions, as the latter are roughly proportional to total fuel use.

One pressing need is for historical open biomass burning emissions. Great strides in assembling interannual estimates of global biomass burning from satellite products have been made (e.g., van der Werf et al., 2003, 2006), but these obviously go back only a short time. Century-scale estimates have been attempted (van Aardenne et al., 2001; Ito and Penner, 2005; Mouillot and Field, 2005; Mouillot et al., 2006), but all researchers acknowledge the great difficulties in being certain of the historical magnitudes and trends. Nevertheless, the patterns of open biomass burning since the industrial revolution will significantly affect aerosol loadings in historical times. Tentative steps have even been taken to estimate historical trends in other natural-source emissions, e.g., Mahowald et al. (2003) on mineral dust emissions, but such work is not yet ready for use by the climate modeling community. The gas phase photochemistry that is responsible for formation of nitric acid is fairly well understood, as is the subsequent fate of HNO_3 – wet and dry deposition and uptake on aerosols, principally by neutralization by ammonia. However emissions inventories of ammonia are subject to great uncertainty historically as well as at present.

Projections of aerosol emissions into the future have been made. Faced with the need to develop future BC and OC emissions for the Third Assessment Report, the IPCC scaled present-day emissions with CO emission forecasts (IPCC, 2001). This was an unsatisfactory approach because of the different factors influencing future emissions of fine particles and CO, particularly the ability to control particle emissions at reasonable cost and the societal imperative of reducing human health effects caused by fine particle inhalation. Forecasts of future BC and OC emissions based on IPCC energy and fuel scenarios have been developed (Streets et al., 2004; Rao et al., 2005) taking care to incorporate the likely future effects of new technology deployment and environmental regulation. The expectation is that global emissions of carbonaceous aerosols will likely remain rather flat or decrease out to 2050. Aerosol emission modelers have been reluctant to venture into the 2050-2100 timeframe on account of the great difficulties of predicting the level of technology application and performance, even if energy modelers can forecast the levels of fuel use by sector. For precursors gases like SO_2, there are many forecasts available; prospective emissions depend strongly on assumptions about future emission controls.

1.3.3. *Aerosol representation in GCMs*

Representation of the climate influence of atmospheric aerosols has been gradually incorporated into GCMs with increasing sophistication. In the IPCC (1990) report, the few transient climate change simulations that were discussed used only increases in greenhouse gases. By the IPCC (1995) report, although most of the simulations still used only greenhouse gases, the direct effect of sulfate aerosols was added to several models (MPI and UKMO). The sulfate aerosol distribution for 1990 was derived from a sulfur cycle model in both cases (Langner and Rodhe, 1991) with estimated past aerosol emissions, and future aerosol loading followed the IS92a sulfur emission scenario (IPCC, 1992). The aerosol forcing contribution was mimicked by increasing the surface albedo. The primary purpose was to establish whether the pattern of warming was altered by including aerosol-induced cooling in regions of high emissions (such as the Eastern U.S. and eastern Asia), although even then improved agreement with the observational record of global mean temperature in the last few decades was noted.

By the time of the IPCC (2001) report, numerous groups were using aerosols in simulations of both the 20th and 21st centuries. The inclusion of the direct effect of sulfate aerosols was necessary, given the models' climate sensitivity and ocean heat uptake, to reproduce the observed global temperature change. Although most models still represented aerosol forcing by increasing the surface albedo, several groups explicitly represented sulfate aerosols in their atmospheric scattering calculations, with geographical distributions determined by off-line tracer model calculations or by separate GCM aerosol simulations. The first model calculations that included the indirect effect of aerosols were also reported.

The most recent IPCC assessment report (2007) summarized the climate change experiments from some 20 modeling groups which have now incorporated representation of a variety of aerosol species, not just sulfates but black and organic carbon, mineral dust, sea salt and in some cases nitrates as well (see Chapter 3, Table 3.3). In addition, there is a greater realization of the importance of including the indirect effect, in part because with the given model sensitivity, the (better resolved) direct effect is now thought to be insufficient to allow proper simulation of observed temperature changes. As in previous assessments, the aerosol distributions that influence both the direct and indirect effect were produced off-line, as opposed to being run in a coupled mode with the climate change simulations. This is a limitation compared with a fully interactive approach in which climate changes are allowed to change the aerosol distribution and hence the aerosol climate forcing.

The fact that models now use multiple aerosol types and often calculate both direct and indirect aerosol effects does not imply that the requisite optical characteristics of the aerosols, or the mechanisms of aerosol/cloud interactions, are well known. Much research needs to be done before the field will be able to reduce the large uncertainties associated with the modeled aerosol forcing (IPCC, 2007). Additionally, one of the major sources of error lies in estimating the emissions of natural and anthropogenic aerosol and their precursors.

1.4 Contents of this report

This report assesses current understanding of aerosol radiative effects on climate, focusing on developments of aerosol measurement and modeling subsequent to the 2001 IPCC assessment report. The Executive Summary presents an overview of the topics addressed in this report. While providing a chapter by chapter summary of topics addressed, it also summarizes the key concepts that are required for the study of aerosol effects on climate. Chapter 1 (this chapter) presents a easily understandable summary of the topics addressed and introduces the reader to the key concepts in addition to providing a framework for further discussion in these chapters.

Chapter 2 provides an assessment of in-situ and remote sensing measurements of aerosol properties, burdens, and radiative forcing. In particular, it discusses the measurement of aerosol properties and their evolution. It provides an overview of current aerosol measurement capabilities and discusses the synergy of measurements and model simulations. The measurement requirements are discussed in the context of needs for an accurate estimation of aerosol radiative effects and forcing. Inadequacies in current measurement capabilities are addressed including aerosol vertical distributioins, direct forcing over land and the lack of accurate aerosol absorption measurements.

Model simulation and estimation of the global and to some extent regional aerosol direct and indirect effects are examined in Chapter 3. In particular, it examines the representations of aerosols that were used in the AR4 runs described in the IPCC (2007) report. The conclusions regarding the emissions and their effects drawn by the IPCC (2007) were based on these runs. These representations are not generally the same as those that were obtained in coupled aerosol-chemistry simulations run with "aerosol models" (in which aerosol sources are prescribed, with transport fields saved off-line from a separate run of the GCM). Similarly, the aerosols in the AR4 runs may differ from those in more recent simulations made with the same models.

Finally, in Chapter 4 issues and procedures that need to be addressed in obtaining a comprehensive understanding of aerosol effects on climate are identified. Future representation of aerosols in climate models is considered in Chapter 4. A more detailed computation of aerosol/chemistry interactions, better calculations of size distributions, and interactions between aerosols and clouds are only a few of the processes that could be incorporated in the future. However, all of these aspects are limited by the level of understanding, and by the computer time necessary for their calculation. Future climate-change experiments will likely be performed at finer horizontal and vertical resolution in order to resolve regional effects, and this too will require increased computational expense. It is therefore not clear how rapidly improved aerosol processes will be included in climate-change experiments; consequently at least for the next set of IPCC simulations the prime mode of operation may continue to be off-line simulations, and saving of aerosol distributions.

Inset 1: Atmospheric and Aerosol properties

Earth's atmosphere is composed primarily of nitrogen and oxygen with much lesser amounts of minor gases such as carbon dioxide, argon and water vapor, and of suspended aerosol particles and cloud particles. Each of these components interacts with solar (or shortwave) and terrestrial (thermal or longwave) radiation in different ways. Gas molecules having a very small size (0.1 nm) compared to the wavelength of the solar radiation (0.3 to ~5 μm) or the terrestrial radiation (greater than 5 μm) predominantly scatter solar radiation by a process known as Rayleigh scattering (Inset 2, below) at the same frequency, thus producing secondary radiation which has well defined angular characteristics. Rayleigh scattered light intensity depends on the 4^{th} power of the light frequency (reciprocal of the wavelength) with the result that blue light is scattered about 10 times more strongly than red light (thus giving rise to blue color of the sky). In addition, gases absorb light in discrete frequencies throughout the solar spectrum, and more so in the thermal infrared (especially near the surface where their densities are high) giving rise to the well known greenhouse effect. Increase in concentration of these molecules throughout the atmosphere, as is observed in the case of carbon dioxide and other trace gases due to human activities such as fossil fuel burning, enhances the greenhouse warming near the surface and thus provides a source of net heating of the surface and lower atmosphere (positive forcing, Table 1).

Aerosol particles on the other hand are much larger than molecules; they range in size (diameter for spherical particles) from a few nanometers (an aggregate of tens of molecules), a result of the process of nucleation, to tens of micrometers, as in the case of sea-salt and desert dust. Cloud particles are typically larger, up to hundreds of micrometers (even larger for rain clouds) a result of condensation of water vapor on the surfaces of aerosols in an atmosphere that is super-saturated (that is, the relative humidity slightly exceeds one hundred percent). Because the wavelength of light is now of the same order as the characteristic size of the particles (aerosols) or are less than the size of cloud particles, the light interaction with the particles is much more complex and is much stronger (per particle) for both scattering (for spherical particles this is known as Mie scattering) and absorption. Typically in an urban atmosphere the number concentration of aerosol particles tends to be high, with the result that the scattering by particles is of the same order (or higher) as that of the more numerous molecules. Some aerosol particles also absorb light. For example, carbonaceous (soot) particles are black and therefore have a relatively high absorption coefficient (Table 1 for definition). In such a case, when the aerosol particles are highly absorbing, the sign of the forcing attributable to aerosols tends to be the same as in the case of absorbing gases. More often though, aerosols tend to be non-absorbing (sulfates and sea-salt) and therefore reflect sunlight back into space providing cooling of the atmosphere. Indeed much attention was paid to this effect of aerosols in the mid- to late- seventies in studying the consequences of a nuclear war between nations in which studies showed that large scale injection of non-absorbing aerosols into the atmosphere (from nuclear explosions) would increase reflection of sunlight back into space thus cooling the surface – a circumstance that was termed "nuclear winter".

Inset 2: Molecular and aerosol light scattering and absorption.

Rayleigh or Molecular Scattering: The oscillating electric field of the solar photon induces an oscillating dipole in the molecule at the same frequency, thus emitting secondary radiation which has well defined angular characteristics (blue shaded area in the figure to the right). Rayleigh scattered light intensity depends on the 4^{th} power of the frequency with the result that blue light is scattered about 10 times stronger than red light (thus giving rise to blue color of the sky).	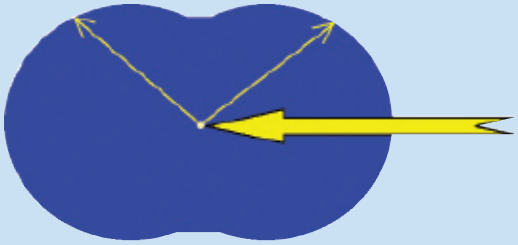 Phase Function for Rayleigh or Molecular scattering when size of molecule d << λ, wavelength of light, shows that forward scattering and backward scattering have equal probability.
Molecular Absorption: Atmospheric molecules such as carbon dioxide, water vapor and oxygen absorb solar and terrestrial radiation in the visible, near IR or thermal IR at specific wavelengths that correspond to their rotational, vibrational and/or electronic frequencies.	 Molecules such as CO_2 and H_2O have dipole moments and therefore strongly absorb radiation at many frequencies or wavelengths. (Figure not to scale).
Aerosol (Mie) Scattering: When particle sizes are large (comparable to the wavelength of light) the scattering cross-section (probability for scattering) increases dramatically. However there are many more molecules than particles in the atmosphere, with the result that the two effects are comparable.	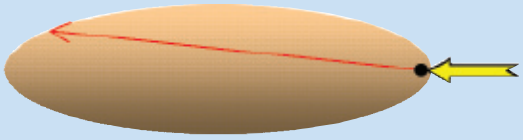 Scattering by large particles (aerosols, cloud droplets, shown here as a black dot) whose size d is approximately equal to λ, wavelength of light, is predominantly in the forward direction (red arrow).
Aerosol Absorption: Particles made of sulfates and sea-salt do not absorb light at solar wavelengths. Soot particles (i.e., those that are black), absorb solar and terrestrial radiation. At those wavelengths, the complex refractive index of these particles has a significant imaginary component.	 Particles with a large imaginary part of the refractive index have significant absorption.

Inset 3: Brief description of key aerosol, cloud, and surface properties that determine the aerosol radiative forcing.

- ***Aerosol extinction coefficient*:** Fraction of radiant flux lost from aerosol scattering and absorption per unit thickness of aerosol, with a unit of m^{-1}.
- ***Aerosol Forcing:*** of a quantity such as solar irradiance or flux is defined as the difference in the quantity with and without aerosols present. Sometimes aerosol forcing just refers to the industrial period in which case the forcing is the change in quantity calculated with aerosols present during the pre-industrial and industrial periods.
- ***Aerosol optical depth (AOD)*:** a measure of aerosol amount in optical sense. It is an e-folding length of the decrease of a direct beam due to the extinction when traveling through the aerosol layer. Changes of AOD with wavelength are usually represented by the Angstrom exponent, with high values of Angstrom exponent indicative of small particles (industrial pollution and biomass burning smoke) and low values representative of large particles (mineral dust and sea-salt).
- ***Aerosol mass extinction (scattering, absorption) efficiency*:** the aerosol extinction (scattering, absorption) coefficient per unit aerosol mass concentration, with a unit of $m^2\,g^{-1}$.
- ***Aerosol phase function*:** a description of the angular distribution of scattering radiation. In practice, the phase function is parameterized with ***asymmetry factor (g)*,** with g=1 for completely forward scattering and g=0 for symmetric scattering. Another relevant parameter is the ***hemispheric backscattered fraction (b)***, a fraction of the scattered intensity that is redirected into the backward hemisphere of the particle and can be derived from measurements made with an integrating nephelometer. The larger the particle size, the more the scattering in the forward hemisphere (i.e., larger g and smaller b).
- ***Aerosol single-scattering albedo (SSA, ω_0)*:** a measure of relative importance of scattering and absorption. It is defined as a ratio of the scattering coefficient to the extinction coefficient. The smaller the SSA, the more absorbing the aerosol is.
- ***Internal mixture vs external mixture:*** Internal mixture is a chemically homogeneous mixture of particles in air, with each particle having about the same chemical composition. For external mixture, individual particles in the aerosol do not have the same chemical compositions or necessarily the same size distribution. The internal mixture has a higher absorption coefficient than the external mixture.
- ***Hydrophilic aerosol vs hydrophobic aerosol:*** Hydrophilic aerosols (e.g., sulfate, sea-salt) can adsorb water vapor from its surroundings and ultimately dissolve, while hydrophobic aerosols (mineral dust) do not adsorb water vapor from its surroundings and dissolve. Hydrophilic aerosols become larger and more scattered with increasing relative humidity of air.
- ***Cloud condensation nuclei (CCN):*** Aerosol particles that act as seeds for the formation of clouds through the condensation of water molecules onto their surfaces at low supersaturation. The activation of aerosol particles to CCN depends on the size and chemical composition of particles.
- ***Cloud albedo:*** Fraction of incident radiant flux reflected by cloud. The cloud albedo depends on the number and size of cloud droplets, and water path. In comparison to clean clouds, polluted clouds have more cloud droplet number and smaller droplet size and are more reflective (i.e., higher cloud albedo).
- ***Surface albedo:*** Fraction of incident radiant flux reflected by surface. It depends not only on surface type but also on geometry of incident light. In general, land has a larger albedo than ocean (glint-free conditions), and desert has a larger albedo than forest. The larger the surface albedo, the less negative the aerosol radiative effect at the TOA is. The TOA aerosol radiative effect can shift from negative (cooling) over ocean to positive (warming) over bright land, if aerosol is partly absorbing.

References:

Ackerman A., O. Toon, D. Stevens, A. Heymsfield, V. Ramanathan, and E. Welton, 2000: Reduction of tropical cloudiness by soot. *Science* **288**:1042—1047.

Albrecht B., 1989: Aerosols, cloud microphysics, and fractional cloudiness. *Science* **245**:1227-1230.

Anderson T., R. Charlson, S. Schwartz, R. Knutti, O. Boucher, H. Rodhe, and J. Heintzenberg, 2003: Climate forcing by aerosols – A hazy picture. *Science* **300**:1103-1104.

Anderson T., R. Charlson, N. Bellouin, O. Boucher, M. Chin, S. Christopher, J. Haywood, Y. Kaufman, S. Kinne, J. Ogren, L. Remer, T. Takemura, D. Tanré, O. Torres, C. Trepte, B. Wielicki, D. Winker, and H. Yu, 2005: An "A-Train" strategy for quantifying direct aerosol forcing of climate. *Bull. Am. Met. Soc.* **86(12)**:1795-1809.

Atwater M., 1970: Planetary albedo changes due to aerosols. *Science* **170(3953)**:64-66.

Bates T., et al., 2006: Aerosol direct radiative effects over the northwestern Atlantic, northwestern Pacific, and North Indian Oceans: estimates based on in-situ chemical and optical measurements and chemical transport modeling. *Atmos. Cehm. Phys.*, **6**:1657-1732.

Bond, T.C., D.G. Streets, K.F. Yarber, S.M. Nelson, J.-H. Woo, and Z. Klimont 2004, A technology-based global inventory of black and organic carbon emissions from combustion, *J. Geophys. Res.*, **109**, D14203, doi:10.1029/2003JD003697.

Bond, T.C., E. Bhardwaj, R. Dong, R. Jogani, S. Jung, C. Roden, D.G. Streets, and N.M. Trautmann, 2007: Historical emissions of black and organic carbon aerosol from energy-related combustion, 1850-2000, *Global Biogeochem. Cycles*, **21**, GB2018, doi:10.1029/2006GB002840.

Charlson R. and M. Pilat, 1969: Climate: The influence of aerosols. *J. Appl. Meteorol.* **8**:1001-1002.

Charlson R., J. Langner, and H. Rodhe, 1990: Sulfate aerosol and climate. *Nature*, **348**:22.

Charlson, R., J. Langner, H. Rodhe, C. Leovy, and S. Warren, 1991: Perturbation of the Northern Hemisphere radiative balance by backscattering from anthropogenic sulfate aerosols. *Tellus*, **43AB**:152-163.

Charlson, R., S. Schwartz, J. Hales, R. Cess, R. J. Coakley, Jr., J. Hansen, and D. Hofmann, 1992: Climate forcing by anthropogenic aerosols. *Science* **255**:423-430.

Coakley J. Jr., R. Cess, and F. Yurevich, 1983: The effect of tropospheric aerosols on the earth's radiation budget: A parameterization for climate models. *J. Atmos. Sci.* **40**:116-138.

Cooke, W.F., and J.J.N. Wilson 1996, A global black carbon aerosol model, *J. Geophys. Res.*, **101**, **19**,395-19,409.

Cooke, W.F., C. Liousse, H. Cachier, and J. Feichter, 1999: Construction of a 1º × 1º fossil fuel emission data set for carbonaceous aerosol and implementation and radiative impact in the ECHAM4 model, *J. Geophys. Res.*, **104**, **22**,137-22,162.

Dentener, F., S. Kinne, T. Bond, O. Boucher, J. Cofala, S. Generoso, P. Ginoux, S. Gong, J.J. Hoelzemann, A. Ito, L. Marelli, J.E. Penner, J.-P. Putaud, C. Textor, M. Schulz, G.R. van der Werf, and J. Wilson, 2006: Emissions of primary aerosol and precursor gases in the years 2000 and 1750 prescribed data-sets for AeroCom, *Atmos. Chem. Phys.,* **6***,* 4321-4344.

Diner D., et al., 2004: PARAGON: An integrated approach for characterizing aerosol climate impacts and environmental interactions. *Bull. Amer. Meteo. Soc.,* **85(10)**:1491-1501.

Fernandes, S.D., N.M. Trautmann, D.G. Streets, C.A. Roden, and T.C. Bond, Global biofuel use, 1850-2000, 2007: *Global Biogeochem. Cycles*, **21**, GB2019, doi:10.1029/2006GB002836.

Ghan S. J., and S.E. Schwartz, 2007: Aerosol Properties and Processes: A Path from Field and Laboratory Measurements to Global Climate Models. Bull. *Amer. Meteorol. Soc*. **88**, 1059–1083.

Guenther, A.,T. Karl, P. Harley, C. Wiedinmyer, P.I. Palmer, and C. Geron, 2006: Estimates of global terrestrial isoprene emissions using MEGAN (Model of Emissions of Gases and Aerosols from Nature), *Atmos. Chem. Phys.,* **6**, 3181-3210.

Gunn, R., and B. Phillips, 1957: An experimental investigation of the effect of air pollution on the initiation of rain. *J. Meteor.* **14**:272-280.

Hansen J., M. Sato, and R. Ruedy, 1997: Radiative forcing and climate response. *J. Geophys. Res.* **102**:6831-6864.

IPCC, 1992: *Climate Change 1992: The Supplementary Report to the IPCC Scientific Assessment.* J. T. Houghton, B. A. Callander and S. K. Varney (eds). Cambridge University Press, Cambridge, UK, 198 pp.

IPCC (Intergovernmental Panel on Climate Change), 1995: Radiative forcing of climate change and an evaluation of the IPCC IS92 emission scenarios, in Climate Change 1994, Cambridge Univ. Press, New York, Cambridge University Press.

IPCC (Intergovernmental Panel on Climate Change), 1996**:** Radiative forcing of climate change, in Climate Change 1995, Cambridge Univ. Press, New York, Cambridge University Press.

IPCC (Intergovernmental Panel on Climate Change), 2001: Radiative forcing of climate change, in Climate Change 2001, Cambridge Univ. Press, New York, Cambridge University Press.

Ito, A., and J.E. Penner, 2005: Historical estimates of carbonaceous aerosols from biomass and fossil fuel burning for the period 1870-2000, *Global Biogeochem. Cycles*, *19*, GB2028, doi:10.1029/2004GB002374.

Junker, C., and C. Liousse, 2006: A global emission inventory of carbonaceous aerosol from historic records of fossil fuel and biofuel consumption for the period 1860-1997, *Atmos. Chem. Phys. Discuss.*, **6**, 4897-4927.

Kahn R., J. Ogren, T. Ackerman, et al., 2004: Aerosol data sources and their roles within PARAGON. *Bull. Amer. Meteor. Soc.* **85**:1511-1522.

Kaufman Y., D. Tanré, and O. Boucher, 2002: A satellite view of aerosols in the climate system. *Nature* **419**:doi:10.1038/nature01091.

Koren I., Y. Kaufman, L. Remer, and J. Martins, 2004: Measurement of the effect of Amazon smoke on inhibition of cloud formation. *Science* **303**:1342.

Langner, J. and H. Rodhe, 1991: A global three-dimensional model of the tropospheric sulfur cycle. *J. Atmos. Chem.*, **13**, 225-263.

Lewis, E. R. and Schwartz S. E., *Sea Salt Aerosol Production: Mechanisms, Methods, Measurements, and Models -- A Critical Review*. Geophysical Monograph Series Vol. 152, (American Geophysical Union, Washington, 2004), 413 pp. ISBN: 0-87590-417-3.

Liou, K. N. and S-C. Ou, 1989: The Role of Cloud Microphysical Processes in Climate: An Assessment From a One-Dimensional Perspective. J. Geophys. Res., **94**: 8599 – 8607.

Liousse, C., J.E. Penner, C. Chuang, J.J. Walton, H. Eddleman, and H. Cachier, 1996: A global three-dimensional model study of carbonaceous aerosols, *J. Geophys. Res.*, **101**, 19,411-19,432.

Mahowald, N., C. Luo, J. del Corral, and C.S. Zender, 2003: Interannual variability in atmospheric mineral aerosols from a 22-year model simulation and observational data, *J. Geophys. Res.*, **108**, 4352-4371.

McCormick, R., and J. Ludwig, 1967: Climate modification by atmospheric aerosols. *Science* **156(3780)**:1358-1359.

Mitchell, J. Jr., 1971: The effect of atmospheric aerosols on climate with special reference to temperature near the Earth's surface. *J. Appl. Meteorol.* **10**:703-714.

Mouillot, F., and C.B. Field, 2005: Fire history and the global carbon budget: A 1° × 1° fire history reconstruction for the 20th century, *Global Change Biol.*, **11**, 398-420.

Mouillot, F., A. Narasimha, Y. Balkanski, J.-F. Lamarque, and C.B. Field, 2006: Global carbon emissions from biomass burning in the 20th century, *Geophys. Res. Lett.*, **33**, L01801, doi:10.1029/2005GL024707.

NRC (National Research Council)**,** 2005: Radiative Forcing of Climate Change: Expanding the Concept and Addessing Uncertainties, National Academy Press, Washington D.C. (Available at http://www.nap.edu/openbook/0309095069/html).

NRC (National Research Council), 2001: Climate Change Sciences: An analysis of some key questions, 42pp., National Academy Press, Washington D.C..

Novakov, T., V. Ramanathan, J.E. Hansen, T.W. Kirchstetter, M. Sato, J.E. Sinton, and J.A. Sathaye, 2003: Large historical changes of fossil-fuel black carbon emissions, *Geophys. Res. Lett.*, **30**, 1324, doi:10.1029/2002GL016345.

Penner J., R. Dickinson, and C. O'Neill, 1992: Effects of aerosol from biomass burning on the global radiation budget. *Science* **256**:1432-1434.

Penner, J.E., H. Eddleman, and T. Novakov,, 1993: Towards the development of a global inventory for black carbon emissions, *Atmos. Environ.*, **27**, 1277-1295.

Rao, S., K. Riahi, K. Kupiainen, and Z. Klimont, 2005: Long-term scenarios for black and organic carbon emissions, *Env. Sc.*, **2**, 205-216.

Schulz M., C. Textor, S. Kinne, et al., 2006: Radiative forcing by aerosols as derived from the AeroCom present-day and pre-industrial simulations. *Atmos. Chem. Phys.*, **6**:5225-5246.

Stern, D.I., 2005: Global sulfur emissions from 1850 to 2000, *Chemosphere*, **58**, 163-175.

Streets, D.G., T.C. Bond, G.R. Carmichael, S.D. Fernandes, Q. Fu, D. He, Z. Klimont, S.M. Nelson, N.Y. Tsai, M.Q. Wang, J.-H. Woo, and K.F. Yarber, 2003: An Inventory of Gaseous and Primary Aerosol Emissions in Asia in the Year 2000, Journal of Geophysical Research, **108**(D21), 8809, doi:10.1029/2002JD003093.

Turco, R.P., O.B. Toon, R.C. Whitten, J.B. Pollack, and P. Hamill, 1983: The global cycle of particulate elemental carbon: a theoretical assessment, in *Precipitation Scavenging, Dry Deposition, and Resuspension*, ed. H.R. Pruppacher et al., pp. 1337-1351, Elsevier Science, New York.

Twomey S., 1977: The influence of pollution on the shortwave albedo of clouds. *J. Atmos. Sci.* **34**:1149-1152.

van Aardenne, J.A., F.J. Dentener, J.G.J. Olivier, C.G.M. Klein Goldewijk, and J. Lelieveld, 2001: A 1° × 1° resolution data set of historical anthropogenic trace gas emissions for the period 1890-1990, *Global Biogeochem. Cycles*, **15**, 909-928.

van der Werf, G.R., J.T. Randerson, G.J. Collatz, and L. Giglio, 2003: Carbon emissions from fires in tropical and subtropical ecosystems, *Global Change Biol.*, **9**, 547-562.

van der Werf, G. R., J.T. Randerson, L. Giglio, G.J. Collatz, P.S. Kasibhatla, and A.F. Arellano Jr. 2006, Interannual variability in global biomass burning emissions from 1997 to 2004. *Atmos. Chem. Phys.,* **6**, 3424-3441.

Yu H., Y. Kaufman, M. Chin, G. Feingold, L. Remer, T. Anderson, Y. Balkanski, N. Bellouin, O. Boucher, S. Christopher, P. DeCola, R. Kahn, D. Koch, N. Loeb, M. S. Reddy, M. Schulz, T. Takemura, and M. Zhou, 2006: A review of measurement-based assessments of aerosol direct radiative effect and forcing. *Atmos. Chem . Phys.* **6**:613-666.

Chapter II. In-Situ and Remote Sensing Measurements of Aerosol Properties, Burdens, and Radiative Forcing

Authors: H. Yu, NASA GSFC/UMBC; **P. Quinn**, NOAA PMEL; **M. Chin**, NASA GSFC; **L. Remer**, NASA GSFC; **G. Feingold**, NOAA ESRL.

Table of Contents

2.1. Introduction

Over the past decade and since the IPCC TAR in particular, a great deal of effort has gone into improving measurement data sets (as summarized in Yu et al., 2006; Bates et al., 2006; Kahn et al., 2004a), including

- Execution of intensive field experiments examining aerosol processes and properties in various aerosol regimes around the globe;
- Establishment and enhancement of ground-based networks measuring aerosol properties and radiative effects;
- Development and deployment of new and enhanced instrumentation, importantly aerosol mass spectrometers examining size dependent composition, and;
- Development and implementation of new and enhanced satellite-borne sensors examining aerosol effects on atmospheric radiation.

These dedicated efforts make it feasible to shift the estimates of aerosol radiative effect and climate forcing from largely model-based as in IPCC TAR to increasingly measurement-based as in the IPCC Fourth Assessment Report (AR4) (IPCC 2007). Satellite measurements that are evaluated, supplemented, and constrained by ground-based remote sensing measurements and in-situ measurements from intensive field campaigns, provide the basis for the regional- to global-scale assessments. Chemical transport models (CTMs) are used to interpolate and supplement the data in regions/conditions where observational data are not available or to assimilate data from various observations for constraining and thereby improving model simulations of aerosol impacts. These developments have played an important role in advancing the scientific understanding of aerosol direct and indirect forcing as documented in the IPCC AR4 (Forster et al., 2007).

In this chapter we review the capabilities of aerosol measurements developed over the past decade, describe the synergies between different measurements and models, and discuss outstanding issues.

2.2. Overview of Aerosol Measurement Capabilities

2.2.1. *Intensive Field Campaigns*

Over the past two decades, more than a dozen intensive field experiments have been conducted to study the physical, chemical, and optical properties and radiative effects of aerosols in a variety of aerosol regimes around the world, as listed in **Table 2.1.** These experiments have been designed with aerosol characterization as the main goal or as one of the major themes in more interdisciplinary studies.

Several of these experiments have been designed to characterize regional aerosol properties in marine environments downwind of known continental aerosol source regions, including:

- The first Aerosol Characterization Experiment (ACE 1) which took place in the Southern Ocean environment south of Australia to characterize background, clean marine aerosol upon which anthropogenic forcings could be imposed (Bates et al., 1998)

Table 2.1: List of major intensive field experiments that are relevant to aerosol research in a variety of aerosol regimes around the globe conducted in the past two decades (adapted from Yu et al., 2006).

Aerosol Regimes	Intensive Field Experiments			Major References
	Name	Location	Time	
Industrial Pollution from North America and West Europe	TARFOX	North Atlantic	July, 1996	Russell et al., 1999
	NEAQS	North Atlantic	July – August, 2002	Quinn and Bates, 2003
	SCAR-A	North America	1993	Remer et al., 1997
	CLAMS	East Coast of U.S.	July-August, 2001	Smith et al., 2005
	INTEX-NA, ICARTT	North America	Summer 2004	Fehsenfeld et al., 2006
	ACE-2	North Atlantic	June – July, 1997	Raes et al., 2000
	MINOS	Mediterranean region	July - August, 2001	Lelieveld et al., 2002
	LACE98	Lindberg, Germany	July-August, 1998	Ansmann et al., 2002
	Aerosols99	Atlantic	January - February, 1999	Bates et al., 2001
Brown Haze in South Asia	INDOEX	Indian subcontinent and Indian Ocean	January - April, 1998 and 1999	Ramanathan et al., 2001b
	ABC	South and East Asia	ongoing	Ramanathan and Crutzen, 2003
Pollution and dust mixture in East Asia	EAST-AIRE	China	March-April, 2005	Li et al., 2007
	ACE-Asia	East Asia and Northwest Pacific	April, 2001	Huebert et al., 2003; Seinfeld et al., 2004
	TRACE-P		March - April, 2001	Jacob et al., 2003
	PEM-West A & B	Western Pacific off East Asia	September-October, 1991 February-March, 1994	Hoell et al., 1996; 1997
Biomass burning smoke in the tropics	BASE-A	Brazil	1989	Kaufman et al., 1992
	SCAR-B	Brazil	August - September, 1995	Kaufman et al., 1998
	LBA-SMOCC	Amazon basin	September-November 2002	Andreae et al., 2004
	SAFARI2000	South Africa and South Atlantic	August - September, 2000	King et al., 2003a
	SAFARI92		September – October, 1992	Lindesay et al., 1996
	TRACE-A	South Atlantic	September-October, 1992	Fishman et al., 1996
Mineral dusts from North Africa and Arabian Peninsula	SHADE	West coast of North Africa	September, 2000	Tanré et al., 2003
	PRIDE	Puerto Rico	June – July, 2000	Reid et al., 2003
	UAE[2]	Arabian Peninsula	August - September, 2004	Reid et al., 2008
Remote Oceanic Aerosol	ACE-1	Southern Oceans	December, 1995	Bates et al., 1998; Quinn and Coffman, 1998

Table 2.2: Summary of major surface networks for the tropospheric aerosol characterization and climate forcing research.

Surface Network	Measured/derived parameters				Spatial coverage	Temporal coverage
	Loading	Size, shape	Absorption	Chemistry		
NASA AERONET	optical depth	fine-mode fraction, Angstrom exponents, asymmetry factor, phase function, non-spherical fraction	single-scattering albedo, absorption optical depth, refractive indices	N/A	~200 sites over global land and islands	1993 onward
DOE ARM					6 sites and 4 mobile facilities in North America, Europe, and Asia	1989 onward
NOAA GMD	near-surface extinction coefficient, optical depth, CN/CCN number concentrations	Angstrom exponent, upscatter fraction, asymmetry factor, hygroscopic growth	single-scattering albedo, absorption coefficient	chemical composition in selected sites and periods	4 baseline stations, several regional stations, aircraft and mobile platforms	1976 onward
AERONET-MAN	optical depth	N/A	N/A	N/A	global ocean	2004-present (periodically)
NASA MPL	vertical distributions of backscatter/extinction coefficient, optical depth	N/A	N/A	N/A	~30 sites in major continents, usually collocated with AERONET and ARM sites and major field experiments	2000 onward
IMPROVE	near-surface mass concentrations and extinction coefficients by species	fine and coarse separately	single-scattering albedo, absorption coefficient	ions, ammonium sulfate, ammonium nitrate, organics, elemental carbon, fine soil	156 national parks and wilderness areas in the U.S.	1988 onward

- The second Aerosol Characterization Experiment (ACE 2) which took place in the subtropical northeast Atlantic Ocean and focused on the European aerosol plume (Raes et al., 2000).
- The Indian Ocean Experiment (INDOEX) which characterized the plumes emanating from the Indian subcontinent and nearby regions as they were transported out over the Indian Ocean (Ramanathan et al., 2001).
- The Asia Aerosol Characterization Experiment (ACE-Asia) which focused on the plume downwind of Asia (Huebert et al., 2003) as did the Transport and Chemical Evolution over the Pacific (TRACE-P) experiment (Jacob et al., 2003).
- The International Consortium for Atmospheric Research on Transport and Transformation (ICARTT) experiment, Tropospheric Aerosol Radiative Forcing Observational Experiment (TARFOX) and several other experiments that focused on the eastern U.S. plume (Fehsenfeld et al., 2006; Russell et al., 1999; Quinn and Bates, 2003).
- The South African Regional Science Initiative (SAFARI) experiment which investigated how the biomass burning smoke from South Africa influences atmospheric chemistry, the radiation budget, and climate (King et al., 2003).
- The SaHAran Dust Experiment (SHADE), Puerto Rico Dust Experiment (PRIDE), and the United Arab Emirates Unified Aerosol Experiment (UAE2) which focused on dust plumes from North Africa and the Arabian Peninsula (Tanré et al., 2003; Reid et al., 2003).

- The DOE Aerosol Intensive Operating Period (AIOP) field studies under the Atmospheric Radiation Measurement (ARM) program that targeted at characterizing aerosol optical properties and radiative influence (Ferrare et al., 2006).
- Field studies that examine aerosol formation and near source evolution in urban regions (Solomon et al., 2003; Zhang et al., 2004; Salcedo et al., 2006).

During each of these comprehensive experiments, aerosols were studied in great detail, using combinations of in-situ and remote sensing observations of physical and chemical properties from various platforms (e.g., aircraft, ship, satellite, and ground-based networks) and numerical modeling. In spite of their relatively short duration, these field experiments have acquired comprehensive data sets of regional aerosol properties that can be compared and compiled to understand the complex interactions of aerosols within the earth and atmosphere system.

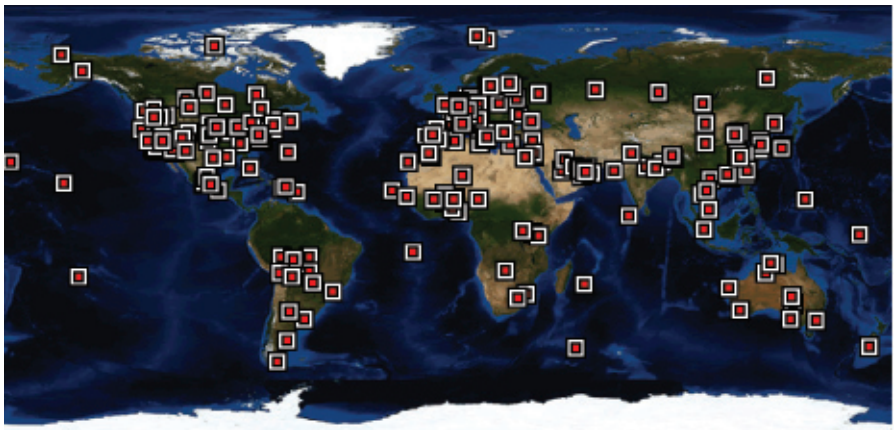

Figure 2.1: Geographical coverage of active AERONET sites in 2006.

2.2.2. *Ground-based Remote Sensing and In-Situ Measurement Networks*

Major surface networks for the tropospheric aerosol characterization and climate forcing research are listed in **Table 2.2**.

2.2.2.1. *Ground-based remote sensing.*

The Aerosol Robotic Network (*AERONET*) program is a federated ground-based remote sensing network of well-calibrated sun photometers and radiometers (http://aeronet.gsfc.nasa.gov). AERONET includes about 200 sites around the world, covering all major tropospheric aerosol regimes (Holben et al., 1998; 2001), as illustrated in **Figure 2.1**. Spectral measurements of sun and sky radiance are calibrated and screened for cloud-free conditions (Smirnov et al., 2000). AERONET stations provide:

- direct, calibrated measurements of spectral aerosol optical depth (AOD or τ) (normally at wavelengths of 440, 670, 870, and 1020 nm) with an accuracy of ±0.015 (Eck et al. 1999), and
- inversion-based retrievals of a variety of effective, column-mean properties, including aerosol single-scattering albedo (*SSA or* ω_0), size distributions, fine-mode fraction, the degree of nonsphericity, phase function, and asymmetry factor (Dubovik et al., 2000; Dubovik and King, 2001; Dubovik et al., 2002; O'Neill, et al., 2004). These retrieved parameters are systematically validated by comparison to emerging in-situ measurements with improved accuracy (e.g., Haywood et al., 2003; Magi et al., 2005; Leahy et al., 2007).

Recent developments associated with AERONET algorithms and data products include:

- simultaneous retrieval of aerosol and surface properties using combined AERONET and satellite measurements (Sinyuk et al., 2007);
- the addition of ocean color and high frequency solar flux measurements;
- the establishment of the Maritime Aerosol Network (MAN) component to monitor aerosols over the World oceans (Smirnov et al., 2006); and
- the extension of observations of cloud optical properties and cloud cover (Marshak et al., 2004; Kaufman and Koren, 2006).

Because of consistent calibration, cloud-screening, and retrieval methods, uniform data are available for all stations, some of which have operated for over 10 years. These data constitute a high-quality, ground-based aerosol climatology and, as such, have been widely used for aerosol process studies as well as for evaluation and validation of model simulation and satellite remote sensing applications (e.g., Chin et al., 2002; Yu et al., 2003, 2006; Remer et al., 2005; Kahn et al., 2005a). In addition, AERONET retrievals of aerosol size distribution and refractive indices have been used in algorithm development for satellite sensors (Remer et al., 2005; Levy et al., 2007a).

AERONET measurements have been complemented by other ground-based aerosol networks with less geographical or temporal coverage, such as the Atmospheric Radiation Measurement (ARM) network (Ackerman and Stokes, 2003) and other networks with multifilter rotating shadowband radiometer (*MFRSR*) (Harrison et al., 1994; Michalsky et al., 2001), the NOAA Global Monitoring Division (*GMD*) network (e.g., Delene and Ogren, 2002; Sheridan and Ogren, 1999), the Interagency Monitoring of Protected Visual Environment (*IMPROVE*) (Malm et al., 1994), and several lidar networks including

- NASA Micro Pulse Lidar Network (MPLNET) (Welton et al., 2001; 2002);
- Regional East Atmospheric Lidar Mesonet (REALM) in North America (Hoff et al., 2002; 2004);
- European Aerosol Research Lidar Network (EARLINET) (Matthias et al., 2004); and
- Asian Dust Network (AD-Net) (e.g., Murayama et al., 2001).
- The aerosol extinction profiles derived from these lidar networks with state-of-the-art techniques (Schmid et al., 2006) are pivotal to a better assessment of aerosol climate forcing and atmospheric responses.

2.2.2.2. *In-situ measurement networks*.

Long-term in-situ measurements of aerosol optical properties and chemical composition have been made in several of the regions where recent intensive field campaigns have been conducted. These measurements are part of the NOAA GMD aerosol monitoring program (Delene and Ogren, 2002; Sheridan and Ogren, 1999; Quinn et al., 2000). The measurement protocols are similar to those used during the intensive campaigns and the measurement periods often encompass the intensive campaign time periods. Hence, they provide a longer-term measure of the means and variability of aerosol properties and context for the shorter duration measurements of the intensive field campaigns.

2.2.3. *Satellite Remote Sensing*

A measurement-based characterization of aerosols on a global scale can only be realized through satellite remote sensing, due to the large spatial and temporal heterogeneities of aerosol distributions. Monitoring aerosols from space has been performed for over two decades and is planned for the coming decade with enhanced capabilities (King et al., 1999; Foster et al., 2007; Lee et al., 2006; Mishchenko et al., 2007a). **Table 2.3** summarizes major satellite measurements currently available for the tropospheric aerosol characterization and climate forcing research.

Early aerosol monitoring from space relied on sensors that were designed for other purposes. The Advanced Very High Resolution Radiometer (*AVHRR*), intended as a weather satellite, provides radiance observations in the visible and near infrared wavelengths that are sensitive to aerosol properties over the ocean (Husar et al., 1997; Mishchenko et al., 1999). Originally intended for ozone monitoring, the ultraviolet channels used for the Total Ozone Mapping Spectrometer (*TOMS*) are sensitive to aerosol absorption with little surface interferences, even over land (Torres et al., 1998). TOMS has proved to be extremely successful in monitoring biomass burning smoke and dust (Herman et al., 1997) and retrieving aerosol single-scattering albedo from space (Torres et al., 2005). A new sensor, the Ozone Monitoring Instrument (*OMI*) aboard Aura, has improved on such advantages. Such historical sensors have provided multi-decadal climatology of aerosol optical depth that has significantly advanced the understanding of aerosol distributions and long-term variability (e.g., Geogdzhayev et al., 2002; Torres et al., 2002; Massie et al., 2004; Mishchenko et al., 2007b).

Over the past decade, satellite aerosol retrievals have become increasingly sophisticated. Now, satellites measure the angular dependence of polarization and radiance in multiple wavelengths in the ultraviolet (UV) through the infrared (IR) at fine temporal and spatial resolution. From these observations, retrieved aerosol products include not only optical depth at one wavelength, but spectral optical depth and particle size over both ocean and land, as well as more direct measurements of polarization and phase function. In addition, cloud screening is much more robust than before and onboard calibration is now widely available. Examples of such new and enhanced sensors include MODerate resolution Imaging Spectroradiometer (*MODIS*, see **Box 2.1**), Multi-angle Imaging SpectroRadiometer (*MISR*, see **Box 2.2**), Polarization and Directionality of the Earth's Reflectance (*POLDER*), OMI, among others. The Clouds and the Earth's Energy System (*CERES*, see **Box 2.3**) measures broadband solar and terrestrial radiances. These radiation measurements in combination with satellite retrievals of aerosol can be used to deduce observational-based aerosol direct effect and forcing.

Complementary to these passive sensors, active remote sensing from space is also making promising progress (see **Box 2.4**). Both the Geoscience Laser Altimeter System (*GLAS*) and the Cloud and Aerosol Lidar with Orthogonal Polarization (*CALIOP*) are collecting essential information about aerosol vertical distributions. Furthermore, the constellation of six afternoon-overpass spacecrafts (as illustrated in **Figure 2.2**), so-called *A-Train* (Stephens et al., 2002) makes it possible for the first time to conduct near simultaneous (within 15-minutes) measurements of aerosols, clouds, and radiative fluxes in multiple dimensions with sensors with complementary capabilities.

Table 2.3: Summary of major satellite measurements currently available for the tropospheric aerosol characterization and climate forcing research.

Category	Properties	Sensor/platform	Parameters	Spatial coverage	Temporal coverage
Column-integrated	Loading	AVHRR/NOAA-series	optical depth	global ocean	1981-present
		TOMS/Nimbus, ADEOS1, EP		global land+ocean	1979-2001
		POLDER-1, -2, PARASOL			1997-present
		MODIS/Terra, Aqua			2000-present (Terra) 2002-present (Aqua)
		MISR/Terra			2000-present
		OMI/Aura			2005-present
	Size, shape	AVHRR/NOAA-series	Angstrom exponent	global ocean	1981-present
		POLDER-1, -2, PARASOL	fine-mode fraction, Angstrom exponent, non-spherical fraction	global land+ocean	1997-present
		MODIS/Terra, Aqua	fine-mode fraction	global land+ocean (better quality over ocean)	2000-present (Terra) 2002-present (Aqua)
			Angstrom exponent		
			Effective radius	global ocean	
			Asymmetry factor		
		MISR/Terra	Angstrom exponent Non-spherical fraction	global land+ocean	2000-present
	Absorption	TOMS/Nimbus, ADEOS1, EP	Absorbing aerosol index, single-scattering albedo, absorbing optical depth	global land+ocean	1979-2001
		OMI/Aura			2005-present
		MISR/Terra	Single-scattering albedo		2000-present
Vertical-resolved	Loading, size, and shape	GLAS/ICESat	Extinction/backscatter	global land+ocean, 16-day repeating cycle, single-nadir measurement	2003-present (~3months/year)
		CALIOP/CALIPSO	Extinction/backscatter, color ratio, depolarization ratio		2006-present

Box 2.1: MODerate resolution Imaging Spectroradiometer

MODIS performs near global daily observations of atmospheric aerosols. Seven of 36 channels (between 0.47 and 2.13 μm) are used to retrieve aerosol properties over cloud and surface-screened areas (Martins et al., 2002; Li et al., 2004). Over vegetated land, MODIS retrieves aerosol optical depth at three visible channels with high accuracy of ±0.05±0.2τ (Kaufman et al., 1997; Chu et al., 2002; Remer et al., 2005; Levy et al., 2007b). Most recently a deep-blue algorithm (Hsu et al., 2004) has been implemented to retrieve aerosols over bright deserts on an operational basis. Because of the greater simplicity of the ocean surface, MODIS has the unique capability of retrieving not only aerosol optical depth with greater accuracy, i.e., ±0.03±0.05τ (Tanré et al., 1997; Remer et al., 2002; 2005), but also quantitative aerosol size parameters (e.g., effective radius, fine-mode fraction of AOD) (Kaufman et al., 2002a; Remer et al., 2005; Kleidman et al., 2005). The fine-mode fraction has been used as a tool for separating anthropogenic aerosol from natural ones and estimating the anthropogenic aerosol direct climate forcing (Kaufman et al., 2005a,b). **Figure 2.3** shows composites of MODIS AOD and fine-mode fraction that illustrate seasonal and geographical variations of aerosol types. Clearly seen from the figure is heavy pollution over East Asia in both months, biomass burning smoke over South Africa, South America, and Southeast Asia in September, heavy dust storms over North Africa and North Atlantic in both months and over northern China in March, and a mixture of dust and pollution plume swept across North Pacific in March.

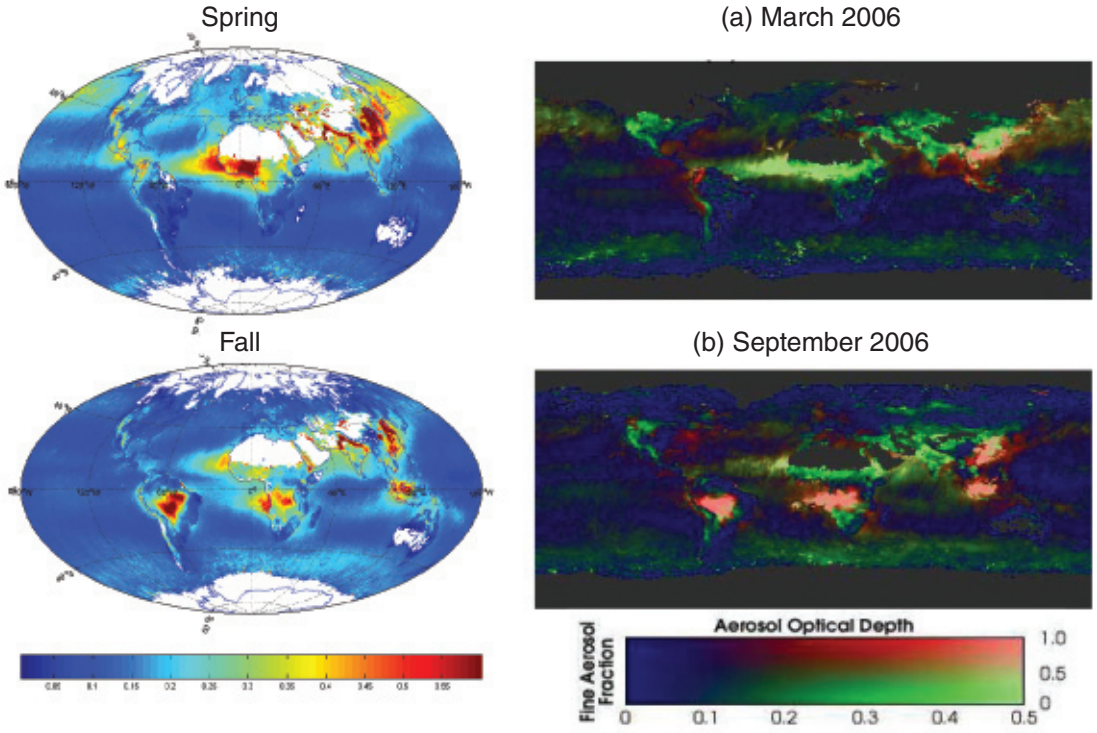

Figure 2.3: Left panel: 7-year climatology of aerosol optical depth at 550 nm. Right panel: A composite of MODIS observed aerosol optical depth (at 550 nm) and fine-mode fraction that shows spatial and seasonal variations of aerosol types. Industrial pollution and biomass burning aerosols are predominated by small particles (shown as red), while mineral dust consists of a large fraction of large particles (shown as green). Bright red and bright green indicate heavy pollution and dust plumes, respectively. The plots are generated from MODIS/Terra Collection 5 data.

Box 2.2: Multi-angle Imaging SpectroRadiometer

MISR, aboard the sun-synchronous polar orbiting satellite Terra, measures upwelling solar radiance in four visible spectral bands and at nine view angles spread out in the forward and aft directions along the flight path (Diner et al., 2002). It acquires global coverage about once per week. A wide range of along-track view angles makes it feasible to more accurately evaluate the surface contribution to the TOA radiances and hence retrieve aerosols over both ocean and land surfaces, including bright desert and sunglint regions (Diner et al., 1998; Martonchik et al., 1998a; 2002; Kahn et al., 2005a). MISR AODs are within 20% or ±0.05 of coincident AERONET measurements (Kahn et al., 2005a; Abdou et al., 2005). The MISR multi-angle data also sample scattering angles ranging from about 60˚ to 160˚ in midlatitudes, yielding information about particle size (Kahn et al., 1998; 2001; 2005a) and shape (Kalashnikova et al., 2005). These quantities are of interest in–and-of themselves for identifying aerosol airmass types, and should also help further refine aerosol retrieval algorithms. MISR also retrieves altitudes of aerosol plumes (biomass burning smoke, volcanic effluent, and mineral dust) where the plumes have discernable spatial contrast (Kahn et al., 2007). **Figure 2.4** is an example that illustrates MISR's capability of characterizing the load, optical properties, and stereo height of near-source fire plumes.

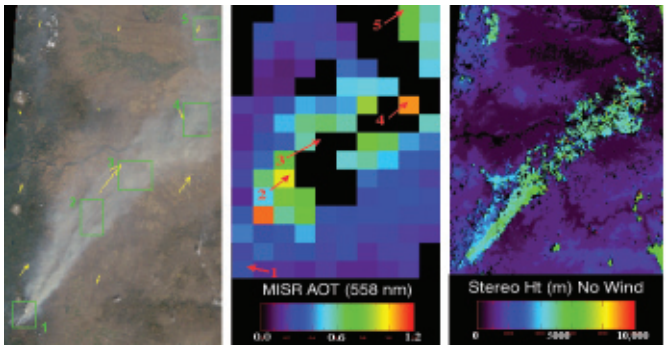

Figure 2.4: Oregon fire on September 4, 2003 as observed by MISR: (a) MISR nadir view of the fire plume, with five patch locations numbered and wind-vectors superposed in yellow; (b) MISR aerosol optical depth at 558 nm; and (c) MISR stereo height without wind correction for the same region (taken from Kahn et al., 2007).

Box 2.3: Clouds and the Earth's Radiant Energy System

CERES measures broadband solar and terrestrial radiances at three channels with a large footprint (e.g., 20 km for CERES/Terra) (Wielicki et al., 1996). It is collocated with MODIS and MISR aboard Terra and with MODIS on Aqua. The observed radiances are converted to the TOA irradiances or fluxes using the Angular Distribution Models (*ADMs*) as a function of viewing angle, sun angle, and scene type (Loeb and Kato, 2002; Zhang et al., 2005a). Such estimates of TOA solar flux in clear-sky conditions can be compared to the expected flux for an aerosol-free atmosphere, in conjunction with measurements of aerosol optical depth from other sensors (e.g., MODIS, and MISR) to derive the aerosol direct effect and climate forcing (Loeb and Manalo-Smith, 2005; Zhang and Christopher, 2003; Zhang et al., 2005b; Christopher et al., 2006). The derived instantaneous value is then scaled to obtain a daily average. A direct use of the coarse spatial resolution CERES measurements would exclude aerosol distributions in partly cloudy CERES scenes. Several approaches that incorporate coincident, high spatial and spectral resolution measurements (e.g., MODIS) have been employed to overcome this limitation (Loeb and Manalo-Smith, 2005; Zhang et al., 2005b).

Box 2.4: Active Remote Sensing of Aerosols

Following a demonstration aboard the U.S. Space Shuttle mission in 1994, the Geoscience Laser Altimeter System (GLAS) was launched in early 2003 to become the first polar orbiting satellite lidar. It provides global aerosol and cloud profiling for a one-month period out of every three-to-six months. It has been demonstrated that GLAS is capable of detecting and discriminating multiple layer clouds, atmospheric boundary layer aerosols, and elevated aerosol layers (e.g., Spinhirne et al., 2005). The Cloud-Aerosol Lidar and Infrared Pathfinder Satellite Observations (CALIPSO), launched on April 28, 2006, is carrying a lidar instrument (Cloud and Aerosol Lidar with Orthogonal Polarization - CALIOP) that has been collecting profiles of the attenuated backscatter at visible and near-infrared wavelengths along with polarized backscatter in the visible channel (Winker et al., 2003). Flying in formation with the Aqua, AURA, POLDER, and CloudSat satellites, this vertically resolved information is expected to greatly improve passive aerosol and cloud retrievals as well as allow the development of new retrieval products (see Kaufman et al., 2003; Léon et al., 2003).

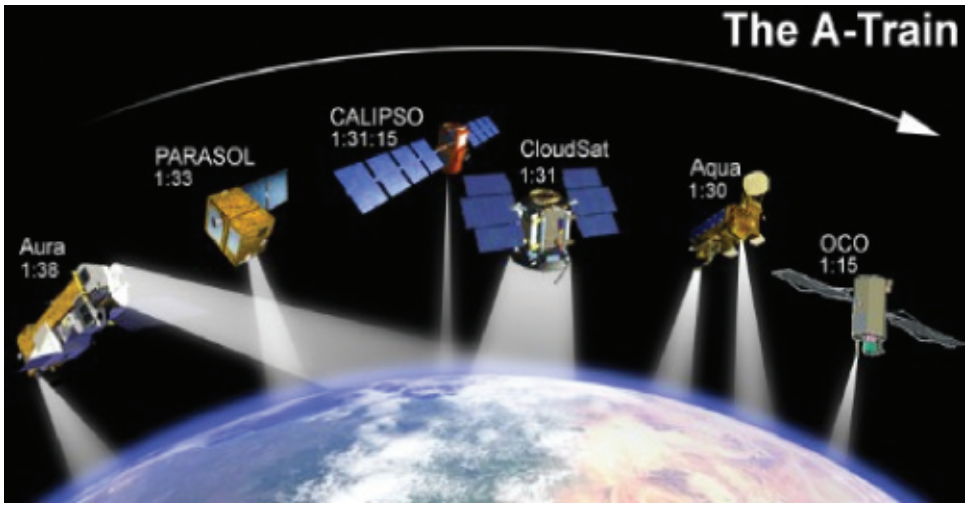

Figure 2.2: A constellation of six spacecrafts with afternoon overpass, so-called A-Train, will provide an unprecedented opportunity of studying aerosols and clouds from the space in multiple dimensions with sensors with complimentary capabilities. The formation of A-Train is expected to complete when OCO is launched in 2008.

The high accuracy of aerosol products (mainly aerosol optical depth) from these new-generation sensors, together with improvements in characterizing the earth's surface and clouds, can help reduce the uncertainties associated with the aerosol direct radiative effect (Yu et al., 2006; and references therein). The retrieved aerosol size parameters can help distinguish anthropogenic aerosols from natural aerosols and hence help assess the anthropogenic aerosol radiative forcing (Kaufman et al., 2005a, b; Bellouin et al., 2005; Christopher et al., 2006; Yu et al., 2006).

Finally, algorithms are being developed to retrieve aerosol absorption or single-scattering albedo from satellite observations (e.g., Kaufman et al., 2002b; Torres et al., 2005). The NASA Glory mission, scheduled to launch in 2008 and to be added to the A-Train, will deploy a multi-angle, multi-spectral polarimeter to determine the global distribution of aerosol and clouds. It will also be able to infer microphysical properties, and chemical composition by source type (e.g., marine, dust, pollution, etc.) of aerosols with accuracy and coverage sufficient for improving quantification of the aerosol direct and indirect effects on climate (Mishchenko et al., 2007b).

2.2.4. *Synergy of Measurements and Model Simulations*

As discussed earlier, aerosols and their climate forcing have been observationally studied through the establishment and enhancement of ground-based networks, the development and implementation of new and enhanced satellite sensors, and the execution of intensive field experiments. However, none of these approaches alone is adequate to characterize large spatial and temporal variations of aerosol physical and chemical properties and to address complex aerosol-climate interactions. Individual approaches have their own strengths and limitations, and are usually complementary. For example, while ground-based networks and intensive field experiments provide the most accurate information about aerosol properties that is required for evaluating and constraining satellite retrievals and model simulations, they are lacking in spatial and/or temporal coverage. Satellite remote sensing can augment the ground networks and field experiments by expanding the temporal and spatial coverage, but can only offer limited retrievable parameters (as determined by sensor's wavelength channels, viewing angles, and polarization capability) and usually only under cloud free conditions. Therefore, the best strategy for characterizing aerosols is to integrate measurements from different satellite sensors with complementary capabilities from sub-orbital measurements.

Models are versatile, although imperfect tools for studying aerosols in both clear and cloudy conditions and providing information on chemical composition that can not be directly observed from satellites. Model simulation is also an indispensable tool for estimating past aerosol forcing and projecting future climate due to changes in atmospheric aerosols. On the other hand, model simulations have large uncertainties because of the difficulties in realistically representing the aerosol life cycle. Along with improving representation of various processes within models, observations are essential for constraining model simulations of aerosol climate impacts through data synthesis.

In the following, we discuss several synergistic approaches to studying aerosols and their climate forcing, including closure studies involving multiple independent data sets, constraint of model aerosol optical properties with in-situ measurements, and integration of satellite observations into models.

Closure Studies: During intensive field experiments, multiple platforms and instruments are deployed to sample the same air mass through a well-coordinated experimental design. Often, several different independent methods are used to measure or derive a single aerosol property or radiative effect. This combination of methods can be used to identify inconsistencies in the measurements and to quantify uncertainties in aerosol characterization and estimates of aerosol radiative effects. This approach, often referred to as a closure study, has been widely employed on both individual measurement platforms (local closure) and in studies involving vertical measurements through the atmospheric column by one or more platforms (column closure) (Quinn et al., 1996; Russell et al., 1997).

As summarized in Bates et al. (2006), aerosol closure studies reveal that the best agreement between measurements occurs for submicrometer, spherical aerosol particles. For submicrometer sulfate/carbonaceous aerosol, measurements of aerosol optical properties and optical depths agree within 10 to 15% and often better. Larger particle sizes present inlet collection efficiency difficulties and non-spherical particles (e.g., dust) lead to differences in instrumental response. Comparisons of optical depth for an aerosol dominated by dust reveal disagreements between methods of up to 35%. Closure studies on DRE reveal uncertainties of about 25% for sulfate/carbonaceous aerosol and 60% for dust. Future

closure studies are needed to integrate surface- and satellite-based radiometric measurements of AOD with in-situ optical, microphysical, and aircraft radiometric measurements. There is also a need to maintain consistency in comparing results and expressing uncertainties (Bates et al., 2006).

Constraining models with in-situ measurements: In-situ measurements of aerosol chemical, microphysical, and optical properties, with a known accuracy based, in part, on closure studies, can be used to constrain regional CTM simulations of aerosol DRE and DCF, as described by Bates et al. (2006). A key step in the approach is assigning empirically derived optical properties to the individual chemical components generated by the CTM for use in a Radiative Transfer Model (RTM). Specifically, regional data from focused, short-duration field programs can be segregated according to aerosol type (sea salt, dust, or sulfate/carbonaceous) based on measured chemical composition and particle size. Corresponding measured optical properties can be carried along in the sorting process so that they, too, are segregated by aerosol type. The so-derived intensive aerosol properties for individual aerosol types, including mass scattering efficiency, single-scattering albedo, and asymmetry factor, and their dependences on relative humidity, are used in place of *a priori* values in CTMs. Bates et al. (2006) show that such constraint leads to about a 30% increase in DRE and DCF estimates in a regional and a global CTM, compared to model calculations based on *a priori* optical properties. Data from short-term, focused experiments are limited in their ability to constrain model-simulated extensive properties of aerosols, such as concentration and AOD, as these properties are much more heterogeneous in space and time than the intensive properties. Long-term in-situ measurements as well as satellite observations are more suited for constraining extensive aerosol properties.

Integration of satellite measurements into model simulations: Global measurements of aerosols (mainly AOD) from satellites can also be used to improve the performance of aerosol model simulations and hence the assessment of the aerosol direct radiative effect through data assimilation or objective analysis process (e.g., Collins et al., 2001; Yu et al., 2003; 2004, 2006; Liu et al., 2005). Both satellite retrievals and model simulations have uncertainties. The goal of data integration is to minimize the discrepancies between them, and to form an optimal estimate of aerosol distributions by combining them with weights inversely proportional to the square of the errors of individual descriptions. Such integration can fill gaps in satellite retrievals and generate global distributions of aerosols that are consistent with ground-based measurements (Collins et al., 2001; Yu et al., 2003, 2006; Liu et al., 2005). Recent efforts have focused on retrieving global sources of aerosol from satellite observations using inverse modeling which may be potentially valuable for reducing large uncertainties of aerosol simulations (Dubovik et al., 2007).

2.3. Assessments of Aerosol Characterization and Climate Forcing

In this section we focus on the assessment of measurement-based aerosol characterization and its use in improving estimates of the direct radiative effect and climate forcing on regional and global scales. In-situ measurements provide highly accurate aerosol chemical, microphysical, and optical properties on a regional basis and for the particular time period of a given experiment. Remote sensing from satellites and ground-based networks provide spatial and temporal coverage that intensive field campaigns lack. Both in-situ measurements and remote sensing have been used to determine key parameters for estimating aerosol direct climate forcing including aerosol single scattering albedo, asymmetry factor, optical depth, and direct radiative effect. Remote sensing has also been providing simultaneous mea-

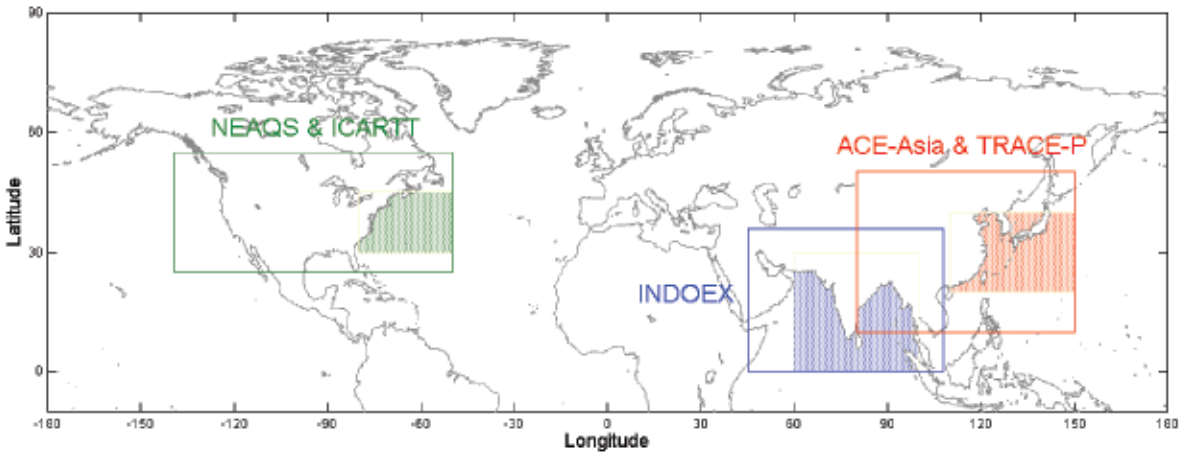

Figure 2.5. Locations of field campaigns that served as the source of data used to constrain model estimates of DRE and DCF in the Bates et al. (2006) study. Solid boxes show the regional CTM domains. Shaded areas show the regions use for the DRE and DCF calculations.

surements of aerosol and radiative fluxes that can be combined to derive aerosol direct radiative effect and climate forcing at the TOA with relaxed requirement for characterizing aerosol intensive properties. We also discuss progress in using both satellite and surface-based remote sensing measurements to study aerosol-cloud interactions and indirect effects.

2.3.1. The Use of Regional Aerosol Chemical and Optical Properties to Improve Model Estimates of DRE and DCF

The wide variety of aerosol data sets from intensive field campaigns provide a rigorous "test bed" for model simulations of aerosol distributions and estimates of DRE and DCF, as demonstrated in Bates et al. (2006). The approach taken by Bates et al. to constrain estimates of DRE and DCF is as follows. CTMs were used to calculate dry mass concentrations of the dominant aerosol species (sulfate, organic carbon, black carbon, sea salt, and dust). In-situ measurements were used to calculate the corresponding optical properties for each aerosol type for use in a radiative transfer model (RTM). Aerosol DRE and DCF estimated by using the empirically derived and a priori optical properties were then compared. In addition, in-situ and ground-based remote measurements were used to check or validate both the CTM and the RTM output.

Here we discuss the details of the aerosol chemical and optical properties in the three regions considered by Bates et al. (see **Figure 2.5**) and the use of these empirically-determined properties in improving model estimates of aerosol burdens, DRE, and DCF. These regions include:

- the Northern Indian Ocean (NIO) where INDOEX took place in 1999.
- the Northwestern Pacific Ocean (NPO) where ACE-Asia took place in 2001.
- the Northwestern Atlantic Ocean (NWA) where the New England Air Quality Study (NEAQS-2002) occurred in 2002 and ICARTT occurred in 2004.

The NIO, NPO, and NWA each have distinct aerosol properties due to differences in upwind sources. Variability in aerosol mass concentration and chemical composition for the three regions is shown

in **Figure 2.6** for the submicrometer (aerodynamic diameter between 0.1 and 1 μm) and supermicrometer (aerodynamic diameter between 1 and 10 μm) aerosol. The data in Figure 6 are based on measurements onboard the NOAA RV *Ronald H. Brown* using standardized sampling protocols which minimizes sampling biases and, hence, allows for a direct comparison of the data from all three experiments (Quinn and Bates, 2005).

Although the mean submicrometer aerosol mass concentrations were similar between the three regions (15 to 20 μg m^{-3}), the aerosol composition differed. INDOEX took place during the dry winter monsoon season, which is characterized by large-scale subsidence and northeasterly flow from the Indian subcontinent to the northern Indian Ocean. Submicrometer aerosol was dominated by sulfate and dust/fly ash with a significant contribution from BC. Emissions of BC from India result primarily from residential combustion (biofuel) with contributions from industry and transportation.

ACE-Asia took place during the spring when dust outbreaks over the Gobi desert are most frequent and intense. The submicrometer aerosol measured during ACE-Asia was primarily sulfate, POM, and dust while the supermicrometer aerosol was dominated by dust. The large supermicrometer mass concentrations measured during ACE-Asia indicate the large aerosol loadings that result from the springtime dust outbreaks.

Sub-micrometer aerosol mass concentrations measured during ICARTT were uniquely dominated by POM and sulfate. Based on modeling studies and statistical comparisons to gas phase volatile organic tracer compounds, the POM appears to be mainly of anthropogenic origin (de Gouw et al., 2005; Quinn et al., 2006).

Several factors contribute to the uncertainty of CTM calculations of size distributed aerosol composition including emissions, aerosol removal by wet deposition, chemical processes involved in the

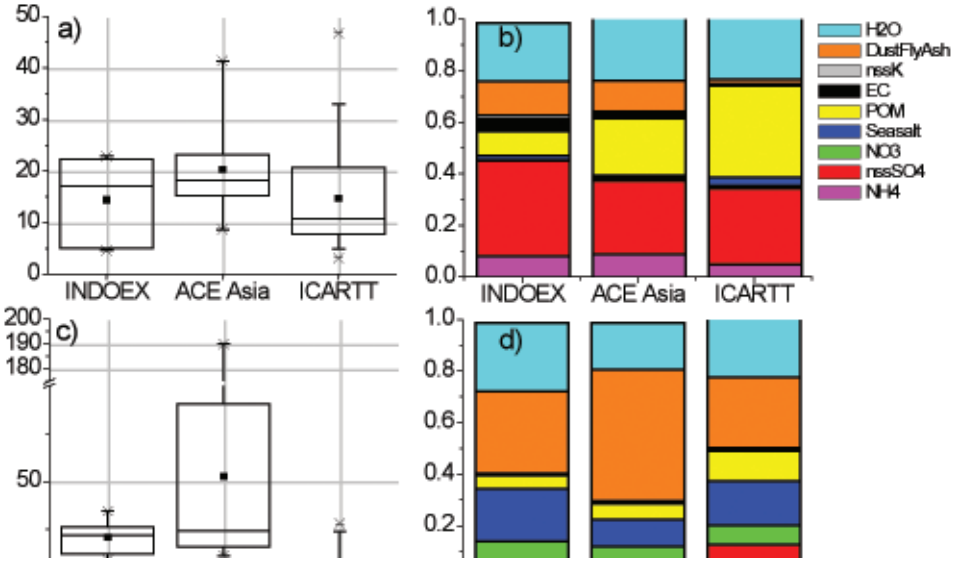

Figure 2.6: Submicrometer aerosol a) mass concentrations and b) mass fractions of the dominant chemical components measured during INDOEX, ACE-Asia, and ICARTT onboard Ronald H. Brown. Similarly, supermicrometer aerosol c) mass concentrations and d) mass fractions of the dominant chemical components measured during INDOEX, ACE-Asia, and ICARTT onboard Ronald H. Brown. Values are shown at the measurement RH of 55±5%.

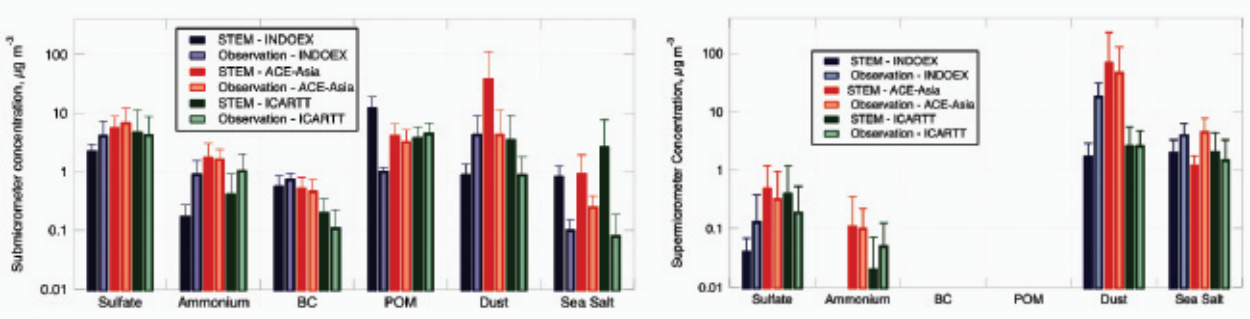

Figure 2.7: Comparison of the mean concentration (μg m^{-3}) and standard deviation of the modeled (STEM) aerosol chemical components with those observed on the RV Ronald H. Brown during INDOEX, ACE-Asia, and ICARTT. After Bates et al. (2006).

formation of secondary aerosols, vertical transport, and meteorological fields including the timing and amount of precipitation, formation of clouds, and relative humidity. In-situ measurements made during the intensive field campaigns described above provide a point of comparison for the CTM generated aerosol distributions at the surface and at discrete points above the surface. Such comparisons are useful for identifying areas where the models need improvement.

The submicrometer, supermicrometer, and sub-10 micrometer aerosol chemical components measured during INDOEX, ACE-Asia, and ICARTT are compared with those calculated with the Sulfate Transport and dEposition Model (*STEM*) (e.g., Carmichael et al., 2002, 2003; Tang et al., 2003, 2004; Bates et al., 2004; Streets et al., 2006a), as shown in **Figure 2.7**. To directly compare the measured (*RV Ronald H. Brown*) and modeled values, the model was sampled at the times and locations of the shipboard measurements every 30 min along the cruise track. The best agreement is found for submicrometer sulfate and BC. Large discrepancies between the modeled and measured values occur for submicrometer POM (INDOEX), dust (ACE-Asia), and sea salt (all regions). In the super-micrometer size range, large disagreements occur for dust (INDOEX) and sea salt (INDOEX and ACE-Asia). The total mass of the supermicrometer aerosol is underestimated by the model by about a factor of 3.

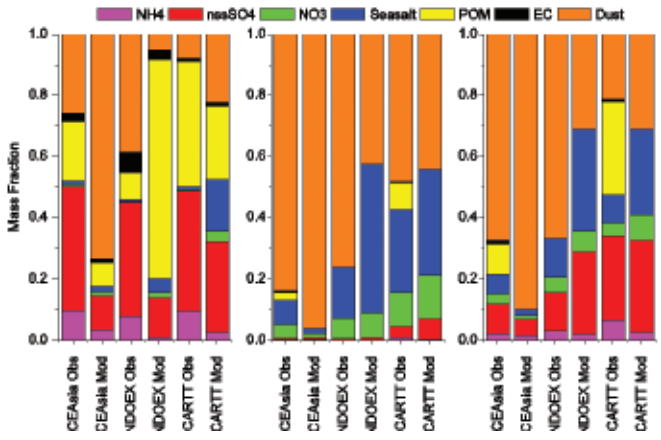

Figure 2.8. Mass fractions of the aerosol chemical components for INDOEX, ACE-Asia, and ICARTT based on shipboard measurements and STEM model calculations. Left panel is submicrometer aerosol, middle panel is supermicrometer aerosol, and right panel is sub-10 micrometer aerosol. After Bates et al. (2006).

A comparison of the modeled and measured mass fractions of the chemical components for the three size ranges is shown in **Figure 2.8**. The model is able to duplicate the measurements to the degree that the sub-micrometer aerosol is composed of a mixture of sulfate, POM, and BC and the supermicrometer aerosol is composed primarily of dust and sea salt. The relative amount of each component is not well-captured by the model for either size range, however. Discrepancies in the measured and modeled dust and sea salt concentrations and mass fractions reflect the large uncertainties in the emission models used for the components. Uncertainties in the column amounts of sea salt and dust are significant as both compo-

nents contribute substantially to AOD and DRE. In addition, both of these components can interact with gas and particle phase species thereby impacting concentrations and size distributions of anthropogenic aerosol components.

Further comparisons made by Bates et al. (2006) between STEM and aircraft-derived component concentrations revealed that 1) model results are better at altitudes less than 2 km due to the uncertainties in modeling vertical transport and removal processes; 2) dust and sea salt are underestimated, likely due to errors in model-calculated emissions and parameterizations of removal processes; and 3) the agreement is best for sulfate due to greater accuracy in emissions, chemical conversion, and removal for this component.

Empirically determined optical properties of interest in the calculation of DRE and DCF are compared for the three regions in **Figure 2.9**. The dependence of these parameters on particle size (submicrometer vs. super-micrometer) and wavelength (450, 550, and 700 nm) is indicated. Single scattering albedo shows a strong dependence on both wavelength and particle size. Values are the lowest for sub-micrometer aerosol measured during INDOEX which corresponds with the relatively large sub-micrometer BC mass fractions observed in NIO region (as shown in Figure 7). Although there is a strong wavelength-dependence of aerosol scattering efficiency, values of mass scattering efficiency are similar among the three geographical regions, indicating that the variability in aerosol size distribution (modal diameter and width) or particle shape is not large enough to lead to significant regional differences (Quinn and Bates, 2005). The hemispheric backscattered fraction, b, derived from measurements made with an integrating nephelometer, is a complex function of particle size and shape.

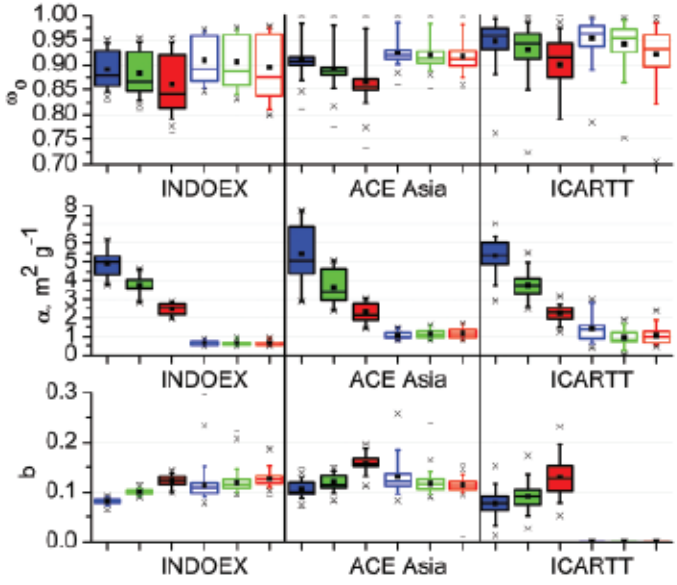

Figure 2.9: Mean and variability in single scattering albedo (ω_o), mass scattering efficiency (α), and backscattered fraction (b) for INDOEX, ACE-Asia, and ICARTT. Submicrometer values are solid bars, supermicrometer values are open bars. Wavelength is indicated by color (blue = 450 nm, green = 550 nm, red = 700 nm). The horizontal lines in the box denote the 25th, 50th, and 75th percentiles. The whisker denotes the 5th and 95th percentiles. The x denotes the 1st and 99th percentile. The square denotes the mean. Values are shown at the measurement RH of 55 ± 5%.

While the data discussed here (chemical composition shown in **Figure 2.6** and optical properties shown in **Figure 2.9**) are representative of conditions in the marine boundary layer during intensive field campaigns, they can be extended to cover a broader spatial and temporal scale through comparisons with surface-based observations and aircraft data during the campaigns, as well as long-term surface network measurements (Bates et al., 2006).

A key step in the Bates et al. approach is assigning empirically derived optical properties to the individual chemical components generated by the CTM for use in the RTM. Carrying the individual components through the RTM calculations (rather than the total aerosol) is required to attribute DRE and DCF to specific aerosol components. However, aerosol optical properties measured during field campaigns are, in general, characteristic of the total aerosol, not the individual species. In order to use the measurements to derive optical properties of individual components, the following assumptions were made: 1) aerosol mass over the ocean regions is present in an accumulation and a coarse mode, 2) sea salt and/or dust are present as external mixtures in the coarse mode (or supermicrometer size range), and 3) sulfate, OC, BC, and ammonium are internally mixed and exist entirely in the accumulation mode (submicrometer size range). Data for the NIO, NWP and NWA were segregated according to aerosol type (sea salt, dust, or sulfate/carbonaceous) based on measured chemical composition and particle size thereby isolating the sulfate/carbonaceous accumulation mode aerosol from the dust and sea salt coarse mode. Measured optical properties were carried along in the sorting process so that they, too, were segregated by aerosol type. As a result of this analysis, optical properties were estimated based on measurements as a function of aerosol size, type (composition), relative humidity, and wavelength.

One outcome of the Bates et al. analysis was a formal parameterization of the enhancement in light scattering due to the uptake of water vapor by aerosol particles [$f_{\sigma sp}(RH)$] for sulfate/carbonaceous aerosol mixtures. Prior to this analysis, both model and measurement studies revealed that POM internally mixed with water soluble salts can reduce the hygroscopic response of the aerosol, which decreases its water content and ability to scatter light at elevated relative humidities (e.g., Saxena et al., 1995; Carrico et al., 2005). Measurements made during INDOEX, ACE-Asia, and ICARTT revealed a substantial decrease in $f_{\sigma sp}(RH)$ with an increasing mass fraction of POM in the accumulation mode. Based on these data, a relationship between $f_{\sigma sp}(RH)$ and the POM mass fraction was developed for accumulation mode sulfate-POM aerosol (Quinn et al., 2005). The relationship is given by

$$f_{\sigma sp}(RH, RH_{ref}) = \sigma_{sp}(\mathrm{RH})/\sigma_{sp}(\mathrm{RH_{ref}}) = [(100 - \mathrm{RH_{ref}})/(100 - \mathrm{RH})]^{\gamma s} \qquad (1)$$

where

$$\gamma_s = 0.9 - 0.6*F_O \qquad (2)$$

and

$$F_o = C_O/(C_O + C_S) \qquad (3).$$

C_O and C_S are the measured mass concentrations of submicrometer POM and sulfate, respectively. The radiative transfer calculations of Bates et al. used the CTM output of C_O and C_S in Equation (3) to determine γ_s.

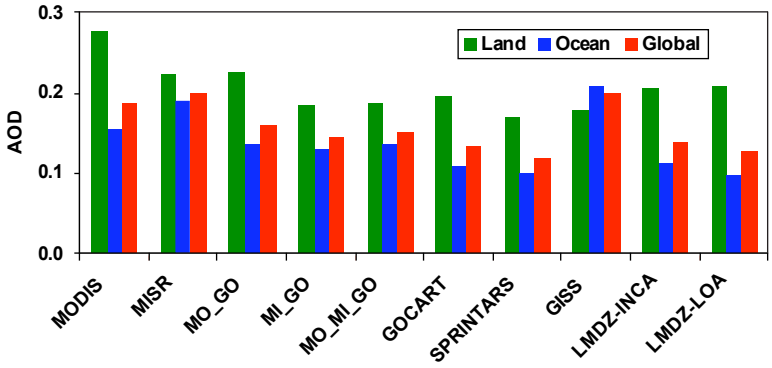

Figure 2.10: Comparison of annual mean aerosol optical depth (AOD) at 550 nm between satellite retrievals, model simulations, and satellite-model integrations averaged over land, ocean, and globe (all limited to 60°S-60°N region) (figure generated from Table 6 in Yu et al., 2006).

To compare the results using the *a priori* and empirically-derived optical properties, Bates et al. calculated DRE and DCF once using the optical properties built into the radiation code (*a priori*) and once using the observed properties (constrained). In addition, two RTMs (GFDL AM2 (GAMDT, 2004) and the University of Michigan (Liu et al., 2007)) were run with input from two different CTMs (STEM and MOZART). Results of the comparison of *a priori* versus constrained RTM runs include the following. The constrained optical properties derived from measurements increased the calculated AOD (34 ± 8%), TOA DRE (32 ± 12%), and TOA DCF (37 ± 7%) relative to runs using the *a priori* values. These increases are due to the larger values of the constrained mass extinction efficiencies relative to the *a priori* values. In addition, differences in AOD due to using the aerosol loadings from MOZART versus those from STEM are much greater than differences resulting from the *a priori* vs. constrained RTM runs. This result reflects the fact that DRE and DCF are linearly proportional to the amount of aerosol present.

The use of empirically-derived aerosol properties to assess model output (both CTM and RTM) and to serve as input to RTM calculations revealed that 1) uncertainties in calculated AOD and DRE are large and due primarily to the large uncertainties in the emissions and burdens of dust and sea salt, 2) the choice of aerosol optical properties (a priori or constrained) is a much smaller source of uncertainty in estimates of AOD, DRE, and DCF than is the choice of chemical transport model that determines the aerosol field for use in the radiative transfer calculations, and 3) the use of constrained optical properties led to values of AOD that were about 30% larger than those based on *a priori* optical properties. Similarly, the use of constrained optical properties led to about a 30% increase in TOA DRE and DCF indicating that AOD, DRE, and DCF, for these experimental regions, may be greater than previously estimated.

2.3.2. *Intercomparisons of Satellite Measurements and Model Simulation of Aerosol Optical Depth*

Given the fact that DRE and DCF are proportional to the amount of aerosol present, it is of first order importance to improve the spatial characterization of aerosol optical depth (AOD) on a global scale. This requires an evaluation of the various remote sensing data sets of AOD and comparison with model-estimates of AOD. The latter comparison is particularly important if we are to use models to predict future climate states. Both remote sensing and model simulation have uncertainties and satellite-model integration is needed to obtain an optimum description of aerosol distribution.

Figure 2.10 shows an intercomparison of annual average aerosol optical depth at 550 nm from two recent aerosol-oriented satellite sensors (MODIS and MISR), five model simulations (GOCART, GISS,

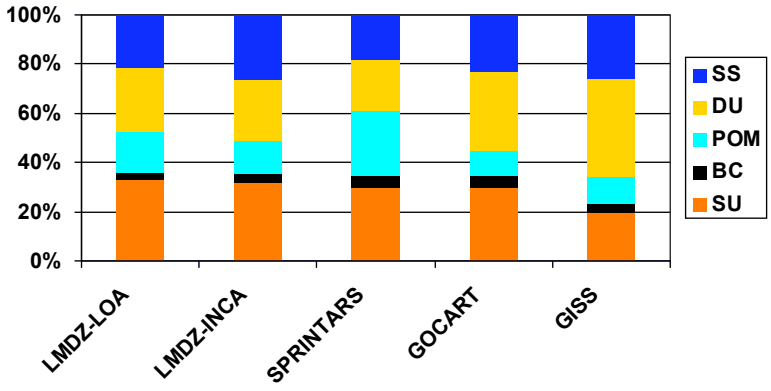

Figure 2.11: Percentage contributions of individual aerosol components (SU – sulfate, BC – black carbon, POM – particulate organic matter, DU – dust, SS – sea-salt) to the total aerosol optical depth (at 550 nm) on a global scale simulated by the five models (data taken from Kinne et al., 2006).

SPRINTARS, LMDZ-LOA, LMDZ-INCA) and three satellite-model integrations (MO_GO, MI_GO, MO_MI_GO). These model-satellite integrations are conducted by using an optimum interpolation approach (Yu et al., 2003) to constrain GOCART simulated AOD with that from MODIS, MISR, or MODIS over ocean and MISR over land, denoted as MO_GO, MI_GO, and MO_MI_GO, respectively. MODIS values of AOD are from Terra Collection 4 retrievals and MISR AOD is based on early post launch retrievals. MODIS and MISR retrievals give a comparable average AOD on the global scale, with MISR greater than MODIS by 0.01~0.02 depending on the season. However, differences between MODIS and MISR are much larger when land and ocean are examined separately: AOD from MODIS is 0.02-0.07 higher over land but 0.03-0.04 lower over ocean than the AOD from MISR. These differences are being reduced by the new MODIS aerosol retrieval algorithms in Collection 5 (Levy et al., 2007b) and the improved radiance calibration in MISR retrievals (Kahn et al., 2005b).

The annual and global average AOD from the five models is 0.19±0.02 (mean ± standard deviation) over land and 0.13±0.05 over ocean, respectively. Clearly, the model-based mean AOD is smaller than both MODIS- and MISR-derived values (except the GISS model). A similar conclusion has been drawn from more extensive comparisons involving more models and satellites (Kinne et al., 2006). On regional scales, satellite-model differences are much larger. These differences could be attributed, in part, to cloud contamination and 3D cloud effects in satellite retrievals (Kaufman et al., 2005b; Wen et al., 2006) or to models missing important aerosol sources/sinks or physical processes (Koren et al., 2007a). The satellite-model integrated products are generally in-between the satellite retrievals and the model simulations, and agree better with AERONET measurements (e.g., Yu et al., 2003).

As in the case of in-situ/model comparisons, there appears to be a relationship between uncertainties in the representation of dust in models and the uncertainty in AOD, and its global distribution. For example, the GISS model generates more dust than the other models (Fig. 2.11), resulting in a closer agreement with MODIS and MISR in the global mean (Fig. 2.10). However, the distribution of AOD between land and ocean is quite different from MODIS- and MISR-derived values.

Figure 2.11 shows larger model differences in the simulated percentage contributions of individual components to the total aerosol optical depth on a global scale, and hence in the simulated aerosol single-scattering properties (e.g., single-scattering albedo, and phase function), as documented in Kinne et al. (2006). This, combined with the differences in aerosol loading (i.e., optical depth) determines the model diversity in simulated aerosol direct radiative effect and forcing, as discussed later.

However, current satellite remote sensing capability is not sufficient to constrain model simulations of aerosol components.

2.3.3. *Remote Sensing Based Estimates of Aerosol Direct Radiative Effect*

AERONET and other surface networks usually provide a set of aerosol optical properties that can be used to calculate the aerosol direct radiative effect (Procopio et al., 2004; Zhou et al., 2005). The calculated aerosol radiative effect can be used to evaluate both satellite remote sensing measurements and model simulations (e.g., Yu et al., 2006). **Figure 2.12** shows the diurnally averaged, normalized aerosol direct effect based on the AERONET data that represent different aerosol types, geographical locations, and surface properties (Zhou et al., 2005). The normalized aerosol direct effect is referred to as *radiative efficiency* (E_τ), defined as a ratio of DRE to τ at 550 nm (Anderson et al., 2005a). The quantity of E_τ is mainly governed by aerosol size distribution and chemical composition (determining the aerosol single-scattering albedo and phase function), surface reflectivity, and solar irradiance, and also to some degree depends on the optical depth because of multiple scattering. The figure demonstrates how the aerosol direct solar effect is determined by a combination of aerosol and surface properties. For example, the radiative effect by South African biomass burning smoke differs significantly from that by South American smoke because of the much stronger light absorption due to smoke generated in South Africa (Dubovik et al., 2002; Eck et al., 2003). Mineral dust from North Africa and the Arabian Peninsula exert a radiative perturbation with a factor of ~2 difference in magnitude, due mainly to considerable spatial variability of surface reflectance in the region (Tsvetsinskaya et al., 2002).

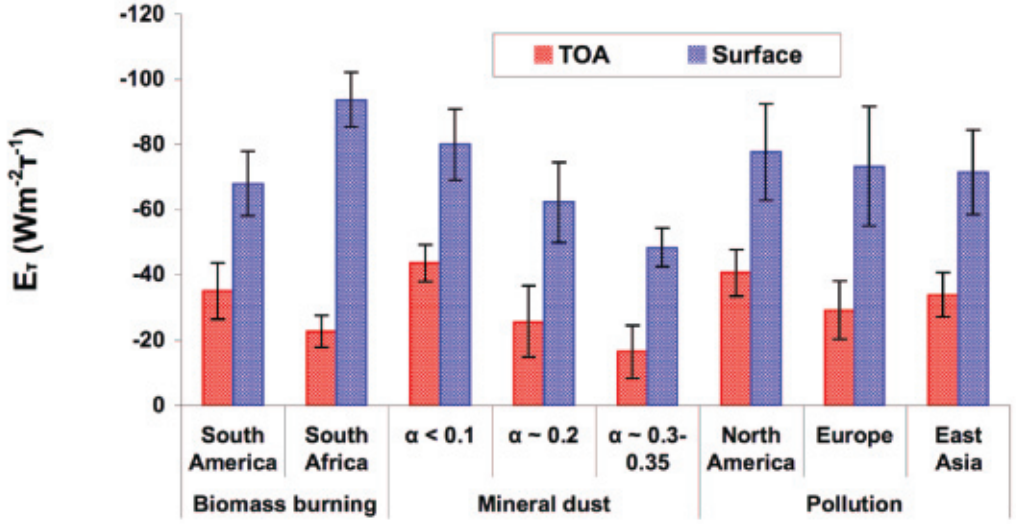

Figure 2.12: The clear-sky radiative efficiency E_τ, defined as the aerosol direct radiative effect (W m^{-2}) per unit aerosol optical depth (τ) at 550 nm, at the TOA and the surface for typical aerosol types and over different geographical regions, which is calculated from AERONET aerosol climatology. The vertical bars represent one standard deviation of Eτ for individual aerosol regimes. α is surface broadband albedo. The figure demonstrates how the aerosol direct solar effect is determined by a combination of aerosol and surface properties. The radiative effect by South African biomass burning smoke differs significantly from that by South America smoke because of stronger absorption of smoke in South Africa. Mineral dust from North Africa and the Arabian Peninsula exerts much different magnitude of radiative perturbation due mainly to considerable spatial variability of surface reflectance in the region (adapted from Zhou et al., 2005)

Table 2.4: Summary of approaches to estimating the aerosol direct radiative effect in three categories: (A) satellite retrievals; (B) satellite-model integrations; and (C) model simulations. (adapted from Yu et al., 2006)

Category	Product	Brief Descriptions	Identified Sources of Uncertainty	Major References
A. Satellite retrievals	MODIS	Using MODIS retrievals of a linked set of AOT, ω_0, and phase function consistently in conjunction with a radiative transfer model (RTM) to calculate TOA fluxes that best match the observed radiances.	Radiance calibration, cloud-aerosol discrimination, instantaneous-to-diurnal scaling, RTM parameterizations	Remer and Kaufman, 2006
	MODIS_A	Splitting MODIS AOD over ocean into mineral dust, sea-salt, and biomass-burning and pollution; using AERONET measurements to derive the size distribution and single-scattering albedo for individual components.	Satellite AOD and FMF retrievals, overestimate due to summing up the compositional direct effects, use of a single AERONET site to characterize a large region	Bellouin et al., 2005
	CERES_A	Using CERES fluxes in combination with standard MODIS aerosol	Calibration of CERES radiances, large CERES footprint, satellite AOD retrieval, radiance-to-flux conversion (ADM), instantaneous-to-diurnal scaling, narrow-to-broadband conversion	Loeb and Manalo-Smith, 2005 ; Loeb and Kato, 2002
	CERES_B	Using CERES fluxes in combination with NOAA NESDIS aerosol from MODIS radiances		
	CERES_C	Using CERES fluxes in combination with MODIS aerosol with new angular models for aerosols		Zhang et al, 2005a,b ; Zhang and Christopher, 2003; Christopher et al., 2006
	POLDER	Using POLDER AOD in combination with prescribed aerosol models (similar to MODIS)	Similar to MODIS	Boucher and Tanré, 2000 ; Bellouin et al., 2003
B. Satellite-model integrations	MODIS_G	Using GOCART simulations to fill AOD gaps in satellite retrievals	Propagation of uncertainties associated with both satellite retrievals and model simulations (but the model-satellite integration approach does result in improved AOD quality for MO_GO, and MO_MI_GO)	* Aerosol single-scattering albedo and asymmetry factor are taken from GOCART simulations; * Yu et al, 2003, 2004, 2006
	MISR_G			
	MO_GO	Integration of MODIS and GOCART AOT		
	MO_MI_GO	Integration of GOCART AOD with retrievals from MODIS (Ocean) and MISR (Land)		
	SeaWiFS	Using SeaWiFS AOD and assumed aerosol models	Similar to MODIS_G and MISR_G, too weak aerosol absorption	Chou et al, 2002
C. Model simulations	GOCART	Offline RT calculations using monthly average aerosols with a time step of 30 min (without the presence of clouds)	Emissions, parameterizations of a variety of sub-grid aerosol processes (e.g., wet and dry deposition, cloud convection, aqueous-phase oxidation), assumptions on aerosol size, absorption, mixture, and humidification of particles, meteorology fields, not fully evaluated surface albedo schemes, RT parameterizations	Chin et al., 2002; Yu et al., 2004
	SPRINTARS	Online RT calculations every 3 hrs (cloud fraction=0)		Takemura et al, 2002, 2005
	GISS	Online model simulations and weighted by clear-sky fraction		Koch and Hansen, 2005; Koch et al., 2006
	LMDZ-INCA	Online RT calculations every 2 hrs (cloud fraction = 0)		Balkanski et al., 2007; Schulz et al., 2006; Kinne et al., 2006
	LMDZ-LOA	Online RT calculations every 2 hrs (cloud fraction=0)		Reddy et al., 2005a, b

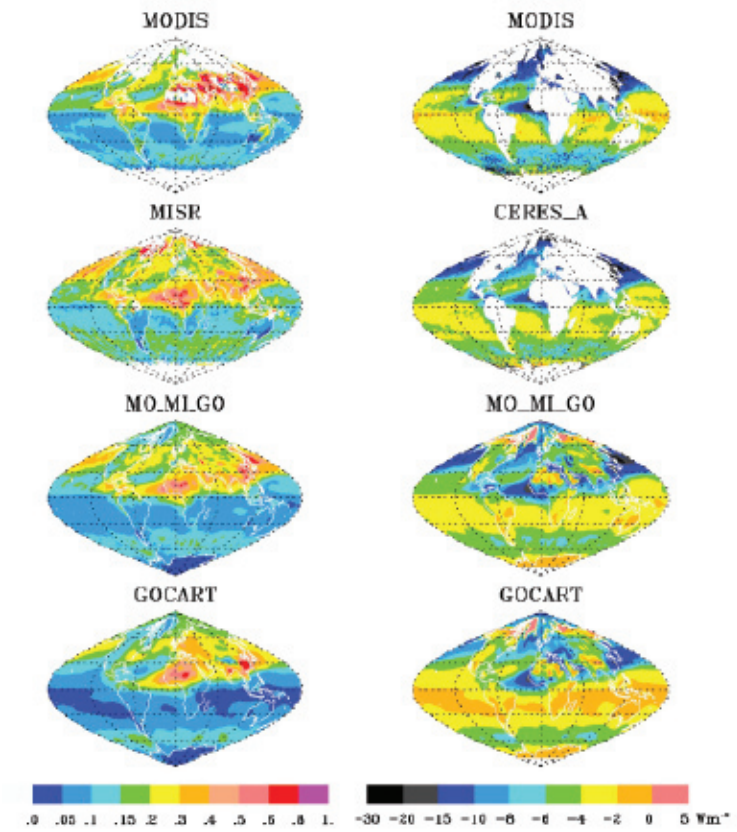

Figure 2.13: Geographical patterns of seasonally (MAM) averaged aerosol optical depth at 550 nm (left panel) and the diurnally averaged clear-sky aerosol direct solar effect (Wm-2) at the TOA (right panel) derived from satellite (Terra) retrievals (MODIS, Remer et al., 2005; Remer and Kaufman, 2006; MISR, Kahn et al., 2005a; and CERES_A, Loeb and Manalo-Smith, 2005), GOCART simulations (Chin et al., 2002; Yu et al., 2004), and GOCART-MODIS-MISR integrations (MO_MI_GO, Yu et al., 2006) (taken from Yu et al., 2006).

Table 2.4 summarizes approaches to estimating the aerosol direct solar effect, including a brief description of methods, identifies major sources of uncertainty, and provides references. These estimates fall into three broad categories, namely (A) satellite-based, (B) satellite-model integrated, and (C) model-based. Since satellite aerosol measurements are generally limited to cloud-free conditions, we focus here on assessments of clear-sky aerosol direct radiative effect and forcing and defer a discussion on complex influences of clouds on the aerosol direct effect and forcing to section 2.4.

Figure 2.13 shows global distributions of aerosol optical depth at 550 nm (left panel) and diurnally averaged clear-sky direct radiative effect at the TOA (right panel) for March-April-May (MAM) based on the different approaches. The direct effect at the surface follows the same pattern as that at the TOA but is significantly larger in magnitude because of aerosol absorption. It appears that different approaches agree on large-scale patterns of aerosol optical depth and the direct effect on solar radiation. In this season, the aerosol impacts in the Northern Hemisphere are much larger than those in the Southern Hemisphere. Dust outbreaks and biomass burning elevate the optical depth to more than 0.3 in large parts of North Africa and the tropical Atlantic. In the tropical Atlantic, TOA cooling as large as -10 Wm^{-2} extends westward to Central America. In highly polluted eastern China, the optical depth is as high as 0.6-0.8, resulting from the combined effects of pollution and biomass burning in the south, and dust outbreaks in the north. The impacts from Asia also extend to the North Pacific, with a TOA cooling of more than -10 Wm^{-2}. Other areas with large aerosol impacts include Western Europe, mid-latitude North Atlantic, and much of South Asia and the Indian Ocean. Over the "roaring forties" in the Southern Hemisphere, high winds generate a large amount of sea-salt. Such elevation of optical depth, along with high solar zenith angle and hence large backscattering to space, results in a band of TOA cooling of more than -4 Wm^{-2}. Some differences exist between different approaches. For

example, the early post-launch MISR retrieved optical depths over the southern hemisphere oceans are higher than MODIS retrievals and GOCART simulations. Over the "roaring forties", the MODIS derived TOA solar flux perturbations are larger than the estimates from other approaches. The "roaring forties" are a difficult region for remote sensing of aerosol and may be affected by cloud artifacts.

Figure 2.14 shows seasonal and annual mean AOD (first row), clear-sky DRE at the TOA (second row) and surface (third row) derived from averaging the satellite-based estimates and satellite-model integrations (i.e., category A and B in Table 2.4) with an equal weight over 13 regions, ocean and land separately. Correspondingly the probability distribution functions of seasonal and regional DREs are shown in **Figure 2.15**. These figures highlight large seasonal and regional variations of aerosol direct radiative effect. The DRE is relatively narrowly distributed at the TOA and over ocean, compared to that at the surface and over land

Figure 2.16 summarizes the measurement- and model-based estimates of clear-sky annually- averaged DRE at both the TOA and surface from 60°S to 60°N. Seasonal DRE values for individual estimates are summarized in **Table 2.5** (**Box 2.5**) and **Table 2.6** (**Box 2.6**), for ocean and land, respectively. Mean, median and standard error ε ($\varepsilon=\sigma/(n-1)^{1/2}$), where σ is standard deviation and n is the number of methods) are calculated for measurement- and model-based estimates separately. Note that while

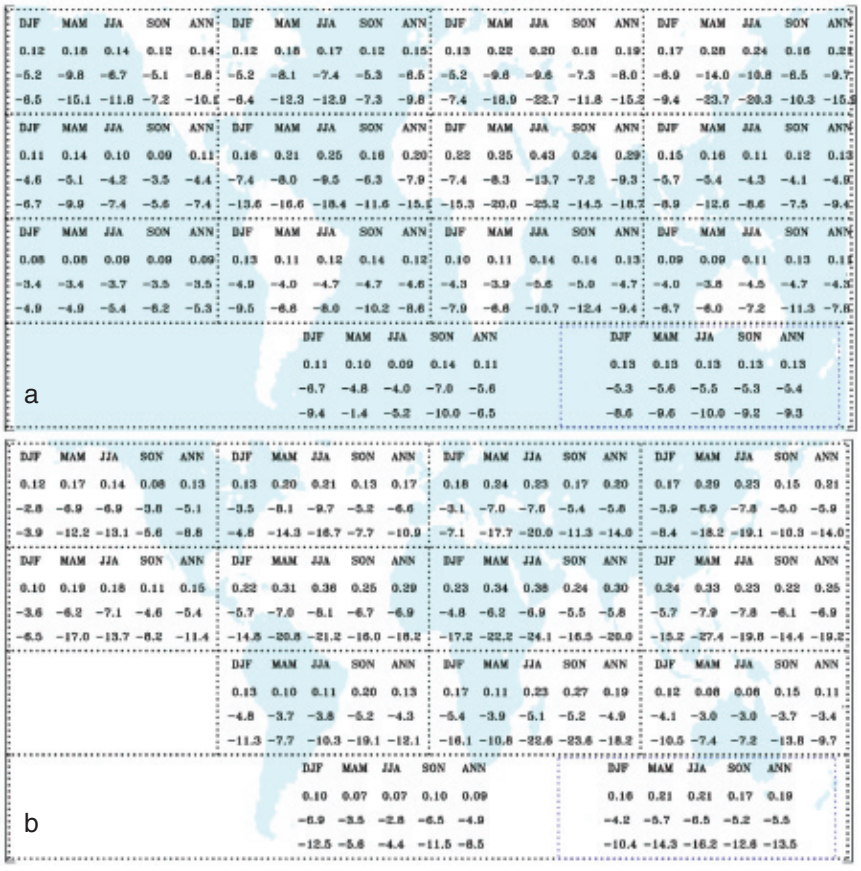

Figure 2.14: Observational-based AOD (first row in each section) and clear-sky DRE (Wm^{-2}) at the TOA (second row) and surface (third row) over 13 oceanic (a) and continental (b) sections (i.e., shadowed areas) derived from equally-weighted average of satellite-based and satellite-model integration-based estimates listed in Table 2. The lower-right boxes are for global oceanic and continental averages, respectively.

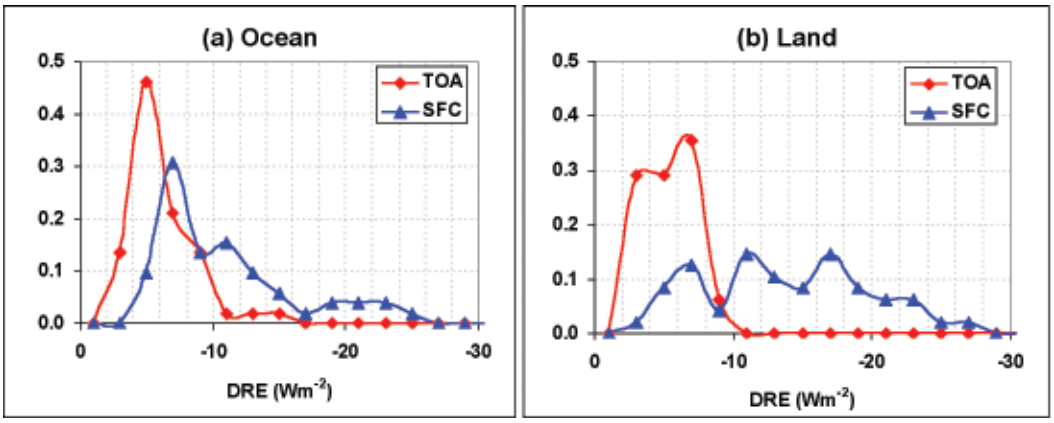

Figure 2.15: Frequency distribution of seasonal and regional average DRE for (a) Ocean and (b) Land, based on sectional and seasonal average data shown in Figure 2.14.

the standard deviation or standard error reported here is not a fully rigorous measure of a true experimental uncertainty, it is indicative of the uncertainty because independent approaches with independent sources of errors are used (see Table 2.4).

For the aerosol direct effect at the TOA and over ocean, a majority of measurement-based and satellite-model integration-based estimates agree with each other within about 10%. On annual average, the measurement-based estimates give the DRE of -5.5±0.2 Wm^{-2} (median±ε) at the TOA and -8.8±0.7 Wm^{-2} at the surface. This suggests that the ocean surface cooling is about 60% larger than the cooling at the TOA.

Model simulations give wide ranges of DRE estimates at both the TOA and surface. The ensemble of five models gives the annual average DRE (median ± ε) of -3.5±0.6 Wm^{-2} and -4.8±0.8 Wm^{-2} at the TOA and surface, respectively. On average, the surface cooling is about 37% larger than the TOA cooling, smaller than the measurement-based estimate of surface and TOA difference of 60%. Large DRE differences between models result from a combination of differences in parameterizations of various aerosol processes and meteorological fields, which are documented under the AEROCOM and Global Modeling Initiative (GMI) frameworks (Kinne et al., 2006; Textor et al., 2006; Liu et al., 2007).

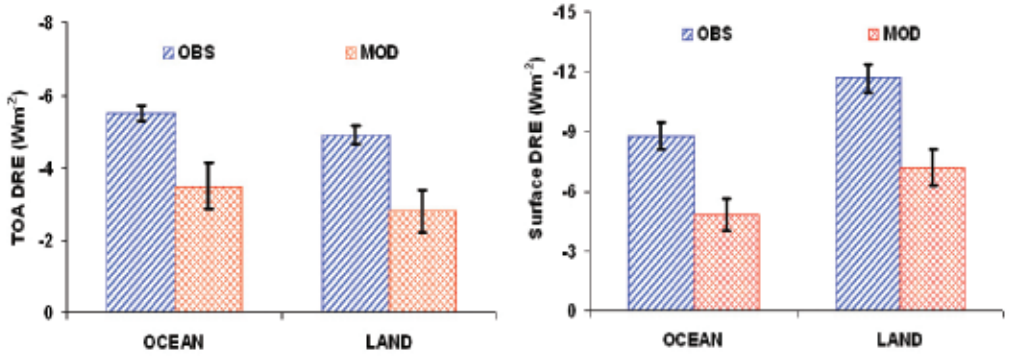

Figure 2.16: Summary of observation- and model-based (denoted as OBS and MOD, respectively) estimates of clear-sky, annual average DRE at the TOA and at the surface. The box and vertical bar represent median and standard error, respectively. (taken from Yu et al., 2006)

Box 2.5 (Table 2.5): Summary of seasonal and annual average clear-sky DRE (Wm^{-2}) at the TOA and the surface (SFC) over global OCEAN derived with different methods and data.

Sources of data: MODIS (Remer & Kaufman, 2006), MODIS_A (Bellouin et al., 2005), POLDER (Boucher and Tanré, 2000; Bellouin et al., 2003), CERES_A and CERES_B (Loeb and Manalo-Smith, 2005), CERES_C (Zhang et al., 2005b), MODIS_G, MISR_G, MO_GO, MO_MI_GO (Yu et al., 2004; 2006), SeaWiFS (Chou et al., 2002), GOCART (Chin et al., 2002; Yu et al., 2004), SPRINTARS (Takemura et al., 2002), GISS (Koch and Hansen, 2005; Koch et al., 2006), LMDZ-INCA (Kinne et al., 2006; Schulz et al., 2006), LMDZ-LOA (Reddy et al., 2005a, b). Mean, median, standard deviation (σ), and standard error (ε) are calculated for observations (Obs) and model simulations (Mod) separately. The last row is the ratio of model median to observational median. (taken from Yu et al., 2006)

Products	DJF		MAM		JJA		SON		ANN	
	TOA	SFC	TOA	SFC	TOA	SFC	TOA	SFC	TOA	SFC
MODIS	-5.9	–	-5.8	–	-6.0	–	-5.8	–	-5.9	–
MODIS_A *	-6.0	-8.2	-6.4	-8.9	-6.5	-9.3	-6.4	-8.9	-6.4	-8.9
CERES_A	-5.2	–	-6.1	–	-5.4	–	-5.1	–	-5.5	–
CERES_B	-3.8	–	-4.3	–	-3.5	–	-3.6	–	-3.8	–
CERES_C	-5.3	–	-5.4	–	-5.2	–	–	–	-5.3	–
MODIS_G	-5.5	-9.1	-5.7	-10.4	-6.0	-10.6	-5.5	-9.8	-5.7	-10.0
MISR_G **	-6.4	-10.3	-6.5	-11.4	-7.0	-11.9	-6.3	-10.9	-6.5	-11.1
MO_GO	-4.9	-7.8	-5.1	-9.3	-5.4	-9.4	-5.0	-8.7	-5.1	-8.8
MO_MI_GO	-4.9	-7.9	-5.1	-9.2	-5.5	-9.5	-5.0	-8.6	-5.1	-8.7
POLDER	-5.7	–	-5.7	–	-5.8	–	-5.6	–	-5.7 -5.2***	-7.7***
SeaWiFS	-6.0	-6.6	-5.2	-5.8	-4.9	-5.6	-5.3	-5.7	-5.4	-5.9
Obs. Mean	-5.4	-8.3	-5.6	-9.2	-5.6	-9.4	-5.4	-8.8	-5.5	-8.7
Obs. Median	-5.5	-8.1	-5.7	-9.3	-5.5	-9.5	-5.4	-8.8	-5.5	-8.8
Obs. σ	0.72	1.26	0.64	1.89	0.91	2.10	0.79	1.74	0.70	1.65
Obs. ε	0.23	0.56	0.20	0.85	0.29	0.94	0.26	0.78	0.21	0.67
GOCART	-3.6	-5.7	-4.0	-7.2	-4.7	-8.0	-4.0	-6.8	-4.1	-6.9
SPRINTARS	-1.5	-2.5	-1.5	-2.5	-1.9	-3.3	-1.5	-2.5	-1.6	-2.7
GISS	-3.3	-4.1	-3.5	-4.6	-3.5	-4.9	-3.8	-5.4	-3.5	-4.8
LMDZ -INCA	-4.6	-5.6	-4.7	-5.9	-5.0	-6.3	-4.8	-5.5	-4.7	-5.8
LMDZ -LOA	-2.2	-4.1	-2.2	-3.7	-2.5	-4.4	-2.2	-4.1	-2.3	-4.1
Mod. Mean	-3.0	-4.4	-3.2	-4.8	-3.5	-5.4	-3.3	-4.9	-3.2	-4.9
Mod. Median	-3.3	-4.1	-3.5	-4.6	-3.5	-4.9	-3.8	-5.4	-3.5	-4.8
Mod. σ	1.21	1.32	1.31	1.84	1.35	1.82	1.36	1.63	1.28	1.6
Mod. ε	0.61	0.66	0.66	0.92	0.67	0.91	0.68	0.81	0.64	0.80
Mod./Obs.	0.60	0.51	0.61	0.50	0.64	0.52	0.70	0.61	0.64	0.55

* High bias may result from adding the DRE of individual components to derive the total DRE (Bellouin et al., 2005).

** High bias most likely results from an overall overestimate of 20% in early post-launch MISR optical depth retrievals (Kahn et al., 2005).

*** Bellouin et al. (2003) use AERONET retrieval of aerosol absorption as a constraint to the method in Boucher and Tanré (2000), deriving aerosol direct effects both at the TOA and the surface.

Box 2.6 (Table 2.6): Summary of seasonal and annual average clear-sky DRE (Wm^{-2}) at the TOA and the surface over global LAND derived with different methods and data.

Sources of data: MODIS_G, MISR_G, MO_GO, MO_MI_GO (Yu et al., 2004, 2006), GOCART (Chin et al., 2002; Yu et al., 2004), SPRINTARS (Takemura et al., 2002), GISS (Koch and Hansen, 2005; Koch et al., 2006), LMDZ-INCA (Balkanski et al., 2007; Kinne et al., 2006; Schulz et al., 2006), LMDZ-LOA (Reddy et al., 2005a, b). Mean, median, standard deviation (σ), and standard error (ε) are calculated for observations (Obs) and model simulations (Mod) separately. The last row is the ratio of model median to observational median. (taken from Yu et al., 2006)

Products	DJF		MAM		JJA		SON		ANN	
	TOA	SFC	TOA	SFC	TOA	SFC	TOA	SFC	TOA	SFC
MODIS_G	-4.1	-9.1	-5.8	-14.9	-6.6	-17.4	-5.4	-12.8	-5.5	-13.5
MISR_G	-3.9	-8.7	-5.1	-13.0	-5.8	-14.6	-4.6	-10.7	-4.9	-11.8
MO_GO	-3.5	-7.5	-5.1	-12.9	-5.8	-14.9	-4.8	-10.9	-4.8	-11.6
MO_MI_GO	-3.4	-7.4	-4.7	-11.8	-5.3	-13.5	-4.3	-9.7	-4.4	-10.6
Obs. Mean	-3.7	-8.2	-5.2	-13.2	-5.9	-15.1	-4.8	-11.0	-4.9	-11.9
Obs. Median	-3.7	-8.1	-5.1	-13.0	-5.8	-14.8	-4.7	-10.8	-4.9	-11.7
Obs. σ	0.33	0.85	0.46	1.29	0.54	1.65	0.46	1.29	0.45	1.20
Obs. ε	0.17	0.49	0.26	0.74	0.31	0.85	0.27	0.75	0.26	0.70
GOCART	-2.9	-6.1	-4.4	-10.9	-4.8	-12.3	-4.3	-9.3	-4.1	-9.7
SPRINTARS	-1.4	-4.0	-1.5	-4.6	-2.0	-6.7	-1.7	-5.2	-1.7	-5.1
GISS	-1.6	-3.9	-3.2	-7.9	-3.6	-9.3	-2.5	-6.6	-2.8	-7.2
LMDZ-INCA	-3.0	-5.8	-4.0	-9.2	-6.0	-13.5	-4.3	-8.2	-4.3	-9.2
LMDZ-LOA	-1.3	-5.4	-1.8	-6.4	-2.7	-8.9	-2.1	-6.7	-2.0	-6.9
Mod. Mean	-2.0	-5.0	-3.0	-7.8	-3.8	-10.1	-3.0	-7.2	-3.0	-7.6
Mod. Median	-1.6	-5.4	-3.2	-7.9	-3.6	-9.3	-2.5	-6.7	-2.8	-7.2
Mod. σ	0.84	1.03	1.29	2.44	1.61	2.74	1.24	1.58	1.19	1.86
Mod. ε	0.42	0.51	0.65	1.22	0.80	1.37	0.62	0.79	0.59	0.93
Mod./Obs.	0.43	0.67	0.63	0.61	0.62	0.63	0.53	0.62	0.58	0.62

Clearly the model-based ensemble estimates of DRE are 30-50% smaller than the measurement-based estimates. As discussed earlier, MODIS retrieved optical depths tend to be overestimated by about 10-15% due to the contamination of thin cirrus and clouds in general (Kaufman et al., 2005b). Such overestimation of optical depth would result in a comparable overestimate of the aerosol direct radiative effect. Other satellite AOD data may have similar contamination, which however has not yet been quantified. For simplicity, we assume a cloud contamination of 10-15% in the measurement-based average DRE. With this correction of cloud contamination, the discrepancy between the measurement-based and model-based estimates of DRE and radiative efficiency would be reduced to 15-40%. On the other hand, the observations may be measuring enhanced AOD and DRE due to processes not well represented in the models including humidification and enhancement of aerosols in the vicinity of

clouds (Koren et al., 2007a). From the perspective of model simulations, uncertainties associated with a number of factors will contribute to the measurement-model discrepancy. Factors determining the AOD should be major reasons for the DRE discrepancy and the constraint of model AOD with well evaluated and bias reduced satellite AOD through a data assimilation approach can reduce the DRE discrepancy significantly. Other factors (such as model parameterization of surface reflectance, and model-satellite differences in single-scattering albedo and asymmetry factor due to satellite sampling bias toward cloud-free conditions) should also contribute, as evidenced by the existence of a large discrepancy in the radiative efficiency (Yu et al., 2006). Significant endeavor is demanded in the future to conduct comprehensive assessments.

Currently, satellite measurements alone are not adequate to characterize complex aerosol properties over complex surfaces and hence can not be used to derive the aerosol direct effect over land with high accuracy. As such, DRE estimates over land have to rely on model simulations and satellite-model integrations. On a global and annual average, the satellite-model integrated approaches derive a median DRE of -4.9 Wm^{-2} at the TOA and -11.7 Wm^{-2} at the surface respectively. The surface cooling is about 2.4 times larger than the TOA cooling because of aerosol absorption.

An ensemble of five model simulations derives a DRE (median ± ε) over land of -2.8±0.6 Wm^{-2} at the TOA and -7.2±0.9 Wm^{-2} at the surface, respectively. These are about 40% smaller than the measurement-based estimates. The measurement-model differences are a combination of differences in aerosol amount (optical depth), single-scattering properties, surface albedo, and radiative transfer schemes (Yu et al., 2006). Seasonal variations of DRE over land, as derived from both measurements and models, are larger than those over ocean.

2.3.4. *Satellite Based Estimates of Anthropogenic Aerosol Direct Climate Forcing*

Satellite instruments do not measure the aerosol chemical composition needed to discriminate anthropogenic from natural aerosol components. Because anthropogenic aerosols are predominately submicron, the fine-mode fraction derived from POLDER, MODIS, or MISR might be used as a tool for deriving anthropogenic aerosol optical depth. This could provide a feasible way to conduct measurement-based estimates of anthropogenic aerosol forcing (Kaufman et al., 2002a). The MODIS-based estimate of anthropogenic AOD is about 0.033 over oceans, consistent with model assessments of 0.03~0.036 even though the total AOD from MODIS is 25-40% higher than the models (Kaufman et al., 2005a). This accounts for 21±7% of the MODIS-observed total aerosol optical depth, compared with about 33% of anthropogenic contributions estimated by the models. The anthropogenic fraction of AOD should be much larger over land (i.e., 47±9% from a composite of several models) (Bellouin et al., 2005), comparable to the 40% estimated by Yu et al. (2006). Similarly, the non-spherical fraction from MISR or POLDER could also be used to separate dust from anthropogenic aerosol (Kahn et al., 2001).

In Kaufman et al. (2005a), it was assumed that all biomass burning aerosol is anthropogenic and all dust aerosol is natural. The better determination of anthropogenic aerosols requires a quantification of biomass burning ignited by lightning (natural origin) and mineral dust due to human induced changes of land cover/land use and climate (anthropogenic origin), which remains uncertain. Recent modeling (Tegen et al., 2004) suggests that the anthropogenic sources of dust contribute less than 10% of the

Table 2.7: Estimates of anthropogenic aerosol optical depth (τant) and clear-sky DCF at the TOA from model simulations (Schulz et al., 2006) and approaches constrained by satellite observations (Kaufman et al., 2005; Bellouin et al., 2005, 2008; Chung et al., 2005; Yu et al., 2006; Christopher et al., 2006; Matsui and Pielke, 2006; Quaas et al., 2008; Zhao et al., 2008).

Data Sources	Ocean		Land		Global		Estimated uncertainty or model diversity for DCF
	τ_{ant}	DCF (Wm^{-2})	τ_{ant}	DCF (Wm^{-2})	τ_{ant}	DCF (Wm^{-2})	
Kaufman et al. (2005)	0.033	-1.4	-	-	-	-	30%
Bellouin et al. (2005)	0.028	-0.8	0.13	-	0.062	-1.9	15%
Chung et al. (2005)	-	-	-	-	-	-1.1	-
Yu et al. (2006)	0.031	-1.1	0.088	-1.8	0.048	-1.3	47% (ocean), 84% (land), and 62% (global)
Christopher et al. (2006)	-	-1.4	-	-	-	-	65%
Matsui and Pielke (2006)	-	-1.6	-	-	-	-	30°S-30°N oceans
Quaas et al. (2008)	-	-0.7	-	-1.8	-	-0.9	45%
Bellouin et al. (2008)	0.021	-0.6	0.107	-3.3	0.043	-1.3	Update to Bellouin et al. (2005) with MODIS Collection 5 data
Zhao et al. (2008)	-	-1.25	-	-	-	-	35%
Schulz et al. (2006)	0.022	-0.59	0.065	-1.14	0.036	-0.77	30-40%; same emissions prescribed for all models

total dust optical depth, although early studies speculated the fraction to be between 0% (Ginoux et al., 2001) and 50% (Tegen and Fung, 1995).

To improve satellite estimates of anthropogenic aerosols and their direct forcing, satellite programs should concentrate on validating and improving retrievals of the aerosol Ångström exponent, and suborbital measurements should be used to derive relationships between the Ångström exponent and fine-mode fraction to allow interpretation of the satellite derived fine-mode optical depth (Anderson et al., 2005b).

There have been several estimates of DCF by anthropogenic aerosols in recent years. **Table 2.7** lists such estimates of TOA DCF that are from model simulations (Schulz et al., 2006) and constrained to some degree by satellite observations (Kaufman et al., 2005a; Bellouin et al., 2005, 2008; Chung et al., 2005; Christopher et al., 2006; Matsui and Pielke, 2006; Yu et al., 2006; Quaas et al.,2008; Zhao et al., 2008). The satellite-based clear-sky DCF by anthropogenic aerosols is estimated to be -1.1 ± 0.37 Wm^{-2} over ocean, about a factor of 2 stronger than model simulated -0.6 Wm^{-2}. Similar DCF estimates are rare over land, but a few studies do suggest that the DCF over land is much more negative than that over ocean (Yu et al., 2006; Bellouin et al., 2005, 2008). On global average, the measurement-based estimate of DCF ranges from -0.9~-1.9 Wm^{-2}, again stronger than the model-based estimate of -0.8 Wm^{-2}. Similar to DRE estimates, satellite-based DCF estimates are rare over land. DCF estimates have larger uncertainty than DRE estimates, particularly over land.

An uncertainty analysis (Yu et al., 2006) partitions the uncertainty for the global average DCF between land and ocean more or less evenly. Five parameters, namely fine-mode fraction (f_f) and anthropogenic fraction of fine-mode fraction (f_{af}) over both land and ocean, and τ over ocean, contribute nearly 80%

of the overall uncertainty in the DCF estimate, with individual shares ranging from 13-20% (Yu et al., 2006). We should point out that these uncertainties presumably represent a lower bound because the sources of error are assumed to be independent. Uncertainties associated with several parameters are also not well defined. Nevertheless, such uncertainty analysis is useful for guiding future research and documenting advances in our understanding.

On global average, anthropogenic aerosols are generally more absorptive than natural aerosols. As such the surface DCF is much more negative than the TOA DCF. Several observation-constrained studies estimate the global average clear-sky DCF at the surface of -4.2 ~ -5.1Wm^{-2} (Yu et al., 2004; Bellouin et al., 2005; Chung et al., 2005; Matsui and Pielke, 2006), which is about a factor of 2 larger in magnitude than the model estimates (e.g., Reddy et al., 2005b).

2.3.5. *Remote Sensing Studies of Aerosol-Cloud Interactions and Indirect Effects*

Satellite views of the Earth inevitably show a planet covered, not by aerosols, but by clouds. The bright white clouds overlying darker oceans or vegetated surface demonstrate the significant effect that clouds have on the Earth's radiative balance. Low clouds reflect incoming sunlight back to space, acting to cool the planet, while high clouds can trap outgoing terrestrial radiation and act to warm the planet. Changes in cloud cover, in cloud vertical development, and cloud optical properties will have strong radiative and therefore, climatic impacts. Furthermore, factors that change cloud development will also change precipitation processes. These changes can alter amounts, locations and intensities of local and regional rain and snowfall, creating droughts, floods and severe weather.

Aerosol particles act as cloud condensation nuclei (*CCN*). Every cloud droplet consists of water condensing onto one or more of these CCN. Thus, for the same amount of liquid water in a cloud, more available CCN will result in a greater number but smaller size of droplets (Twomey, 1977). A cloud with smaller but more numerous droplets will be brighter and reflect more sunlight to space. This is the aerosol indirect radiative effect. However, because the droplets are smaller they may inhibit collision-coalescence in the cloud, suppressing particle growth that stops drizzle and other precipitation and extends cloud lifetime (Albrecht et al. 1989). In a cloud with strong updrafts, the cloud may eventually precipitate, but only after higher altitudes are reached that result in taller cloud tops, more lightning and greater chance of severe weather (Rosenfeld and Lensky, 1998; Andreae et al., 2004).

On the other hand, because aerosols themselves are radiatively active, they can change atmospheric conditions (temperature, stability) that also influences cloud development and properties (Hansen et al, 1997; Ackerman et al., 2000). Thus, aerosols affect clouds both through changing cloud droplet size distributions, and by changing the atmospheric environment of the cloud.

The AVHRR satellites have observed relationships between columnar aerosol loading and retrieved cloud microphysics and cloud brightness over the Amazon Basin that are consistent with the theories explained above (Kaufman and Nakajima, 1993; Kaufman and Fraser, 1997; Feingold et al., 2001). Other studies have linked cloud and aerosol microphysical parameters or cloud albedo and droplet size using satellite data applied over the entire global oceans (Wetzel and Stowe, 1999; Nakajima et al., 2001; Han et al., 1998). Using these correlations with estimates of aerosol increase from the pre-industrial era, estimates of anthropogenic aerosol indirect radiative forcing fall into the range of -0.7 to -1.7 Wm^{-2} (Nakajima et al., 2001).

Introduction of the more modern instruments (POLDER and MODIS) have allowed more detailed observations of relationships between aerosol and cloud parameters. Cloud cover can both decrease and increase with increasing aerosol loading (Koren et al., 2004; Kaufman et al., 2005; Koren et al., 2005; Sekiguchi et al., 2003; Yu et al., 2007). Aerosol absorption appears to be an important factor in determining how cloud cover will respond to increased aerosol (Kaufman and Koren, 2006; Jiang and Feingold, 2006). Different responses of cloud cover to increased aerosol could also be correlated with atmospheric thermodynamic and moisture structure (Yu et al., 2007). Observations in the MODIS data show that aerosol loading correlates with enhanced convection and greater production of ice anvils in the summer Atlantic Ocean (Koren et al., 2005), which conflicts with previous results that used AVHRR and could not isolate convective systems from shallow clouds (Sekiguchi et al., 2003).

In recent years, surface-based remote sensing has also been applied to address aerosol effects on cloud microphysics. This method offers some interesting insights, and is complementary to the global satellite view. Surface remote sensing can only be applied at a limited number of locations, and therefore lacks the global satellite view. However, these surface stations yield high temporal resolution data and because they sample aerosol below, rather than adjacent to clouds they do not suffer from "cloud contamination". With the appropriate instrumentation (lidar) they can measure the local aerosol entering the clouds, rather than a column-integrated aerosol optical depth.

Feingold et al. (2003) used data collected at the Atmospheric Radiation Measurement (*ARM*) site to allow simultaneous retrieval of aerosol and cloud properties, with the combination of a Doppler cloud radar and a microwave radiometer to retrieve cloud drop effective radius r_e profiles in non-precipitating (radar reflectivity Z < -17 dBZ), ice-free clouds. Simultaneously, sub-cloud aerosol extinction profiles were measured with a lidar to quantify the response of drop sizes to changes in aerosol properties. The microwave radiometer made it possible to sort the cloud data according to liquid water path (*LWP*), consistent with Twomey's (1977) conceptual view of the aerosol impact on cloud microphysics. With high temporal/spatial resolution data (on the order of 20's or 100's of meters), realizations of aerosol-cloud interactions at the large eddy scale were obtained. Moreover, by examining updrafts only (using the radar Doppler signal), the role of updraft in determining the response of r_e to changes in aerosol (via changes in drop number concentration N_d) was examined. Analysis of data from 7 days showed that turbulence intensifies the aerosol impact on cloud microphysics.

In addition to radar/microwave radiometer retrievals of aerosol and cloud properties, surface based radiometers such as the MFRSR (Michalsky et al., 2001) have been used in combination with a microwave radiometer to measure an average value of r_e during daylight when the solar elevation angle is sufficiently high (Min and Harrison, 1996). Using this retrieval, Kim et al. (2003) performed analyses of the r_e response to changes in aerosol at the same continental site, and instead of using extinction as a proxy for CCN, they used a surface measurement of the aerosol light scattering coefficient. Their analysis spanned much longer time periods and their data included a range of different aerosol conditions. A similar study was conducted by Garrett et al. (2004) at a location in the Arctic. The advantage of the MFRSR/microwave radiometer combination is that it derives r_e from cloud optical depth and LWP and it is not sensitive to large drops as the radar is. Its drawback is that it can only be applied to clouds with extensive horizontal cover during daylight hours.

In conclusion, observational estimates of aerosol indirect radiative effects are still in their infancy. Effects on cloud microphysics that result in cloud brightening have to be balanced by effects on cloud

lifetime, cover, vertical development and ice production. Aerosol type and specifically the absorption properties of the aerosol may cause different cloud responses. Early estimates of observationally based aerosol indirect forcing range from -0.7 to -1.7 Wm^{-2} (Nakajima et al, 2001) and -0.6 to -1.2 Wm^{-2} (Sekiguchi et al., 2003), depending on the estimate for aerosol increase from pre-industrial times and whether aerosol effects on cloud fraction are also included in the estimate.

2.4. Outstanding Issues

Despite substantial progress in the assessment of the aerosol radiative effect and forcing as summarized in section 2.2 and 2.3, several important issues remain, and significant efforts are required to address them.

2.4.1. *Aerosol Vertical Distributions*

Vertical distributions of aerosols are crucial to quantifying the aerosol direct effect in the thermal infrared and in cloudy conditions, interpreting the satellite observed aerosol-cloud correlations, and understanding the atmospheric response to aerosol radiative forcing.

Due to its large size, mineral dust can cause warming in the thermal infrared, both at the TOA and at the surface. Therefore, estimates of aerosol direct effect on solar radiation should represent an upper bound of the aerosol net direct effect (on total radiative fluxes). The warming effect could be significant, as suggested by a few observational studies (Highwood et al., 2003; Haywood et al., 2005; Zhang and Christopher, 2003; Slingo et al., 2006). However, current estimates of the warming effects in the thermal infrared remain highly uncertain, because of lack of observations of vertical distributions of aerosol in the thermal infrared range (Sokolik et al., 2001; Lubin et al., 2002). In addition, the scattering effect in the thermal infrared domain is generally neglected in most GCMs, which may lead to an underestimate of the thermal infrared aerosol effect (Dufresne et al., 2002).

Calculations of the cloudy-sky aerosol direct effect require an adequate characterization of vertical distributions of aerosols and three-dimensional fields of clouds, especially for absorbing aerosols. The surface cooling in climatologically cloudy conditions is comparable to that under clear conditions, while the TOA effect could switch from cooling in clear conditions to warming in overcast conditions (Keil and Haywood, 2003). Note that substantial differences currently exist in simulations of aerosol vertical distributions (Penner et al., 2002; Textor et al., 2006) and limited measurements do not suffice for the estimate of the cloudy-sky DRE and DCF. This is manifested by a large diversity in the calculated whole-sky to clear-sky ratio for the TOA DCF (Schulz et al., 2006; Chung et al., 2005; Reddy and Boucher, 2004; Takemura et al., 2001; Jacobson, 2001), as summarized in **Figure 2.17**. The ratio ranges from +0.5 to -0.1 (i.e., shifting from clear-sky cooling to whole-sky warming), with an average of 0.26, and standard deviation of 0.17.

The emerging ground-based aerosol lidar networks and spaceborne lidars and radars (Stephens et al., 2001) will help improve the understanding of the aerosol direct forcing in cloudy conditions and the thermal infrared range. The lidar measurements can also well constrain the aerosol-induced atmospheric heating rate increment that is essential for assessing atmospheric responses to the aerosol radiative forcing (e.g., Yu et al., 2002; Feingold et al., 2005; Lau et al., 2006).

2.4.2. *Aerosol Direct Forcing over Land*

The land surface reflection is large, heterogeneous, and anisotropic, which complicates aerosol retrievals and determination of the aerosol direct effect. For example, the lack of a dust signal over the deserts (Hsu et al., 2000) is apparently attributable to the large heterogeneity of surface reflectance as documented by high-resolution MODIS land albedo retrievals (Tsvetsinskaya et al., 2002). The current-generation satellite sensors like MODIS and MISR are improving the characterization of land surface reflection by measuring its wavelength dependence and angular distribution at high resolution. This offers a promising opportunity for inferring the aerosol direct effect over land from satellite measurements of radiative fluxes (e.g., CERES) and from critical reflectance techniques (Fraser and Kaufman, 1985; Kaufman, 1987). Such satellite-based estimates should be comprehensively evaluated against those calculated from AERONET measurements (Zhou et al., 2005) and intensive field experiments (as summarized in Yu et al., 2006).

2.4.3. *Aerosol Absorption*

Aerosol absorption and single-scattering albedo are strong functions of the size of particles, the state of mixture, the shape, the wavelength and the relative humidity. A characterization of aerosol absorption or SSA is complicated by instrumental errors and modeling inadequacies, as summarized in Heintzenberg et al. (1997), Reid et al. (2005), and Bond and Bergstrom (2006). The global assessment of aerosol absorption and SSA represents a major challenge in efforts to quantify the direct forcing (Yu et al., 2006) and aerosol-cloud interactions (Kaufman and Koren, 2006).

Instrument calibration for aerosol absorption measurements is challenging, because aerosol absorption typically has a much smaller magnitude than aerosol scattering (Heintzenberg et al., 1997; Bond and Bergstrom, 2006). Determining aerosol absorption by subtracting measured scattering from measured

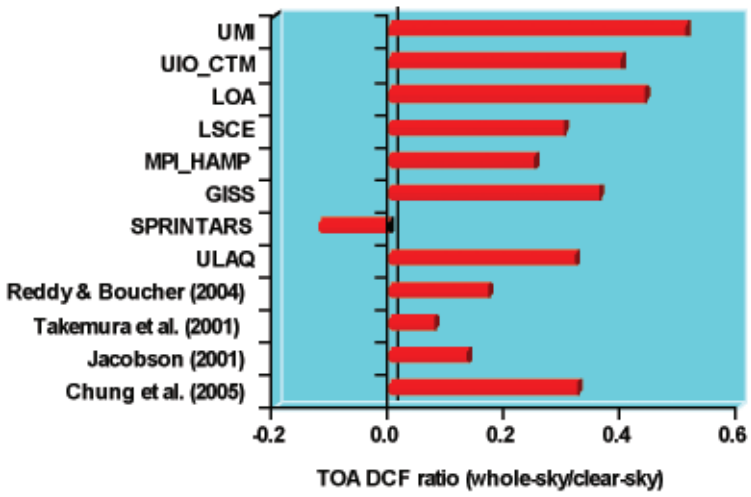

Figure 2.17: Summary of model-based estimates of whole-sky to clear-sky ratio for the TOA DCF. Model simulations are taken from Schulz et al. (2006), except otherwise specified.

extinction could have large uncertainties. Recent employment of photoacoustic methods (Arnott et al., 1997) and cavity ring down extinction cells (Strawa et al., 2002) will significantly improve the accuracy of SSA measurement. In-situ measurements are generally conducted at low relative humidity and effects of water uptake on aerosol absorption are poorly understood (Redemman et al., 2001).

Model simulations of aerosol compositions have large diversities, as shown in **Figure 2.11**. It is necessary to constrain model simulations with optical models consistent with in-situ measurements of aerosol physical and optical properties (Bond and Bergstrom, 2006). While nonabsorbing aerosols don't directly contribute to aerosol absorption, it is necessary to better characterize the evolution of nonabsorbing aerosols such as hydrophilic sulfate and their interactions with black carbon (BC) in models (Stier et al., 2006). The mixing of sulfate and BC can turn initially hydrophobic BC to a hydrophilic state and hence enhance removal by wet scavenging and decrease BC abundance and absorption. In addition, the presence of sulfate also can increase the BC absorption efficiency through internal mixing and increasing the amount of diffuse solar radiation. The first mechanism prevails in remote regions, reducing aerosol absorption. Near source regions, the second mechanism could prevail and hence enhance the solar absorption (Stier et al., 2006).

Inverse methods have been widely used in both ground and satellite remote sensing, providing aerosol absorption information over large geographical areas and during long time periods. The theoretical uncertainty of the AERONET retrieval of SSA is 0.03 for AOD greater than 0.3 (Dubovik et al., 2002). Similarly, at large AOD the estimated AERONET uncertainty for absorptive optical depth is 0.01 (Dubovik and King, 2000; Dubovik et al., 2001). It is important to pursue validation against independent measurements because a recent study has shown a factor of 2-4 discrepancy between the AERONET retrievals and the simulated absorptive optical depths (Sato et al., 2003). This discrepancy would imply significant errors in the global burden of black carbon and/or the absorptive efficiency of black carbon (perhaps related to aerosol mixing state, morphology, or size distribution) (Sato et al., 2003; Martins et al., 1998; Jacobson, 2000; 2001). On the other hand, a comparison of in-situ to AERONET absorption over the Chesapeake Bay indicated that the latter may be biased high (Magi et al., 2005). AERONET Version 2 retrievals of aerosol SSA are expected to be more accurate due to improved characterization of seasonal, spectral, and BRDF of surface reflection and the SSA retrievals over bright surfaces are substantially lower than that in Version 1 (Leahy et al., 2007). This warrants a reexamination of discrepancies/agreements between AERONET retrievals and in-situ measurements (Haywood et al., 2003; Magi et al., 2005). It is essential to pursue a better understanding of the uncertainty of in-situ measured and remote sensing inversed SSA in a robust way and accordingly a synthesis of different data sets for yielding regional characterization of aerosol absorption with well-defined uncertainty (Leahy et al., 2007).

Satellite methods for quantifying SSA and absorption have been developed and partially validated at UV wavelengths (Torres et al., 2005), although the retrieval has large uncertainties associated with its sensitivity to the height of the aerosol layer and it is unclear at present how these UV results can be extended to visible wavelengths. Examining satellite images in dusty conditions (Kaufman et al., 2001; Moulin et al., 2001) suggests that mineral dust absorption could be much weaker than previously believed (e.g., Patterson et al., 1977) and widely used in model simulations, corroborated by in-situ and ground-based remote sensing measurements (e.g., Clarke and Charlson, 1985; Dubovik et al., 2002; Cattrall et al., 2003; Haywood et al., 2003). This finding could partly explain the measurement-model

discrepancies in aerosol direct radiative effect (e.g., Yu et al., 2004). It is thus important to reevaluate and improve model simulations of mineral dust aerosol radiative effect by explicitly accounting for the dependence on mineralogy and morphology of dust (Sokolik and Toon, 1999; Sokolik et al., 2001; Balkanski et al., 2007). Views in and out of sunglint can be used to retrieve total aerosol extinction and scattering, respectively, thus constraining aerosol absorption over oceans (Kaufman et al., 2002b). However, the technique requires highly accurate retrievals of aerosol scattering properties including the real part of the refractive index. Only a polarization instrument can provide that information. The technique will be applied to the collocated MODIS and PARASOL data in the A-Train. The technique will also be applied to APS data from the Glory mission.

2.4.4. *Diurnal Cycle*

Significant efforts are demanded to capture the diurnal cycle of aerosol direct forcing in order to better assess aerosol impacts on climate. AERONET measurements show that the daytime variability depends on location and aerosol type, with the variation as large as 40% for biomass burning smoke and urban/industrial pollution near the sources, and essentially negligible for dust (Smirnov et al., 2002). From the perspective of satellite remote sensing, the diurnal variation of aerosols can be better characterized by geostationary satellites (*GOES*) (Christopher and Zhang, 2002b; Wang et al., 2003). However, these satellites generally lack the information required to characterize aerosol types. The synergistic use of low earth orbit (for characterizing aerosol type) and geostationary earth orbit satellite data should be used to retrieve aerosol optical depth and its diurnal variations (Costa et al., 2004a, 2004b). MODIS flying on the twin EOS satellites, namely Terra and Aqua, can also be used to some extent to examine aerosol diurnal variations, i.e., from late morning (10:30 LT) to early afternoon (13:30 LT) (Remer et al., 2006; Ichoku et al., 2005).

Clouds can modulate the aerosol direct solar effect significantly and daytime variation of clouds needs to be adequately characterized. The aerosol direct effect also depends on surface reflection, and the anisotropy of surface reflection further complicates the calculation of the diurnal cycle of the aerosol radiative effect (Yu et al., 2004). With satellite remote sensing providing angular and spectral variations of surface reflection (e.g., Moody et al., 2005; Martonchik et al., 1998; 2002), it is feasible to better characterize the complexity of surface reflection and its interaction with aerosol extinction through the use of the black-sky and white-sky albedo for direct beam and diffuse light, respectively (Yu et al., 2004, 2006).

2.4.5. *Aerosol-Cloud Interactions and Indirect Forcing*

Remote sensing estimates of aerosol indirect forcing are still rare and uncertain. Basic processes still need to be understood on regional and global scales. Uncertainties will likely increase before they decrease as new processes and their feedbacks become known. Remote sensing observations of aerosol-cloud interactions and aerosol indirect forcing are now simple correlations between variables, in which cause-and-effects are inferred. However, such inferences are not proven. The most difficult aspect of inferring aerosol effects on clouds from the observed relationships is separating aerosol effects from meteorological effects when aerosol loading itself is often correlated with the meteorology. While satellite studies provide indispensable information on aerosol-cloud interaction, future work will need to combine satellite observations with in-situ validation and modeling interpretation.

2.4.6. *Long-term Trends of Aerosols and Radiative Fluxes*

To detect long-term trends of aerosols, satellite retrievals of aerosol optical depth should have high accuracy and a synergy of aerosol products from multiple sensors (historical sensors and modern sensors) to construct as long a record as possible. Historical sensors like TOMS and AVHRR have provided multi-decadal climatology of aerosol optical depth (Torres et al., 2002; Geogdzhayev et al., 2002), which have been used to analyze trends of aerosol optical depths in Asia (e.g., Massie et al., 2004) and over global ocean (Mishchenko et al., 2007b). These products should be extended to a longer period by incorporating data from modern sensors (e.g., MODIS, MISR, OMI, and others). Such extensions should be built upon our understanding and reconciliation of AOD differences among different sensors or platforms (Jeong et al., 2005). A good deal of effort is needed to address this fundamental issue. An emerging 7-year climatology of high quality AOD data from modern sensors, though not as long as records from historic sensors, has been used to examine the interannual variations of aerosol (Koren et al., 2007b) and shall contribute significantly to the study of aerosol trends.

Broadband direct solar radiation is measured at meteorological stations around the world. These long-term observations can be used to derive average aerosol optical depth over the solar spectrum, thus having the potential to detect changing aerosol conditions on a decadal scale (Luo et al., 2001). However such aerosol optical depth retrievals still need to be evaluated using independent measurements from other surface observations, such as AERONET and MFRSR.

Analysis of long-term records of surface solar radiation suggests significant trends during past decades (e.g., Stanhill and Cohen, 2001; Wild et al., 2005; Pinker et al., 2005). While a significant and widespread decline in surface solar radiation occurred up to 1990 (so-called *dimming*), a sustained increase has been observed in the most recent decade. Speculation suggests that such trends result from decadal changes of aerosols and an interplay of aerosol direct and indirect effects (Stanhill and Cohen, 2001; Wild et al., 2005; Streets et al., 2006b; Norris and Wild, 2007). Other studies suggest that the measured changes in surface solar radiation are local, not global in nature (Alpert et al., 2005). However, reliable observations of aerosol trends are needed before these speculations can be proven or disproven. In addition to the aerosol optical depth, we also need to quantify changes in aerosol composition because of changes in industrial practices, environmental regulations, and biomass burning emissions (Novakov et al., 2003; Streets et al., 2004; Streets and Aunan et al., 2005). Such compositional changes will affect the aerosol single-scattering albedo and size distribution, which in turn will affect the surface solar radiation (e.g., Qian et al., 2007). However such data are currently rare and subject to large uncertainties. A better understanding of aerosol-radiation-cloud interactions is badly needed to attribute the observed radiation changes to aerosol changes with less ambiguity.

2.5. Concluding Remarks

Since the concept of aerosol-radiation-climate interactions was first proposed around 1970, substantial progress has been made in determining the mechanisms and magnitudes of these interactions, particularly in the last ten years. Such advancement has greatly benefited from significant improvements in aerosol measurements and increasing sophistication of model simulations. In particular, the establishment of ground-based aerosol networks such as AERONET and the execution of intensive field

experiments in a variety of aerosol regimes have collected invaluable datasets that serve as a baseline for constraining and evaluating satellite retrievals and model simulations. New and enhanced satellite sensors, such as POLDER, MODIS, and MISR, are measuring aerosols on a global scale and with good accuracy. CERES measures broadband solar and thermal infrared fluxes that are used to derive the aerosol direct radiative effect and forcing.

As a result of these improvements, we now have a much improved knowledge of aerosol properties and their interaction with solar radiation on regional and global scale. Intensive field campaigns conducted in major aerosol regimes around the globe and the emerging ground-based aerosol networks have resulted in better characterization of regional aerosol, including its chemical, microphysical, and radiative properties. Uncertainties associated with them can be well understood through conducting closure studies of over-determined data from multiple platforms and instruments. Aerosol closure studies reveal that for submicrometer, spherical (e.g., sulfate, carbonaceous aerosol) meaurements of aerosol optical properties and optical depths agree within 15% and often better. For dust dominated aerosol, measurements of aerosol optical depth disagree by up to 35% between methods, due to inlet collection efficiency and instrumental response difficulties resulting from its larger particle size and non-sphericity. Closure studies on DRE reveal uncertainties of about 25% for sulfate/carbonaceous aerosol and 60% for dust (Bates et al., 2006)

The accumulated comprehensive data sets of regional aerosol properties provide a rigorous "test bed" and strong constraint for satellite retrievals and model simulations of aerosols and their direct radiative effect and climate forcing. In Bates et al. (2006), in-situ measurements from three major aerosol characterization experiments were used to derive optical properties for individual aerosol types (i.e., sulfate/carbonaceous, dust, and sea-salt aerosol) that are of interest in the calculation of aerosol direct radiative effect, including wavelength-dependent mass extinction efficiency, single-scattering albedo, backscatter and asymmetry factor, and humidification factor for aerosol scattering. Such empirically determined aerosol optical properties were then used to constrain calculations of AOD and DRE in two CTM models. The so-constrained AOD and DRE increase by about 30%, compared to calculations based on the *a priori* optical properties.

For all of their advantages, field campaigns are inherently limited by their relatively short duration and small spatial coverage. Satellite remote sensing can augment field campaigns by expanding the temporal and spatial coverage. Surface networks provide high temporal resolution records but also benefit from the expanded spatial resolution provided by satellites. The multi-spectral MODIS measures global distributions of aerosol optical depth (τ) on a daily scale, with high accuracy of $\pm 0.03 \pm 0.05\tau$ over oceans. The annual average τ at 550 nm is about 0.14 over the global oceans. Based on the MODIS fine-mode and background aerosol fraction, about 21% of the 0.l4 is estimated to be contributed by human activities. The multi-angle MISR can evaluate the surface reflectance and retrieve aerosols simultaneously over all kinds of surfaces, including bright deserts. MISR derives an annual average AOD of 0.23 at 550 nm over global land with an uncertainty of ~20% or ±0.05. A combination of MODIS over-ocean and MISR over-land retrievals gives a global average of aerosol optical depth of about 0.17 at 550 nm, which is 20% larger than an ensemble average of 0.14 of five global aerosol models. It is possible that such discrepancy can be largely reduced by correcting cloud artifacts in satellite retrievals, and by including complex cloud-aerosol physical processes in models.

The high-accuracy of MODIS and MISR aerosol products and broadband flux measurements from CERES, together with simultaneous improvements in surface and cloud characterizations in these sensors, make it feasible to obtain observational constraints for the aerosol direct effect. A number of measurement-based approaches consistently estimate the cloud-free DRE (on solar radiation) at the top-of-atmosphere to be about -5.5±0.2 Wm^{-2} (median ± standard error from various methods) over global ocean. At the ocean surface, the DRE is estimated to be -8.8±0.7 Wm^{-2}. Over land, deriving the aerosol direct effect from the flux measurements such as that from CERES is complicated by a large and highly heterogeneous surface reflection. An integration of satellite retrievals and model simulations yields a DRE of -4.9±0.7 Wm^{-2} and -11.8±1.9 Wm^{-2} at the TOA and surface, respectively. Overall, in comparison to that over ocean, the DRE estimates over land are more poorly constrained by observations and have larger uncertainties. At regional scales, differences between measurement-based approaches or between measurements and models are larger than those at a global scale.

An ensemble of five model simulations gives a DRE that is about 30-50% smaller than the measurement-based estimate. Such discrepancy could be reduced to 15-40% after accounting for cloud contamination in satellite retrievals. The integration of satellite and surface measurements into a *CTM* proves to be a promising and essential approach to producing an optimal description of aerosol distributions and hence aerosol radiative.

Using the quantitative separation of fine and coarse aerosol in enhanced new-generation satellite sensors, the cloud-free DCF by anthropogenic aerosols is estimated to be -1.1±0.37 Wm^{-2} over ocean, about a factor of 2 stronger than model simulated -0.6 Wm^{-2}. Similar DCF estimates are rare over land, but a few studies do suggest that the DCF over land is much more negative than that over ocean. On global average, the measurement-based estimate of DCF ranges from -0.9~ -1.9 Wm^{-2}, again stronger than the model-based estimate of -0.8 Wm^{-2}. Overall, DCF estimates have larger uncertainty than DRE estimates do.

The use of high-quality aerosol measurements from remote sensing and in-situ techniques, along with the improved performance of model simulations in the past decade, has resulted in a new estimate of aerosol climate forcing with reduced uncertainties in IPCC AR4. The aerosol direct climate forcing is estimated to be -0.5±0.4 Wm^{-2} with a medium-low level of scientific understanding. The indirect forcing due to the cloud albedo effect for liquid water clouds is estimated to be -0.7 (ranging from -1.1 to +0.4) Wm^{-2}, with a low level of scientific understanding (Forster et al., 2007). In fact, such progress in quantifying the aerosol direct and indirect forcing plays an exclusively important role in the more definitive assessment of the global anthropogenic radiative forcing as *virtually certainly positive* and conversely *exceptionally unlikely negative* in IPCC AR4 (Haywood and Schulz, 2007).

Despite the substantial progress, several important issues remain, such as measurements of aerosol size distribution, particle shape, absorption, and vertical profiles, and detection of aerosol long-term trend and establishment of its connection with the observed trends of solar radiation reaching the surface. Significant efforts are needed to address them. Current observational capability needs to be continued to construct a long-term data record with consistent accuracy and high quality that can be used to detect long-term trends of aerosol. Along with algorithm refinement for better aerosol optical depth retrievals, future measurements should focus on improved retrievals of such aerosol properties as size distribution, particle shape, absorption, and vertical distribution. Coordinated sub-orbital measurements need to be conducted in context of evaluating and validating remote sensing measurements.

These new measurements are essential to reducing uncertainties associated with the estimate of aerosol climate forcing, in particular the anthropogenic fraction of aerosol, aerosol TOA forcing over land, aerosol forcing at the surface, and aerosol induced increment of atmospheric heating rate profile. Coordinated research strategy need to be developed to synthesize measurements from multiple platforms and sensors for a better characterization of complex aerosol system and to integrate remote sensing measurements into models for a stronger constraint of model simulations.

Finally, *aerosol-cloud interactions* continue to be an enormous challenge from both the observational and modeling perspectives, and progress is crucial if we are to improve our ability to predict climate change. The relatively short lifetimes of aerosol particles (order of days), in addition to the even shorter timescales for cloud formation and dissipation (10s of minutes) make this a particularly difficult challenge. Moreover, the problem requires addressing an enormous range of spatial scales, from the microscale to the global scale. A methodology for integrating observations (in-situ and remote) and models at the range of relevant temporal/spatial scales is crucial if we are to make progress on this problem.

References

Abdou W., D. Diner, J. Martonchik, C. Bruegge, R. Kahn, B. Gaitley, and K. Crean, 2005: Comparison of conincident MISR and MODIS aerosol optical depths over land and ocean scenes containing AERONET sites. *J. Geophys. Res.* **110:** D10S07, doi:10.1029/2004JD004693.

Ackerman A., O. Toon, D. Stevens, A. Heymsfield, V. Ramanathan, and E. Welton, 2000: Reduction of tropical cloudiness by soot. *Science* **288**:1042-1047.

Ackerman T., and G. Stokes, 2003: The Atmospheric Radiation Measurement Program. *Physics Today* **56**:38-44.

Albrecht B., 1989: Aerosols, cloud microphysics, and fractional cloudiness. *Science* **245**:1227-1230.

Alpert P., P. Kishcha, Y. Kaufman, and R. Schwarzbard, 2005: Global dimming or local dimming? Effect of urbanization on sunlight availability. *Geophys. Res. Lett.* **32:**L17802, doi: 10.1029/GL023320.

Anderson T., R. Charlson, S. Schwartz, R. Knutti, O. Boucher, H. Rodhe, and J. Heintzenberg, 2003a: Climate forcing by aerosols - A hazy picture. *Science* **300**:1103-1104.

Anderson T., R. Charlson, D. Winker, J. Ogren, and K. Holmén, 2003b: Mesoscale variations of tropospheric aerosols. *J. Atmos. Sci.,* **60**:119-136.

Anderson T., R. Charlson, N. Bellouin, O. Boucher, M. Chin, S. Christopher, J. Haywood, Y. Kaufman, S. Kinne, J. Ogren, L. Remer, T. Takemura, D. Tanré, O. Torres, C. Trepte, B. Wielicki, D. Winker, and H. Yu, 2005a.: An "A-Train" strategy for quantifying direct aerosol forcing of climate. *Bull. Am. Met. Soc.* **86**:1795-1809.

Anderson T., Y. Wu, D. Chu, B. Schmid, J. Redemann, and O. Dubovik, 2005b: Testing the MODIS satellite retrieval of aerosol fine-mode fraction. *J. Geophys. Res.* **110**: D18204, doi:10.1029/2005JD005978.

Andreae M. O., D. Rosenfeld, P. Artaxo, et al., 2004: Smoking rain clouds over the Amazon. *Science* **303**:1337– 1342.

Arnott W., H. Moosmuller, and C. Rogers, 1997: Photoacoustic spectrometer for measuring light absorption by aerosol: instrument description. *Atmos. Environ.* **33**:2845-2852.

Balkanski Y., M. Schulz, T. Claquin, and S. Guibert, 2007: Reevaluation of mineral aerosol radiative forcings suggests a better agreement with satellite and AERONET data. *Atmos. Chem. Phys.* **7**:81-95.

Bates T., B. Huebert, J. Gras, F. Griffiths, and P. Durkee (1998): The International Global Atmospheric Chemistry (IGAC) Project's First Aerosol Characterization Experiment (ACE-1) - Overview. *J. Geophys. Res*. **103:**16,297-16,318.

Bates T., P. Quinn, D. Coffman, D. Covert, T. Miller, J. Johnson, G. Carmichael, S. uazzotti, D. Sodeman, K. Prather, M. Rivera, L. Russell, and J. Merrill, 2004: Marine boundary layer dust and pollution transport associated with the passage of a frontal system over eastern Asia. *J. Geophys. Res.* **109:**doi:10.1029/2003JD004094.

Bates T., et al., 2006: Aerosol direct radiative effects over the northwestern Atlantic, northwestern Pacific, and North Indian Oceans: estimates based on in-situ chemical and optical measurements and chemical transport modeling. *Atmos. Cehm. Phys.*, **6**:1657-1732.

Bellouin N., O. Boucher, D. Tanré, and O. Dubovik, 2003: Aerosol absorption over the clear-sky oceans deduced from POLDER-1 and AERONET observations. *Geophys. Res. Lett.* **30**:1748, doi:10.1029/2003GL017121.

Bellouin N., O. Boucher, J. Haywood, and M. Reddy, 2005: Global estimates of aerosol direct radiative forcing from satellite measurements. *Nature* **438**:1138-1140, doi:10.1038/nature04348.

Bellouin N., A. Jones, J. Haywood, and S.A. Christopher, 2008: Updated estimate of aerosol direct radiative forcing from satellite observations and comparison against the Hadley Centre climate model. *J. Geophys. Res.* **113**:D10205, doi:10.1029/2007JD009385.

Bond T., and R. Bergstrom, 2006: Light absorption by carbonaceous particles: An investigative review. *Aerosol Sci. Technol*. **40**:27-67.

Boucher O., and D. Tanré, 2000: Estimation of the aerosol perturbation to the Earth's radiative budget over oceans using POLDER satellite aerosol retrievals. *Geophys. Res. Lett.* **27**:1103-1106.

Brennan J., Y. Kaufman, I. Koren, I., and R. Li, 2005: Aerosol-cloud interaction — misclassification of MODIS clouds in heavy aerosol. *IEEE Trans. Geos. Rem. Sens.* **43(4)**:911-915.

Carmichael G., G. Calori, H. Hayami, I. Uno, S. Cho, M. Engardt, S. Kim, Y. Ichikawa, Y. Ikeda, J. Woo, H. Ueda and M. Amann, 2002: The Mics-Asia study: Model intercomparison of long-range transport and sulfur deposition in East Asia. *Atmos. Environ.* **36**:175-199.

Carmichael G., Y. Tang, G. Kurata, I. Uno, D. Streets, N. Thongboonchoo, J. Woo, S. Guttikunda, A. White, T. Wang, D. Blake, E. Atlas, A. Fried, B. Potter, M. Avery, G. Sachse, S. Sandholm, Y. Kondo, R. Talbot, A. Bandy, D. Thorton and A. Clarke, 2003: Evaluating regional emission estimates using the TRACE-P observations. *J. Geophys. Res.* **108**:8810, doi:10.1029/2002JD003116.

Carrico C. et al., 2005: Hygroscopic growth behavior of a carbon-dominated aerosol in Yosemite National Park. *Atmos. Environ.* **39**:1393 – 1404.

Cattrall C., K. Carder, and H. Gordon, 2003: Columnar aerosol single-scattering albedo and phase function retrieved from sky radiance over the ocean: Measurements of Saharan dust. *J. Geophys. Res.* **108**:4287, doi:10.1029/2002JD002497.

Charlson, R., S. Schwartz, J. Hales, R. Cess, R. J. Coakley, Jr., J. Hansen, and D. Hofmann, 1992: Climate forcing by anthropogenic aerosols. *Science* **255**:423-430.

Chin M., R. Rood, S. Lin, J. Muller, and A. Thompson, 2000a: Atmospheric sulfur cycle simulated in the global model GOCART: Model description and global properties. *J. Geophys. Res.* **105**:24671-24687.

Chin M., D. Savoie, B. Huebert, A. Bandy, D. Thornton, T. Bates, P. Quinn, E. Saltzman, and W. De Bruyn, 2000b: Atmospheric sulfur cycle simulated in the global model GOCART: Comparison with field observations and regional budgets. *J. Geophys. Res.*, **105**:24689-24712.

Chin M., P. Ginoux, S. Kinne, O. Torres, B. Holben, B. Duncan, R. Martin, J. Logan, A. Higurashi, and T. Nakajima, 2002: Tropospheric aerosol optical thickness from the GOCART model and comparisons with satellite and sun photometer measurements. *J. Atmos., Sci.* **59**:461-483.

Chin M., P. Ginoux, R. Lucchesi, B. Huebert, R. Weber, T. Anderson, S. Masonis, B. Blomquist, A. Bandy, and D. Thornton, 2003: A global aerosol model forecast for the ACE-Asia field experiment. *J. Geophys. Res.,* **108**:8654, doi:10.1029/2003JD003642,.

Chin, M., D. Chu, R. Levy, L. Remer, Y. Kaufman, B. Holben, T. Eck, and P. Ginoux, 2004: Aerosol distribution in the northern hemisphere during ACE-Asia: Results from global model, satellite observations, and sunphotometer measurements. *J. Geophy. Res.* **109**:D23S90, doi:10.1029/2004JD004829.

Chou M., P. Chan, and M. Wang, 2002: Aerosol radiative forcing derived from SeaWiFS-retrieved aerosol optical properties. *J. Atmos. Sci.*. **59**:748-757.

Christopher S., and J. Zhang, 2002a: Shortwave aerosol radiative forcing from MODIS and CERES observations over the oceans. *Geophys. Res., Lett.* **29**:1859, doi:10.1029/2002GL014803.

Christopher S., J. Zhang, Y. Kaufman, and L. Remer, 2006: Satellite-based assessment of top of atmosphere anthropogenic aerosol radiative forcing over cloud-free oceans. *Geophys. Res. Lett.* **33:**L15816.

Chu D., Y. Kaufman, C. Ichoku, L. Remer, D. Tanré, and B. Holben, 2002: Validation of MODIS aerosol optical depth retrieval over land. *Geophys. Res. Lett.* **29**, doi:10.1029/2001/GL013205.

Chung C., V. Ramanathan, D. Kim, and I. Podgomy, 2005: Global anthropogenic aerosol direct forcing derived from satellite and ground-based observations. *J. Geophys. Res.* **110:**D24207, doi:10.1029/2005JD006356.

Clarke A., and R. Charlson, 1985: Radiative properties of the background aerosol: Absorption component of extinction. *Science* **229**:263-265.

Collins W., P. Rasch, B. Eaton, B. Khattatov, J. Lamarque, and C. Zender, 2001.: Simulating aerosols using a chemical transport model with assimilation of satellite aerosol retrievals: Methodology for INDOEX. *J. Geophys. Res.* **106**:7313—7336.

Costa M., A. Silva, and V. Levizzani, 2004a: Aerosol characterization and direct radiative forcing assessment over the ocean. Part I: Methodology and sensitivity analysis. *J. Appl. Meteorol.* **43:**1799-1817.

Costa M., A. Silva AM, and V. Levizzani, 2004b: Aerosol characterization and direct radiative forcing assessment over the ocean. Part II: Application to test cases and validation. *J. Appl. Meteorol.* **43:**1818-1833.

de Gouw J., et al., 2005: Budget of organic carbon in a polluted atmosphere: Results from the New England Air Quality Study in 2002. *J. Geophys. Res.* **110:**D16305, doi:10.1029/2004JD005623.

Delene D. and J. Ogren, 2002: Variability of aerosol optical properties at four North American surface monitoring sites. *J. Atmos. Sci.* **59**:1135-1150.

Deuzé J., F. Bréon, C. Devaux, P. Goloub, M. Herman, B. Lafrance, F. Maignan, A. Marchand, F. Nadal, G. Perry, and Tanré, D.: Remote sensing of aerosols over land surfaces from POLDER-ADEOS-1 polarized measurements. *J. Geophys. Res.* **106**:4913-4926, 2001.

Diner, D., J. Beckert, T. Reilly, et al., 1998: Multiangle Imaging SptectrRadiometer (MISR) description and experiment overview. *IEEE Trans. Geosci. Remote. Sens.* **36**:1072-1087.

Diner D., J. Beckert, G. Bothwell and J. Rodriguez, J2002: Performance of the MISR instrument during its first 20 months in Earth orbit. *IEEE Trans. Geosci. Remote Sens.* **40**:1449-1466.

Diner D., T. Ackerman, T. Anderson, et al.: Progressive Aerosol Retrieval and Assimilation Global Observing Network (PARAGON): An integrated approach for characterizing aerosol climatic and environmental interactions. *Bull. Amer. Meteo. Soc.,* **85**:1491-1501.

Dubovik O., A. Smirnov, B. Holben, M. King, Y. Kaufman, and Slutsker, 2000: Accuracy assessments of aerosol optical properties retrieved from AERONET sun and sky radiance measurements. *J. Geophys. Res.* **105**:9791-9806.

Dubovik O., and M. King, 2000: A flexible inversion algorithm for retrieval of aerosol optical properties from Sun and sky radiance measurements. *J. Geophys. Res.,* **105:**20673-20696.

Dubovik O., B. Holben, T. Eck, A. Smirnov, Y. Kaufman,]M. King, D. Tanré, and I. Slutsker, 2002: Variability of absorption and optical properties of key aerosol types observed in worldwide locations. *J. Atmos. Sci.* **59:**590-608.

Dubovik O., T. Lapyonok, Y. Kaufman, M. Chin, P. Ginoux, and A. Sinyuk, 2007: Retrieving global sources of aerosols from MODIS observations by inverting GOCART model, *Atmos. Chem. Phys. Discuss.* **7**:3629-3718.

Dufresne J., C. Gautier, P. Ricchizzi, and Y. Fouquart, 2002: Longwave scattering effects of mineral aerosols. *J. Atmos. Sci.,* **59**:1959-1966.

Eck T., B. Holben, J. Reid, O. Dubovik, A. Smirnov, N. O'Neill, I. Slutsker, and S. Kinne, 1999: Wavelength dependence of the optical depth of biomass burning, urban and desert dust aerosols. *J. Geophys. Res.* **104**:31333-31350.

Eck T., B. Holben, and J. Reid, et al., 2003: High aerosol optical depth biomass burning events: A comparison of optical properties for different source regions. *Geophys. Res. Lett.*, **30**:2035, doi:10.1029/2003GL017861.

Fehsenfeld F., et al., 2006:International Consortium for Atmospheric Research on Transport and Transformation (ICARTT): North America to Europe—Overview of the 2004 summer field study. *J. Geophys. Res.,* **111:**D23S01, doi:10.1029/2006JD007829.

Feingold G., W. Eberhard, D. Veron, and M. Previdi, 2003: First measurements of the Twomey aerosol indirect effect using ground-based remote sensors. *Geophys. Res. Lett.* **30**:1287, doi:10.1029/2002GL016633.

Feingold, G., Remer, L. A., Ramaprasad, J. and Kaufman, Y. J., 2001: Analysis of smoke impact on clouds in Brazilian biomass burning regions: An extension of Twomey's approach., J. Geophys. Res., **106**, 22,907-922,922.

Feingold G., H. Jiang, and J. Harrington, 2005: On smoke suppression of clouds in Amazonia. *Geophys. Res. Lett.* **32**:L02804, doi:10.1029/2004GL021369.

Ferrare R., D. Turner, L. Brasseur, W. Feltz, O. Dubovik, and T. Ackerman, 2001: Raman lidar measurements of the aerosol extinction-to-backscatter ratio over the Southern Great Plains. *J. Geophys. Res.,* **106**:20333-20347.

Ferrare R., G. Feingold, S. Ghan, J. Ogren, B. Schmid, S.E. Schwartz, and P. Sheridan, 2006: Preface to special section: Atmospheric Radiation Measurement Program May 2003 Intensive Operations Period examining aerosol properties and radiative influences. *J. Geophys. Res.* **111:**D05S01, doi:10.1029/2005JD006908.

Forster P., et al., 2007: Changes in Atmospheric Constituents and in Radiative Forcing. *In: Climate Change 2007: The Physical Science Basis, Contribution of Working Group I to the Fourth Assessment Report of the Intergovermental Panel on Climate Change* [Solomon, S., et al. (eds.)], Cambridge University Press, Cambridge, UK, and New York, NY, USA.

Fraser R. and Y. Kaufman, 1985: The relative importance of aerosol scattering and absorption in Remote Sensing. *Transactions on Geoscience and Remote Sensing,* GE-**23**:625-633.

GAMDT - Geophysical Fluid Dynamics Laboratory (GFDL) Global Atmospheric Model Development Team, 2004: The new GFDL global atmosphere and land model AM2-LM2: Evaluation with prescribed SST Simulations. *J. Climate,* **17:**4641-4673.

Garrett T., C. Zhao, X. Dong, G. Mace, and P. Hobbs, 2004: Effects of varying aerosol regimes on low-level Arctic stratus. *Geophys. Res. Lett.* **31:**L17105, doi:10.1029/2004GL019928.

Geogdzhayev I., M. Mishchenko, W. Rossow, B. Cairns, B., and A. Lacis, 2002: Global two-channel AVHRR retrievals of aerosol properties over the ocean for the period of NOAA-9 observations and preliminary retrievals using NOAA-7 and NOAA-11 data. *J. Atmos. Sci.*, **59**:262--278.

Ginoux P., M. Chin, I. Tegen, J. Prospero, B. Holben, O. Dubovik, and S. Lin, 2001: Sources and distributions of dust aerosols simulated with the GOCART model. *J. Geophys. Res.* **106:**20225-20273.

Ginoux P., J. Prospero, O. Torres, and M. Chin, 2004: Long-term simulation of dust distribution with the GOCART model: Correlation with the North Atlantic Oscillation. *Environ. Modeling and Software* **19**:113-128.

Han, Q., W. B. Rossow, J. Chou, and R. M. Welch, Global survey of the relationship of cloud albedo and liquid water path with droplet size using ISCCP, 1998: *J. Clim*., **11**, 1516– 1528.

Hansen J., M. Sato, and R. Ruedy, 1997: Radiative forcing and climate response. *J. Geophys. Res.* **102**:6831-6864.

Harrison L., J. Michalsky, and J. Berndt, 1994: Automated multifilter rotating shadowband radiometer: An instrument for optical depth and radiation measurements. *Applied Optics* **33**:5118-5125.

Haywood J. and K. Shine, 1995: The effect of anthropogenic sulfate and soot aerosol on the clear sky planetary radiation budget. *Geophys. Res. Lett*. **22**:603-606.

Haywood J., and O. Boucher, 2000: Estimates of the direct and indirect radiative forcing due to tropospheric aerosols: A review. *Rev. Geophys.* **38**:513-543.

Haywood J., P. Francis, S. Osborne, M. Glew, N. Loeb, E. Highwood, D. Tanré, E. Myhre, P. Formenti, and E. Hirst, 2003: Radiative properties and direct radiative effect of Saharan dust measured by the C-130 aircraft during SHADE: 1.Solar spectrum. *J. Geophys. Res.* **108**:8577, doi:10.1029/2002JD002687.

Haywood J., S. Osborne, and S. Abel, 2004: The effect of overlying absorbing aerosol layers on remote sensing retrievals of cloud effective radius and cloud optical depth. *Quart. J. Roy. Met. Soc.* **130**:779-800.

Haywood J., R. Allan, I. Culverwell, T. Slingo, S. Milton, J. Edwards, and N. Clerbaux, 2005: Can desert dust explain the outgoing longwave radiation anomaly over the Sahara during July 2003? *J. Geophys. Res.* **110**:D05105, doi:10.1029/2004JD005232.

Haywood J., and M. Schulz, 2007: Causes of the reduction in uncertainty in the anthropogenic radiative forcing of climate between IPCC (2001) and IPCC (2007). *Geophys. Res. Lett.* **34**:L20701, doi:10.1029/2007GL030749.

Heintzenberg J., H. Graf, R. Charlson, and P. Warneck, 1996: Climate forcing and the physicochemical life cycle of the atmospheric aerosol - Why do we need an integrated, interdisciplinary global research programme? *Beitr. Phys. Atmosph.* **69**:261-271.

Heintzenberg J., R. Charlson, A. Clarke, et al., 1997: Measurements and modeling of aerosol single-scattering albedo: progress, problems and prospects. *Beitr.Phys. Atmosph.* **70**:249-263.

Herman J., P. Bhartia, O. Torres, C. Hsu, C. Seftor, and E. Celarier, 1997: Global distribution of UV-absorbing aerosols from Nimbus-7/TOMS data. *J. Geophys. Res.* **102**:16911--16922.

Highwood E., J. Haywood, M. Silverstone, S. Newman, and J. Taylor 2003: Radiative properties and direct effect of Saharan dust measured by the C-130 aircraft during Saharan Dust Experiment (SHADE): 2. Terrestrial spectrum. *J. Geophys. Res.* **108**: 8578, doi:10.1029/2002JD002552.

Hoff R. et al., 2002: Regional East Atmospheric Lidar Mesonet: REALM, in *Lidar Remote Sensing in Atmospheric and Earth Sciences*, edited by L. Bissonette, G. Roy, and G. Vallée, pp. 281-284, Def. R&D Can. Valcartier, Val-Bélair, Que..

Hoff R., J. Engel-Cox, N. Krotkov, S. Palm, R. Rogers, K. McCann, L. Sparling, N. Jordan, O. Torres, and J. Spinhirne, 2004: Long-range transport observations of two large forest fire plumes to the northeastern U.S., in *22nd International Laser Radar Conference, ESA Spec. Publ., SP-***561**:683-686.

Holben B., T. Eck, I. Slutsker, et al., 1998: AERONET - A federated instrument network and data archive for aerosol characterization. *Remote Sens. Environ.* **66**:1-16.

Holben B., D. Tanré, A. Smirnov, et al., 2001: An emerging ground-based aerosol climatology: aerosol optical depth from AERONET. *J. Geophys. Res.* **106**:12067-12098.

Horvath H., 1993: Atmospheric light absorption -- A review. *Atmos. Environ.* **27A**:293-317.

Hsu N., S. Tsay, M. King, and J. Herman, 2004: Aerosol properties over bright-reflecting source regions. *IEEE Trans. Geosci. Remote Sens.* **42:**557-569.

Hsu N., J. Herman, and C. Weaver, 2000: Determination of radiative forcing of Saharan dust using combined TOMS and ERBE data. *J. Geophys. Res.* **105**:20649-20661.

Huebert B., T. Bates, P. Russell, G. Shi, Y. Kim, K. Kawamura, G. Carmichael, and T. Nakajima, 2003: An overview of ACE-Asia: strategies for quantifying the relationships between Asian aerosols and their climatic impacts. *J. Geophys. Res*. **108**:8633, doi:10.1029/2003JD003550.

Husar R., J. Prospero, and L. Stowe, 1997: Characterization of tropospheric aerosols over the oceans with the NOAA advanced very high resolution radiometer optical thickness operational product. *J. Geophys. Res.* **102**:16889-16909.

Ichoku C., L. Remer, and T. Eck, 2005: Quantitative evaluation and intercomparison of morning and afternoon MODIS aerosol measurements from Terra and Aqua satellites. *J. Geophys. Res.* **110**:D10S03, doi:10.1029/2004JD004987.

IPCC (Intergovernmental Panel on Climate Change), 2001: Radiative forcing of climate change, in Climate Change 2001, Cambridge Univ. Press, New York, Cambridge University Press, 2001.

Jacob D., J. Crawford, M. Kleb, V. Connors, R.J. Bendura, J. Raper, G. Sachse, J. Gille, L. Emmons, and C. Heald, 2003: The Transport and Chemical Evolution over the Pacific (TRACE-P) aircraft mission: design, execution, and first results. *J. Geophys. Res.* **108:**9000, 10.1029/2002JD003276.

Jacobson M., 2000: A physically-based treatment of elemental carbon optics: Implications for global direct forcing of aerosols. *Geophys. Res. Lett*. **27**:217-220.

Jacobson M., 2001: Strong radiative heating due to the mixing state of black carbon in atmospheric aerosols. *Nature* **409**:695-697.

Jeong M., Z. Li, D. Chu, and S. Tsay, 2005: Quality and Compatibility Analyses of Global Aerosol Products Derived from the Advanced Very High Resolution Radiometer and Moderate Resolution Imaging Spectroradiometer. *J. Geophys. Res.* **110**:D10S09, doi:10.1029/2004JD004648.

Jiang, H., and G. Feingold, 2006: Effect of aerosol on warm convective clouds: Aerosol-cloud-surface flux feedbacks in a new coupled large eddy model. *J. Geophys. Res.*, **111**: D01202, doi:10.1029/2005JD006138.

Kahn R., W. Li, C. Moroney, D. Diner, J. Martonchik, and E. Fishbein, 2007: Aerosol source plume physical characteristics from space-based multiangle imaging. *J. Geophys. Res.* **112**:D11205, doi:10.1029/2006JD007647.

Kahn R., R. Gaitley, J. Martonchik, D. Diner, K. Crean, and B. Holben, 2005a: MISR global aerosol optical depth validation based on two years of coincident AERONET observations. *J. Geophys. Res.*

110:D10S04, doi:10.1029/2004JD004706.
Kahn R., W. Li, J. Martonchik, C. Bruegge, D. Diner, B. Gaitley, W. Abdou, O. Dubovik, B. Holben, A. Smirnov, Z. Jin, and D. Clark, 2005b: MISR low-light-level calibration, and implications for aerosol retrieval over dark water. *J. Atmos. Sci.* **62:**1032-1052.
Kahn R., J. Ogren, T. Ackerman, et al., 2004a: Aerosol data sources and their roles within PARAGON. *Bull. Amer. Meteor. Soc.* **85**:1511-1522.
Kahn R., J. Anderson, T. Anderson, et al., 2004b: Environmental snapshots from ACE-Asia. *J. Geophys. Res.* **109**:doi:2003JD004339.
Kahn R., P. Banerjee, and D. McDonald, 2001: The sensitivity of multiangle imaging to natural mixtures of aerosols over ocean. *J. Geophys. Res.* **106**:18219-18238.
Kalashnikova O., R. Kahn, I. Sokolik, and W. Li, 2005: The ability of multi-angle remote sensing observations to identify and distinguish mineral dust types: Optical models and retrievals of optically thick plumes. *J. Geophys. Res.* **110**:D18S14, doi:10.1029/2004JD004550.
Kaufman Y., 1987: Satellite Sensing of Aerosol Absorption, *J. Geophys. Res.*, **92:**4307-4317.
Kaufman, Y. J. and Nakajima, T., 1993: Effect of Amazon smoke on cloud microphysics and albedo-Analysis from satellite imagery, *J. Applied Meteor*. **32**:729-744.
Kaufman, Y. and R. Fraser, 1997: The effect of smoke particles on clouds and climate forcing. *Science* **277**:1636-1639.
Kaufman Y., D. Tanré, L. Remer, E. Vermote, A. Chu, and B. Holben, 1997: Operational remote sensing of tropospheric aerosol over land from EOS moderate resolution imaging spectroradiometer. *J. Geophys. Res.* **102**:17051-17067.
Kaufman Y., B. Holben, D. Tanré, I. Slutsker, A. Smirnov, and T. Eck, 2000: Will aerosol measurements from Terra and Aqua polar orbiting satellites represent daily aerosol abundance and properties? *Geophys. Res. Lett.* **27**:3861-3864.
Kaufman Y., D. Tanré, O. Dubovik, A. Karnieli, and L. Remer, 2001: Absorption of sunlight by dust as inferred from satellite and ground-based measurements. *Geophys. Res., Lett.* **28**:1479-1482.
Kaufman Y., D. Tanré, and O. Boucher, 2002a: A satellite view of aerosols in the climate system. *Nature* **419**: doi:10.1038/nature01091.
Kaufman Y., J. Martins, L. Remer, M. Schoeberl, and M. Yamasoe, 2002b: Satellite retrieval of aerosol absorption over the oceans using sunglint. *Geophys. Res. Lett.* **29**: 1928, doi:10.1029/2002GL015403.
Kaufman Y., J. Haywood, P. Hobbs, W. Hart, R. Kleidman, and B. Schmid, 2003: Remote sensing of vertical distributions of smoke aerosol off the coast of Africa. *Geophys. Res. Lett.* **30**:1831, doi:10.1029/2003GL017068.
Kaufman Y., O. Boucher, D. Tanré, M. Chin, L. Remer, and T. Takemura, 2005a: Aerosol anthropogenic component estimated from satellite data. *Geophys. Res. Let.* **32**: L17804, doi:10.1029/2005GL023125.
Kaufman Y., L. Remer, D. Tanré, R. Li, R. Kleidman, S. Mattoo, R. Levy, T. Eck, B. Holben, C. Ichoku, J. Martins, and I. Koren, 2005b: A critical examination of the residual cloud contamination and diurnal sampling effects on MODIS estimates of aerosol over ocean. *IEEE Trans. on Geoscience & Remote Sensing,* **43**:2886-2897.
Kaufman, Y. J., I. Koren, L. A. Remer, D. Rosenfeld and Y. Rudich, 2005: The effect of smoke, dust, and pollution aerosol on shallow cloud development over the Atlantic Ocean, *Proc. Nat. Acad. Sci.*, **102**:11207-11212.

Kaufman, Y. J. and Koren, I., 2006: Smoke and pollution aerosol effect on cloud cover. *Science* **313**:655-658.

Keil A., and J. Haywood, 2003: Solar radiative forcing by biomass burning aerosol particles during SAFARI-2000: A case study based on measured aerosol and cloud properties. *J. Geophys. Res.* **108**:8467, doi:10.1029/2002JD002315.

Kim B.-G., S. Schwartz, M. Miller, and Q. Min, 2003: Effective radius of cloud droplets by ground-based remote sensing: Relationship to aerosol. *J. Geophys. Res.* **108**:4740, doi:10.1029/2003JD003721.

King M., Y. Kaufman, D. Tanré, and T. Nakajima, 1999: Remote sensing of tropospheric aerosols: Past, present, and future. *Bull. Am. Meteorol. Soc.* **80**:2229-2259.

King M., S. Platnick, C. Moeller, Revercomb, and D. Chu, 2003: Remote sensing of smoke, land, and clouds from the NASA ER-2 during SAFARI 2000. *J. Geophys. Res.* **108:**8502, doi:10.1029/2002JD003207.

Kinne S., M. Schulz, C. Textor, et al., 2006: An AeroCom initial assessment -- optical properties in aerosol component modules of global models. *Atmos. Chem. Phys.* **6**:1815-1834.

Kleidman R., N. O'Neill, L. Remer, Y. Kaufman, T. Eck, D. Tanré, O. Dubovik, and B. Holben, 2005: Comparison of Moderate Resolution Imaging Spectroradiometer (MODIS) and Aerosol Robotic Network (AERONET) remote-sensing retrievals of aerosol fine mode fraction over ocean. *J. Geophys. Res.* **110**:D22205, doi:10.1029/2005JD005760.

Koch D., and J. Hansen, 2005: Distant origins of Arctic black carbon: A Goddard Institute for Space Studies ModelE experiment. *J. Geophys. Res.* **110**: D04204, doi:10.1029/2004JD005296.

Koch D., G. Schmidt, and C. Field, 2006: Sulfur, sea salt and radionuclide aerosols in GISS ModelE. *J. Geophys. Res.* **111**:D06206, doi:10.1029/2004JD005550.

Koren I., Y. Kaufman, L. Remer, and J. Martins, 2004: Measurement of the effect of Amazon smoke on inhibition of cloud formation. *Science* **303**:1342.

Koren, I., Kaufman, Y. J., Rosenfeld, D., Remer, L. A. and Rudich, Y., 2005: Aerosol invigoration and restructuring of Atlantic convective clouds, *Geophys. Res. Lett.*, **32**:doi:10.1029/2005GL023187.

Koren I., L. Remer, Y. Kaufman, Y. Rudich, and J. Martins, 2007a: On the twilight zone between clouds and aerosols. *Geophys. Res. Lett.* **34**:L08805, doi:10.1029/2007GL029253.

Koren I., L. Remer, and K. Longo, 2007b: Reversal of trend of biomass burning in the Amazon. *Geophys. Res. Lett.* **34**: L20404, doi:10.1029/2007GL031530.

Lau K., M. Kim, and K. Kim, 2006: Asian summer monsoon anomalies induced by aerosol direct forcing - the role of the Tibetan Plateau. *Climate Dynamics* **36**:855-864, doi:10.1007/s00382-006-10114-z.

Leahy L., T. Anderson, T. Eck, and R. Bergstrom, 2007: A synthesis of single scattering albedo of biomass burning aerosol over southern Africa during SAFARI 2000. *Geophys. Res. Lett.* **34:**L12814, doi:10.1029/2007GL029697.

Lee T., et al., 2006: The NPOESS VIIRS day/night visible sensor. *Bull. Amer. Meteorol. Soc.* **87**:191-199.

Léon J., D. Tanré, J. Pelon, Y. Kaufman, J. Haywood, and B. Chatenet, 2003: Profiling of a Saharan dust outbreak based on a synergy between active and passive remote sensing. *J. Geophys. Res.* **108**:8575, doi:10.1029/2002JD002774.

Levy R., L. Remer, and O. Dubovik, 2007a: Global aerosol optical properties and application to MODIS aerosol retrieval over land. *J. Geophys. Res.* **112**:D13210, doi:10.1029/2006JD007815.

Levy R., L. Remer, S. Mattoo, E. Vermote, and Y. Kaufman, 2007b: Second-generation algorithm for retrieving aerosol properties over land from MODIS spectral reflectance. *J. Geophys. Res.* **112**:D13211, doi:10.1029/2006JD007811.

Li Z., et al., 2007: Preface to special section on East Asian studies of tropospheric aerosols: An international regional experiment (EAST-AIRE). *J. Geophys. Res.* **112:**D22s00, doi:10.0129/2007JD008853.

Liu H., R. Pinker, and B. Holben, 2005: A global view of aerosols from merged transport models, satellite, and ground observations. *J. Geophys. Res.* **110**:D10S15, doi:10.1029/2004JD004695.

Liu X., J. Penner, B. Das, D. Bergmann, J. Rodriguez, S. Strahan, M. Wang, and Y. Feng, 2007: Uncertainties in global aerosol simulations: Assessment using three meteorological data sets. *J. Geophys. Res.*, **112**:D11212, doi: 10.1029/2006JD008216.

Li R., Y. Kaufman, W. Hao, I. Salmon, and B. Gao, 2004: A technique for detecting burn scars using MODIS data. *IEEE Trans. on Geoscience & Remote Sensing* **42**:1300-1308.

Loeb N., and S. Kato, 2002: Top-of-atmosphere direct radiative effect of aerosols over the tropical oceans from the Clouds and the Earth's Radiant Energy System (CERES) satellite instrument. *J. Climate* **15**:1474-1484.

Loeb N., and N. Manalo-Smith, 2005: Top-of-Atmosphere direct radiative effect of aerosols over global oceans from merged CERES and MODIS observations. *J. Clim.* **18**:3506-3526.

Lubin D., S. Satheesh, G. McFarquar, and A. Heymsfield, 2002: Longwave radiative forcing of Indian Ocean tropospheric aerosol. *J. Geophys. Res.* **107**:8004, doi:10.1029/2001JD001183.

Luo Y., D. Lu, X. Zhou, W. Li, and Q. He, 2001: Characteristics of the spatial distribution and yearly variation of aerosol optical depth over China in last 30 years. *J. Geophys. Res.* **106**:14501, doi:10.1029/2001JD900030.

Magi B., P. Hobbs, T. Kirchstetter, T. Novakov, D. Hegg, S. Gao, J. Redemann, and B. Schmid, 2005: Aerosol properties and chemical apportionment of aerosol optical depth at locations off the United States East Coast in July and August 2001. *J. Atmos. Sci.* **62**:919-933.

Malm W., J. Sisler, D. Huffman, R. Eldred, and T. Cahill, 1994: Spatial and seasonal trends in particle concentration and optical extinction in the United States. *J. Geophys. Res.* **99:**1347-1370.

Marshak, A., Knyazikhin, Y., Evans, K., and Wiscombe, W.: The "RED versus NIR" plane to retrieve broken-cloud optical depth from ground-based measurements. *J. Atmos. Sci.* **61:**1911-1925, 2004.

Martins J., P. Artaxo, C. Liousse, J. Reid, P. Hobbs, and Y. Kaufman, 1998: Effects of black carbon content, particle size, and mixing on light absorption by aerosols from biomass burning in Brazil. *J. Geophys. Res.* **103**:32041-32050, 1998.

Martins J., D. Tanré, L. Remer, Y. Kaufman, S. Mattoo, and R. Levy, 2002: MODIS cloud screening for remote sensing of aerosol over oceans using spatial variability. Geophys. Res. Lett. **29:**10.1029/2001GL013252.

Martonchik J., D. Diner, B. Pinty, M. Verstraete, R. Myneni, Y. Knjazikhin, and H. Gordon, 1998b: Determination of land and ocean reflective, radiative, and biophysical properties using multiangle imaging. *IEEE Trans. Geosci. Remote Sens.* **36**:1266-1281.

Martonchik J., D. Diner,R. Kahn, M. Verstraete, B. Pinty, H. Gordon, and T. Ackerman, 1998a: Techniques for the Retrieval of aerosol properties over land and ocean using multiangle data. *IEEE Trans. Geosci. Remt. Sensing* **36**:1212-1227

Martonchik J., D. Diner, K. Crean, and M. Bull, 2002: Regional aerosol retrieval results from MISR. *IEEE Trans. Geosci. Remote Sens.* **40**:1520-1531.

Massie S., O. Torres, and S. Smith, 2004: Total ozone mapping spectrometer (TOMS) observations of increases in Asian aerosol in winter from 1979 to 2000. *J. Geophys. Res.*, **109**:D18211, doi:10.1029/2004JD004620.

Matsui T., and R. Pielke, Sr., 2006: Measurement-based estimation of the spatial gradient of aeroosl radiative forcing. *Geophys. Res. Lett.* **33**: L11813, doi:10.1029/2006GL025974.

Matthis I., A. Ansmann, D. Müller, U. Wandinger, and D. Althausen, 2004: Multiyear aerosol observations with dual-wavelength Raman lidar in the framework of EARLINET. *J. Geophys. Res.* **109**:D13203, doi:10.1029/2004JD004600.

Michalsky J., J. Schlemmer, W. Berkheiser, et al., 2001: Multiyear measurements of aerosol optical depth in the Atmospheric Radiation Measurement and Quantitative Links program. *J. Geophys. Res.* **106:**12099-12108.

Miller R., R. Cakmur, J. Perlwitz, D. Koch, G. Schmidt, I. Geogdzhayev, P. Ginoux, C. Prigent, and I. Tegen, 2006: Mineral dust aerosols in the NASA Goddard Institute for Space Sciences ModelE atmospheric general circulation model. *J. Geophys. Res.*, **111**:D06208, doi:10.1029/2005JD005796.

Min Q., and L.C. Harrison, 1996: Cloud properties derived from surface MFRSR measurements and comparison with GEOS results at the ARM SGP site. *Geophys. Res. Lett.* **23:**1641- 1644.

Mishchenko M., I. Geogdzhayev, B. Cairns, W. Rossow, and A. Lacis, 1999: Aerosol retrievals over the ocean by use of channels 1 and 2 AVHRR data: Sensitivity analysis and preliminary results. *Appl. Opt.*, **38**:7325-7341.

Mishchenko M., et al., 2007a: Accurate monitoring of terrestrial aerosols and total solar irradiance. *Bull. Amer. Meteorol. Soc.* **88**:677-691.

Mishchenko M., et al., 2007b: Long-term satellite record reveals likely recent aerosol trend. *Science* **315**:1543.

Moody E., M. King, S. Platnick, C. Schaaf, and F. Gao, 2005: Spatially complete global spectral surface albedos: value-added datasets derived from Terra MODIS land products. *IEEE Trans. Geosci. Remote Sens.* **43**:144-158.

Moulin C., H. Godon, V. Banzon, and R. Evans, 2001: Assessment of Sahran dust absorption in the visible from SeaWiFS imagery. *J. Geophys. Res.* **106**:18239-18249.

Murayama T., N. Sugimoto, I. Uno, I., et al., 2001: Ground-based network observation of Asian dust events of April 1998 in East Asia. *J. Geophys. Res.* **106**:18346-18359.

NRC (National Research Council)**,** 2005: Radiative Forcing of Climate Change: Expanding the Concept and Addessing Uncertainties, National Academy Press, Washington D.C. (Available at http://www.nap.edu/openbook/0309095069/html).

NRC (National Research Council), 2001: Climate Change Sciences: An analysis of some key questions, 42pp., National Academy Press, Washington D.C..

Nakajima, T., Higurashi, A., Kawamoto, K. and Penner, J. E., 2001: A possible correlation between satellite-derived cloud and aerosol microphysical parameters., *Geophys. Res. Lett*. **28**:1171-1174.

Norris J., and M. Wild, 2007: Trends in aerosol radiative effects over Europe inferred from observed cloud cover, solar "dimming", and solar "brightening". *J. Geophys. Res.* **112**:D08214, doi:10.1029/2006JD007794.

Novakov T., V. Ramanathan, J. Hansen, T. Kirchstetter, M. Sato, J. Sinton, and J. Sathaye, 2003: Large historical changes of fossil-fuel black carbon emissions. *Geophys. Res. Lett.* **30**:1324, doi:10.1029/2002GL016345.

O'Neill N., T. Eck, A. Smirnov, B. .Holben, and S. Thulasiraman, 2003: Spectral discrimination of coarse and fine mode optical depth. J. Geophys. Res., 108(D17), 4559, doi:10.1029/2002JD002975.

Patterson E., D. Gillete, and B. Stockton, 1977: Complex index of refraction between 300 and 700 nm for Sahara aerosol. *J. Geophys. Res.* **82**:3153-3160.

Penner J., R. Dickinson, and C. O'Neill, 1992: Effects of aerosol from biomass burning on the global radiation budget. *Science* **256**:1432-1434.

Penner J., R. Charlson, J. Hales, et al., 1994: Quantifying and minimizing uncertainty of climate forcing by anthropogenic aerosols, *Bull. Amer. Meteorol. Soc.* **75**:375-400.

Penner J., S. Zhang, M. Chin, et al., 2002: A comparison of model- and satellite-derived aerosol optical depth and reflectivity. *J. Atmos. Sci.* **59**:441--460.

Pinker R., B. Zhang, and E. Dutton, 2005: Do satellite detect trends in surface solar radiation? *Science* **308**:850-854.

Qian Y., W. Wang, L Leung, and D. Kaiser, 2007: Variability of solar radiation under cloud-free skies in China: The role of aerosols. *Geophys. Res. Lett.* **34**:L12804, doi:10.1029/2006GL028800.

Quaas J., O. Boucher, N. Bellouin, and S. Kinne, 2008: Satellite-based estimate of the direct and indirect aerosol climate forcing. *J. Geophys. Res.* **113:**D05204, doi:10.1029/2007JD008962.

Quinn P., T. Anderson, T. Bates, R. Dlugi, J. Heintzenberg, W. Von Hoyningen-Huene, M. Kumula, P. Russel, and E. Swietlicki, 1996: Closure in tropospheric aerosol-climate research: A review and future needs for addressing aerosol direct shortwave radiative forcing. *Contrib. Atmosph. Phys*. **69**:547-577.

Quinn P., D. Coffman, V. Kapustin, T.S. Bates and D.S. Covert, 1998: Aerosol optical properties in the marine boundary layer during ACE 1 and the underlying chemical and physical aerosol properties. *J. Geophys. Res.* **103:**16547 - 16563.

Quinn P. T. Bates, T. Miller, D. Coffman, J. Johnson, J. Harris, J. Ogren, G. Forbes, G., T. Anderson, D. Covert, and M. Rood, 2000: Surface submicron aerosol chemical composition: What fraction is not sulfate? *J. Geophys. Res.* **105**:6785 - 6806.

Quinn P., and T. Bates, 2003: North American, Asian, and Indian haze: Similar regional impacts on climate? *Geophys. Res. Letts.* **30**:1555, doi:10.1029/2003GL016934.

Quinn P. and T. Bates, 2005: Regional Aerosol Properties: Comparisons from ACE 1, ACE 2, Aerosols99, INDOEX, ACE Asia, TARFOX, and NEAQS. *J. Geophys. Res.* **110:**D14202, doi:10.1029/2004JD004755,.

Quinn P., et al., 2005: Impact of particulate organic matter on the relative humidity dependence of light scattering: A simplified parameterization. *Geophys. Res. Lett.,* **32:**L22809, doi:101029/2005GL024322.

Quinn P., T. Bates, D. Coffman, T. Onasch, D. Worsnop, T. Baynard, J. de Gouw, P. Goldan, W. Kuster, E. Williams, J. Roberts, B. Lerner, A. Stohl, A. Pettersson, and E. Lovejoy, 2006: Impacts of sources and aging on submicrometer aerosol properties in the marine boundary layer across the Gulf of Maine. *J. Geophys. Res.* **111:**D23S36, doi:10.1029/2006JD007582.

Raes F., T. Bates, F. McGovern, and M. van Liedekerke, 2000: The 2nd Aerosol Characterization Experiment (ACE-2): General overview and main results. *Tellus* **52B:**111–125.

Ramanathan V., and A. Vogelmann, 1997: Greenhouse Effect, Atmospheric Solar Absorption, and the Earth's Radiation Budget: From the Arrhenius-Langely Era to the 1990's. *Ambio* ***26*:**38-46.

Ramanathan V., P. Crutzen, J. Lelieveld, et al., 2001: Indian Ocean Experiment: An integrated analysis of the climate forcing and effects of the great Indo-Asian haze. *J. Geophys. Res.* **106**:28371-28398.

Ramanathan V., and P. Crutzen, 2003: Atmospheric Brown "Clouds". *Atmos. Environ.* **37**:4033-4035.

Reddy M., and O.Boucher, 2004: A study of the global cycle of carbonaceous aerosols in the LMDZT general circulation model. *J. Geophys. Res.* **109**:D14202, doi:10.1029/2003JD004048.

Reddy M., O. Boucher, C. Venkataraman, S. Verma, J.-F. Le´on, N. Bellouin, and M. Pham, 2004: General circulation model estimates of aerosol transport and radiative forcing during the Indian Ocean Experiment. *J. Geophys. Res.* **109**:D16205, doi:10.1029/2004JD004557.

Reddy M., O. Boucher, N. Bellouin, M. Schulz, Y. Balkanski, J. Dufresne, and M. Pham, 2005a: Estimates of multi-component aerosol optical depth and direct radiative perturbation in the LMDZT general circulation model. *J. Geophys. Res.* **110**:D10S16, doi:10.1029/2004JD004757.

Reddy M., O. Boucher, Y. Balkanski, and M. Schulz, 2005b: Aerosol optical depths and direct radiative perturbations by species and source type. *Geophys. Res. Lett.* **32**: L12803, doi:10.1029/2004GL021743.

Redemann J., P. Russell, and P. Hamill, 2001: Dependence of aerosol light absorption and single-scattering albedo on ambient relative humidity for sulfate aerosols with black carbon cores. *J. Geophys. Res.* **106**:27485-27495.

Redemann J., S. Masonis, B. Schmid, T. Anderson, P. Russell, J. Livingston, O. Dubovik, and A. Clarke, 2003: Clear-column closure studies of aerosols and water vapor aboard the NCAR C-130 during ACE-Asia, 2001. *J. Geophys. Res.* **108:**8655, doi:10.1029/2003JD003442.

Reid J., J. Kinney, and D. Wesphal, et al., 2003: Analysis of measurements of Saharan dust by airborne and groundbased remote sensing methods during the Puerto Rico Dust Experiment (PRIDE). *J. Geophys. Res.* **108**:8586, doi:10.1029/2002JD002493.

Reid J., T. Eck, S. Christopher, R. Koppmann, O. Dubovik, D. Eleuterio, B. Holben, E. Reid, and J. Zhang, 2005: A review of biomass burning emissions part III: intensive optical properties of biomass bunring particles, *Atmos. Chem. Phys.* **5**:827-849.

Reid J., et al., 2008: An overview of UAE2 flight operations: Observations of summertime atmospheric thermodynamic and aerosol profiles of the southern Arabian Gulf. *J. Geophys. Res.* (Submitted).

Remer L., S. Gassó, D. Hegg, Y. Kaufman, and B. Holben, 1997: Urban/industrial aerosol: ground based sun/sky radiometer and airborne in-situ measurements. *J. Geophys. Res.* **102**:16849-16859.

Remer L., D. Tanré, Y. Kaufman, C. Ichoku, S. Mattoo, R. Levy, D. Chu, B. Holben, O. Dubovik, A. Smirnov, J. Martins, R. Li, and Z. Ahman, 2002: Validation of MODIS aerosol retrieval over ocean. *Geophys. Res. Lett.* **29**:doi:10.1029/2001/GL013204.

Remer L., Y. Kaufman, D. Tanré, S. Mattoo, D. Chu, J. Martins, R. Li, C. Ichoku, R. Levy, R. Kleidman, T. Eck, E. Vermote, and B. Holben, 2005: The MODIS aerosol algorithm, products and validation. *J. Atmos. Sci.* **62**:947-973.

Remer L., and Y. Kaufman, 2006: Aerosol direct radiative effect at the top of the atmosphere over cloud free ocean derived from four years of MODIS data. *Atmos. Chem. Phys.* **6**:237-253.

Remer L., Y. Kaufman, and R. Kleidman, 2006: Comparison of three years of Terra and Aqua MODIS aerosol optical thickness over the global oceans. *IEEE Geosci. Remote Sens. Lett.* **3:**537-540.

Rosenfeld D., and I. Lansky, 1998: Satellite-based insights into precipitation formation processes in continental and maritime convective clouds. *Bull. Am. Meteorol. Soc.* **79:**2457-2476.

Russell P., S. Kinne, and R. Bergstrom, 1997: Aerosol climate effects: local radiative forcing and column closure experiments. *J. Geophys. Res.* **102**:9397-9407.

Russell P., J. Livingston, P. Hignett, S. Kinne, J. Wong, A. Chien, R. Bergstrom, P. Durkee, and P. Hobbs, 1999: Aerosol-induced radiative flux changes off the United States mid-Atlantic coast: comparison of values calculated from sun photometer and in-situ data with those measured by airborne pyranometer. *J. Geophys. Res.* **104**:2289-2307.

Salcedo D., T. B. Onasch, K. Dzepina, M. R. Canagaratna, Q. Zhang, J.A. Huffman, P. F. DeCarlo, J. T. Jayne, P. Mortimer, D. R. Worsnop, C. E. Kolb, K. S. Johnson, B. Zuberi, L. C. Marr, R. Volkamer, L. T. Molina, M. J. Molina, B. Cardenas, R. M. BernabÎ, C. M‡rquez, J. S. Gaffney, N. A. Marley, A. Laskin, V. Shutthanandan, Y. Xie, W. Brune, R. Lesher, T. Shirley, and J. L. Jimenez, 2006: Characterization of ambient aerosols in Mexico City during the MCMA-2003 campaign with Aerosol Mass Spectrometry: results from the CENICA Supersite. *Atmos. Chem. Phys.* **6**:925-946.

Sato M., J. Hansen, D. Koch, A. Lacis, R. Ruedy, O. Dubovik, B. Holben, M. Chin, and T. Novakov, 2003: Global atmospheric black carbon inferred from AERONET. *Proc. Nat. Aca. Sci.* **100**:6319-6324.

Saxena P., L. Hildemann, P. McMurry, and J. Seinfeld, 1995: Organics alter hygroscopic behavior of atmospheric particles. *J. Geophys. Res.* **100:**18755-18770.

Schaaf C., F. Gao, A. Strahler, et al., 2002: First operational BRDF, albedo and nadir reflectance products from MODIS. *Remote Sens. Environ.* **83**:135-148.

Schmid B., R. Ferrare, C. Flynn, R. Elleman, D. Covert, A. Strawa, E. Welton, D. Turner, H. Jonsson, J. Redemann, J. Eilers, K. Ricci, A. Hallar, M. Clayton, J. Michalsky, A. Smirnov, B. Holben, and J. Barnard, 2006: How well do state-of-the-art techniques measuring the vertical profile of tropospheric aerosol extinction compare? *J. Geophys. Res.* **111:** doi:10.1029/2005JD005837, 2006.

Schulz M., C. Textor, S. Kinne, et al., 2006: Radiative forcing by aerosols as derived from the AeroCom present-day and pre-industrial simulations. *Atmos. Chem. Phys.*, **6**:5225-5246.

Sekiguchi, M., T. Nakajima, K. Suzuki, et al., A study of the direct and indirect effects of aerosols using global satellite data sets of aerosol and cloud parameters *J. Geophys. Res*, 108, NO. D22, 4699, doi:10.1029/2002JD003359, 2003

Seinfeld J., R. Kahn, T. Anderson, R. Charlson, R. Davies, D. Diner, S. Schwartz, and B. Wielicki, 2004: Scientific objectives, measurement needs, and challenges motivating the PARAGON aerosol initiative. *Bull. Amer. Meteo. Soc.* **85**:1503-1509.

Sheridan P., and J. Ogren, 1999: Observations of the vertical and regional variability of aerosol optical properties over central and eastern North America. *J. Geophys. Res.* **104**:16793-16805.

Slingo A., T. Ackerman, R. Allan, et al., 2006: Observations of the impact of a major Saharan dust storm on the atmospheric radiation balance. *Geophys. Res. Lett.* **33**:L24817, doi:10.1029/2006GL027869.

Smirnov A., B. Holben, T. Eck, O. Dubovik, and I. Slutsker, 2000: Cloud screening and quality control algorithms for the AERONET database. *Rem. Sens. Env.* **73**:337-349.

Smirnov A., B. Holben, T. Eck, I. Slutsker, B. Chatenet, and R. Pinker, 2002: Diurnal variability of aerosol optical depth observed at AERONET (Aerosol Robotic Network) sites. *Geophys. Res. Lett.* **29:**2115, doi:10.1029/2002GL016305.

Smirnov A., B. Holben, S. Sakerin, D. Kabanov, I. Slutsker, M. Chin, T. Diehl, L. Remer, R. Kahn, A. Ignatov, L. Liu, M. Mishchenko, T. Eck, T. Kucsera, D. Giles, and O. Kopelevich, 2006: Ship-based aerosol optical depth measurements in the Atlantic Ocean, comparison with satellite retrievals and GOCART model. *Geophys. Res. Lett.* **33:**L14817, doi: 10.1029/2006GL026051.

Sokolik I., and O. Toon, 1999: Incorporation of mineralogical composition into models of the radiative properties of mineral aerosol from UV to IR wavelengths. *J. Geophys. Res.* **104**:9423-9444, doi:10.1029/1998JD200048.

Sokolik I., D. Winker, G. Bergametti, et al., 2001: Introduction to special section: outstanding problems in quantifying the radiative impacts of mineral dust. *J. Geophys. Res.* **106**:18015-18027.

Solomon P. A., W. Chameides, R. Weber, A. Middlebrook, C. S. Kiang, A. G. Russell, A. Butler, B. Turpin, D. Mikel, R. Scheffe, E. Cowling, E. Edgerton, J. St. John, J. Jansen, P. McMurry, S. Hering, and T. Bahadori, 2003: Overview of the 1999 Atlanta Supersite Project. *J. Geophys. Res.* **108(D7):**8413, doi:10.1029/2001JD001458

Spinhirne J., S. Palm, W. Hart, D. Hlavka, and E. Welton, 2005: Cloud and Aerosol Measurements from the GLAS Space Borne Lidar: initial results. *Geophys. Res. Let.* **32**:L22S03, doi:10.1029/2005GL023507.

Stanhill G., and S. Cohen, 2001: Global dimming: a review of the evidence for a widespread and significant reduction in global radiation with discussion of its probable causes and possible agricultural consequences. *Agricul. Forest Meteorol.* **107**:255-278.

Stephens G., R. Engelen, M. Vaughan, and T. Anderson: Toward retrieving properties of the tenuous atmosphere using space-based lidar measurements. *J. Geophys. Res.* **106**:28143-28157.

Stephens G., D. Vane, R. Boain, G. Mace, K. Sassen, Z. Wang, A. Illingworth, E. O'Conner, W. Rossow, S. Durden, S. Miller, R. Austin, A. Benedetti, and C. Mitrescu, 2002: The CloudSat mission and the A-Train. *Bull. Amer. Meteo. Soc.* **83**:1771-1790.

Stier P., J. Seinfeld, S. Kinne, J. Feichter, and O. Boucher, 2006: Impact of nonabsorbing anthropogenic aerosols on clear-sky atmsopheric absorption. *J. Geophys. Res.* **111**:D18201, doi:10.1029/2006JD007147.

Strawa A., R. Castaneda, T. Owano, P. Baer, and B. Paldus, 2002: The measurement of aerosol optical properties using continuous wave cavity ring-down techniques. *J. Atm. Ocean. Tech.* **20**:454-465.

Streets D., and K. Aunan, 2005: The importance of China's household sector for black carbon emissions. *Geophys. Res. Lett.* **32**:L12708, doi:10.1029/2005GL022960.

Streets D., T. Bond, T. Lee, and C. Jang, 2004: On the future of carbonaceous aerosol emissions. *J. Geophys. Res.* **109**:D24212, doi:10.1029/2004JD004902.

Streets D., Q. Zhang, L. Wang, K. He, J. Hao, Y. Tang, and G. Carmichael, 2006a: Revisiting China's CO emissions after TRACE-P: Synthesis of inventories, atmospheric modeling and observations *J. Geophys. Res.* **111:**D14306, doi:10.1029/2006JD007118.

Streets D., Y. Wu, and M. Chin, 2006b: Two-decadal aerosol trends as a likely explanation of the global dimming/brightening transition. *Geophys. Res. Lett.* **33**:L15806, doi:10.1029/2006GL026471.

Takemura T., H. Okamoto, Y. Maruyama, A. Numaguti, A. Higurashi, and T. Nakajima, 2000: Global three-dimensional simulation of aerosol optical thickness distribution of various origins. *J. Geophys. Res.* **105**:17853-17873.

Takemura T., T. Nakajima, O. Dubovik, B. Holben, and S. Kinne, 2002: Single-scattering albedo and radiative forcing of various aerosol species with a global three-dimensional model. *J. Climate*, **15**:333-352.

Takemura, T., T. Nozawa,S. Emori, T. Nakajima, and T. Nakajima, 2005: Simulation of climate response to aerosol direct and indirect effects with aerosol transport-radiation model. *J. Geophys. Res.* **110**:D02202, doi:10.1029/2004JD005029.

Tang Y., G. Carmichael, I. Uno, J. Woo, G. Kurata, B. Lefer, R. Shetter, H. Huang, B. Anderson, M. Avery, A. Clarke and D. Blake, 2003: Influences of biomass burning during the Transport and Chemical Evolution Over the Pacific (TRACE-P) experiment identified by the regional chemical transport model. *J. Geophys. Res.* **108:**8824, doi:10.1029/2002JD003110.

Tang Y., G. Carmichael, J. Seinfeld, D. Dabdub, R. Weber, B. Huebert, A. Clarke, S. Guazzotti, D. Sodeman, K. Prather, I. Uno, J. Woo, D. Streets, P. Quinn, J. Johnson, C. Song, A. Sandu**,** R. Talbot and J. Dibb, 2004: Three-dimensional simulations of inorganic aerosol distributions in East Asia during spring 2001. *J. Geophys. Res.* **109**:D19S23, doi:10.1029/2003JD004201.

Tanré D., Y. Kaufman, M. Herman, and S. Mattoo, 1997: Remote sensing of aerosol properties over oceans using the MODIS/EOS spectral radiances. *J. Geophys. Res.*, **102**:16971-16988.

Tanré D., J. Haywood, J. Pelon, J. Léon, B. Chatenet, P. Formenti, P. Francis, P. Goloub, E. Highwood, and G. Myhre, 2003: Measurement and modeling of the Saharan dust radiative impact: Overview of the Saharan Dust Experiment (SHADE). *J. Geophys. Res.* **108**:8574, doi:10.1029/2002JD003273.

Tegen I., and I. Fung, 1995: Contribution to the atmospheric mineral aerosol load from land surface modification. *J. Geophys. Res.* **100**:18707-17726.

Tegen I., M. Werner, S. Harrison, and K. Kohfeld, 2004: Relative importance of climate and land use in determining present and future global soil dust emission. *Geophy. Res. Lett.* **31**:L05105, doi:10.1029/2003GL019216.

Textor C., M. Schulz, S. Guibert, et al., 2006: Analysis and quantification of the diversities of aerosol life cycles within AEROCOM. *Atmos. Chem. Phys.* **6**:1777-1813.

Torres O., P. Bhartia, J. Herman, Z. Ahmad, and J. Gleason, 1998: Derivation of aerosol properties from satellite measurements of backscattered ultraviolet radiation: Theoretical bases. *J. Geophys. Res.* **103**:17009-17110.

Torres O., P. Bhartia, J. Herman, A. Sinyuk, P. Ginoux, and B. Holben, 2002: A long-term record of aerosol optical depth from TOMS observations and comparison to AERONET measurements. *J. Atmos. Sci.* **59**:398--413.

Torres O., P. Bhartia, A. Sinyuk, E. Welton, and B. Holben, 2005: Total Ozone Mapping Spectrometer measurements of aerosol absorption from space: Comparison to SAFARI 2000 ground-based observations. *J. Geophys. Res.* **110**:D10S18, doi:10.1029/2004JD004611.

Tsvetsinskaya E., C. Schaaf, F. Gao, et al., 2002: Relating MODIS-derived surface albedo to soils and rock types over Northern Africa and the Arabian Peninsula. *Geophys. Res. Lett.* **29**:1353, doi:10.1029/2001GL014096.

Twomey S., 1977: The influence of pollution on the shortwave albedo of clouds. *J. Atmos. Sci.* **34**:1149-1152.

Wang J., S. Christopher, F. Brechtel, J. Kim, B. Schmid, J. Redemann, P. Russell, P. Quinn, and B. Holben, 2003: Geostationary satellite retrievals of aerosol optical thickness during ACE-Asia. *J. Geophys. Res.* **108**:8657, 10.1029/2003JD003580.

Welton E., K. Voss, P. Quinn, P. Flatau, K. Markowicz, J. Campbell, J. Spinhirne, H. Gordon, and J. Johnson, 2002: Measurements of aerosol vertical profiles and optical properties during INDOEX 1999 using micro-pulse lidars. *J. Geophys. Res.* **107**:8019, doi:10.1029/2000JD000038.

Welton E., J. Campbell, J. Spinhirne, and V. Scott, 2001: Global monitoring of clouds and aerosols using a network of micro-pulse lidar systems, in *Lidar Remote Sensing for Industry and Environmental Monitoring*, U. N. Singh, T. Itabe, N. Sugimoto, (eds.), *Proc. SPIE*, **4153**:151-158.

Wen G., A. Marshak, and R. Cahalan, 2006: Impact of 3D clouds on clear sky reflectance and aerosol retrieval in a biomass burning region of Brazil. *IEEE Geo. Rem. Sens. Lett.* **3**:169-172.

Wetzel, M. A. and Stowe, L. L.: Satellite-observed patterns in stratus microphysics, aerosol optical thickness, and shortwave radiative forcing. 1999: *J. Geophys. Res.*, **104**:31287-31299.

Wielicki B., B. Barkstrom, E. Harrison, R. Lee, G. Smith, and J. Cooper, 1996: Clouds and the Earth's radiant energy system (CERES): An Earth observing system experiment. *Bull. Amer. Meteo. Soc.* **77**:853-868.

Wild M., H. Gilgen, A. Roesch, et al., 2005: From dimming to brightening: Decadal changes in solar radiation at Earth's surface. *Science* **308**:847-850.

Winker D., J. Pelon, and M. McCormick, 2003: The CALIPSO mission: spaceborne lidar for observation of aerosols and clouds. *Proc. SPIE* **4893**:1-11.

Yu H., S. Liu, and R. Dickinson, 2002: Radiative effects of aerosols on the evolution of the atmospheric boundary layer. *J. Geophys. Res.* **107:**4142, doi:10.1029/2001JD000754.

Yu H., R. Dickinson, M. Chin, Y. Kaufman, B. Holben, I. Geogdzhayev, and M. Mishchenko, 2003: Annual cycle of global distributions of aerosol optical depth from integration of MODIS retrievals and GOCART model simulations. *J. Geophys. Res.* **108**:4128, doi:10.1029/2002JD002717.

Yu H., R. Dickinson, M. Chin, Y. Kaufman, M. Zhou, L. Zhou, Y. Tian, O. Dubovik, and B. Holben, 2004: The direct radiative effect of aerosols as determined from a combination of MODIS retrievals and GOCART simulations. *J. Geophys. Res.* **109**:D03206, doi:10.1029/2003JD003914.

Yu H., Y. Kaufman, M. Chin, G. Feingold, L. Remer, T. Anderson, Y. Balkanski, N. Bellouin, O. Boucher, S. Christopher, P. DeCola, R. Kahn, D. Koch, N. Loeb, M. S. Reddy, M. Schulz, T. Take-

mura, and M. Zhou, 2006: A review of measurement-based assessments of aerosol direct radiative effect and forcing. *Atmos. Chem . Phys.* **6**:613-666.

Yu H., R. Fu, R. Dickinson, Y. Zhang, M. Chen, and H. Wang, 2007: Interannual variability of smoke and warm cloud relationships in the Amazon as inferred from MODIS retrievals. *Remote Sens. Environ.* **111**:435-449.

Zhang J., and S. Christopher, 2003: Longwave radiative forcing of Saharan dust aerosols estimated from MODIS, MISR, and CERES observations on Terra. *Geophys. Res. Lett.* **30**:2188, doi:10.1029/2003GL018479.

Zhang J., S. Christopher, L. Remer, and Y. Kaufman, 2005a: Shortwave aerosol radiative forcing over cloud-free oceans from Terra. I: Angular models for aerosols. *J. Geophys. Res.* **110**:D10S23, doi:10.1029/2004JD005008.

Zhang J., S. Christopher, L. Remer, and Y. Kaufman, 2005b: Shortwave aerosol radiative forcing over cloud-free oceans from Terra. II: Seasonal and global distributions. *J. Geophys. Res.* **110**:D10S24, doi:10.1029/2004JD005009.

Zhang Q., C.O. Stanier, M.R. Canagaratna, J.T. Jayne, D.R. Worsnop, S.N. Pandis, and J.L. Jimenez, 2004; Insights into the chemistry of new particle formation and growth events in Pittsburgh based on aerosol mass spectrometry. Environ. Sci. Technol. 38(18):4797 -4809, 10.1021/es035417u S0013-936X(03)05417-8.

Zhao T. X.-P., H. Yu, I. Laszlo, M. Chin, and W.C. Conant, 2008: Derivation of component aerosol direct radiative forcing at the top of atmosphere for clear-sky oceans. *J. Quant. Spectro. Rad. Trans.* **109:**1162-1186.

Zhou M., H. Yu, R. Dickinson, O. Dubovik, and B. Holben, 2005: A normalized description of the direct effect of key aerosol types on solar radiation as estimated from AERONET aerosols and MODIS albedos. *J. Geophys. Res.* **110**:D19202, doi:10.1029/2005JD005909.

Acronyms and Symbols

ABC	Asian Brown Cloud
ACE	Aerosol Characterization Experiment
AD-Net	Asian Dust Network
ADEOS	Advanced Earth Observation Satellite
ADM	Angular Dependence Models
AeroCom	Aerosol model and observation intercomparison project
AERONET	Aerosol Robotic Network
AI	Aerosol Index
AIOP	Aerosol Intensive Operative Period
AOD (τ)	Aerosol optical depth
APS	Aerosol Polarimetry Sensor
AR4	IPCC Forth Assessment Report
ARM	Atmospheric Radiation Measurements
AVHRR	Advanced Very High Resolution Radiometer
A-Train	Constellation of six afternoon overpass satellites
BASE-A	Biomass Burning Airborne and Spaceborne Experiment Amazon and Brazil
BRDF	Bidirectional Reflectance Distribution Function
CALIOP	Cloud and Aerosol Lidar with Orthogonal Polarization

1	CALIPSO	Cloud Aerosol Infrared Pathfinder Satellite Observations
2	CCN	Cloud Condensation Nuclei
3	CCRI	Climate Change Research Initiative
4	CCSP	Climate Change Science Program
5	CERES	Clouds and the Earth's Radiant Energy System
6	CLAMS	Chesapeake Lighthouse and Aircraft Measurements for Satellite campaign
7	CTM	Chemical Transport Model
8	DAAC	Distributed Active Archive Center
9	DCF	Direct climate forcing (anthropogenic aerosols)
10	DRE	Direct radiative effect (total aerosols)
11	EARLINET	European Aerosol Research Lidar Network
12	EAST-AIRE	East Asian Studies of Tropospheric Aerosols: An International Regional Experiment
13	EOS	Earth Observing System
14	ERBE	Earth Radiation Budget Experiment
15	$E\tau$	Radiative Efficiency (aerosol radiative effect normalized by AOD)
16	GCM	General Circulation Model
17	GEOS	Goddard Earth Observing System
18	GFDL	Geophysical Fluid Dynamics Laboratory (NOAA)
19	GHGs	Greenhouse Gases
20	GISS	Goddard Institute for Space Studies (NASA)
21	GLAS	Geoscience Laser Altimeter System
22	GMD	Global Modeling Division (NOAA)
23	GMI	Global Modeling Initiative
24	GOCART	Goddard Chemistry Aerosol Radiation and Transport
25	GOES	Geostationary Operational Environmental Satellite
26	GSFC	Goddard Space Flight Center (NASA)
27	ICARTT	International Consortium for Atmospheric Research on Transport and Transformation
28	ICESat	Ice, Cloud, and Land Elevation Satellite
29	IMPROVE	Interagency Monitoring of Protected Visual Environment
30	INCA	Interactions between Chemistry and Aerosol (LMDz model)
31	INDOEX	Indian Ocean Experiment
32	INTEX-NA	Intercontinental Transport Experiment – North America
33	IPCC	Intergovermental Panel on Climate Change
34	IR	Infrared radiation
35	LBA	Large-Scale Biosphere-Atmosphere Experiment in Amazon
36	LMDZ	Laboratoire de Météorologie Dynamique with Zoom
37	LOA	Laboratoire d' Optique Atmosphérique
38	LOSU	Level of Scientific Understanding
39	LWP	Liquid Water Path
40	MAN	Maritime Aerosol Network
41	MFRSR	Multifilter Rotating Shadowband Radiometer
42	MINOS	Mediterranean Intensive Oxidant Study
43	MISR	Multi-angle Imaging SpectroRadiometer
44	MODIS	Moderate Resolution Imaging Spectroradiometer
45	MPLNET	Micro Pulse Lidar Network
46		

NASA	National Aeronautics and Space Administration
NEAQS	New England Air Quality Study
NOAA	National Oceanography and Atmosphere Administration
NPOESS	National Polar-orbiting Operational Environmental Satellite System
NPP	NPOESS Preparatory Project
OMI	Ozone Monitoring Instrument
PARASOL	Polarization and Anisotropy of Reflectance for Atmospheric Science coupled with Observations from a Lidar
PEM-West	Western Pacific Exploratory Mission
POLDER	Polarization and Directionality of the Earth's Reflectance
POM	Particulate Organic Matter
PRIDE	Pueto Rico Dust Experiment
REALM	Regional East Atmospheric Lidar Mesonet
RH	Relative Humidity
RTM	Radiative Transfer Model
SAFARI	South Africa Regional Science Experiment
SCAR-A	Smoke, Clouds, and Radiation – America
SCAR-B	Smoke, Clouds, and Radiation - Brazil
SeaWiFS	Sea-viewing Wide Field-of-view Sensor
SHADE	Saharan Dust Experiment
SMOCC	Smoke, Aerosols, Clouds, Rainfall and Climate
SPRINTARS	Spectral Radiation-Transport Model for Aerosol Species
SSA (ω_0)	Aerosol Single-Scattering Albedo
STEM	Sulfate Transport and Deposition Model
TAR	IPCC Third Assessment Report
TARFOX	Tropospheric Aerosol Radiative Forcing Observational Experiment
TOA	Top-Of-Atmosphere
TOMS	Total Ozone Mapping Spectrometer
TRACE-A	Transport and Chemical Evolution over the Atlantic
TRACE-P	Transport and Chemical Evolution over the Pacific
UAE^2	United Arab Emirates Unified Aerosol Experiment
UV	Ultraviolet radiation

Chapter III. Modeling the Effects of Aerosols on Climate

Author: D. Rind, NASA GISS, **G. Feingold**, NOAA ESRL; **S. E. Schwartz**, DOE BNL.

Table of Contents

3.1. Introduction

A primary conclusion of the recent IPCC (2007) report is the elevation of man's influence on the warming climate to the category of "very likely". This conclusion is based on among other things the ability of models to simulate the global and to some extent regional variations of temperature over the past 100 years. When anthropogenic effects are included, the simulations can reproduce the observed warming; when they are not, the models do not get very much warming at all. Practically all of the models run for this assessment (approximately 20) produce this distinctive result.

Behind this relative unanimity, however, is an inconvenient truth: in order to produce the observed temperature increase trend, models must use very uncertain aerosol forcing. The greenhouse gas change by itself produces warming in models that exceeds that observed on average by some 40% (IPCC, 2007). Cooling associated with aerosols reduces this warming to the correct level. However, to achieve this response, different climate models use differing aerosol forcings, both direct (aerosol scattering and absorption of short and longwave radiation) and indirect (aerosol effect on cloud cover reflectivity and lifetime), whose magnitudes differ markedly. Kiehl (2007) using nine of the IPCC (2007) AR4 climate models found that they had a factor of three forcing difference in the aerosol contribution for the 20th century. The differing aerosol forcing is the prime reason why models whose climate sensitivity varies by almost a factor of three can produce the 'right' answer. Hence the uncertainty in IPCC (2007) anthropogenic climate simulations for the past 100 years should really be much greater than stated (Schwartz et al., 2007; Kerr, 2007). To clarify this issue, we first review how aerosol radiative forcing is estimated.

3.1.1. *Calculating aerosol radiative forcing*

Two different approaches are used to assess the aerosol effect on climate. "Forward modeling" studies incorporate different aerosol types and attempt to explicitly calculate the aerosol radiative forcing. From this approach, IPCC (2007) concluded that the best estimate of aerosol direct radiative forcing (compared with preindustrial times) is –0.5 [±0.4] Wm^{-2}, with the contributions as follows: sulfate, –0.4 [±0.2] Wm^{-2}; fossil fuel organic carbon, –0.05 [±0.05] Wm^{-2}; fossil fuel black carbon, +0.2 [±0.15] Wm^{-2}; biomass burning, +0.03 [±0.12] Wm^{-2}; nitrate, –0.1 [±0.1] Wm^{-2} ; and mineral dust, –0.1 [±0.2] Wm^{-2}. The radiative forcing due to the cloud albedo or brightness effect (also referred to as first indirect or Twomey effect) is estimated to be –0.7 [–1.1, +0.4] Wm^{-2}. No estimate was specified for the second indirect effect, associated with cloud lifetime (which was deemed a 'feedback' rather than a forcing). The total negative radiative forcing due to aerosols according to IPCC (2007) estimates is therefore –1.2 Wm^{-2} [range –0.6 to –2]; in contrast the greenhouse warming (including tropospheric ozone) is estimated to be about 3 Wm^{-2}, hence tropospheric aerosols reduce this influence by 40% [20-80%].

The other method of calculating aerosol forcing is called the 'inverse approach' – it is assumed that the observed climate change is primarily the result of the known climate forcing contributions. If one assumes a climate sensitivity (or a range of sensitivities), one can determine what the total forcing had to be to produce the observed temperature change. The aerosol forcing is then deduced as a residual after subtraction of the GHG forcing along with other known forcings from the total value. Studies of this nature come up with aerosol forcing ranges of –0.6 to –1.7 Wm^{-2} (Knutti et al., 2002, 2003; IPCC Chap.9); -0.4 to –1.6 Wm^{-2} (Gregory et al., 2002); and -0.4 to –1.4 Wm^{-2} (Stott **et al**., 2006).

Anderson et al. (2003) reviewing the full magnitude of "forward modeling" studies noted that the results showed a much wider range than appears in the IPCC report, with negative values as large as –4 Wm^{-2}, obviously outside of the range of the inverse estimates. They concluded that either these more extreme forward calculations are incorrect, or natural variability is being underestimated, or climate sensitivity is much larger than anticipated. We return to this discussion in section 3.4. Next we review how the modeling of aerosol radiative forcing for the IPCC AR4 report was carried out.

3.1.2. *Modeling aerosol direct radiative forcing*

In the prescribed climate modeling simulations conducted for the IPCC (2007) AR4 report, a scenario of aerosol sulfur concentrations in the atmosphere was made available to the different modeling groups. It used the historical reconstruction of sulfur emissions by Lefohn et al. (1999) rescaled to the SRES (1990) [Special Report on Emission Scenarios, prepared for IPCC, 1990] values to avoid discontinuities with future climate projections. The sources were then run in the French LMD chemical transport and transformation model to produce column average aerosol distributions over the globe (Boucher and Pham, 2002). At least four GCMs employed this distribution, although it was not mandatory, and many did not, preferring their own approaches. The global sulfur emission estimates from different studies are well constrained, with seven different reconstructions of sulfur emissions having a standard deviation of less than 20% among them for the time period between 1890 and 1990 (IPCC, 2007). However, the modeling groups which didn't use the Boucher and Pham distribution had to convert time-dependent sulfur emissions to regionally dependent sulfate concentrations and optical depth, and the techniques used were model-dependent. For example, NCAR incorporated historical SO_2 emissions from the data set of Smith et al. (2001) into the MOZART global chemical transport model to produce its sulfate distribution. GFDL also used MOZART with time-varying aerosols. GISS used time-varying aerosols in a version of the full GCM that included additional aerosol-related processes, with the distributions saved for use in the climate-change simulations. As will be shown, the varying procedures resulted in varying sulfate concentrations. And as the models also use different aerosol radiative characteristics along with differing atmospheric radiation schemes, the subsequent radiative forcing is even more model-dependent.

As an illustration of the uncertainty to be found, shown in **Table 3.1** are the various global sulfate aerosol loads, optical depths and direct radiative forcings relative to preindustrial times in aerosol and climate models published since the Third Annual IPCC report (TAR) {adapted from IPCC 2007, Table 2.4} (see Section 1 for the distinction between aerosol models and climate models). These may be thought of as the "extensive" properties of the aerosols. Also indicated (in the last three columns) are the "intensive" properties, the mass scattering efficiency, forcing per optical depth, and forcing relative to the mass of aerosol ("normalized forcing"). While the amount of aerosol may be considered a product of the model's sources and sinks ('extensive influences) which influence its optical depth, the efficiency with which an aerosol scatters (i.e., the intensity) translates this aerosol loading into radiative forcing. Considerable variation exists in each of these quantities, with the standard deviation about 40% of the average radiative forcing. Note that the range shown in the table does not necessarily indicate the range in the IPCC climate change experiments, but is indicative of the level of understanding during the time the IPCC AR4 simulations were being carried out. A more direct comparison between several of the GCMs used for the 20th century climate change experiments is provided in Section 3.2.

Note the following model abbreviations for this and similar tables:
CCM3: Community Climate Model; GEOSCHEM: Goddard Earth Observing System-Chemistry; GISS: Goddard Institute for Space Studies; SPRINTARS: Spectral Radiation-Transport Model for Aerosol Species; LMD: Laboratoire de Meteorologie Dynamique; LOA: Laboratoire d'Optique Atmospherique; GATORG: Gas, Aerosol Transport and General circulation model; PNNL: Pacific Northwest National Laboratory; UIO-CTM: Univeristy of Oslo CTM; UIO-GCM: University of Oslo

Table 3.1. Sulfate load, optical depth and radiative all-sky forcing in different models. For model designation and appropriate references, see IPCC, 2007, Table 2.4, from which this was adapted. Note that the different GISS model results arise from different aerosol physics packages.

# Model	Sulfate load (mg m^{-2})	Optical Depth (0.55 μm)	Radiative Forcing (Wm^{-2})	Mass scat. efficiency $m^2 g^{-1}$	Forcing per Opt. Depth $W m^{-2}$	Normalized forcing $W g^{-1}$
PUBLISHED SINCE IPCC, 2001						
A CCM3	2.23		-0.56			-251
B GEOSCHEM	1.53	0.018	-0.33	11.8	-18	-216
C GISS	3.3	0.022	-0.65	6.7	-30	-197
D GISS	3.27		-0.96			-294
E GISS*	2.12		-0.57			-269
F SPRINTARS	1.55	0.015	-0.21			-135
G LMD	2.76		-0.42			-152
H LOA	3.03	0.03	-0.41	9.9	-14	-135
I GATORG	3.06		-0.32			-105
J PNNL	5.5	0.042	-0.44	7.6	-10	-80
K UIO-CTM	1.79	0.019	-0.37	10.6	-19	-207
L UIO-GCM	2.28		-0.29			-127
AEROCOM (different models used identical emissions)						
M UMI	2.64	0.02	-0.58	7.6	-29	-220
N UIO-CTM	1.7	0.019	-0.36	11.2	-19	-212
O LOA	3.64	0.035	-0.49	9.6	-14	-135
P LSCE	3.01	0.023	-0.42	7.6	-18	-140
Q ECHAM5-HAM	2.47	0.016	-0.46	6.5	-29	-186
R GISS**	1.34	0.006	-0.19	4.5	-32	-142
S UIO-GCM	1.72	0.012	-0.25	7.0	-21	-145
T SPRINTARS	1.19	0.013	-0.16	10.9	-12	-134
U ULAC	1.62	0.02	-0.22	12.3	-11	-136
Average A-L	**2.8**	**0.024**	**-0.46**	**9.3**	**-18**	**-181**
Average M-U	**2.15**	**0.018**	**-0.35**	**8.6**	**-21**	**-161**
Minimum A-U	**1.19**	**0.006**	**-0.96**	**4.5**	**-10**	**-80**
Maximum A-U	**5.50**	**0.042**	**-0.16**	**12.3**	**-32**	**-294**
rel std dev A-L	**0.40**	**0.41**	**0.44**	**0.23**	**0.40**	**0.38**
rel std dev M-U	**0.39**	**0.45**	**0.43**	**0.30**	**0.37**	**0.22**

*Note that the the aerosol scheme used in this version of the GCM is totally different than that in the GISS climate model discussed below.

** The AEROCOM GISS model uses totally different sources than were used for the historic simulations.

GCM; UMI: University of Michigan; LSCE: Laboratoire des Sciences du Climat et de l'Enviornment; ECHAMS5-HAM: European Centre Hamburg with Hamburg Aerosol Module; ULAQ: University of lL'Aquila.

As expected the relative standard deviations of the intensive properties were somewhat lower than those of the extensive variables, but of comparable magnitude and therefore contributing substantially to the variance in the total radiative forcing. The extensive and intensive properties of the several models are compared in **Figure 3.1**. It is seen that there can be substantial variation in intensive variables, and that even for models that exhibit similar normalized forcing, there can be compensation between mass scattering efficiency and forcing per optical depth.

The values (and relative standard deviations, RSDs) of mass scattering efficiency and normalized forcing have been examined in an intercomparison of radiative transfer models (Boucher et al, 1998). That study showed that for a well specified aerosol (size, composition, relative humidity) the mass scattering

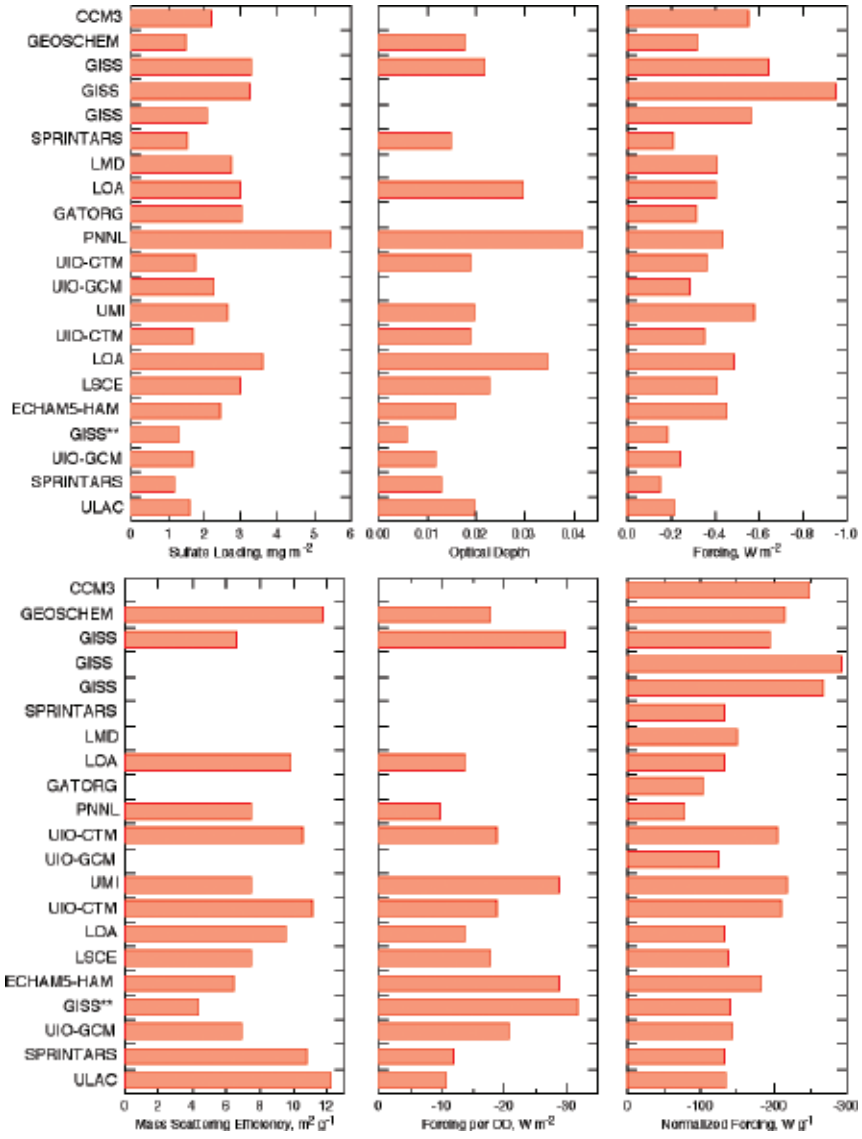

Figure 3.1 Extensive (top) and intensive (bottom) aerosol properties of models in Table 3.1. Note that scales of negative quantities are reversed so that the magnitudes of all plotted quantities increase to the right.

efficiency as determined by the several models agrees quite precisely (**Figure 3.2**, left). The rather low values of mass scattering efficiency by the several GCMs (< 9 m^2 g^{-1}) (**Figure 3.1**) suggests that the particle radii were all considerably lower than the mode radius 0.33 µm, a radius value that would give a much greater mass scattering efficiency of about 20 m^2 g^{-1}. The spread in GCM mass scattering efficiency (27% RSD) is likely due to the spread in the size distributions assumed or calculated in the several models, which could arise from both the intrinsic size distribution and the environmental relative humidity experienced by the aerosols in the different models.

For the radiative transfer calculations leading to determination of normalized forcing in the model intercomparison of Boucher et al. (1998), the atmospheric conditions (relative humidity profile) and surface reflectance were also quite well specified, resulting in a RSD of 8% in normalized forcing at the particle radius corresponding to the greatest normalized forcing (**Figure 3.2**, right). The much greater spread in this quantity for the GCMs examined in Table 3.1 (33% RSD) would appear more a consequence of variations in aerosol properties (cf. the 27% RSD in mass scattering efficiency) than of differences in the radiative transfer algorithms. The mode radius of the sulfate particles inferred from the normalized forcing is considerably less than that inferred from the mass scattering efficiency; the reason for this is not known.

In summary, the differences among models in the direct radiative effect of sulfate aerosols appear to be associated primarily with different magnitudes of sulfate loading, different size distributions of the sulfate aerosol, and different relative humidity influences. Ideally, these are all aspects which should be able to be constrained by observations, if not now then with continuing research.

For the other aerosol constituents, the climate modelers used perhaps even more diverse approaches, in part because the historical variation with time of other aerosol sources is less well-known. For example, the NCAR group scaled their current black and organic carbonaceous aerosols from present-day to earlier years using a global scaling for population. The GISS group used time-and spatially-varying emis-

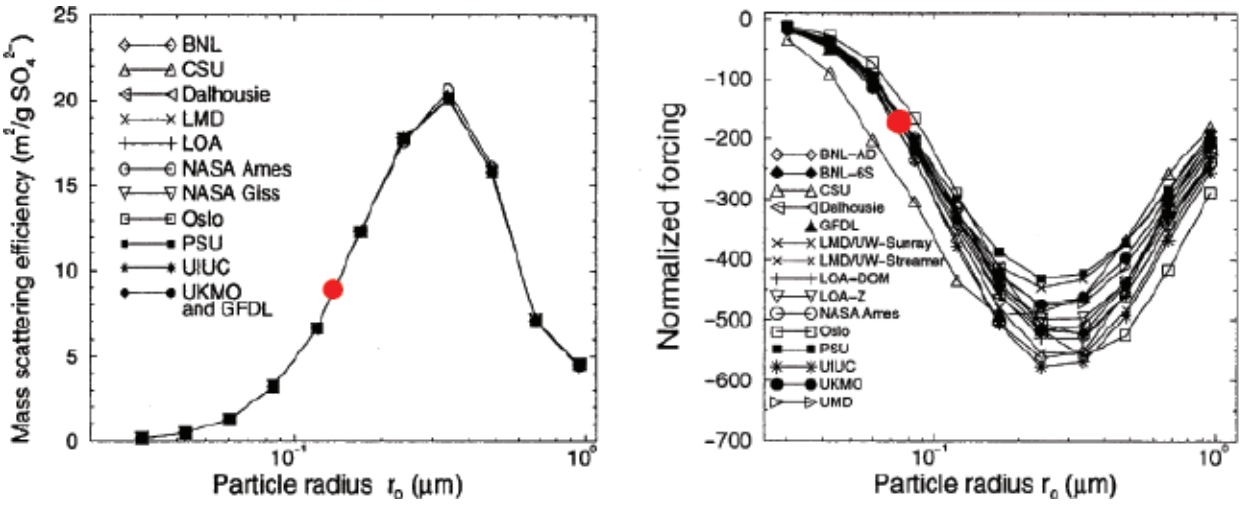

Fig 3.2. Mass scattering efficiency (left) and global-average normalized forcing (forcing per sulfate loading, W m-2 /(g m-2) or W g-1) (right) as evaluated by 15 radiation transfer models for a well specified aerosol (ammonium sulfate at 80% relative humidity) and well specified surface albedo, as a function of particle radius. (Boucher et al., 1998). Red circles denote ordinate values corresponding to averages of models in Table 3.1.

sions based on fuel use, but then normalized the black carbon (BC) and organic carbon (OC) amounts to obtain best correspondence with the present day with AERONET data (Hansen et al., 2007). GFDL ran MOZART simulations two years every decade from 1869-2000 with varying emissions [historical emissions produced by scaling present-day values based on the EDGAR-HYDE historical emissions inventory (Van Ardenne et al., 2001)] but the same present-day wind fields, with year-to-year variations imposed by linear interpolation. As with sulfate, further differences arose because of the use of differing aerosol optical characteristics and differing radiation schemes.

Table 3.2: As in Table 3.1 for the carbonaceous aerosols: particulate organic matter (POM) and black carbon (BC). From IPCC 2007 Table 2.5.

# Model	POM LOAD (mg POM m^{-2})	POM Optical Depth (0.55μm)	POM Radiative Forcing (Wm^{-2})	mass scat effic, m^2 g^{-1}	forcing per OD, W m^{-2} OD-1	Normalized forcing, W/g	BC LOAD (mg BC m^{-2})	BC RAD. FORCING (Wm^{-2})	Normalized forcing, W/g
PUBLISHED SINCE IPCC, 2001									
A SPRINTARS			-0.24					0.36	
B LOA	2.33	0.016	-0.25	6.9	-16	-107	0.37	0.55	1486
C GISS	1.86	0.017	-0.26	9.1	-15	-140	0.29	0.61	2103
D GISS	1.86	0.015	-0.3	8.1	-20	-161	0.29	0.35	1207
E GISS	2.39		-0.18			-75	0.39	0.5	1282
F GISS	2.49		-0.23			-92	0.43	0.53	1233
G SPRINTARS	2.67	0.029	-0.27	10.9	-9	-101	0.53	0.42	792
H GATORG	2.56		-0.06	0.0		-23	0.39	0.55	1410
I MOZGN	3.03	0.018	-0.34	5.9	-19	-112			
J CCM							0.33	0.34	1030
K UIO-GCM							0.3	0.19	633
AEROCOM (different models used identical emissions)									
L UMI	1.16	0.006	-0.23	5.2	-38	-198	0.19	0.25	1316
M UIO-CTM	1.12	0.0058	-0.16	5.2	-28	-143	0.19	0.22	1158
N LOA	1.41	0.0085	-0.16	6.0	-19	-113	0.25	0.32	1280
O LSCE	1.5	0.0079	-0.17	5.3	-22	-113	0.25	0.3	1200
P ECHAM5-HAM	1	0.0077	-0.01	7.7	-1	-10	0.16	0.2	1250
Q GISS	1.22	0.006	-0.14	4.9	-23	-115	0.24	0.22	917
R UIO-GCM	0.88	0.0045	-0.06	5.1	-13	-68	0.19	0.36	1895
S SPRINTARS	1.84	0.02	-0.1	10.9	-5	-54	0.37	0.32	865
T ULAC	1.71	0.0075	-0.09	4.4	-12	-53	0.38	0.08	211
Average A-K	**2.38**	**0.019**	**-0.24**				**0.38**	**0.44**	
Average L-T	**1.32**	**0.008**	**-0.13**				**0.35**	**0.25**	
Average A-T	1.83	0.012	-0.18	5.6	-17	-99	0.31	0.35	1182
Average A-T	**0.42**	**0.006**	**0.08**				**0.08**	**0.13**	
Std. Dev. L-T	**0.32**	**0.005**	**0.05**				**0.08**	**0.08**	
Rel Std Dev A-T	0.36	0.60	0.53	0.43	0.54	0.49	0.32	0.42	0.36
Expected			0.61					0.49	

Again, as an illustration of present uncertainty, shown in **Table 3.2** {from IPCC 2007, Table 2.5} are estimates of anthropogenic carbonaceous aerosol forcing from aerosol and climate models published since the TAR. Organic carbon forcing ranges from –0.06 to –0.34 Wm^{-2} whereas black carbon values range from 0.08 to 0.61 Wm^{-2}; relative standard deviations among the models are about 30% in both cases. As was true for sulfate aerosols, the relative standard deviations of the intensive variables are as large or larger than those of the extensive variables and with rather extreme outlier values.

Additionally, even the choice of which aerosols to incorporate was left open to the modelers. Presented in **Table 3.3** {adapted from SAP 1.1 Table 5.2} are the time-varying aerosol forcings employed in the different climate model simulations of the last 100 years for IPCC AR4. As can be seen, all the climate models used a sulfate aerosol direct effect, while fewer than half incorporated a sulfate aerosol indirect forcing; about half used black carbon and organic carbon forcing; and about a quarter used mineral dust and sea salt (which should not generally affect anthropogenic forcing differences).

3.1.3 *Modeling the aerosol indirect effect*

Whether modelers incorporated an indirect aerosol cloud forcing was also left up to them, and as noted fewer than half the groups incorporated such forcing for sulfates. Shown in **Figure 3.3** {from IPCC 2007 Fig. 2.14} are results from published model studies indicating the different radiative forcing values from the first indirect effect (cloud albedo). This cloud albedo effect ranges from –0.22 to –1.85 Wm^{-2}; the lowest estimates of the derivations from simulations that constrained representation

	MODEL	G	O	SD	SI	BC	OC	MD	SS
1	CCCma-CGCM3.1(T47)								
2	CCSM3								
3	CNRM-CM3								
4	CSIRO-Mk3.0								
5	ECHAM5/MPI-OM								
6	FGOALS-g1.0								
7	GFDL-CM2.0								
8	GFDL-CM2.1								
9	GISS-AOM								
10	GISS-EH								
11	GISS-ER								
12	INM-CM3.0								
13	IPSL-CM4								
14	MIROC3.2(medres)								
15	MIROC3.2(hires)								
16	MRI-CGCM2.3.2								
17	PCM								
18	UKMO-HadCM3								
19	UKMO-HadGEM1								

Table 3.3 Greenhouse gas and tropospheric aerosol forcings used in IPCC simulations of 20th century climate change. Forcings used are: well-mixed greenhouse gases (G), tropospheric and stratospheric ozone (O), sulfate aerosol direct (SD) and indirect effects (SI), black carbon (BC) and organic carbon aerosols (OC), mineral dust (MD), and sea salt (SS). Adapted from IPCC 1.1, Table 5.2.

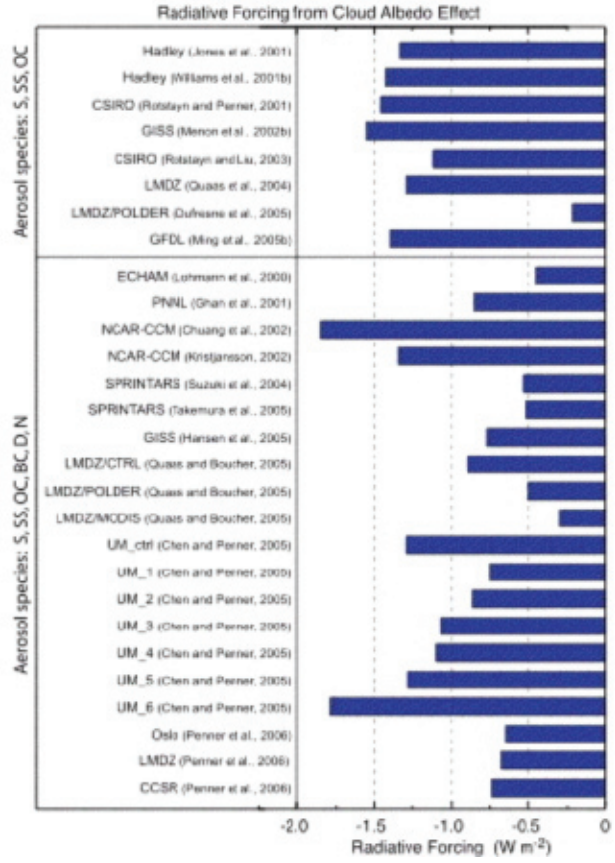

Fig. 3.3. Radiative forcing from the cloud albedo effect (1st aerosol indirect effect) in the global climate models used in IPCC 2007 (IPCC Fig. 2.14). For additional model designations and references, see IPCC 2007, chapter 2.

of aerosol effects on clouds with satellite measurements. In view of the difficulty of quantifying this effect remotely, it is not clear whether this constraint provides an improved estimate.

[In the following figure, species included in the lower part of the panel include sulfate, sea salt, organic and back carbon, dust and nitrates; in the top panel only sulfate, sea salt and organic carbon.]

Most models do not incorporate the second indirect effect (on cloud lifetimes, due to the alteration in cloud droplet sizes and precipitation efficiency). However, Hansen et al. (2007) argue that the effect can be substantial; in that study, it was estimated that increased cloud lifetimes (rather than cloud brightness) could help in producing the 'required' –1.2 Wm^{-2}. Models in general do not agree on the relative importance of the albedo and lifetime effects. For example, the ratio of second to first indirect effects ranges from about 0.2 to 1.4 in the models reviewed by Lohmann and Feichter (2005). Differences in models are likely related to the aerosol microphysical parameterizations employed, as well as to assumptions about the aerosol background.

It is obvious that modelers have used quite different approaches to produce the aerosol forcing that has resulted in bringing model simulations into line with observations. As noted by Kiehl (2007), the aerosol cooling has been greater in models with larger climate sensitivity. Most of these simulations were conducted several years ago, in time for the IPCC (2007) report. Since then there have been additional studies comparing aerosol observations with what the climate models actually used. In the next section we review the results of those studies, and examine the implications for the ability of models to reproduce the climate record of the last century.

3.2. Comparison of Aerosol Direct Effect in Observations and GCMs

Several comparisons have been made between observations and the aerosols used in GCMs. We will discuss two United States models in detail, from the Goddard Institute for Space Studies (GISS) and the Geophysical Fluid Dynamics Laboratory (GFDL). The purpose in presenting these comparisons is to help elucidate how modelers go about assessing their aerosol components, and the difficulties that entails. Here we are concerned with the aerosols that were actually used in the climate model experiments for AR4. Comparisons with observations have already led to some improvements that can be implemented in climate models for subsequent climate change experiments (e.g., Koch et al., 2006). This aspect is discussed further in chapter 4.

The three parameters that define the aerosol radiative forcing are the aerosol optical depth, the single scattering albedo [at the reference wavelength of 0.55 μm] and the phase function or asymmetry factor (all of which are wavelength dependent). The aerosol optical depth (τ) is indicative of how much aerosol exists in the column, and specifically relates to the magnitude of interaction between the aerosols and short- or longwave radiation. The greater the optical depth, the greater the interaction, and for shortwave (solar) radiation and reflective aerosols, that results in greater cooling. The single scattering albedo (ϖ) indicates the degree of short or long wave absorption versus the fraction of optical depletion that is due to scattering rather than absorption. The higher the value of ϖ, the smaller the absorption, and again for solar radiation, the greater the cooling for the planet as a whole. The phase function or asymmetry factor relates to the angle of scattering; when the scattering is primarily backward, solar radiation is reflected out toward space and cooling predominates. This last aspect is related to the size of the particles; for bigger particles, relative to the wavelength of the light being scattered, more radiation is scattered forward, and hence cooling is reduced. An indication of the particle size is provided by another parameter, the Ångstrom exponent (Å), which is a measure of wavelength dependence; for typical tropospheric aerosols, the Ångstrom exponent for scattering tends to be inversely dependent on particle size; up to a certain point, larger values of Å are thus associated with smaller aerosols and greater cooling. These parameters are further related; for example, for a given composition, the ability of a particle to scatter radiation decreases more rapidly with decreasing size than does its ability to absorb, so models at a given wavelength can vary ϖ by varying Å. In the following sub-section, we review the realism of these features in the GISS model to illustrate more precisely the impact of modeling choices.

3.2.1. *The GISS Model*

The aerosols and aerosol forcing in the GISS model have been assessed by Liu et al. (2006). The GISS aerosol climatology is obtained from chemistry-transport model simulations that produce monthly mean height distributions of aerosol mass densities at each grid box (Koch, 2001). The spatial distributions of sulfate, sea salt, nitrate, dust, black carbon and organic carbon aerosols are described in Schmidt et al. (2006), and in greater detail by Liu et al. (2006).

Aerosol optical depth can be related to aerosol mass loading as

$$\tau = \frac{3Q_{ext}M}{4\pi\rho r_{eff}}$$

where M is the aerosol mass loading per unit area, Q_{ext} is the extinction efficiency factor (related to the phase function and single scattering albedo), r_{eff} is the effective radius (related to the particle size distribution and hence Ångstrom coefficient), and ρ is the specific density of the aerosol. This relationship is a simplification for the relatively large particles that contribute appreciably to mass concentration (a full derivation is included as Appendix A.1). Note that the particle size, density and extinction coefficient implicitly vary with height, due to variations in both their concentration and relative humidity, which influences these characteristics.

Therefore, to convert the aerosol mass loadings to optical properties, the size distribution and phase functions must be assigned. Dry size effective radii are specified for each of the aerosol types, and laboratory-measured phase functions are employed for all solar and thermal wavelengths [see the list of references in Liu et al. (2006); be advised, however, that questions remain concerning the pertinence of laboratory-determined refractive indices for the organic carbon and black carbon that exist in the atmosphere where, as but one example, internal mixtures can influence the refractive properties.] With these specifications, the optical thickness and scattering optical properties of the various aerosols are defined for the somewhat arbitrarily specified (dry) particle sizes. In addition, for hygroscopic aerosols (sulfate, nitrate, sea salt and organic carbon), formulas are used for the particle growth of each aerosol as a function of relative humidity, including the change in density and refractive index. In practice, look-up tables for extinction coefficients (i.e., aerosol refractive properties) as a function of relative humidity are employed based on laboratory measurements [see Schmidt et al., 2006 for details, but again the accuracy of these measurements is not fully established. The field observations discussed in Chapter 2 provide a reality check.] While the aerosol distribution is prescribed as monthly mean values, the relative humidity component of the extinction is updated each hour.

The GISS climate model aerosol distribution and properties used for 1990 and subsequent years is compared with satellite data sets from MODIS (the particular version used is referred to as "collection 4 data without deep blue retrieval over deserts"), MISR, POLDER and AVHRR, with additional data from TOMS and ground-based measurements (AERONET). The GISS climate model does not vary its aerosols after 1990, so comparisons with satellite retrievals after that date are all being made with the same model values. The GCM comparisons are for cloud-free conditions, theoretically consistent with the satellite aerosol retrievals being used (although determination of when a cloud is present by satellite is not always unequivocal); the GISS model has either cloud-free or cloud-covered grid boxes at each point in time (there is no partial cloud cover), and thus there is no ambiguity for the model in this regard. Satellite measurements are also subject to errors arising from both measurement uncertainty and assumptions in converting from radiance to optical depth.

Here, following Liu et al. (2006), we compare modeled and observed aerosol characteristics. Shown in **Figure 3.4 a,b** (adapted from Liu et al., 2006 Fig. 1a,b) are the global optical depth distributions of aerosols from the GISS model along with the various observational data sets for the two solstice seasons. Qualitative agreement is apparent, with generally higher burdens in Northern Hemisphere summer, and seasonal variations of smoke over southern Africa and South America, as well as wind blown dust over northern African and the Persian Gulf. Aerosol optical depth in both model and observations is smaller away from land. Note that there are differences among the observational data sets themselves, due at least in part to characteristics of the retrievals. For example, over land, POLDER retrieves aerosol properties only in the accumulation mode (i.e., small aerosols). Disagreement among observational data sets obviously makes model validation more difficult.

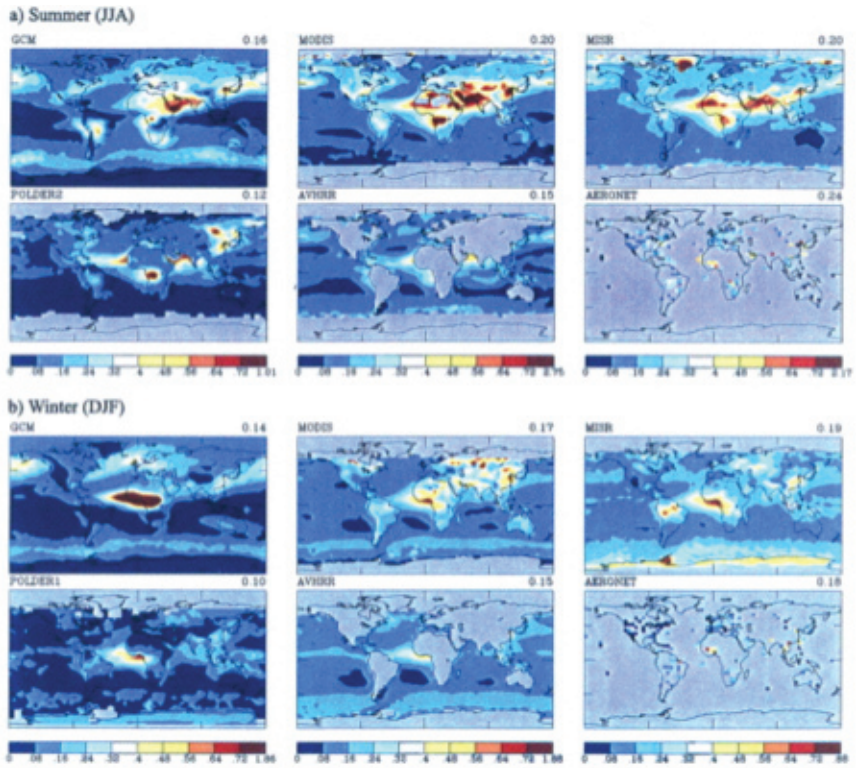

Fig. 3.4. GISS climate model aerosol optical depth at 0.55 μm in June-August (a) and December-February (b) compared with satellite observations (MODIS, MISR, POLDER and AVHRR) as well as surface-based observations (AERONET). Note all satellite comparisons presented are for clear-sky conditions. From Liu et al. (2006).

These comparisons include both natural and anthropogenic aerosols. Errors in modeling natural aerosols do not necessarily affect calculations of the direct aerosol influence on climate change, at least to first order, but they do affect the assessment of the anthropogenic component of the total aerosol characteristics.

There are, however, considerable discrepancies between the model and observations. Overall, the GISS GCM has reduced aerosol optical depths compared with the satellite data (a global, clear-sky average of about 80% compared with MODIS and MISR data), although it is in better agreement with AERONET ground-based measurements in some locations (note that the input aerosol values were

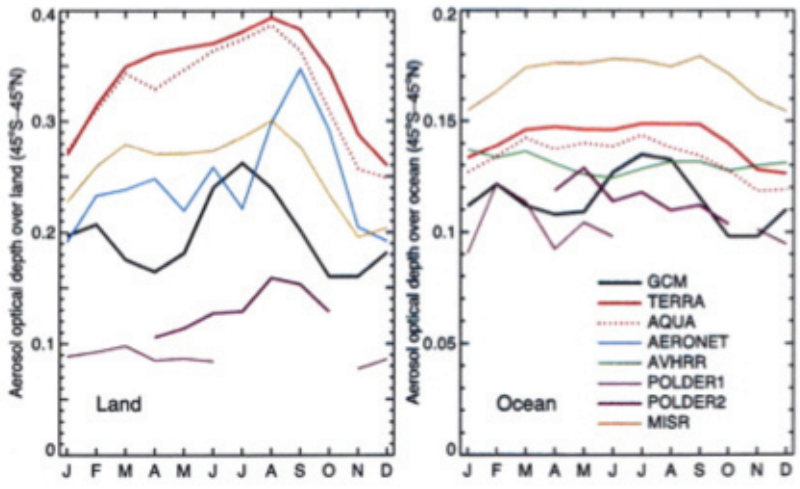

Fig. 3.5. Seasonal dependence of the area weighted monthly mean aerosol optical depth in the GISS climate model (GCM) and observational data sets. From Liu et al. (2006).

calibrated with AERONET data). The model values over the Sahel in Northern Hemisphere winter and the Amazon in Southern Hemisphere winter are excessive, indicative of errors in the biomass burning distributions, at least partially associated with an older biomass burning source estimate (the source used here was from Liousse et al., 1996).

The seasonal distribution of the aerosol optical depth is shown in **Figure 3.5** {adapted from Liu et al., 2006, Fig. 4} (the legends "Terra" and "Aqua" refer to the MODIS instruments on board each of these satellites). While the absolute value of the differences are as large among the observations themselves as they are between the GISS model and some observations, the seasonal dependence in the GISS

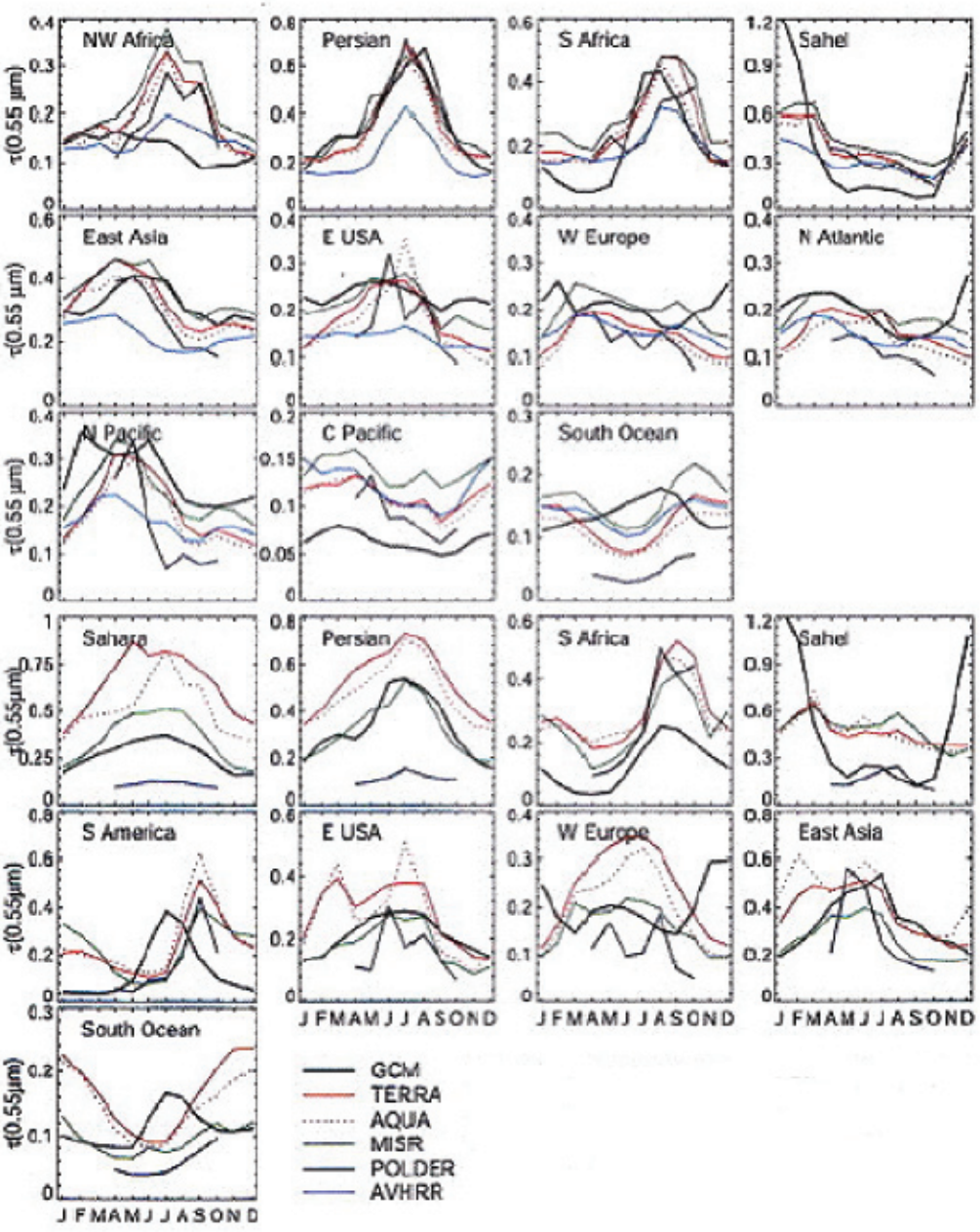

Fig. 3.6. Regional analysis of the monthly mean aerosol optical depth at 0.55 μm in the GISS GCM and from observations, over water surfaces (top three rows) and over land (bottom three rows). From Liu et al., (2006).

model appears different, with, for example, spring and fall minima in optical depth that is not seen in observations.

Because of the heterogeneous nature of its forcing, aerosol impacts are often viewed in terms of their geographical influence on radiation and temperature. Shown in **Figure 3.6** {adapted from Liu et al., 2006 Fig. 7} is a regional comparison of the optical depths as a function of month. Despite the global-average mismatch, the model seasonal variation is in qualitative agreement with the observations for many of these locations, all of which represent major aerosol regimes. The relative contributions of the different aerosol types to the optical depth in these regions is given in **Figure 3.7** {adapted from Liu

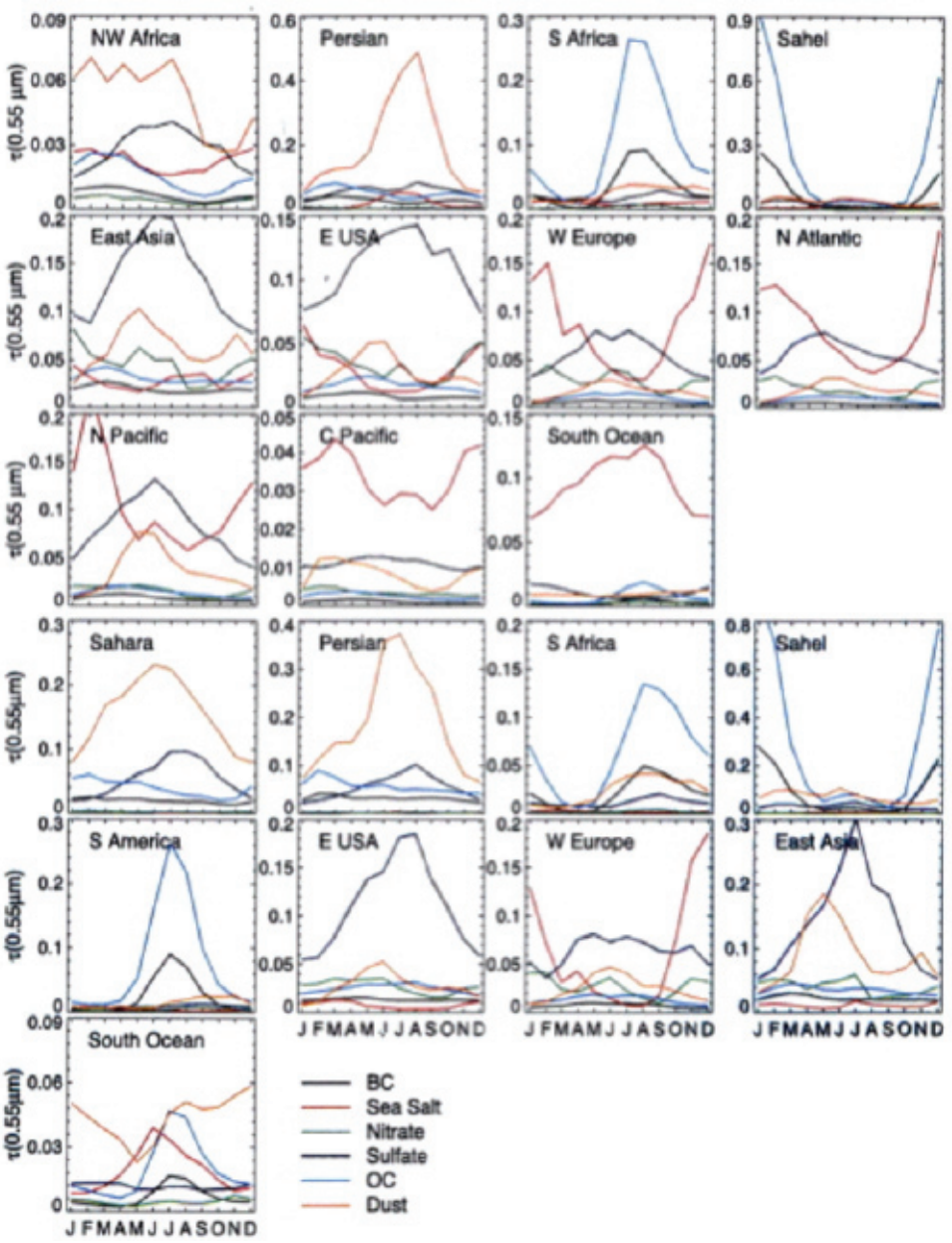

Fig. 3.7. Contributions of each aerosol component in the GCM to the total optical depth at 0.55 μm in the various regions. From Liu et al. (2006).

et al., 2006 Fig. 8}. In combination with **Figure 3.6** one can see that the higher model values in the Sahel during January are due to organic carbon aerosols from biomass burning. A primary discrepancy in the seasonal cycle occurs in the Southern Hemisphere ocean region (30°S-60°S) where the model shows a maximum in austral winter, opposite to what appears in the observations. Given that winds are strongest in winter, one would expect the sea salt concentration to be maximum at that time, as in the model parameterization; potential cloud cover contamination in this region may be influencing the observations from all the satellite data sets. Nevertheless, as shown by Koch et al. (2006), this model has excessive sea salt aerosols in the Southern Ocean. In addition, the seasonal variation may actually be controlled by sulfate from DMS oxidation and biomass burning transported from southern Africa and South America, hence the opposite model seasonal cycle may be also be associated with problems due to these sources. Determining the reason for model/data mismatches requires multiple experiments and various types of observations.

The Ångstrom exponent in the model and observations is shown in **Figure 3.8** {adapted from Liu et al., 2006, Fig. 2a,b}. This parameter is important because the particle size distribution affects the efficiency of scattering of both short and longwave radiation, as discussed earlier.

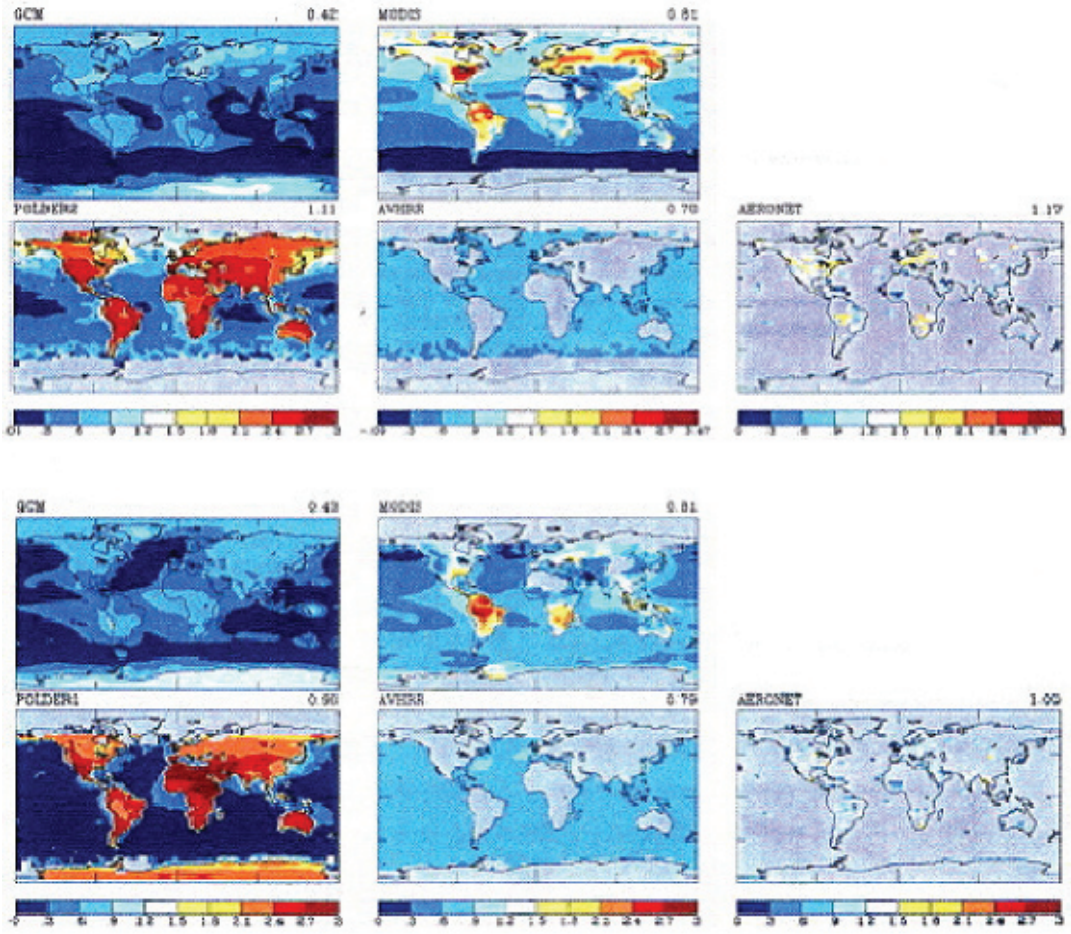

Fig. 3.8. GISS GCM Ångstrom exponent compared with observations for June-August (top two rows) and December-February (bottom two rows). Global numbers (area-weighted with missing data skipped) are shown in the right hand corner. From Liu et al. (2006).

As can be seen in the figure, there are large differences among the data sets themselves, and between the observations and the model. Since the Ångstrom exponent is calculated as the logarithmic derivative of aerosol optical depths between two wavelengths, small differences in optical depth as a function of wavelength are magnified; in addition the instruments each use somewhat different wavelengths to make this calculation (e.g., MODIS uses 0.47-0.66 μm over land, and 0.55-0.85 μm over ocean; POLDER uses 0.55-0.865 μm over both land and ocean, AERONET uses 0.47-0.85 μm over land, and AVHRR uses 0.65-0.8 μm). The data sets show higher values over land and lower values over open ocean, due to the increased sea salt component of ocean aerosols (sea salt has a larger particle size). POLDER values are again larger because of the restriction to the accumulation mode (identified at least in part by the Ångstrom value). The GISS model data can be seen to be biased low (e.g., by comparison with MODIS); one explanation would be that the aerosol dry sizes in the GISS GCM climatology are set too large, which would be consistent with the GISS aerosol optical depths being lower than in the satellite observations. The average effective radius in the GISS model appears to be 0.3-0.4 μm, whereas the observational data indicates a value more in the range of 0.2-0.3 μm (Liu et al., 2006).

The model's single scattering albedo (at 0.55 μm) is compared with observations in **Figure 3.9** {adapted from Liu et al. 2006, Fig. 11}. This parameter is important because the higher the value, the less absorption relative to scattering, and the more the aerosols cool the climate, as determined by net radiation at the top of the atmosphere. At the same time, a smaller single scattering albedo reduces the energy available at the surface (as more is absorbed in the atmosphere). Hansen et al. (1997) calculate that the transition from global cooling to heating occurs at a single scattering albedo of ~0.91 with interactive clouds (~0.86 with fixed clouds).

Compared with AERONET data (version 2) {**Figure 3.10**, adapted from Liu et al., 2006, Fig. 12}, the GISS GCM appears to overestimate the single scattering albedo in general (although it underestimates it in Northern Africa and the Persian Gulf), perhaps because black carbon absorption is excessive, or because the particle size is too large.

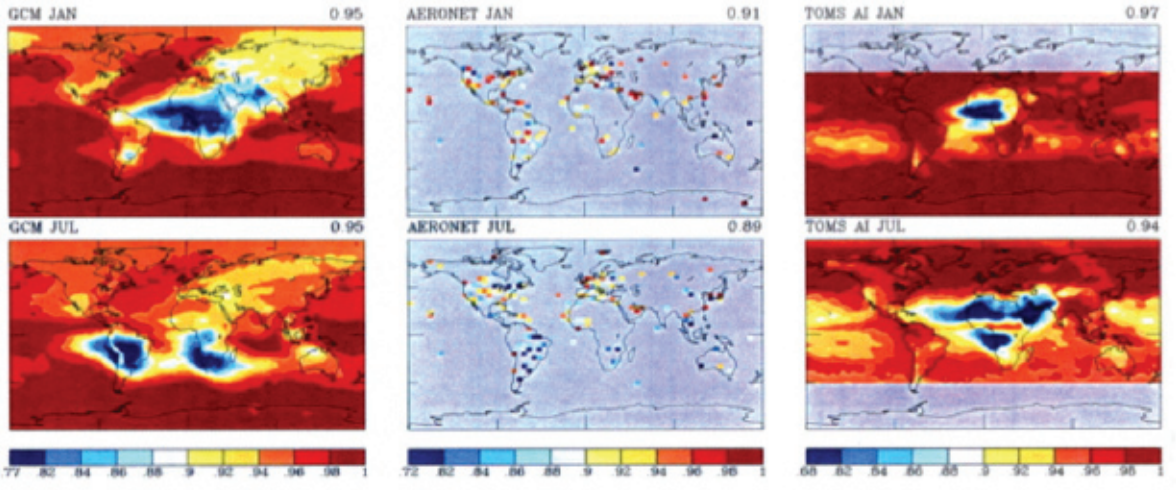

Fig. 3.9. January and July monthly mean single scattering albedo compared with AERONET and TOMS data. The TOMS Aerosol Index (AI) (at 0.32 μm for 1990 has been rescaled as (ϖ=1-0.1 x AI) to roughly resemble the GCM single scattering albedo. Area-weighted global means are given in the top right-hand corner. From Liu et al. (2006).

To summarize these results: while there are many realistic aspects of the GISS aerosol climatology for the 1990 and later time period, the results suggest that the prescribed sizes are too large, and the optical depth is too small. These are related effects (see equation 1), so both could be improved by reducing the particle size, although as discussed in Chapter 2, errors in aerosol optical depth are primarily due to

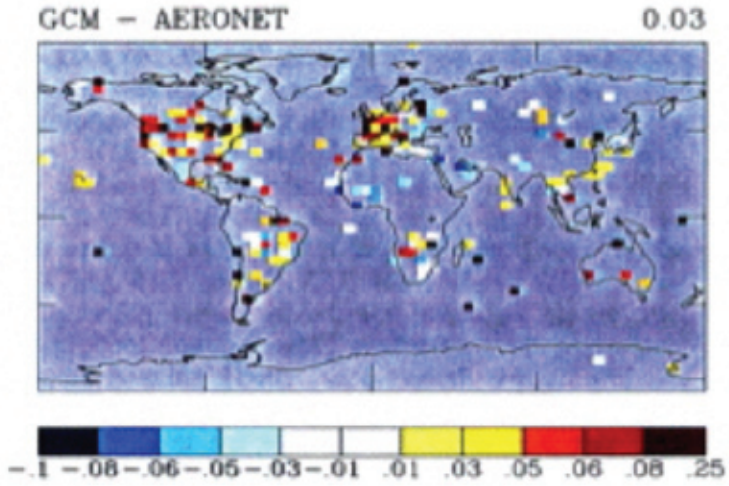

Fig. 3.10. GISS GCM minus AERONET single scattering albedo. The value for this GISS model is reported at 0.55 μm while the selected AERONET wavelength is 0.44 μm. From Liu et al. (2006).

sources and transports, not aerosol properties. Underestimation of optical depth leads to underestimation of the aerosol cooling influence. On the other hand, the single scattering albedo appears to be too large, which could be associated with the black carbon emissions used in the aerosol model from which these values are derived. This effect overestimates the aerosol cooling at the top of the atmosphere; it might be ameliorated by redistributing the black carbon aerosol optical depths. Improving all of these features simultaneously while still keeping a reasonable seasonal variation is not a straightforward task, and it is unclear what influence it will have on the net aerosol radiative forcing. Therefore, this comparison does not provide a clear indication of how direct aerosol radiative forcing in the GISS model relates to observations.

To better understand the accuracy of the direct aerosol radiative forcing, Penner et al. (2002) compared model simulations with AVHRR aerosol optical depth and ERBE clear sky reflectance retrievals. The GISS model in use at that time had reduced aerosol optical depths compared with observations at low and southern latitudes, and overall reduced clear-sky shortwave radiative fluxes of several Wm^{-2} at the top of the atmosphere on the global average. As discussed in that study, it is possible that this reduced flux is associated with incomplete cloud screening from the satellite data rather than a model discrepancy; alternatively, there could be a missing non-sea salt open-ocean source that would increase aerosol optical depths in the region 10°N-30°S. One difference between the GISS model used then and the current version used for climate change experiments is that the newer model has an increased single scattering albedo for dust, which would make it somewhat more reflective.

Combining the Penner et al. (2002) and Liu et al. (2006) studies leads to the conclusion that the GISS model may underestimate the organic and sea salt optical thicknesses, and overestimate the influence of black carbon aerosols in the biomass burning regions. To the extent that is true, it would indicate the GISS model underestimates the direct aerosol cooling effect in a substantial portion of the tropics,

If this is due to a missing natural source, errors in the model burden of naturally-produced aerosols such as DMS, sea salt and some organic molecules will not by themselves directly affect cooling relative to preindustrial simulations. They will also not affect future climate change experiments if they are not expected to change significantly, but they could influence the absorption and wet removal of anthropogenic aerosols through internal mixing and scattering.

An additional concern for climate change simulations relates to the aerosol trend in the GISS model. As noted above, the aerosols in the model are kept fixed after 1990. In fact, the observed trend shows a reduction in tropospheric aerosol optical thickness from 1990 through the present, at least over the oceans (Mischenko et al., 2007). Hansen et al. (2007) suggested that the deficient warming in the GISS model over Eurasia post-1990 was due to the lack of this trend. Indeed, a possible conclusion from the Penner et al. (2002) study was that the GISS model overestimated the aerosol optical thickness (presumably associated with anthropogenic aerosols) poleward of 30°N,. However, when an alternate experiment reduced the aerosol optical depths, the polar warming became excessive (Hansen et al., 2007). Another possibility could be that the lack of sufficient warming over Eurasia was the result of the model's insufficiently positive NAO/AO phase for this time period (hence a dynamic issue, independent of aerosols). Again, clarifying this issue requires numerous modeling experiments and various types of observations.

3.2.2. *The GFDL Model*

The comparison of observations with the GFDL model reported in the literature is not nearly as extensive as that for the GISS model. Nevertheless, some of the assessments discussed above were performed for this model as well. A comparison between the different models will be given in the next section.

The aerosols used in the GFDL climate experiments are obtained from simulations performed with the MOZART 2 model (Model for Ozone and Related chemical Tracers) (Horowitz et al., 2003) except for dust, which uses sources from Ginoux et al. (2001) and wind fields from NCEP/NCAR reanalysis data. It includes most of the same aerosol species as in the GISS model (although it does not include nitrates), and, as in the GISS model, relates the dry aerosol to wet aerosol optical depth (for sulfate and sea salt but not organic carbon) via the relative humidity. While the parameterizations come from different sources, both models maintain a very large growth in particle size when the relative humidity exceeds 90%. For more details see Ginoux et al. (2006), from which this comparison with observations is based.

Overall, the GFDL global mean aerosol mass loading is within 30% of that of other studies (Chin et al., 2002; Tie et al., 2005; Reddy et al., 2005), except for sea salt which is 2 to 5 times smaller. However, the aerosol optical depth for sulfate (τ = 0.1) is 2.5 times that of other studies, while the organic carbon value is considerably smaller (on the order of 1/2). Both of these differences are influenced by the relationship with relative humidity, which in the GFDL model for sulfate is allowed to grow up to 100% (but is maintained constant for organic carbon).

Shown in **Figure 3.11** {adapted from Ginoux et al. 2006, Fig. 7} is the comparison of the mean optical depth with AVHRR and MODIS data for the time period 1996-2000. The global mean value over the ocean (0.15) is in good agreement with AVHRR data (0.14 in Fig.3.11) but there are significant

differences regionally, with the model overestimating the value in the northern mid latitude oceans and underestimating it in the southern ocean. Comparison with MODIS also shows good agreement globally (0.15 in Fig. 3.11), but in this case indicates large disagreements over land, with the model producing excessive aerosol optical depth over industrialized countries and underestimating the effect over biomass burning regions.

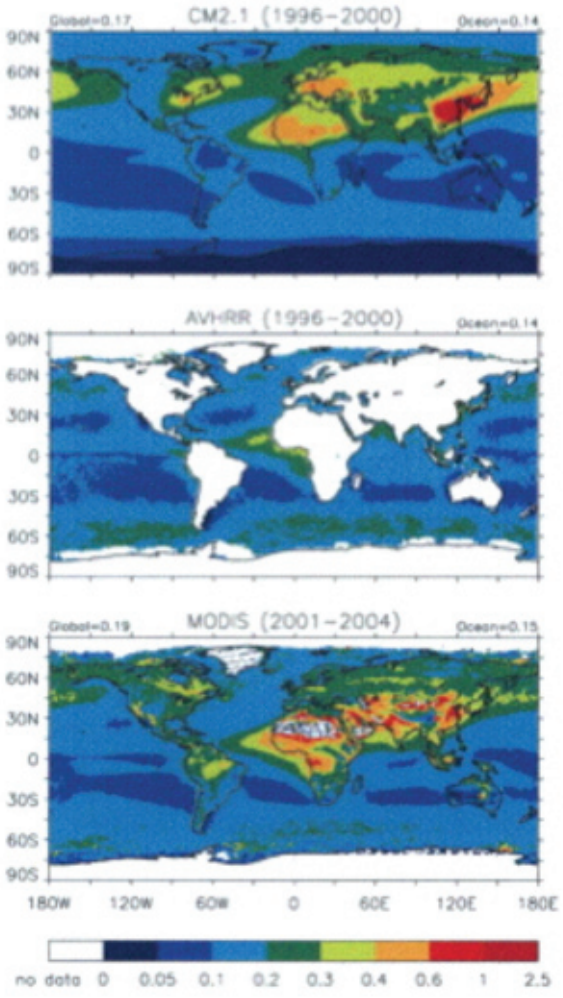

Fig. 3.11. Comparison of mean optical depth at 0.55 μm in the GFDL model C2.1 (1996-2000 average) (top) with AVHRR (1996-2000 average) (middle) and MODIS (2001-2004 average) (bottom). From Ginoux et al. (2006).

Comparison with AERONET data is given in **Figure 3.12** {adapted from Ginoux et al., 2006, Fig. 8}. The correlation between simulated and observed values is 0.6. In agreement with the satellite comparison, the model overestimates the aerosol optical depth in polluted regions of the Northern Hemisphere by a factor of 2 and underestimates the optical depth in biomass burning regions by a factor of 2.

Comparisons of the model's results have also been performed with other data sets (e.g., from the University of Miam; from the IMPROVE program at sites located in U.S. National Parks; and from the EMEP program at stations spread about 27 countries in Europe; for appropriate references, see Genoux et al., 2006). The results show that sulfate optical depth is overestimated in spring and summer (and underestimated in winter) in many regions, including Europe and North America, due perhaps to the relative humidity relationship at high humidities, or perhaps to insufficient removal mechanisms. Organic and black carbon aerosols are also overestimated in polluted regions by a factor of two, where-

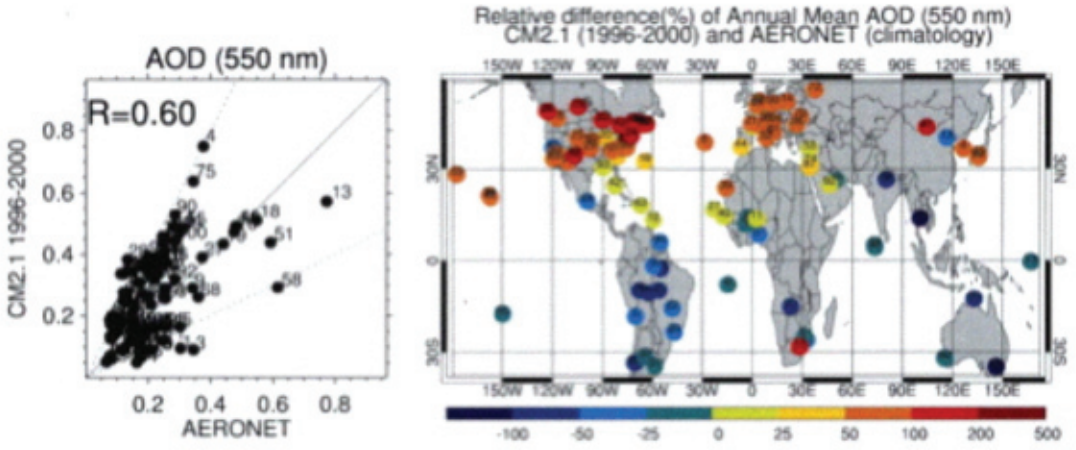

Fig. 3.12. Comparison of GFDL GCM aerosol optical depth at 0.55 μm with aerosol observations (left) and relative differences at each location (right). From Ginoux et al. (2006).

as organic carbon aerosols are elsewhere underestimated by factors of 2 to 3. Dust concentrations at the surface agree with observations to within a factor of 2 in most places where significant dust exists, although over the southwest U.S. it is a factor of 10 too large. Sea salt surface concentrations are underestimated by more than a factor of 2. Over the oceans, the excessive sulfate optical depths compensate for the low sea salt values; this is not true over the southern ocean where, in the real world, high wind speeds result in large amounts of sea salt, so here the model's total optical depth is underestimated by a factor of 2.

Therefore, from an optical depth standpoint, the good global-average agreement masks an excessive aerosol loading over the Northern Hemisphere (in particular, over the northeast U.S. and Europe) and an underestimate over biomass burning regions and the southern oceans. No specific comparison was given for particle size or single-scattering albedo, but the excessive sulfate would likely produce too high a value of reflectivity relative to absorption except in some polluted regions where black carbon (an absorbing aerosol) is also overestimated.

3.2.3. *Model Intercomparisons*

The above discussion, along with Tables 3.1 and 3.2, allows for some synthesis as to the realism of these models' aerosol distribution and how the models rank with respect to other models. With respect to observations, first for sulfates, the GISS model has values less than or equal to the observed for optical depth and radiative impact, while the GFDL model overestimates it by a factor of two. The comparison shown in Table 3.1 indicates that the GISS model direct effect for sulfate is among the highest of the models reviewed; this would imply that the GFDL model values are too large within the context of other models.

For black carbon with respect to observations, the GISS model appears to overestimate its influence in the biomass burning regions and underestimate it elsewhere, while the GFDL model is somewhat the reverse: it overestimates it in polluted regions, and underestimates it in biomass burning areas. The global comparison shown in Table 3.2 indicates the GISS model has values similar to those from other

models, which might be the result of such compensating errors. The GISS and GFDL models have relatively similar global-average black carbon contributions, and the same appears true for organic carbon.

The GISS model has a much larger sea-salt contribution than does GFDL (or indeed other models), a result that is dominated by the southern hemisphere distribution.

As for regional variations, an approximate comparison of the GISS and GFDL model optical depths can be obtained by comparing **Fig. 3.11** with **Figs. 3.4**. Overall there is reasonable agreement in magnitude, with some regional differences, e.g., polluted regions at mid-latitudes have greater optical depth in the GFDL model, while GISS values are larger in low latitude biomass burning regions. The contributions to this clear-sky direct effect from the different aerosol components shows a greater disparity (**Fig. 3.13 a,b**), as can be seen for example over the Southern Ocean, where the primary influence is sea salt in the GISS model {Fig. 3.13 (left), from Lacis, 2007, personal communication}, while in the GFDL model it is sulfate {Fig. 3.13 (right) adapted from Ginoux et al., 2006}. Ginoux et al. (2006) suggest that the sulfate result is due to excessive relative humidity contribution at the highest humidities, although the GISS model uses a formulation that also produces large increases at the highest humidities and its results are very different. The particularities in the parameterization of sulfate removal from the atmosphere may be involved. Since the GISS global optical depth is 0.15 and the GFDL value is 0.17, these regional proportional differences can also be used to indicate component optical depth differences.

No extensive published comparison with observations is available from the NCAR model, but CCSP 3.2 reviewed some characteristics of the aerosol loading from that model with respect to the GFDL and GISS

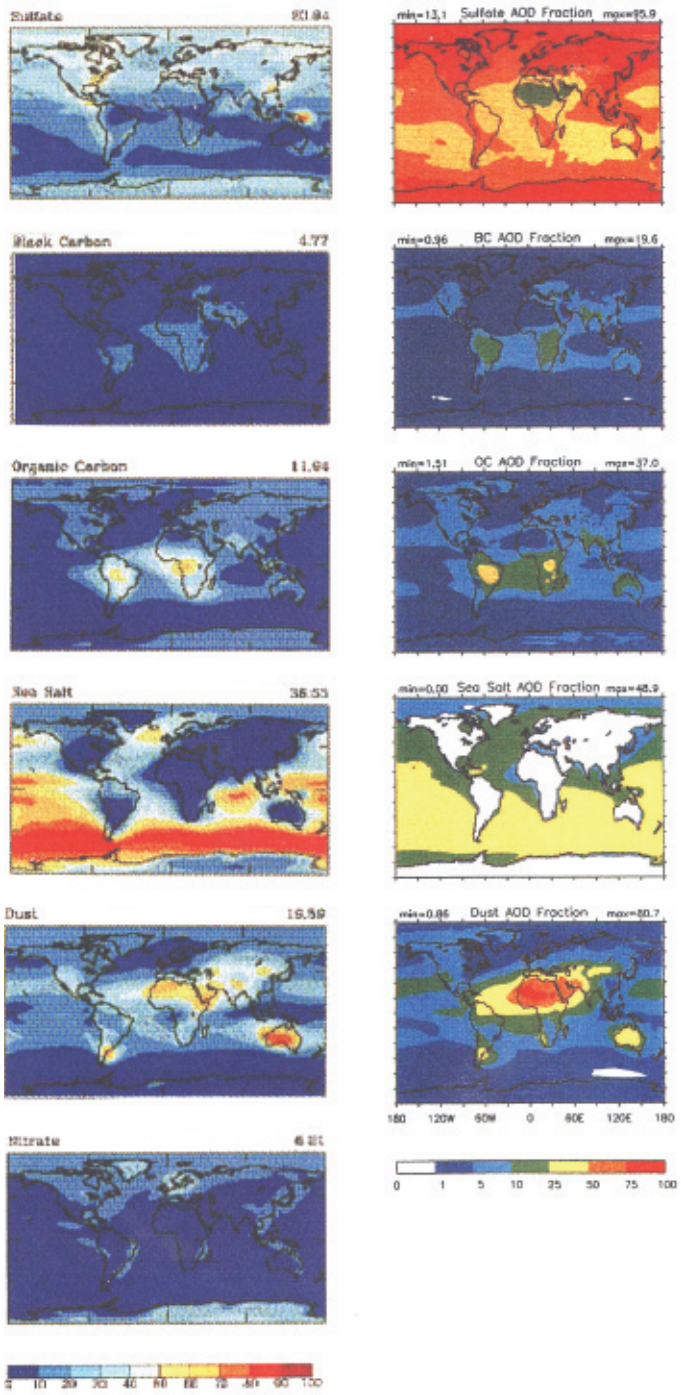

Fig. 3.13. Percentage of aerosol optical depth in the GISS (left) and GFDL (right) models associated with the different components. GFDL does not have nitrate aerosols. Note the different color bars. From Liu et al. (2006) and Ginoux et al. (2006).

values. Sulfates provide the greatest contribution to total aerosol optical depth in the NCAR model for present day donations; its sulfate optical depth is greater than in the GISS model but less than for GFDL (where it dominates the total). The NCAR sea salt value is considerably smaller than that for GISS (where it dominates the total). Hence the NCAR total aerosol optical depth is only about 2/3 the GISS and GFDL values, and appears to be too small compared with satellite retrievals.

The global average direct aerosol radiative forcing at the top of the atmosphere as calculated by various models, including several variants of the GISS model, and as inferred from observations, is presented in **Figure 3.14** {adapted from IPCC 2007 Fig. 2.13}. Note the wide range of forcing. Even amongst the various GISS model simulations the magnitude differs substantially. Part of this result is due to changing aerosol sources or sulfate production in clouds in the different GISS studies, but a major influence is the question of whether aerosol particles are internally or externally mixed (see Section 3.2d). The comparison with observations suggests that most models underestimate the direct effect on a global scale, although the differences only amount to a few tenths Wm^{-2} (and the observations themselves have significant uncertainties – see Chapter 2).

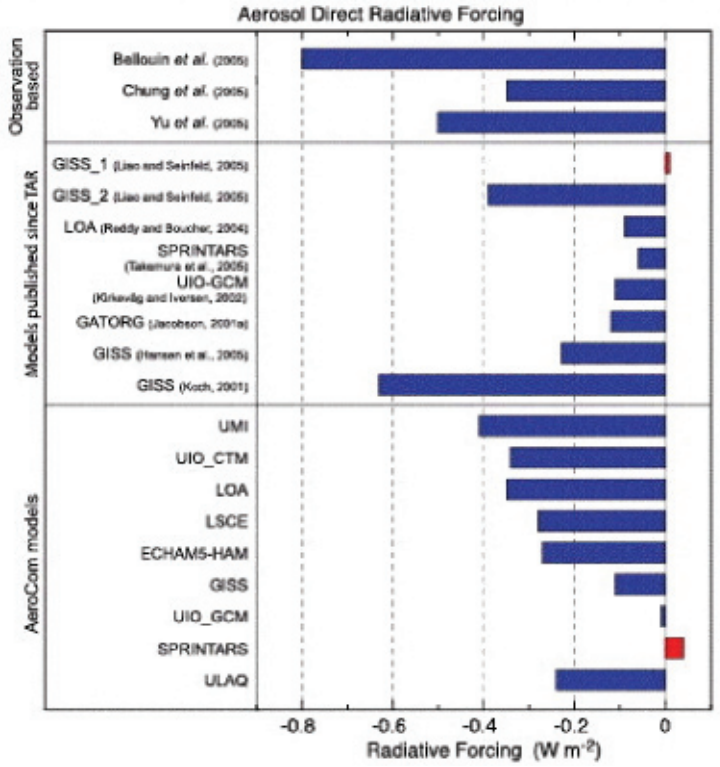

Figure 3.14. Aerosol direct radiative forcing in various climate and aerosol models. Observed values are shown in the top section. From IPCC (2007).

A further comparison can be made with the chemical transport models that participated in the Aerocom intercomparison (see also Table 3.2) (Schulz et al., 2006). Aerosol and radiative results from these models are shown in **Figure 3.15** {adapted from IPCC 2007 Fig. 2.12}. The total aerosol optical depth is somewhat lower in these models than in the observations, similar to the GISS model results (however MODIS tends to overestimate aerosol optical depth over land, where MISR is more realistic). With respect to the radiative forcing due to anthropogenic aerosols, at the top of the atmosphere,

the Aerocom models had negative forcings of -0.5-2 Wm^{-2} in biomass burning and polluted regions, with small, positive forcing elsewhere (Fig. 3.15, lower left). The GISS model {Figure 3.16, upper left, adapted from Lacis 2007 personal communication} has occasional larger negative values in polluted regions, and somewhat stronger positive forcing at the highest latitudes. The differences are even larger at the surface, with the GISS model exceeding –4 Wm^{-2} over large regions (Fig. 3.16, lower left), an

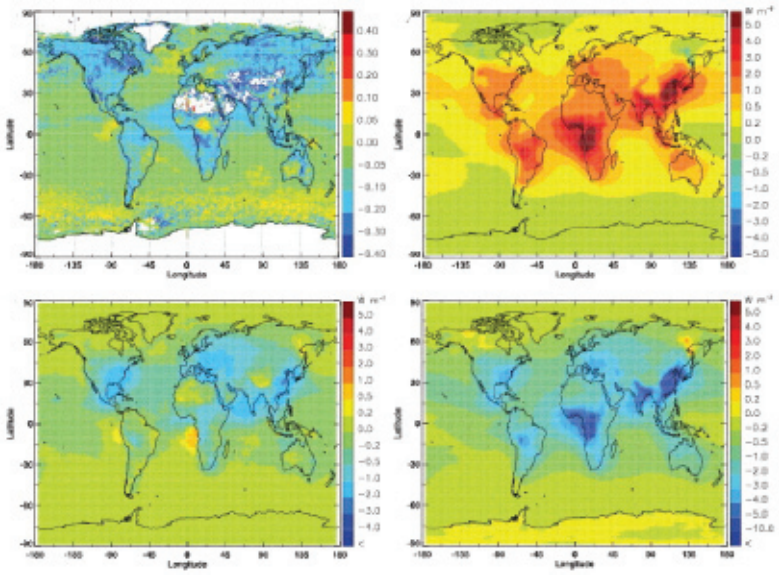

Fig. 3.15. Average results from the nine AeroCom models listed in Table 3.2. Upper left: difference in aerosol optical depth between the models and MODIS data [note the expanded scale compared with that in the lower right]; lower left, upper right and lower right: anthropogenic aerosol shortwave radiative forcing at the top of the atmosphere, of the atmosphere, and at the surface, respectively.

effect only seen in particular regions in the average of the Aerocom models (Fig. 3.15, lower right). This would seem to be due to larger optical depths in the GISS climate model in these regions, specifically the enhancement of black and organic carbon assumed for the climate change simulations (as indicated in the introduction, this was to better match AERONET data. The GISS model version contributed to AEROCOM lacked such enhancement.). The bias in the other GISS aerosol parameters, such as the single-scattering albedo (too high) and particle size (too large) would actually give smaller surface forcing.

A prerequisite to accurately representing aerosols in chemical transport models and climate models is understanding the chemical reactions responsible for aerosol formation. Numerous issues remain uncertain, and the full scope of the problem is outside the framework of this document. A discussion of one important issue relating to secondary organic aerosol formation is included as Appendix A.2.

Some of the conclusions derived from the comparison of the GISS and GFDL climate models illustrate results that are applicable to models in general, including aerosol models. From an assessment of more than 20 aerosol model simulations used for Aerocom intercomparison, Kinne et al. (2006) concluded that aerosol models being run in 2005 do a better job of matching total optical thicknesses from observations than was true in 2002, but there are large differences among aerosol types in how it is done (a conclusion also reached by Schulz et al., 2006). This will affect the direct anthropogenic radiative forcing, which depends on the components (particularly for sulfates, organic and black carbon aerosols). Model mean aerosol concentrations look to be too large over land (outside of the tropics), and too small over oceans and tropical land. Model aerosol sizes are too large over the Northern Hemi-

sphere, and too small over biomass burning regions. The vertical distribution of aerosols differs among models. There are also large model differences in dust, carbonaceous aerosols, the aerosol water mass, and the absorption potential (because of large differences in aerosol composition); in general, models have too little aerosol absorption. Bates et al. (2006) found that in polluted regions the chief causes of the inter-model differences for the clear sky, direct forcing are the differences in emissions, followed by differences in wet removal. However, even when emissions are harmonized, removal processes and transport differences produce large variations among the models (Textor et al., 2007).

3.2.4. *Additional considerations*

Also shown in **Fig. 3.16** (right column) is the aerosol long wave forcing, which will also be affected by the particular aerosol characteristics used in each model. However, compared to the short wave forcing, the values are on the order of 10%, and therefore insignificant considering the other uncertainties. Of more importance is the vertical distribution of the aerosols. This aspect is of secondary importance

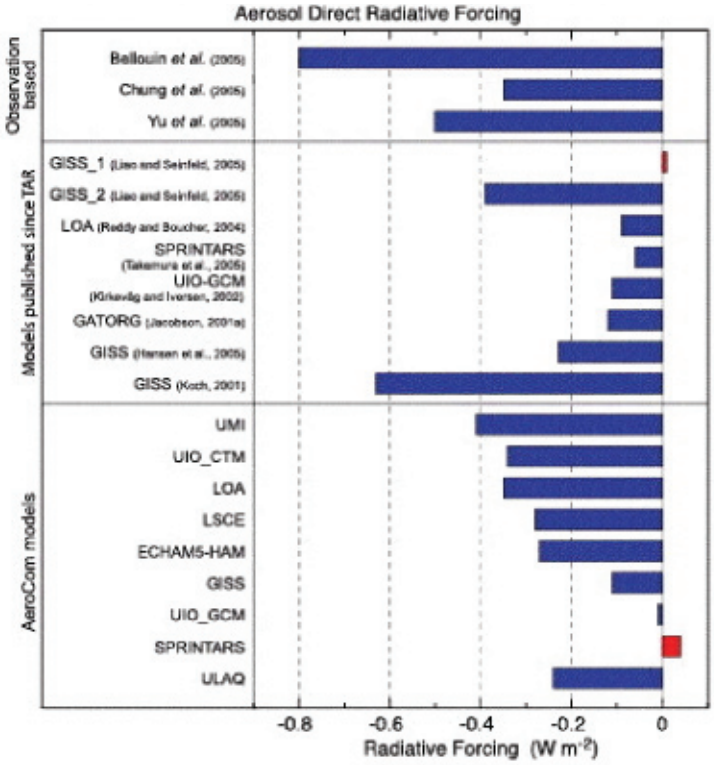

Fig. 3.16. Direct radiative forcing by anthropogenic aerosols in the GISS model (including sulfates, BC, OC and nitrates). Short wave forcing at the top and bottom of the atmosphere are shown in the top left and bottom left panels. The corresponding thermal forcing (discussed later) is indicated in the right hand panels. From Lacis et al. (2007) (personal communication).

for non-absorbing aerosols (except when considering humidification effects and the vertical distribution of water vapor), but absorbing aerosols will reradiate energy depending on their temperature (and hence altitude). Presented in **Fig. 3.17** {adapted from Lacis 2007 personal communication} is the mean pressure level for aerosols in the GISS model for January and July. Sulfate and sea salt lead to the average aerosol being located in the lowest 3 km, but the altitudes to which biomass burning aerosols are lofted has a large impact on their net radiative forcing. This feature needs to be compared with observations and among the models.

Most climate model simulations incorporating different aerosol types have been made using external mixtures, i.e., the evaluation of the aerosols and their radiative properties are calculated separately for each aerosol types. Observations indicate that aerosols commonly consist of internally mixed particles, and these 'internal mixtures' can have very different radiative impacts; compare, for example, the GISS-1 (internal mixture) and GISS-2 (external mixture) model results shown in **Figure 3.14**, a difference between slight warming and significant cooling (due to both changes in radiative properties of the mixtures, and changes in aerosol amount). The more sophisticated aerosol mixtures now being initiated in different modeling groups may well end up producing very different direct (and indirect) forcing values.

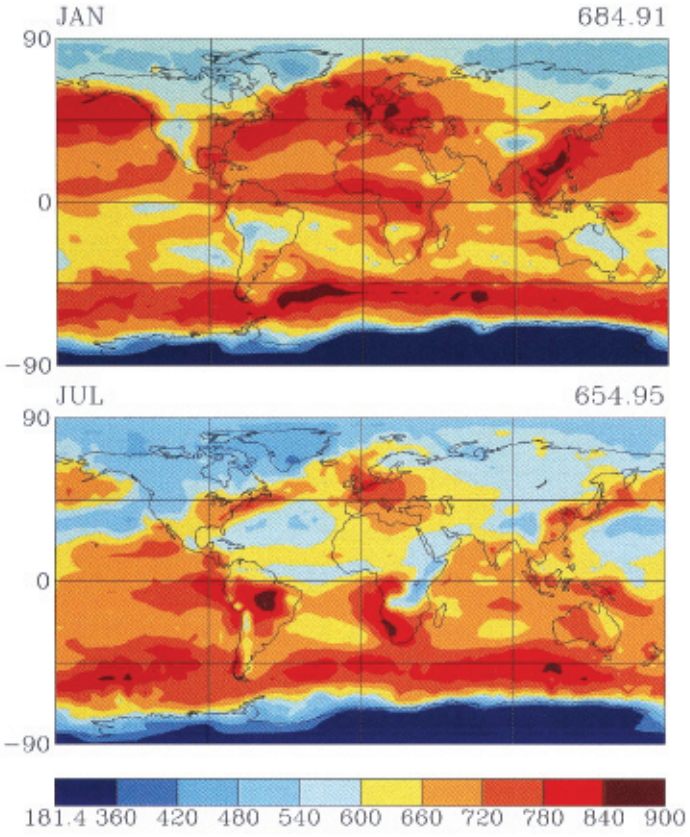

Fig. 3.17. Mean pressure level of the GISS GCM aerosol for January and July (Lacis, 2007, personal communication).

Finally, comparisons with satellite data are concerned with clear-sky aerosol optical thickness and radiative effect. As shown in **Fig. 3.18** {adapted from Lacis, 2007, personal communication}, the aerosol optical depth is larger in cloudy-sky conditions because of the hygroscopic nature of sulfate, which is modeled as a function of relative humidity. Aerosols above or below clouds do not have any significant direct scattering effects, since the cloud reflectivity is much larger. (Absorbing aerosols above clouds would have a strong positive forcing.) However, recent work (Wen et al., 2007) indicates that the enhanced reflections of light between clouds can even have a strong impact on the direct radiative effect of aerosol residing in cloud-free regions. These aspects illustrate the complexity of the system and the difficulty of representing aerosol radiative influences in GCMs, whose cloud distribution is somewhat problematic. And of course aerosols in cloudy regions can affect the clouds themselves, as are discussed in the next section.

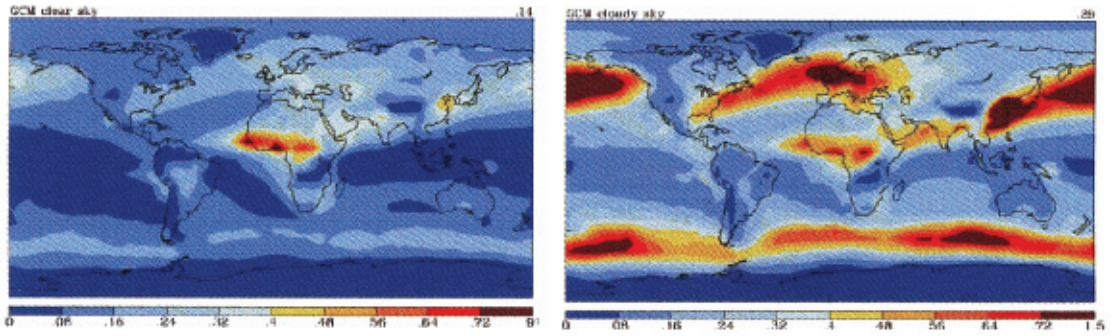

Fig. 3.18. GISS aerosol optical depth for clear skies (left) and cloudy-sky conditions (right). Global mean values at 0.55 μm are shown in upper right hand corners. From Lacis 2007, personal communication.

3.3. Comparison of the Aerosol Indirect Effect in GCMs

3.3.1. Aerosol effects on clouds and radiation

A subset of the aerosol particles can act as cloud condensation nuclei (CCN) and/or ice nuclei (IN). Increases in aerosol particle concentrations, therefore, may increase the ambient concentrations of CCN and IN, affecting cloud properties. For a fixed cloud liquid water content, a CCN increase will lead to more cloud droplets, and so the cloud droplet size will decrease. That effect leads to brighter clouds, the enhanced albedo then being referred to as the 'cloud albedo effect' (Twomey, 1977). If the droplet size is smaller, it may take longer to rainout, leading to an increase in cloud lifetime, hence the 'cloud lifetime' effect (Albrecht, 1989). As noted in Table 3.3, approximately one-third of the models used for the IPCC 20th century climate change simulations incorporated an aerosol indirect effect, generally (though not exclusively) associated with sulfates.

The representation of these first and second indirect effects as relatively simple constructs in GCMS will be considered below. However, it is becoming increasingly clear from studies based on high resolution simulations of aerosol-cloud interactions that there is a great deal of complexity that is unresolved in GCMs. We return to this point in section 3.3.3.

The net radiative forcing produced in various model studies associated with the cloud albedo effect was shown in **Figure 3.3**. It ranges from –0.25 to –1.8 Wm^{-2}. The IPCC estimate given in the introduction ranges from +0.4 to –1.1 Wm^{-2}, with a 'best-guess' estimate of –0.7 Wm^{-2}.

Most models did not incorporate the 'cloud lifetime effect'. Hansen et al. (2005) compared this latter influence (in the form of time-averaged "cloud area" or cloud cover increase) with the cloud albedo effect. In contrast to the discussion in IPCC (2007), they argue that the cloud cover effect is more likely to be the dominant one, as suggested both by cloud-resolving model studies (Ackerman et al., 2004) and satellite observations (Kaufman et al., 2005). The cloud albedo effect may be partly offset by reduced cloud thickness accompanying aerosol pollutants, hence a meteorological (cloud) rather than aerosol effect (see the discussion in Lohmann and Feichter, 2005). (The distinction between meteorological feedback and aerosol forcing can become quite opaque.) Nevertheless, both aerosol

indirect effects were utilized in the GISS model, related to an increase in aerosol cloud droplet number concentration, a function of sulfate, nitrate, black carbon and organic carbon concentration. Only the low altitude cloud influence was modeled, principally because there are greater aerosol concentrations at low levels, and because low clouds currently have greater cloud radiative forcing. [The influence on high altitude clouds, associated with IN changes, is a relatively unexplored area for GCMs and as well for process-level understanding.]

A comparison of the GISS direct and two indirect effects is shown in **Figure 3.19** {adapted from Hansen et al., 2005, Figure 13}. As parameterized, the second indirect effect produced somewhat greater negative radiative forcing and cooling, but this was the result of constants tuned to give that response. Geographically, it appears that the 'cloud cover' effect produced slightly more cooling in the Southern Hemisphere than did the 'cloud albedo' response, with the reverse being true in the Northern Hemisphere.

There are many different aspects that can explain the large divergence of indirect effects in models (Fig. 3.3). To explore this in more depth, Penner et al. (2006) used three different GCMs to analyze the differences between models for the first indirect effect, as well as a combined first plus second indirect effect. The models all had different cloud and/or convection schemes.

In the first experiment, the monthly average aerosol mass and size distribution of, effectively, sulfate aerosol were prescribed, and all models followed the same prescription for parameterizing the cloud droplet number concentration as a function of aerosol concentration. In that sense, the only difference

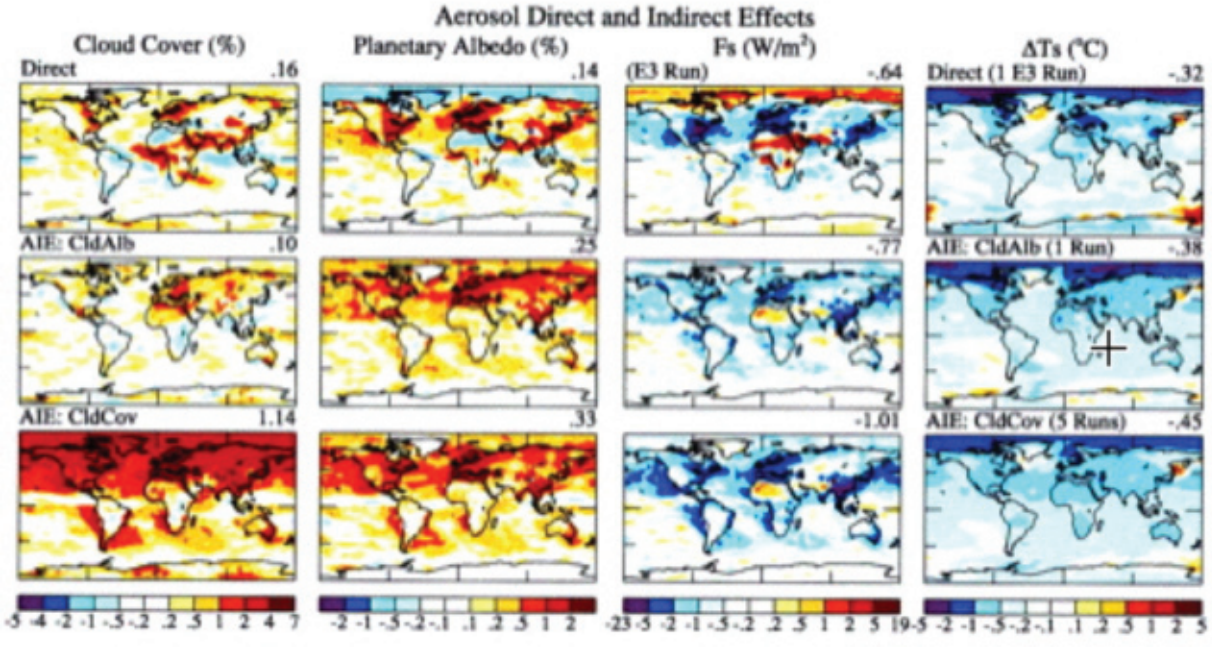

Fig. 3.19. Anthropogenic impact on cloud cover, planetary albedo, radiative flux at the surface (while holding sea surface temperatures and sea ice fixed) and surface air temperature change from the direct aerosol forcing (top row), the 1st indirect effect (second row) and the second indirect effect (third row). The temperature change is calculated from years 81-120 of a coupled atmosphere simulation with the GISS model. From Hansen et al., (2005).

among the models was their separate cloud formation and radiation schemes. The different models all produced a similar droplet effective radii, and therefore shortwave cloud forcing, and change in net outgoing whole sky radiation between pre-industrial times and the present. Hence the first indirect effect was not a strong function of the cloud or radiation scheme. The results for this and the following experiments are presented in **Figure 3.20**, where the experimental results are shown sequentially from left to right {adapted from Penner et al., 2006 Fig. 5} for the whole sky effect, and in Table 3.4 {adapted from Penner et al., 2006, Table 3} for the clear-sky and cloud forcing response as well.

In the second experiment, the aerosol mass and size distribution were again prescribed, but now each model used its own formulation for relating aerosols to droplets. In this case one of the models produced larger effective radii and therefore a much smaller first indirect aerosol effect (Figure 3.20, Table 3.4). However, even in the two models where the effective radius change and net global forcing were similar, the spatial patterns of cloud forcing differ, especially over the biomass burning regions of Africa and South America.

The third experiment allowed the models to relate the change in droplet size to change in precipitation efficiency (i.e., they were now also allowing the second indirect effect - smaller droplets being less efficient rain producers – as well as the first). The models utilized the same relationship for autoconversion of cloud droplets to precipitation. All models produced an increase in cloud liquid water path, and all produced a smaller effect on cloud fraction in (absolute value) than in the previous experiments with the first indirect effect. For two of the models the net impact on outgoing shortwave radiation was to increase the negative forcing by about 20%, while in the third model (which had the much smaller first indirect effect) the radiative forcing was magnified by a factor of three.

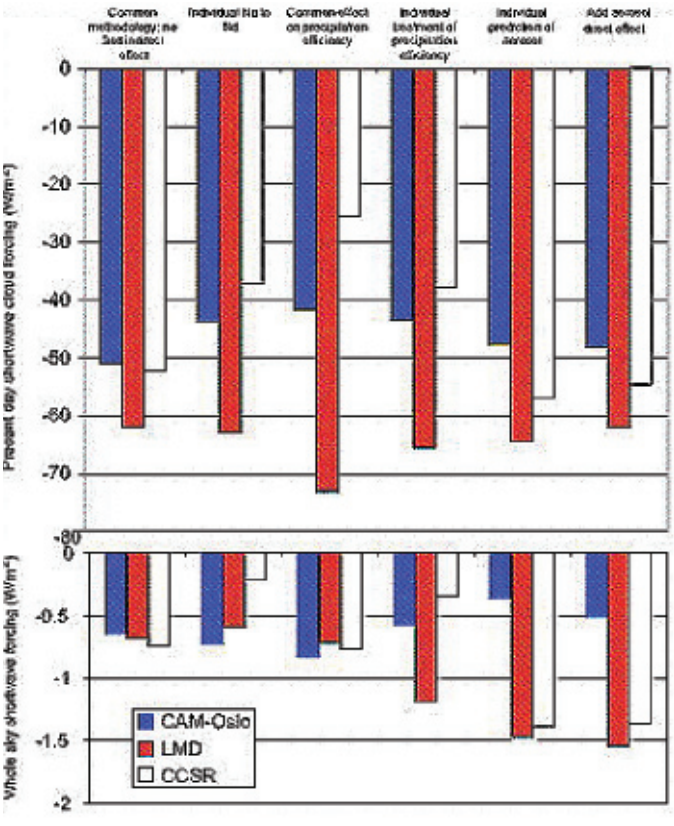

Fig. 3.20. Global average present day short wave cloud forcing at the top of the atmosphere (top) and change in whole sky net outgoing shortwave radiation (bottom) between the present-day and pre-industrial simulations for each model in each experiment. From Penner et al. 2006.

Table 3.4. Differences in present day and pre-industrial outgoing solar radiation in the different experiments. From Penner et al. (2006).

	exp. 1	exp. 2	exp. 3	exp. 4	exp. 5	exp. 6
Whole-sky						
CAM-Oslo	-0.648	-0.726	-0.833	-0.580	-0.365	-0.518
LMD-Z	-0.682	-0.597	-0.722	-1.194	-1.479	-1.553
CCSR	-0.739	-0.218	-0.773	-0.350	-1.386	-1.386
Clear-sky						
CAM-Oslo	-0.063	-0.066	-0.026	0.014	-0.054	-0.575
LMD-Z	-0.054	0.019	-0.066	-0.066	-0.126	-1.034
CCSR	0.018	-0.0068	-0.045	-0.008	0.018	-1.168
CAM-Oslo	-0.548	-0.660	-0.807	-0.595	-0.311	0.056
LMD-Z	-0.628	-0.616	-0.752	-1.128	-1.353	-0.518
CCSR	-0.757	-0.212	-0.728	-0.342	-1.404	-0.200

In the fourth experiment, the models were now each allowed to use their own formulation to relate aerosols to precipitation efficiency. This introduced some additional changes in the whole sky shortwave forcing (Fig. 3.20).

In the fifth experiment, models were allowed to produce their own aerosol concentrations, but were given common sources. This produced the largest changes in the radiative forcing in several of the models. Within any one model, therefore, the change in aerosol concentration has the largest effect on droplet concentrations and effective radii. This experiment too resulted in large changes in radiative forcing.

In the last experiment, the aerosol direct effect was included, based on the full range of aerosols used in each model. While the impact on the whole-sky forcing was not large, the addition of aerosol scattering and absorption primarily affected the change in clear sky radiation (**Table 3.4**).

The results of this study emphasize that in addition to questions concerning cloud physics, the differences in aerosol concentrations among the models (i.e., Figs. 3.4, 3.11 and 3.15) play a strong role in inducing differences in the indirect effect(s), as well as the direct one.

Observational constraints on climate model simulations of the indirect effect with satellite data (e.g. MODIS) have been performed previously in a number of studies (e.g. Storelvmo et al. 2006, Lohmann et al. 2006, Quaas et al. 2006, Menon et al. 2007). These have been somewhat limited since satellite retrieved data do not have the vertical profiles needed to resolve aerosol and cloud fields (e.g. cloud droplet number and liquid water content), and the temporal resolution of simultaneous retrievals of aerosol and cloud products are usually not available at a frequency of more than one a day. Thus, the indirect effect, especially the second indirect effect, remains, to a large extent, unconstrained by satellite observations. However, improved measurements of aerosol vertical distribution from the newer generation of sensors on the A-train platform may provide a better understanding of changes to cloud properties from aerosols.

3.3.2. *Additional aerosol influences*

Various observations have empirically related aerosols injected from biomass burning or industrial processes to reductions in rainfall (e.g., Warner, 1968; Eagan et al., 1974; Andreae et al., 2004; Rosenfeld, 2000). There are several potential mechanisms associated with this response.

In addition to the two indirect aerosol effects noted above, a process denoted as the 'semi-direct" effect involves the absorption of solar radiation by aerosols such as black carbon, within or in the vicinity of clouds. The absorption increases the temperature, lowering the relative humidity, producing evaporation and hence a reduction in cloud liquid water. The impact of this process depends strongly on what the effective aerosol absorption actually is; the more absorbing the aerosol, the larger the potential positive forcing on climate (by reducing low level clouds and allowing more solar radiation to hit the surface). This effect is responsible for shifting the critical value of ϖ (separating aerosol cooling from aerosol warming) from 0.86 with fixed clouds to 0.91 with varying clouds (Hansen et al., 1997). Reduction in cloud cover and liquid water is one way aerosols could reduce rainfall.

More generally, aerosols can alter the location of solar radiation absorption within the system, and this aspect alone can alter climate and precipitation even without producing any change in net radiation at the top of the atmosphere (the usual metric for climate impact). By decreasing solar absorption at the surface, aerosols (from both the direct and indirect effects) reduce the energy available for evapotranspiration, potentially resulting in a decrease in precipitation. This effect has been suggested as the reason for the decrease in pan evaporation over the last 50 years (Roderick and Farquhar, 2002). This decline in solar radiation at the surface appears to have ended in the 1990s (Wild et al., 2005), perhaps because of reduced aerosol emissions in industrial areas (Kruger and Grasl, 2002).

Energy absorption by aerosols above the boundary layer can also inhibit precipitation by warming the air at altitude relative to the surface, i.e., increasing atmospheric stability. The increased stability can then inhibit convection, affecting both rainfall and atmospheric circulation (Ramanathan et al., 2001; Chung and Zhang, 2004). To the extent that aerosols decrease droplet size and reduce precipitation efficiency, this effect by itself could result in lowered rainfall values locally. In their latest simulations, Hansen et al. (2007) did find that the indirect aerosol effect reduced tropical precipitation; however, the effect is similar regardless of which of the two indirect effects is used, and also similar to the direct effect, so it is likely the result of aerosol induced cooling at the surface and consequent reduced evapotranspiration more than anything else. Similar conclusions were reached by Yu et al. (2002) and Feingold et al. (2005).

The local precipitation change, through its impacts on dynamics and soil moisture, can have large positive feedbacks. Harvey (2004) concluded from assessing the response to aerosols in 8 coupled models that the aerosol impact on precipitation was larger than on temperature. He also found that the precipitation impact differed substantially among the models, with little correlation among them.

3.3.3. *Results based on high resolution modeling of aerosol-cloud interactions*

By necessity, the representation of the interaction between aerosol and clouds in GCMs is poorly resolved. This stems in large part from the fact that GCMs do not resolve convection on their large grids

(order several hundred km), that their treatment of cloud microphysics is rather crude, and that as discussed previously, their representation of aerosol needs improvement. Superparametrization efforts (where standard cloud parameterizations in the GCM are replaced by resolving clouds in each grid column of the GCM via a cloud resolving model, e.g., Grabowski, 2004) could lead the way for the development of more realistic cloud fields and thus improved treatments of aerosol-cloud interactions in large-scale models. However these are just being incorporated in models that resolve both cloud and aerosols. Detailed cloud parcel models have been developed to focus on the droplet activation problem (under what conditions droplets actually start forming) and questions associated with the first indirect effect. The coupling of aerosol and cloud modules to dynamical models that resolve the large turbulent eddies associated with vertical motion and clouds (henceforth, large eddy simulations or LES, with grid sizes of ~ 100 m and domains ~ 10 km) has proven to be a powerful tool for representing the details of aerosol-cloud interactions together with feedbacks (e.g., Feingold et al. 1994; Kogan et al. 1994; Stevens et al, 1996; Feingold et al. 1999; Ackerman et al. 2004). In this section we explore some of the complexity in the aerosol indirect effects revealed by such studies to illustrate how difficult parameterizing these effects properly in GCMs could really be.

a. The first indirect effect

The relationship between aerosol and drop concentrations (or drop sizes) is a key piece of the first indirect effect puzzle. It should not however, be equated to the first indirect effect which concerns itself with the resultant radiative forcing. A huge body of measurement and modeling work points to the fact that drop concentrations do indeed increase with increasing aerosol. The main unresolved questions relate to the degree of this effect, and the relative importance of aerosol size distribution, composition and updraft velocity in determining drop concentrations (for a review, see McFiggans et al., 2006). Studies indicate that the aerosol number concentration and size distribution are the most important factors. Updraft velocity (unresolved by GCMs) is particularly important under polluted conditions.

Although there are likely some composition effects that may have significant effect on drop number concentrations, composition is regarded as relatively unimportant compared to the other parameters (Fitzgerald, 1975; Feingold, 2003; Ervens et al., 2005; Dusek et al., 2006). Nevertheless, there are times when composition has a noticeable effect (see Appendix A.3). It has been stated that the significant complexity in aerosol composition can be modeled, for the most part, using fairly simple parameterizations that reflect the soluble and insoluble fractions (e.g., Rissler et al. 2004), yet composition cannot be ignored (an example is shown in Appendix A.3). Furthermore, chemical interactions cannot be overlooked. A large uncertainty remains concerning the impact of organic species on cloud droplet growth kinetics, and thus cloud droplet formation. Cloud drop size is affected by wet scavenging, which depends on composition. And future changes in composition will presumably arise due to biofuels/biomass burning and a reduction in sulfate emissions, which emphasizes the need to include composition changes in climate models when assessing the first indirect effect. The "sulfate plus insoluble" paradigm may become less applicable than is currently the case.

The updraft velocity, and its change as climate warms, may be the Achilles heel of GCMs because it is a key part of convection and the spatial distribution of condensate, as well as droplet activation. Numerous solutions to this problem have been sought, including estimation of vertical velocity based on predicted turbulent kinetic energy from boundary layer models (Lohmann et al., 1999; Larson et al.,

2001) and PDF representations of subgrid quantities, such as vertical velocity and the vertically-integrated cloud liquid water ('liquid water path', or LWP) (Pincus and Klein, 2000; Golaz et al., 2002a,b; Larson et al., 2005). Embedding cloud resolving models within GCMs is also being actively pursued (Grabowski et al. 1999; Randall et al., 2003). Numerous other details come into play; for example, the treatment of cloud droplet activation in GCM frameworks is often based on the assumption of adiabatic conditions, which may overestimate the sensitivity of cloud to changes in CCN (Sotiropoulou et al., 2006, 2007). It will take extensive observations, under difficult conditions, to clarify the requisite cloud and aerosol physics.

b. Other indirect effects

The second indirect effect is often referred to as the "cloud lifetime effect", based on the premise that clouds that do not precipitate will live longer. In GCMs the "lifetime effect" is equivalent to changing the representation of precipitation production and can be parameterized as an increase in cloud area or cloud cover (e.g., Hansen et al., 2005). The second indirect effect hypothesis relates increased aerosol to increased drop concentrations, smaller drops, suppressed collision-induced rain, and longer cloud lifetime. It is curious that, other than the suppression of rain in warm clouds (Warner 1968), there is no clear observational support for this chain of events. Results from ship-track studies show that cloud water may increase or decrease in the tracks (Coakley and Walsh, 2002) and satellite studies suggest similar results for warm boundary layer clouds (Han et al. 2002). Ackerman et al. (2004) used LES to show that in stratocumulus, cloud water may increase or decrease in response to increasing aerosol depending on the relative humidity of the air overlaying the cloud. Wang et al. (2003) showed that all else being equal, polluted stratocumulus clouds tend to have lower water contents than clean clouds because the small droplets associated with polluted clouds evaporate more readily and induce an evaporation-entrainment feedback that dilutes the cloud. This result was confirmed by Xue and Feingold (2006) and Jiang and Feingold (2006) for shallow cumulus, where pollution particles were shown to decrease cloud fraction. Furthermore, Xue et al. (2007) suggested that there may exist two regimes: the first, a precipitating regime at low aerosol concentrations where an increase in aerosol will suppress precipitation and increase cloud cover (Albrecht, 1989); and a second, non precipitating regime where the enhanced evaporation associated with smaller drops will decrease cloud water and cloud fraction.

Finally, the question of possible effects of aerosol on cloud lifetime was examined by Jiang et al. (2006) who tracked hundreds of cumulus clouds generated by LES from their formative stages until they dissipated. They showed there was no effect of aerosol on cloud lifetime, and that cloud lifetime was dominated by dynamical variability.

It could be argued that the representation of these complex feedbacks in GCMs is not warranted until a better understanding of the processes is at hand. Moreover, until GCMs are able to represent cloud scales, it is questionable what can be obtained by adding microphysical complexity to poorly resolved clouds. A better representation of aerosol-cloud interactions in GCMs therefore depends on our ability to improve representation of aerosols and clouds, as well as their interaction. We return to this discussion in the next chapter.

3.4. Impacts of Aerosols on Model Climate Simulations

It was noted in the introduction that aerosol cooling is essential in order for models to produce the observed global temperature rise over the last century, at least models with climate sensitivities in the range of 3°C for doubled CO_2 (or ~0.75°C/Wm^{-2}). Here we discuss this in somewhat more detail.

Hansen et al. (2007) show that in the GISS model well-mixed greenhouse gases produce a warming of close to 1°C between 1880 and the present {**Table 3.5** adapted from Hansen et al., 2007 Table 1}. The direct effect of tropospheric aerosols as calculated in that model produces cooling of close to –0.3°C between those same years, while the indirect effect (represented in that study as cloud cover change) produces an additional cooling of similar magnitude [note that in contrast, in the general model result quoted in IPCC (2007), the radiative forcing from indirect aerosols is twice that of the direct effect].

The time dependence of the total aerosol forcing as well as the individual species components is shown in **Figure 3.21** {adapted from Hansen et al., 2007 Fig.3c}. The resultant warming, of ~0.5°C including these and other forcings (Table 3.5), is less than observed. Hansen et al. (2007) further show that a reduction in sulfate optical thickness and the direct aerosol effect by 50%, which also reduced the aerosol indirect effect by 18%, results in the aerosol negative forcing from 1880 to 2003 being –0.91 Wm^{-2} (down from –1.37 Wm^{-2} with this revised forcing). The model now warms 0.75°C over that time period, closer to the observed warming of 0.8°C. Hansen et al. (op cit.) defend this change by noting that sulfate aerosol removal over North America and western Europe during the 1990s led to a cleaner atmosphere. Note that the comparisons shown in the previous section suggest that the GISS model already underestimates aerosol optical depths; it is thus trends that are the issue here.

Table 3.5. Climate forcings (1880-2003) used to drive GISS climate simulations, along with the surface air temperature changes obtained for several periods. Instantaneous (Fi), adjusted (Fa), fixed SST (Fs) and effective (Fe) forcings are defined in Hansen et al. 2005. From Hansen et al., 2007.

Forcing Agent	**Forcing Wm^{-2} (1880-2003)**				**ΔT surf °C [Year to 2003]**			
	Fi	**Fa**	**Fs**	**Fe**	**1880**	**1900**	**1950**	**1979**
Well-mixed GHGs	2.62	2.50	2.65	2.72	.96	.93	.74	.43
Stratospheric H_2O	-	-	.06	.05	.03	.01	.05	.00
Ozone	.44	.28	.26	.23	.08	.05	.00	-.01
Land Use	-	-	-.09	-.09	-.05	-.07	-.04	-.02
Snow Albedo	.05	.05	.14	.14	.03	.00	.02	-.01
Solar Irradiance	.23	.24	.23	.22	.07	.07	.01	.02
Strat Aerosols	.00	.00	.00	.00	-.08	-.03	-.06	.04
Trop. Aer., Direct	-.41	-.38	-.52	-.60	-.28	-.23	-.18	-.10
Trop. Aer., 2nd IE	-	-	-.87	-.77	-.27	-.29	-.14	-.05
Sum of Above	**-**	**-**	**1.86**	**1.9**	**.49**	**.44**	**.40**	**.30**
All Forcings at once	**-**	**-**	**1.77**	**1.75**	**.53**	**.61**	**.44**	**.29**

This is not the only example of inverse-reasoning (Anderson et al., 2003), in which model simulations incorporate aerosols calibrated to bring the temperature change results closer to observations. The magnitude of the indirect effect, as discussed by Hansen et al. (2005) is roughly tuned to produce the required response. The authors justify this approach by claiming that paleoclimate data indicate a climate sensitivity of close to 0.75°(±0.25) C/Wm^{-2}, and therefore something close to this magnitude of negative forcing is reasonable. Even this stated range leaves significant uncertainty in climate sensitivity and the magnitude of the aerosol negative forcing. Furthermore, IPCC (2007) concluded that paleoclimate data is *not* capable of narrowing the range of climate sensitivity, nominally 0.375 to 1.13 °C/Wm^{-2}, because of uncertainties in paleoclimate forcing and response, so from this perspective the total aerosol forcing is even less constrained than the GISS estimate. Hansen et al. (2007) acknowledge that (in their words) "an equally good match to observations probably could be obtained from a model with larger sensitivity and smaller net forcing, or a model with smaller sensitivity and larger forcing".

The GFDL model results for global mean ocean temperature change (down to 3 km depth) for the time period 1860 to 2000 is shown in **Figure 3.22** {adapted from Delworth et al., 2005, Fig. 1}, along with the different contributing factors (Delworth et al., 2005). This is the same GFDL model whose aerosol distribution was discussed previously. The aerosol forcing produces a cooling on the order of 50% that of greenhouse warming (generally similar to that calculated by the GISS model, Table 3.5). Similar reasoning concerning the somewhat arbitrary nature of the aerosol forcing applies to this model conclusion, in particular concerning the indirect aerosol cooling.

The general model response noted by IPCC, as discussed in the introduction, was that the total aerosol effect of –1.2 Wm^{-2} reduced the greenhouse forcing of some 3 W m^{-2} by about 40%, in the neighborhood of the GFDL and GISS forcings. Since the average model sensitivity was close to 0.75 Wm^{-2},

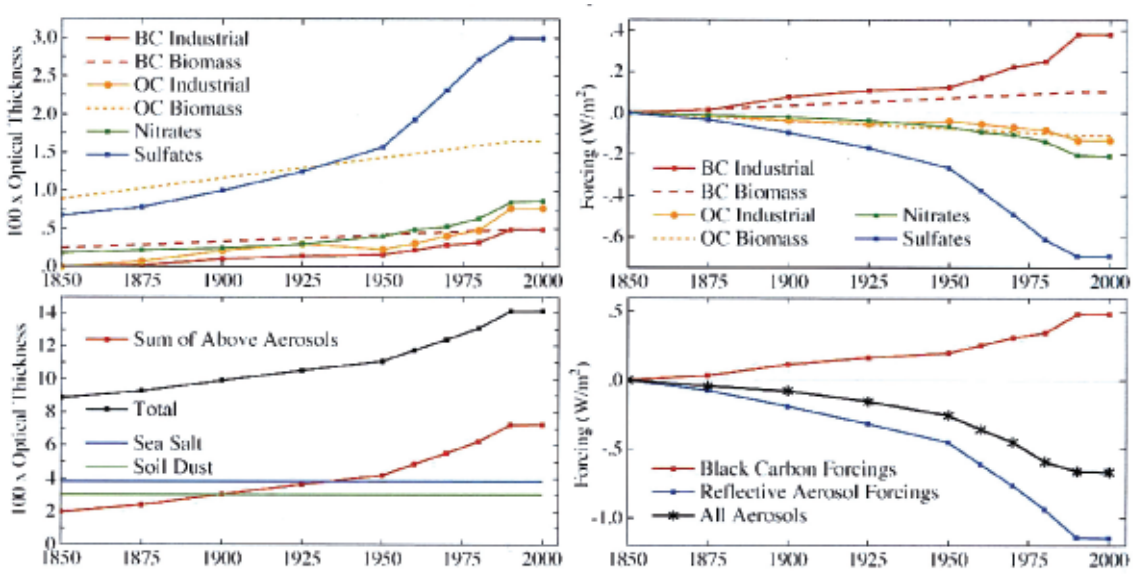

Fig. 3.21. Time dependence of aerosol optical thickness (left) and effect climate forcing (right). Note that as specified, the aerosol trends are all 'flat' from 1990 to 2000. From Hansen et al. (2007).

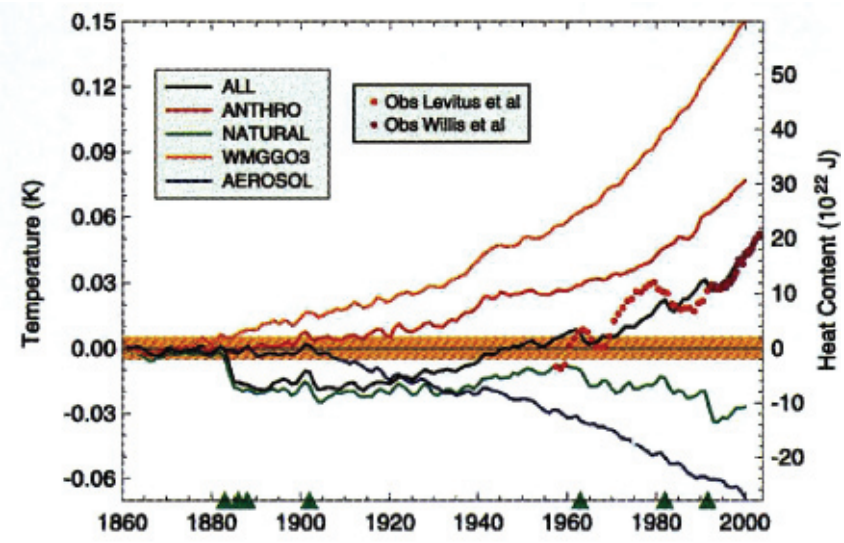

Fig. 3.22. Change in global mean ocean temperature (left axis) and ocean heat content (right axis) for the top 3000 m due to different forcings in the GFDL model. WMGG includes all greenhouse gases and ozone; NATURAL includes solar and volcanic aerosols (events shown as green triangles on the bottom axis). Observed ocean heat content changes are shown as well. From Delworth et al., 2005.

similar to the sensitivities of these models, the necessary negative forcing is therefore similar. The agreement cannot therefore be used to validate the actual aerosol effect until climate sensitivity itself is better known.

Is there some way to distinguish between greenhouse gas and aerosol forcing that would allow the observational record to indicate how much of each was really occurring? This question of attribution has been the subject of numerous papers, and the full scope of the discussion is beyond the range of this report. It might be briefly noted that Zhang et al. (2006) using results from several GCMs and including both spatial and temporal patterns, found that the climate responses to greenhouse gases and sulfate aerosols are correlated, and separation is possible only occasionally, especially at global scales and during summer when the aerosol effect on solar absorption is likely to be bigger. The conclusions concerning this appear to be model and method-dependent: using time-space distinctions as opposed to trend detection may work differently in different models (Gillett et al., 2002a). Using multiple models helps primarily by providing larger-ensemble sizes for statistics (Gillett et al., 2002b). However, even distinguishing between the effect of different aerosol types is difficult. Jones et al. (2005) concluded that currently the pattern of temperature change due to black carbon is indistinguishable from the sulfate aerosol pattern. In contrast, Hansen et al. (2005) found that absorbing aerosols produce a different global response than other forcings, and so may be distinguishable. Overall, the similarity in response to all these very different forcings is undoubtedly due to the importance of climate feedbacks in amplifying the forcing, whatever be its nature.

Distinctions in the climate response do appear to arise in the vertical, where absorbing aerosols produce warming that is exhibited throughout the troposphere and into the stratosphere, whereas reflective aerosols cool the troposphere but warm the stratosphere (Hansen et al., 2005). Delworth et al. (2005) noted that in the ocean, the cooling effect of aerosols extended to greater depths, due to the thermal instability associated with cooling the ocean surface. Hence the temperature response at levels both above and below the surface may provide an additional constraint on the magnitudes of each of these forcings.

3.5. Implications of comparisons of modeled and observed aerosols for climate model simulations.

The comparisons in subsections 2 and 3 suggest (tentatively) that models may underestimate aerosol concentrations and the direct effect over the oceans and in the Southern Hemisphere, and over land in the tropics, while overestimating it over land in the Northern Hemisphere. If so, the global average response would be more accurate than the hemispheric differentiation. The fact that the total optical depth is in better agreement between models than the individual components means that even with similar optical depths, the aerosol direct forcing effect may be quite different (as it is in the difference models, e.g., Fig. 3.12).

The indirect effect is strongly influenced by the aerosol concentrations, so if the above discrepancies are true, the indirect effect will also have these shortcomings. If that proves to be the case, than the model simulations of anthropogenic warming over land in the Northern Hemisphere would be underestimated (aerosol cooling being too large), while the warming is overestimated in other regions. It is, however, important to distinguish between those aerosols that are expected to change with time and those that are not; model discrepancies concerning the latter category will not affect the climate change simulations nearly as strongly. And errors in absorbing aerosols (e.g., black carbon) will have somewhat of an opposite climate influence from errors in reflecting aerosols (e.g., sulfates).

This type of speculation can only be better quantified when aerosol observations and models are improved. The pathway to this objective is discussed in the following chapter.

References

Ackerman, A. S., M. P. Kirkpatrick, D. E. Stevens and O. B. Toon, 2004: The impact of humidity above stratiform clouds on indirect aerosol climate forcing. *Nature*, **432**, 1014-1017.

Albrecht, B. 1989: Aerosols, cloud microphysics and fractional cloudiness. *Science*, **245**, 1227-1230.

Anderson, T. L., R. J. Charlson, S. E. Schwartz, R. Knutti, O. Boucher, H. Rodhe and J. Heintzenberg, 2003: Climate forcing by aerosols – a hazy picture. *Science*, **300**, 1103-1104.

Andreae, M. O., D. Rosenfeld, P. Artaxo, A. A. Costa, G. P. Frank, K. M. Longo and M. A. F. Silvas-Dias, 2004: Smoking rain clouds over the amazon. *Science*, **303**, 1337-1342.

Bates, T. S. et al., 2006: Aerosol direct radiative effects over the northwest Atlantic, northwest Pacific, and North Indian Oceans: estimates based on in-situ chemical and optical measurements and chemical transport modeling. *Atmos. Chem. Phys. Discuss.*, **6**, 175-362.

Boucher, O., and M. Pham, 2002: History of sulfate aerosol radiative forcings. *Geophys. Res. Lett.*, **29**, 22–25.

Chin, M. et al., 2002: Tropospheric aerosol optical depth from the GOCART model and comparisons with satellite and Sun photometer measurements. *J. Atmos. Sci.*, **59**, 461-483.

Chung, C. E. and G. Zhang, 2004: Impact of absorbing aerosol on precipitation. *J.* Geophys. *Res.*, **109**, doi:10.1029/2004JD004726.

Coakley, J. A. Jr. and C. D. Walsh, 2002: Limits to the Aerosol Indirect Radiative Effect Derived from Observations of Ship Tracks. *J. Atmos. Sci.*, **59**, 668-680

Delworth, T. L., V. Ramaswamy and G. L. Stenchikov, 2005: The impact of aerosols on simulated ocean temperature and heat content in the 20th century. *Geophys. Res. Lett.*, **32**, doi:10.1029/2005GL024457.

Dusek, U., G. P. Frank, L. Hildebrandt, J. Curtius, S. Walter, D. Chand, F. Drewnick, S. Hings, D. Jung, S. Borrmann, and M. O. Andreae (2006), Size matters more than chemistry in controlling which aerosol particles can nucleate cloud droplets, *Science*, *312*, 1375-1378.

Eagan, R. c., P. V. Hobbs and L. F. Radke, 1974: Measurements of cloud condensation nuclei and cloud droplet size distributions in the vicinity of forest fires. *J. Appl. Meteor.*, **13**, 553-557.

Ervens, B., G. Feingold, and S. M. Kreidenweis, 2005: The influence of water-soluble organic carbon on cloud drop number concentration. *J. Geophys. Res.*, **110,** D18211, doi:10.1029/2004JD005634.

Feingold, G., B. Stevens, W.R. Cotton, and R.L. Walko, 1994: An explicit microphysics/LES model designed to simulate the Twomey Effect. *Atmospheric Research*, **33**, 207-233.

Feingold, G., W. R. Cotton, S. M. Kreidenweis, and J. T. Davis, 1999: Impact of giant cloud condensation nuclei on drizzle formation in marine stratocumulus: Implications for cloud radiative properties. *J. Atmos. Sci.*, **56**, 4100-4117.

Feingold, G., 2003: Modeling of the first indirect effect: Analysis of measurement requirements. *Geophys. Res. Lett.*, **30**, No. 19, doi:10.1029/2003GL017967.

Feingold, G., H. Jiang, and J. Y. Harrington, 2005: On smoke suppression of clouds in Amazonia. *Geophys. Res. Lett.*, **32**, No. 2, L02804, 10.1029/2004GL021369.

Fitzgerald, J. W., 1975: Approximation formulas for the equilibrium size of an aerosol particle as a function of its dry size and composition and the ambient relative humidity, *J. Appl. Meteor.* **14**, 1044-1049.

Gillett, N.P., et al., 2002a: Reconciling two approaches to the detection of anthropogenic influence on climate. *J. Clim.*, **15**, 326–329.

Gillett, N.P., et al., 2002b: Detecting anthropogenic influence with a multimodel ensemble. *Geophys. Res. Lett.*, **29,** doi:10.1029/2002GL015836.

Ginoux, P., M. Chin, I. Tegen, J. M. Prospero, B. Holben, O. Dubovik and S.-J. Lin, 2001: Sources and distributions of dust aerosols simulated with the GOCART model. *J. Geophys. Res.*, **20**, 20255-20273.

Ginoux, P., L. W. Horowitz, V. Ramaswamy, I. V. Geogdzhayev, B. N. Holben, G. Stenchikov and X. Tie, 2006: Evaluation of aerosol distribution and optical depth in the Geophysical Fluid Dynamics Laboratory coupled model CM2.1 for present climate. *J. Geophys. Res.*, **111**, doi:10.1029/2005JD006707.

Golaz, J-C., V. E. Larson, and W. R. Cotton, 2002a: A PDF-based model for boundary layer clouds. Part I: Method and model description, *J. Atmos. Sci*., **59**, 3540-3551.

Golaz, J-C., V. E. Larson, and W. R. Cotton, 2002b: A PDF-based model for boundary layer clouds. Part II: Model results. *J. Atmos. Sci*., **59**, 3552-3571.

Grabowski, W.W., 2004: An improved framework for superparameterization. *J. Atmos. Sci*., **61**, 1940-52.

Grabowski, W.W., X. Wu, and M.W. Moncrieff, 1999: Cloud resolving modeling of tropical cloud systems during Phase III of GATE. Part III: Effects of cloud microphysics, *J. Atmos. Sci*., **56**, 2384-2402.

Gregory, J.M., et al., 2002: An observationally based estimate of the climate sensitivity. *J. Clim.*, **15,** 3117–3121.
Han, Q. Y., W. B. Rossow, J. Zeng, and R. M. Welch, 2002: Three different behaviors of liquid water path of water clouds in aerosol-cloud interactions. *J. Atmos. Sci.*, **59**, 726-735.
Hansen, J., M. Sato and R. Ruedy, 1997: Radiative forcing and climate response. *J. Geophys. Res.*, **102**, 6831-6864.
Hansen, J., et al., 2005: Efficacy of climate forcings. *J. Geophys. Res.*, **110**, doi:10.1029/2005JD005776, 45pp.
Hansen, J. et al., 2007: Climate simulations for 1880-2003 with GISS model E. *J. Geophys. Res.*, in press.
Harvey, L.D.D., 2004: Characterizing the annual-mean climatic effect of anthropogenic CO_2 and aerosol emissions in eight coupled atmosphere-ocean GCMs. *Clim. Dyn.,* **23**, 569–599.
IPCC, 2007: Climate Change 2007: *The Physical Science Basis. Contribution of Working Group I to the Fourth Assessment Report of the Intergovernmental Panel on Climate Change* [Solomon, S., D. Qin, M. Manning, Z. Chen, M. Marquis, K.B. Avery, M. Tignor and H.L. Miller (eds.)]. Cambridge University Press, Cambridge, United Kingdom and New York, NY, USA, 996 pp.
Jiang, H., and G. Feingold, 2006: Effect of aerosol on warm convective clouds: Aerosol-cloud-surface flux feedbacks in a new coupled large eddy model. *J. Geophys. Res.*, **111**, D01202, doi:10.1029/2005JD006138.
Jiang, H., H. Xue, A. Teller, G. Feingold, and Z. Levin, 2006: Aerosol effects on the lifetime of shallow cumulus. *Geophys. Res. Lett.*, **33**, doi: 10.1029/2006GL026024.
Jones, G.S., et al., 2005: Sensitivity of global scale attribution results to inclusion of climatic response to black carbon. *Geophys. Res. Lett.*, **32**, L14701, doi:10.1029/2005GL023370.
Kaufman, Y. J., I. Koren, L. A. Remer, D. Rosenfeld and Y. Rudich, 2005: The effect of smoke, dust and pollution aerosol on shallow cloud development over the Atlantic Ocean. *Proc. Natl. Acad. Sci.*, **102**, 11207-11212.
Kerr, R., 2007: Another global warming icon comes under attack. *Science*, **317**, 28.
Kiehl, J. T., 2007: Twentieth century climate model response and climate sensitivity. *Geophys. Res. Lett.*, **34**, doi:10.1029/2007GL031383.
Kinne, S., et al., 2006: An AeroCom initial assessment: optical properties in aerosol component modules of global models. *Atmos. Chem. Phys*. **6**, 1815–1834.
Knutti, R., T.F. Stocker, F. Joos, and G.-K. Plattner, 2002: Constraints on radiative forcing and future climate change from observations and climate model ensembles. *Nature,* **416,** 719–723.
Knutti, R., T.F. Stocker, F. Joos, and G.-K. Plattner, 2003: Probabilistic climate change projections using neural networks. *Clim. Dyn.*, **21**, 257– 272.
Koch, D., 2001: Transport and direct radiative forcing of carbonaceous and sulfate aerosols in the GISS GCM. *J. Geophys. Res.*, **106**, 20311-20332.
Koch, D., G. A. Schmidt and C. V. Field, 2006: Sulfur, sea salt and radionuclide aerosols in GISS Model E. *J. Geophys. Res.*, **111**, doi:10.1029/2004JD005550.
Kogan, Y. L., D. K. Lilly, Z. N. Kogan, and V. Filyushkin, 1994: The effect of CCN regeneration on the evolution of stratocumulus cloud layers. *Atmos. Res.*, **33**, 137- 150.
Kruger, O. and Grasl, H., 2002: The indirect aerosol effect over Europe. *Geophys. Res. Lett.*, **29**, doi:10.1029/2001GL014081.

Larson, V. E., R. Wood, P. R. Field, J.-C. Golaz, T. H. Vonder Haar, and W. R. Cotton, 2001: Small-scale and mesoscale variability of scalars in cloudy boundary layers: One-dimensional probability density functions, *J. Atmos. Sci*., **58**, 1978-1996.

Larson, V.E., J.-C. Golaz, H. Jiang and W.R. Cotton, 2005: Supplying local microphysics parameterizations with information about subgrid variability: Latin hypercube sampling, *J. Atmos. Sci.*, **62,** 4010-4026.

Lefohn, A. S., J. D. Husar and R. B. Husar, 1999: Estimating historical anthropogenic global sulfur emission patterns for the period 1850-1990. *Atm. Env.*, **33**, 3435-3444.

Liousse, C., J. E. Penner, C. Chuang, J. J. Walton, H. Eddleman and H. Cachier, 1996: A three-dimensional model study of carbonaceous aerosols. *J. Geophys. Res.*, **101**, 19411-19432.

Liu, L., A. A. Lacis, B. E. Carlson, M. I. Mishchenko, and B. Cairns, 2006: Assessing Goddard Institute for Space Studies ModelE aerosol climatology using satellite and ground-based measurements: A comparison study. *J. Geophys. Res.*, **111**, doi:10.1029/2006JD007334.

Lohmann, U., J. Feichter, C. C. Chuang, and J. E. Penner, 1999: Prediction of the number of cloud droplets in the ECHAM GCM, *J. Geophys. Res.*, **104**, 9169-9198.

Lohmann, U. and J. Feichter, 2005: Global indirect aerosol effects: a review. *Atmos. Chem. Phys.*, **5**, 715-737.

Lohmann, U., I. Koren and Y.J. Kaufman, 2006: Disentangling the role of microphysical and dynamical effects in determining cloud properties over the Atlantic, *Geophys. Res. Lettr.,* **33**, L09802.

McFiggans, G., P. Artaxo, U. Baltensberger, H. Coe, M.C. Facchini, G. Feingold, S. Fuzzi, M. Gysel, A. Laaksonen, U. Lohmann, T. F. Mentel, D. M. Murphy, C. D. O'Dowd, J. R. Snider, E. Weingartner, 2006: The effect of physical and chemical aerosol properties on warm cloud droplet activation. *Atmos. Chem. Phys.*, **6**, 2593-2649.

Menon, S., A.D. Del Genio, Y.J. Kaufman, R. Bennartz, D. Koch, N. Loeb and D. Orlikowski, 2007: Analyzing signatures of aerosol-cloud interactions from satellite retrievals and the GISS GCM. J. Geophys. Res., In Review.

Mishchenko, M. I. And I. V. Geogdzhayev, 2007: GACP data show potential climate impact of aerosols. *GEWEX*, **17**, 4-5.

Nakicenovic, N. et al., 2000: *Special Report on Emissions Scenarios: A Special Report of Working Group III of the Intergovernmental Panel on Climate Change*, Cambridge University Press, Cambridge, U.K., 599 pp.

Penner, J. E. et al., 2002: A comparison of model- and satellite-derived aerosol optical depth and reflectivity. *J. Atmos. Sci.*, **59**, 441-460.

Penner, J. E., et al. 2006: Model intercomparison of indirect aerosol effects. *Atmos. Chem. Phys., Discuss.*, **6**, 1579-1617.

Pincus, R., and S.A. Klein, 2000: Unresolved spatial variability and microphysical process rates in large-scale models, *J. Geophys. Res.*, **105**, 27,059-27,065.

Quaas, J., O. Boucher and U. Lohmann, 2006: Constraining the total aerosol indirect effect in the LMDZ GCM and ECHAM4 GCMs using MODIS satellite data. *Atmos. Chem. Phys. Disc.,* **5**, 9669-9690.

Ramanathan, V., P. J. Crutzen, J. T. Kiehl and D. Rosenfeld, 2001: Aerosols, climate and the hydrological cycle. *Science*, **294**, 2119-2124.

Randall, D., M. Khairoutdinov, A. Arakawa, and W. Grabowski, 2003: Breaking the cloud parameterization deadlock, *Bull. Amer. Meteorol. Soc.*, **84**, 1547-1564.

Reddy, M. S., O. Boucher, N. Bellouin, M. Schulz, Y. Balkanski, J.-L. Dufresne and M. Pham, 2005: Estimates of global multicomponent aerosol optical depth and radiative perturbation in the Laboratoire de Meteorologie Dynamique general circulation model. *J/ Geophys. Res.*, **110**, doi:10.1029/2004JD004757.

Rissler, J., E. Swietlicki, J. Zhou, G. Roberts, M. O. Andreae, L. V. Gatti, and P. Artaxo 2004: Physical properties of the sub-micrometer aerosol over the Amazon rain forest during the wet-to-dry season transition – comparison of modeled and measured CCN concentrations, *Atmos. Chem. Phys.,* **4**, 2119-2143.

Roderick, M. L. and G. D. Farquhar, 2002: The cause of decreased pan evaporation over the past 50 years. *Science*, **298**, 1410-1411.

Rosenfeld, D., 2000: Suppression of rain and snow by urban and industrial air pollution. *Science,* **287**, 1793-1796.

SAP 1.1, 2006: Temperature Trends in the Lower Atmosphere. T. R. Karl, S. J. Hassol, C. D. Miller and W. L. Murray, editors. Available from the Global Change Research Information Office, Washington, D.C. 164pp.

Schmidt, G. A., et al., 2006: Present-day atmospheric simulations using GISS Model E: Comparison to in-situ, satellite and reanalysis data. *J. Clim.*, **19**, 153-192.

Schulz, M. et al., 2006: Radiative forcing by aerosols as derived from the AeroCom present-day and pre-industrial simulations. *Atmos. Chem. Phys*., **6**, 5225–5246.

Schwartz, S. E., R. J. Charlson and H. Rodhe, 2007: Quantifying climate change – too rosy a picture? *Nature Reports*, *Climate Change*, **2**, 23-24.

Smith, S.J., Pitcher, H. and Wigley, T.M.L., 2001: Global and regional anthropogenic sulfur dioxide emissions. *Global and Planetary Change* 29, 99- 119.

Sotiropoulou, R.E.P, Nenes, A., Adams, P.J., Seinfeld, J.H. (2007) Cloud condensation nuclei prediction error from application of Kohler theory: Importance for the aerosol indirect effect, *J.Geoph. Res.*, **112**, D12202, doi:10.1029/2006JD007834

Sotiropoulou, R.E.P, Medina, J., Nenes A. (2006) CCN predictions: is theory sufficient for assessments of the indirect effect?, *Geoph.Res.Let.*, **33**, L05816, doi:10.1029/2005GL025148

Stevens, B., G. Feingold, R. L. Walko and W. R. Cotton, 1996: On elements of the microphysical structure of numerically simulated non-precipitating stratocumulus. J. Atmos. Sci., 53, 980-1006.

Storlevmo, T., J.E. Kristjansson, G. Myhre, M. Johnsud, and F. Stordal, 2006: Combined observational and modeling based study of the aerosol indirect effect, *Atmos. Chem. Phys. Dis*., **6**, 3757-3799.

Stott, P.A., et al., 2006: Observational constraints on past attributable warming and predictions of future global warming. *J. Clim.*, **19**, 3055– 3069.

Textor, C., et al., 2007: The effect of harmonized emissions on aerosol properties in global models - an AeroCom experiment. *Atmos. Chem.Phys. D*isc., 2007.

Tie, X. et al., 2005: Assessment of the global impact of aerosols on tropospheric oxidants. *J. Geophys. Res.*, **110**, doi:10.1029/2004JD005359.

Twomey, S. A., 1977: The influence of pollution on the shortwave albedo of clouds. *J. Atmos. Sci.*, **34**, 1149-1152.

Van Ardenne, J. A., Dentener, F. J., Olivier, J. G. J., Klein, Goldewijk, C. G. M., and Lelieveld, J., 2001: A 1° x 1° resolution data set of historical anthropogenic trace gas emissions for the period 1890–1990. *Global Biogeochem. Cycl*. **15**, 909–928.

Wang, S., Q. Wang, and G. Feingold, 2003: Turbulence, condensation and liquid water transport in numerically simulated nonprecipitating stratocumulus clouds. *J. Atmos. Sci.*, **60**, 262-278.

Warner, J., 1968: A reduction of rain associated with smoke from sugar-cane fires—An inadvertent weather modification, *J. App. Meteor.,* **7**, 247–251.

Wen, G., A. Marshak, R. F. Cahalan, L. A. Remer, R. G. Kleidman, 2007: 3-D aerosol cloud radiative interaction observed in collocated MODIS and ASTER images of cumulus cloud fields. J. Geophys. Res., 112, No, D13, D1320410.1029/2006JD008267

Wild, M., et al., 2005: From dimming to brightening: decadal changes in solar radiation at Earth's surface. *Science*, **308**, 847-850.

Xue, H., G. Feingold, and B. Stevens, 2007: Aerosol effects on clouds, precipitation, and the organization of shallow cumulus convection. *J. Atmos. Sci.*, in press.

Xue, H., and G. Feingold, 2006: Large eddy simulations of trade-wind cumuli: Investigation of aerosol indirect effects. *J. Atmos. Sci.*, **63**, 1605-1622.

Yu H., S. C. Liu, and R. E. Dickinson, 2002: Radiative effects of aerosols on the evolution of the atmospheric boundary layer, *J. Geophys. Res.*, **107** (D12), doi:10.1029/2001JD000754.

Zhang, X., F.W. Zwiers, and P.A. Stott, 2006: Multi-model multi-signal climate change detection at regional scale. *Journal of Climate,* **19**, 4294-4307.

Appendix A.1

An approximate relation between aerosol optical depth and aerosol mass loading may be developed as follows. The local mass concentration for a single particulate component of an aerosol is given as an integral over size distribution as

$$m = \frac{4\pi\rho}{3}\int r^3 n(r)\,dr \tag{1}$$

where is the size distribution of the aerosol normalized such that $\int n(r)dr = N$ where N is the total number concentration. For multiple aerosol species

$$m = \sum m_i = \frac{4\pi}{3}\int r^3 [\sum \rho_i(r) n_i(r)]dr = \frac{4\pi}{3}\sum \rho_i \int r^3 n_i(r)dr \tag{2}$$

where the latter equality holds if the density of the individual aerosol species is independent of radius, a good approximation for particles sufficiently large to contribute appreciably to mass concentration. Finally the column mass burden (amount of aerosol particulate matter per Earth surface area) is

$$M = \int m(z)\,dz = \frac{4\pi}{3}\int\left\{\sum \rho_i(z)\int r^3 n_i(r,z)\,dr\right\}dz \tag{3}$$

where the dependence of particle size and density on height z is explicitly noted; such dependence is to be expected both through the intrinsic dependence of aerosol loading on height that results from prior mixing and transformation processes, and through the dependence relative humidity with height and the dependence of particle size on relative humidity (which can be quite strong, especially for high relative humidity as might be encountered near the top of the boundary layer). This mass burden can in turn be expressed in terms of a weighted average density of the aerosol in the column $\langle\rho\rangle$ as

$$M = \frac{4\pi}{3}\langle\rho\rangle\int\left\{\int r^3 n(r)\,dr\right\}dz \tag{4}$$

where

$$\langle \rho \rangle = \frac{\int \{ \sum \rho_i(z) \int r^3 n_i(r,z) dr \} dz}{\int \{ \int r^3 n(r) dr \} dz} \quad (5)$$

Similarly the local extinction coefficient of the aerosol particulate matter is given for a single component aerosol as

$$\sigma_{ep}(\lambda) = \int r^2 Q_e(r,\lambda) n(r) dr \quad (6)$$

where Q_e (r, λ) is the extinction efficiency factor, a function of particle size, composition (through index of refraction) and wavelength. The extinction coefficient is related to the phase function and the single scattering albedo of the aerosol. Again for a multicomponent aerosol

$$\sigma_{ep}(\lambda) = \sum \sigma_{ep,\,i}(\lambda) = \sum \int r^2 Q_{e,\,i}(r,\lambda) n_i(r) dr \quad (7)$$

Finally the aerosol optical depth is given as the integral of extinction coefficient with height:

$$\tau(\lambda) = \int \sigma_{ep}(\lambda, z) dz = \sum \{ \int r^2 Q_{e,\,i}(r,\lambda,z) n_i(r,z) dr \} \quad (8)$$

where the extinction efficiency implicitly depends on height through the dependence of index of refraction on composition, which even for a single component aerosol will vary with varying relative humidity through the dependence of index of refraction on water content of the particulate matter. This wavelength dependent optical depth can in turn be expressed in terms of a weighted average scattering efficiency in the column (also wavelength dependent) $\langle Q_e(\lambda) \rangle$ as

$$\tau(\lambda) = \langle Q_e(\lambda) \rangle \int \{ \int r^2 n(r) dr \} dz \quad (9)$$

where

$$\langle Q_e(\lambda) \rangle = \frac{\sum \{ \int r^2 Q_{e,\,i}(r,\lambda,z) n_i(r,z) dr \}}{\int \{ \int r^2 n(r) dr \} dz} \quad (10)$$

Hence the aerosol optical depth is related to the column mass burden as

$$\tau(\lambda) = \frac{3 \langle Q_e(\lambda) \rangle M}{4\pi \langle \rho \rangle r_{eff}} \quad (11)$$

where the effective radius r_{eff} is given by its usual definition (ratio of third to second moments of the distribution; Hansen and Travis, 1974) integrated over the aerosol column as

$$r_{eff} = \frac{\int \{ \int r^3 n(r) dr \} dz}{\int \{ \int r^2 n(r) dr \} dz} \quad (12)$$

and is an intensive aerosol property that is related to the Ångström exponent.

Appendix A.2

Several recent studies have pointed to formation of secondary organic aerosol in amounts and at rates that cannot be accounted for in current chemical modeling. In aircraft measurements in urban-influenced air in New England DeGouw et al (2005) found that particulate organic matter (POM) was highly correlated with secondary anthropogenic gas-phase species, strongly suggesting that the POM derived from secondary anthropogenic sources. This is illustrated in **Figure A2.1**, which shows scatterplots of submicrometer POM versus acetylene (a primary emitted species) and isopropyl nitrate (a secondary organic species formed by atmospheric reactions of primary emitted species) The increase in submicrometer POM with increasing photochemical age could not be explained by the removal of aromatic precursors alone, suggesting that other species must have contributed and/or that the mechanism for POM formation is more efficient than previously assumed.

A further example is aerosol production in Mexico City, **Figure A2.2**, that showed amounts of secondary organic aerosol (SOA) produced from anthropogenic volatile organic carbon at rates as much as

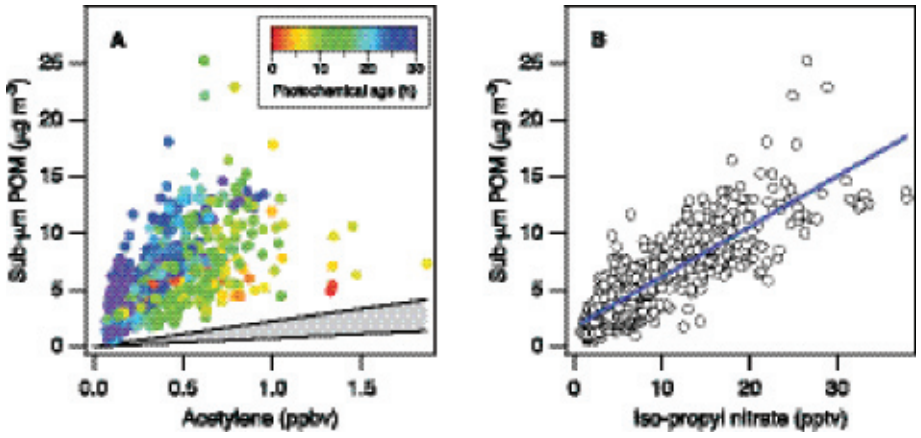

Figure A2.1. Scatterplots of the submicrometer particulate organic matter (POM) measured during the 1992 New England Air Quality Study versus (a) acetylene and (b) isopropyl nitrate. The colors of the data points in a denote the photochemical age as determined by the ratios of compounds of known OH reactivity; the gray area shows the range of ratios between submicrometer POM and acetylene typical of urban air. Modified from De Gouw et al. (2006).

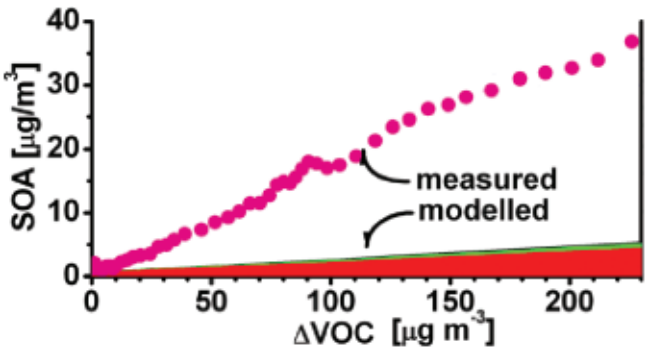

Figure A2.2. Measured and modeled secondary organic aerosol (SOA) formation in Mexico City on April 9 2003. Comparison of measured and modeled concentration of secondary organic aerosol SOA versus concentration of volatile organic carbon VOC calculated to have been oxidized. Shaded areas indicate the calculated amount of SOA-mass concentration attributed to aromatics (red), alkenes (green), alkanes (black). Modified from Volkamer et al (2006).

eight-fold greater than predicted by current models. Also contrary to current understanding, much of the excess secondary organic aerosol is formed from first-generation oxidation products.

The production of organic aerosol downwind of Mexico City has been further examined more recently in aircraft studies by normalizing the aerosol to carbon monoxide to account for dilution. Aerosol composition was determined by mass spectrometry, which showed the increasing dominance of the organic component of the aerosol over roughly one day of photochemical processing, **Figure A2.3**. The measured increase in organic aerosol exceeded the modeled increase, based on laboratory experiments and measured volatile organic carbon, by an order of magnitude.

The amount of organic aerosol formed by atmospheric reactions can be much greater than expected on the basis of present photochemical models, which are derived from theory and laboratory experiments. Aircraft measurements of organic carbon aerosol over the northwest Pacific revealed unexpectedly high concentrations in the free troposphere (FT) 10–100 times higher than computed with a global chemical transport model including a standard simulation of secondary organic aerosol formation based on empirical fits to smog chamber data. The same model was able to reproduce the observed vertical profiles of sulfate and elemental carbon aerosols, which exhibit sharp decreases from the boundary layer to the FT due to wet scavenging. The results were attributed to a large, sustained source of SOA in the FT from oxidation of long-lived volatile organic compounds. This SOA constituted the dominant component of the measured aerosol mass in the FT. In simulations of reactions forming secondary organic aerosol downwind of London Johnson et al (2006) found it necessary to increase the partitioning of organic into the aerosol phase by a factor of 500 over the partition coefficient that had been developed to simulate laboratory smog chamber studies.

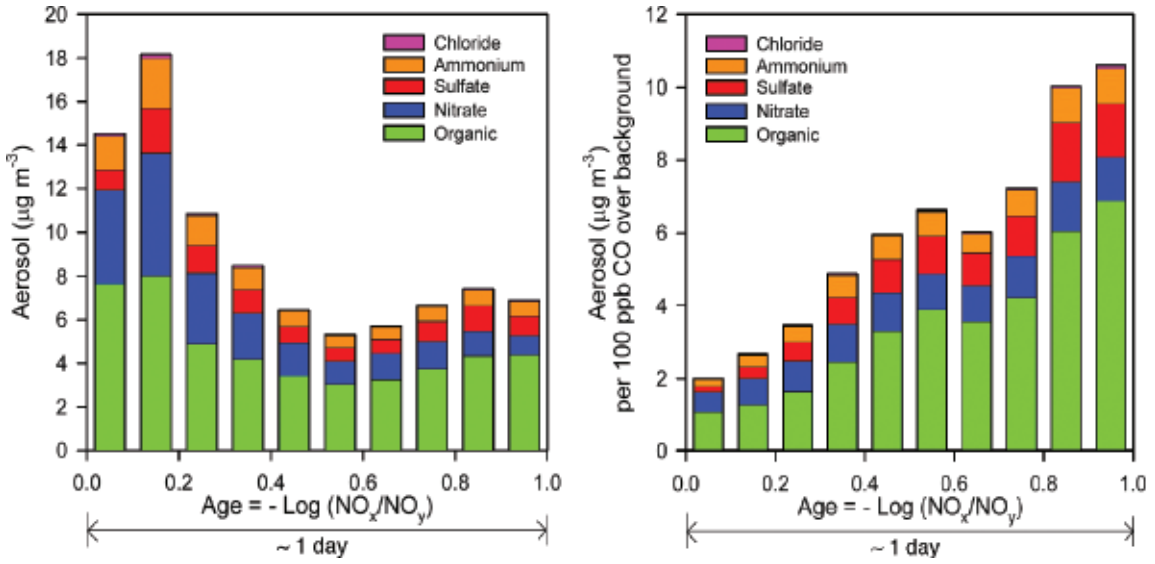

Figure A2.3. Measurements of the concentration of aerosol constituents by airborne aerosol mass spectrometry downwind of Mexico City, left, and normalized to excess carbon monoxide, right, to account for dilution. Measurements are binned according to photochemical age as determined from ratio of nitrogen oxides (NO_x = NO + NO_2) to higher oxidation products of these oxides, NOy, mainly nitric acid. Modified from Kleinman et al. (2007).

Another important recent finding that may have major implications to understanding and modeling organic aerosol comes from a series of laboratory and chemical transport modeling studies that identified and quantified aerosol formation from the oxidation of isoprene (Kroll et al, 2006; Henze and Seinfeld, 2006). The atmospheric oxidation of gas-phase hydrocarbons leads to the formation of low-volatility products that partition into the condensed phase; the resulting secondary organic aerosol accounts for a substantial fraction of global organic aerosol loading and hence has an important influence on climate. Large biogenic hydrocarbons (terpenes and sesquiterpenes) have long been believed to be the primary source of SOA on a global scale; although the biogenic hydrocarbon, isoprene, the second most abundant hydrocarbon in the earth's atmosphere after methane, is emitted in much larger quantities (~500 Tg yr^{-1}) than the terpenes, because of its low molecular weight it has generally been believed not to form SOA in appreciable amounts. However in recent environmental chamber experiments, photooxidation of isoprene has been shown to produce SOA in small but appreciable quantities (mass yields of 1-5%). Because of the large source strength of isoprene, even these small yields imply a major SOA source missing from previous atmospheric models. Inclusion of SOA formation from isoprene in a global chemical transport model was found to more than double the predicted SOA loading. This work indicates that isoprene may be the single most important contributor to SOA on a global scale, with important implications for global climate. The availability of a model representation of this process will allow it to be incorporated into large scale chemical transport models and climate models.

References

De Gouw, J. A., et al., 2005: Budget of organic carbon in a polluted atmosphere: Results from the New England Air Quality Study in 2002, *J. Geophys. Res*., **110**, D16305, doi:10.1029/2004JD005623.

Heald, C. L., D. J. Jacob, R. J. Park, L. M. Russell, B. J. Huebert, J. H. Seinfeld, H. Liao, and R. J. Weber, 2005: A large organic aerosol source in the free troposphere missing from current models, *Geophys. Res. Lett.*, **32**, L18809, doi:10.1029/2005GL023831.

Henze, D. K. and Seinfeld, J. H., 2006: Global secondary organic aerosol from isoprene oxidation. Geophys. Res. Lett. 33, L09812, doi:10.1029/2006GL025976.

Johnson D., S.R. Utembe, M.E. Jenkin, R.G. Derwent, G.D. Hayman, M.R. Alfarra, H. Coe and G. McFiggans, 2006: Simulating regional scale secondary organic aerosol formation during the TORCH 2003 campaign in the southern UK, *Atmos. Chem and Phys.* **6**: 403-418.

Kleinman, L. I., Springston, S. R., Daum, P. H., Lee, Y.-N., Nunnermacker, L. J., Senum, G. I., Wang, J., Weinstein-Lloyd, J., Alexander, M. L., Hubbe, J., Ortega, J., Canagaratna, M. R., and Jayne, J., 2007: The time evolution of aerosol composition over the Mexico City plateau. *Atmos. Chem. Phys. Discuss*. **7**, 14461-14509.

Kroll, J. H., Ng, N. L., Murphy, S. M., Flagan, R. C., and Seinfeld, J. H., 2006: Secondary organic aerosol formation from isoprene photooxidation. *Environ. Sci. Technol.* **40**, 1869-1877, doi:10.1021/es0524301.

Volkamer, R., J. L. Jimenez, F. San Martini, K. Dzepina, Q. Zhang, D. Salcedo, L. T. Molina, D. R. Worsnop, and M. J. Molina, 2006: Secondary organic aerosol formation from anthropogenic air pollution: Rapid and higher than expected, *Geophys. Res. Lett.*, **33**, L17811, doi:10.1029/2006GL026899.

Appendix A.3

An example of the importance of composition when parameterizing the first indirect effect is shown in **Figure A3.1**. Physical measurements, of the dependence of critical supersaturation of particles as a function of their diameter, show marked differences above and below a shallow stratus deck in the vicinity of Pt. Reyes, CA. Here the two diagonal lines (slope of -3/2 on a logarithmic plot of supersaturation vs dry diameter) indicates the dependence of critical supersaturation on particle size for constant composition according to the Köhler theory of cloud drop activation. Departure from this dependence indicates dependence on composition. The difference in critical supersaturation for two ionic substances, sodium chloride and ammonium sulfate, is about 32%, e.g., an increase from 0.2 to 0.26%, a substantial increase. Shown on the figure are measurements above and below a cloud deck off the coast of northern California. Activation of the above-cloud particles of the same size requires a greater supersaturation, and activation of particles at both altitudes requires a supersaturation about three times as high as would be expected for particles consisting entirely of inorganic salts; also shown for reference are measurements made in the eastern Caribbean, which are consistent with an inorganic salt composition. Simultaneous measurements of bulk composition show a greater organic fraction above clouds than below. Measurements of size dependent composition confirm that this organic fraction is greatest in the diameter range corresponding to the CCN measurements, 40 - 200 nm. In the absence of the chemical measurements the reasons for the differences in critical supersaturation would not be known; in the absence of the physical measurements the consequences of the differences in composition would not be known.

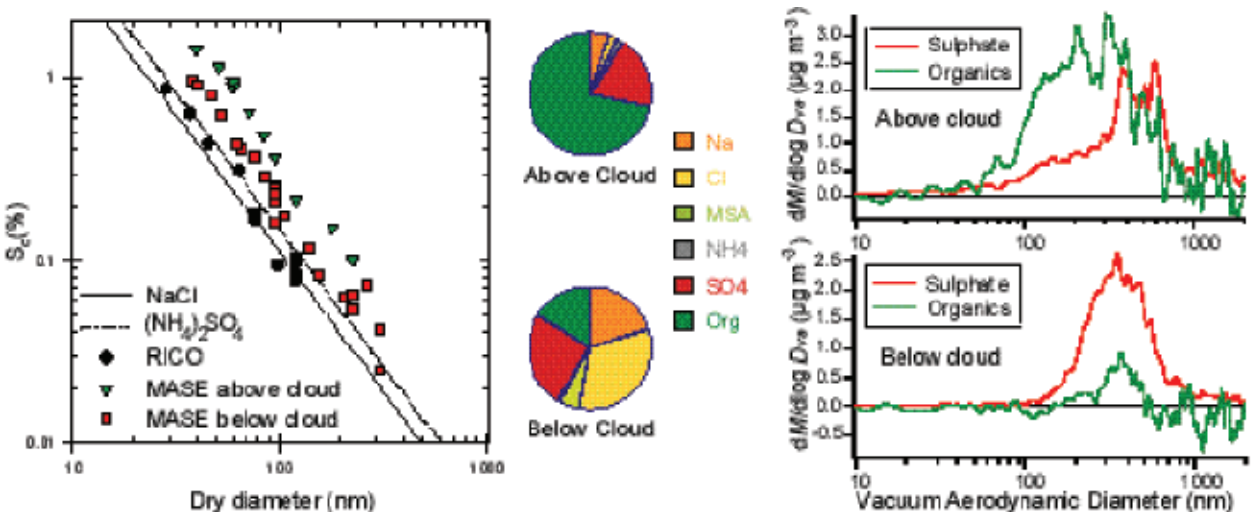

Figure A3.1. Example of difference in CCN activity of aerosols and relation to composition below (110-170 m) and above (400-470 m) clouds measured off the coast of California, north of San Francisco, on July 25, 2005. Left panel shows critical supersaturation as a function of particle size; also shown for comparison are measurements made in clean maritime air in the eastern Caribbean boundary layer and the theoretical dependence for two soluble salts, sodium chloride and ammonium sulfate (J. Hudson, Desert Research Institute, unpublished measurements; Hudson, 1989; Hudson and Da, 1996). Pie charts (middle panel) show ionic composition measured by PILS (particle into liquid sampler) and organic fraction inferred by difference from total volume, inferred from light scattering at low relative humidity and assumed mass scattering efficiency of 3.3 m2 g^{-1}; below cloud mass concentration 8.1 ± 0.3 µg m^{-3}; above cloud, 3.8 ± 0.2 µg m^{-3} (Y.-N. Lee, Brookhaven National Laboratory, unpublished measurements). Right panel shows the distribution of sulfate and organic mass with particle size above cloud (top) and below cloud (bottom) measured by aerosol mass spectrometry (M. Alexander, Pacific Northwest National Laboratory, unpublished measurements). From Ghan and Schwartz (2007).

References

Ghan S. J., and Schwartz S. E., 2007: Aerosol Properties and Processes: A Path from Field and Laboratory Measurements to Global Climate Models. *Bull. Amer. Meteorol. Soc*. **88**, 1059–1083.

Hudson J. G. and Da X., 1996: Volatility and size of cloud condensation nuclei. *J. Geophys. Res.* **101**, 4435-4442.

Chapter IV. Way Forward

Authors:. **D. Rind**, NASA GISS; **H. Yu**, NASA GSFC/UMBC; **S. E. Schwartz**, DOE BNL; **R. N. Halthore**, NASA HQ/NRL.

Table of Contents

4.1 Introduction

The previous chapters have emphasized that while we have made progress in understanding aerosol forcing of the climate system, there are still many uncertainties. To put the work in perspective, serious investigation of this issue has only been occurring for about the last 20 years. Given all the complexities, such as the varying aerosol types and emissions, uncertain refractive indices, great heterogeneity, and the added issue of interactions with clouds, it is not hard to believe that work of at least that many more years will be necessary before we can define aerosol forcing with a sufficient degree of confidence. And without improved understanding of how much aerosols have offset the better known greenhouse gas forcing for the last 150 years, we cannot use the past temperature record to determine the climate sensitivity over that time, or indeed the likely magnitude of climate response to future greenhouse gas (and aerosol) increases.

As discussed in Chapter 2, improved observations are already helping us to obtain an empirical estimate of the current direct effect of aerosols on climate, independent of models. Continued and even better observations are needed to refine this estimate. To be able to estimate climate forcing due to the indirect effect of aerosols, via their impact on cloud reflectivity and lifetime, will require much more extensive and coordinated campaigns. While choice of a target accuracy requirement for aerosol forcing is somewhat subjective (Schwartz, 2004), a possible target might be ± 0.3 W m^{-2}, comparable to the uncertainty associated with forcing by tropospheric ozone.

Predictions of the future effects of aerosols will have to rely on models, and as indicated in Chapter 3, the current state of observations is inadequate to allow us to assess model performance for anything other than total optical depth (and even that is somewhat uncertain, especially over land). Models produce much more in the way of specificity concerning aerosol distributions than the observations can verify. Improving observations for the purpose of validating models is another future goal.

Models also need to specify aerosol emissions and various aerosol properties. Modelers have also developed crude parameterizations for the interactions of aerosols with clouds. Better observations of all these particulars need to be obtained; many are in situ and in cloudy regimes, so we will need more than just surface or satellite platforms. This then is a third category of observational needs, to enable us to improve the various components of aerosol models.

On the modeling side, given the interactive nature of aerosols and climate, the most realistic results will ultimately be obtained when climate models incorporate aerosols "on-line" as part of their climate change simulations. This will require improved understanding, obtained both from observations of how aerosols are acting within the climate system, and laboratory assessments of aerosol physics/atmospheric chemistry. It will also require improved model meteorology, including better simulation of parameters directly affecting aerosols such as clouds and precipitation. These parameters are obviously important for their own purposes in modeling the climate system. Currently, climate models exhibit substantial error in shortwave cloud albedo in zonal monthly means, even when driven by observed sea surface temperature (Bender et al, 2006), the errors arising from errors in cloud amount and/or reflectivity. It is clear that models must accurately represent such cloud properties accurately if they are to be trusted for reliably calculating the future climate that would result from alternative scenarios of emissions of greenhouse gases, aerosols and aerosol precursors.

Coupling aerosol calculations into the standard climate models will require increased computational power, since many of the interactions are quite computer-intensive – and this will be competing with other computational demands, such as the desire for finer horizontal resolution.

In the rest of this chapter we discuss the primary observational and modeling needs, recognizing that the two are highly interactive, with observations helping to improve models, and models indicating what observations and what degree of accuracy are needed.

4.2 Requirements for Future Research – Observations

As noted above, observations are needed to observe aerosol radiative forcing directly and to improve models, in a variety of ways. We review the relevant types of needed research.

4.2.1. *In-situ measurements of aerosol properties and processes*

Recent work has shown the ubiquity of organic aerosols, especially secondary organic aerosols, and rapid rates of production of organic particulate matter, especially in photochemically active air influenced by recent urban emissions of hydrocarbons and nitrogen oxides. Recent measurements have also shown the widespread occurrence of new particle formation events; these are particularly important

as they influence the dynamics of aerosol evolution affecting optical and cloud nucleating properties. Large scale field campaigns, e.g., ICARTT, MILAGRO, have been particularly valuable in studying aerosol evolution processes and in identification especially of the rapid formation of secondary organic aerosol. The advantage of such studies is that they bring to bear many measurement capabilities, multiple aircraft platforms. Clearly such campaigns are required in the future, with enhanced measurement capabilities, especially for the organic precursor gases. Such field campaigns also serve to provide highly detailed data sets for development and/or evaluation of models describing aerosol evolution.

In addition to such large scale campaigns there is a requirement for a dispersed network of aerosol research observatories examining aerosol size-distributed composition and the relation between size-distributed composition, hygroscopic growth, optical properties, and CCN properties. Such systematic measurements are necessary do develop understanding of these relation and to test representation of this understanding in models. A set of such measurements, analogous to dispersed networks of measurements of aerosol optical depth, are necessary to evaluate the performance of hemispheric or global scale models that would calculate these properties. Such a dispersed network, in conjunction with surface based measurements of aerosol optical depth and column light scattering (e.g., AERONET) would provide many measurement constraints on remote-sensing determination of aerosol properties. Finally such a network would provide important ground truth for satellite determinations of aerosol properties.

4.2.2. *Laboratory studies of aerosol evolution and properties*

While field measurements can identify processes that are occurring in the ambient atmosphere, it is difficult to determine the rates of these processes and the dependence of these rates on controlling variables. Such information is necessary as input to models representing these processes. For such determinations laboratory studies are essential, for example to determine the dependence of the rate of new particle formation on the concentrations of precursor gases (sulfuric acid, ammonia, water vapor, specific organic compounds) and on other controlling variables such as temperature.

Analogously, laboratory studies can provide information in a controlled environment of hygroscopic growth, light scattering and absorption, and particle activation for aerosols of specific known composition, allowing development of suitable mixing rules and evaluation of parameterizations of such mixing rules.

4.2.3. *Surface- and satellite-based remote sensing*

Current remote sensing capabilities need to be maintained for constructing a long-term data record with consistent accuracy and high quality suitable for detecting changes of aerosols over decadal time scale. In future missions, satellite capabilities should be enhanced to acquire high quality measurements of aerosol size distribution, particle shape, absorption, and vertical profile with adequate spatial and temporal coverage. Multi-sensor studies are required to achieve maximized capability for characterizing multitudes of the global aerosol system. Observations should be explored to constrain model simulations via inversion and assimilation methods.

Continuation and enhancement of current observational capabilities. The global aerosol system is a moving target, changing over a wide range of time and spatial scales. To assess its climate impacts, it is necessary to construct a long-term data record with consistent accuracy and high quality suitable for detecting changes of aerosols over decadal time scale. Thus there is a need to maintain and increase ground-based and satellite observational networks with an eye to maintaining a consistent measurement strategy that spans decades. Long term surface-based networks such as the NOAA GMD sites, and NASA AERONET network have been for more than a decade providing essential information on aerosol properties that are vital for satellite validation, model evaluation, and climate change assessment. Current satellite capabilities with the designed lifetime of a few years must be continued for detecting the long-term trend and properties of aerosols on a global scale. Strategic plans need to be developed in a timely and systems manner to minimize the discontinuity of observational capability as the current sensors age. Observational capabilities also need to be augmented to improve the characterization of vertical distribution, absorption, size distribution, and type of aerosols. Surface remote sensing should be enhanced with more routine measurements of size-distributed composition, more lidar profiling of vertical features, and improved measurements of aerosol absorption with the state-of-art techniques such as photoacoustic methods and cavity rind down extinction cells. For satellite remote sensing, a multi-angle, multi-spectral polarimeter with sufficiently high accuracy and adequate spatial coverage is needed to acquire information on aerosol size distribution, absorption, and type. The Glory mission scheduled to launch late this year will provide high quality measurements, but Glory is severely limited in its global coverage, and partially limited in its spatial resolution. An alternative would be to develop remote sensing techniques that derive aerosol absorption properties in context with the properties of the underlying surface. Active lidar sensor in space, particularly the High Spectral Resolution Lidar (HSRL) should provide the additional capabilities for determining aerosol extinction above clouds. Aerosols, clouds, precipitation, weather and climate are inherently intertwined as one holistic global system. As observation systems and models are improved for better estimates of aerosol characteristics and forcing, similar improvements are needed for measurements of cloud properties, precipitation, water vapor and temperature profiles, and underlying surface properties. A summary of current, follow-on and future needs of major aerosol measurement requirements from space is provided in **Table 4.1**.

Synergy of aerosol and radiation measurements from multiple platforms and sensors. A wealth of data has been collected from diverse platforms and sensors. Individual sensors or platforms have both strengths and limitations and no single type of observation is adequate for characterizing the complex aerosol system. As such, the best strategy is to make a synergistic use of measurements from multiple platforms/sensors with complementary capabilities. The synergy can be performed through integrating retrieved products from individual platforms and/or sensors for a better characterization of multitudes of aerosols, and/or fusing multi-satellite radiance measurements for joint retrievals of new, standalone parameters. The constellation of six afternoon-overpass spacecrafts, so-called A-Train, provides an unprecedented opportunity for such synergy because they conduct near simultaneous measurements of aerosols, clouds, and radiative fluxes in multiple dimensions with sensors with complementary capabilities, such as multi-spectral, multi-angle, and polarization measurements of aerosol column from radiometers and vertical distributions of aerosols and clouds from lidar and radar. Some promising progress made in recent years needs to be advanced with a good deal of effort when data from the most recently launched CALIPSO and CloudSat are emerging. A combination of polar-orbiting and geostationary satellites, with multi-spectral measurements from a polar-orbiting

satellite providing constraints to retrievals from a geostationary satellite, would monitor the daytime cycle of aerosols with a better accuracy than a geostationary satellite alone. More coordinated suborbital measurements are also required for validating and complementing satellite observations. To digest and make the best use of a pool of measurements from different platforms, a coordinated research strategy and international collaboration need to be developed.

Determination of anthropogenic component of aerosols and their radiative forcing. This is an important question necessary to be addressed in order to gain better understanding and assessment of human influences on climate. While satellite instruments do not measure the aerosol chemical composition needed to discriminate anthropogenic from natural aerosol components, they can measure such aerosol microphysical properties as particle size and shape. Given that anthropogenic aerosol is dominated by submicron or fine-mode particles and mineral dust is largely non-spherical, the fine-mode fraction, non-spherical fraction, and depolarization of aerosol extinction from modern sensors such as MODIS, MISR, POLDER, and CALIOP have been used to estimate anthropogenic aerosol component and the direct radiative forcing. Substantial efforts are needed to further explore and improve such approaches. For example, removal of contributions of fine-mode portion of dust and maritime aerosol has been empirically determined from satellite observations in specific regions without accounting for their possible temporal and spatial variations. These issues need to be further examined. Comparisons of approaches using different microphysical properties are mutually beneficial. Satellite measurement-based assessment of direct climate forcing by anthropogenic aerosol has been applied only to oceans because of the limited capability of current satellite sensors in retrieving aerosol size information over land. The NASA Glory Mission using a multi-angle, multi-spectral polarimeter will acquire information on aerosol size distribution, absorption, and type with good accuracy that will improve estimates of the anthropogenic contribution of aerosols. Finally but not

Table 4.1 Summary of status and future needs of major aerosol measurement requirements from space for the tropospheric aerosol characterization and climate forcing research.

Requirements	Current Status	Scheduled Follow-on	Future Needs
optical depth	AVHRR (since 1981) TOMS (1979-2001) POLDER (since 1997) MODIS (since 2000) MISR (since 2000) OMI (since 2004)	VIIRS on NPP (2009) and NPOESS to maintain MODIS capabilities OMPS on NPP (2009) to maintain OMI capabilities	A *multi-angle, multi-spectral polarimeter* is needed to acquire aerosol optical depth, particle size, shape, and absorption with high accuracy and adequate spatial coverage.
particle size/shape	AVHRR (since1981) POLDER (since 1997) MODIS (since 2000) MISR (since 2000)	APS on Glory (2008) to provide optical depth, particle size/shape, and absorption, but limited to sub-satellite ground track	A *multi-beam, high-spectral resolution lidar* is needed to acquire vertical profiles of aerosol extinction and size/shape information with high accuracy and adequate spatial coverage.
absorption	TOMS (1979-2001) MISR (since 2000) OMI (since 2004)		A *coordinated research strategy* is needed to develop sub-orbital programs for evaluating and validating satellite remote sensing measurements.
vertical profiles	GLAS (since 2003) CALIOP (since 2006)	N/A	

least, satellite-based estimates of anthropogenic component desperately need to be evaluated and validated with in-situ measurements. The in-situ measurements should be conducted in the context of evaluating and validating satellite remote sensing approaches, focusing on measuring aerosol microphysical properties and anthropogenic fraction in the column.

Detection of aerosol long-term trends and attribution of the observed radiation trends to aerosols. This is an important yet challenging issue that needs to be addressed with substantial effort in coming years. It requires a construction of consistent multi-decadal data records with climate data quality. To get as long data records as possible, it requires a use of data from historic sensors like AVHRR and TOMS that should be extended to observations from modern sensors currently on orbit and scheduled to launch. Some analyses of aerosol optical depth climatology have emerged very recently, using either historic sensors for multi-decadal trends or modern sensors for short-term tendencies of change. However the results from these studies are not always consistent. It thus requires a good understanding and reconciliation of existing differences before a merger of aerosol products from historic and modern satellite sensors. A close examination of relevant issues associated with individual sensors is urgently needed, including sensor calibration, algorithm assumptions, cloud screening, data sampling and aggregation, among others. Trend analyses on regional scales are particularly needed and should be encouraged, given the documented regional differences in the emission trends. The satellite-based trend analysis should also be performed in conjunction with long-term surface-based Sun photometer networks and a construction of aerosol emissions and multi-decadal model simulations. It is even more challenging to unambiguously establish connections between aerosol trends and the observed trends of radiation (e.g., dimming or brightening). The attribution of the observed radiation trends to aerosol changes requires the detection of trends not only for aerosol optical depth, but also aerosol compositions and sizes that determine aerosol single-scattering albedo and asymmetry factor and hence the aerosol radiative forcing. Unfortunately reliable data for the latter don't exist. Given that current understanding of aerosol effects on clouds is far from complete, initial efforts should focus on establishing aerosol-radiation connections under cloud-free conditions.

Integration of remote sensing and in-situ measurements into models. Aerosol models provide an essential tool for estimating the past aerosol forcing and projecting future climate change. There is a need to encourage "cross pollination" between observations and models. To reduce model uncertainties, continuous efforts are required for improving the characterization of the aerosol life cycle. One of the largest uncertainties associated with the model calculations of aerosol and their radiative forcing is the emissions of aerosol and aerosol precursors and the resulting burdens. Aerosol sinks, such as wet deposition, also tend to be poorly characterized as a result of the difficulty in representing cloud and precipitation processes and lack of observations. Models should aim to improve the performance based on information provided by observational results, which include not only the measures of aerosol optical depth but also the observed relationships between parameters. Observations should be explored to aid models in determining sources and sinks of aerosols via inverse methods. It is also of great importance to integrate satellite and in-situ measurements into global models. There have been some preliminary efforts that integrate satellite retrieved columnar AOD as well as empirically determined optical properties with model simulations. A coordinated research strategy needs to be developed for integrating the emerging CALIPSO observed three-dimensional aerosol extinction into aerosol models. Schemes of surface albedo characterization in global models also need to be evaluated and constrained with emerging measurements from new-generation satellite sensors.

4.3. Requirements for Future Research - Modeling

The comparisons with aerosol observations have already led to some improvement in GCMs, particularly with respect to the realism of some sources and processes. For example, Koch et al. (2006) included species dissolution in stratiform clouds that reduced the atmospheric load of most soluble aerosols, since it increased the scavenging of these aerosols by large-scale rainfall. But as an indication of the problems encountered with such 'improvements', despite using increased natural sulfur emissions, this new process causes sulfate to be less than observed, and suggests the need for additional sulfur oxidation mechanisms (Koch et al., 2006). Due to the uncertainties in sources and removal processes, there are many degrees of freedom in the system, and changes in one component may well necessitate different choices or the inclusion of even more processes associated with other components.

The *sine qua non* for improving model simulations of aerosols is that modelers must be able to tell what constitutes an improvement. Many of the comparisons with observations shown for aerosol models in Chapter 2, and the GISS and GFDL GCMs in Chapter 3, are less than definitive because of disagreements among the observing platforms. Knowing the right answer(s) is clearly important for the aerosol characteristics themselves, but also for the associated radiative forcing. The number one priority for improving models is to obtain improved observations of aerosol component distributions and radiative forcing.

4.3.1 Required modeling improvements

The aerosol component distributions are affected primarily by sources, removal mechanisms and atmospheric transport. Calculation of the aerosol radiative forcing requires information on their radiative properties. We discuss the modeling needs in each of these areas.

Emissions. A discussion of the current status of understanding of sources was provided in Chapter 1. Improvements in specifying emissions requires better observations and laboratory studies, but the subject is included here under the modeling category since aerosol emissions are the most important factor in determining the model distribution and loading of the different aerosol components.

We need to have a systematic determination of emissions of primary particles, including size-distributed composition, and of aerosol precursor gases. Additionally emission inventories are required for the twentieth century to serve as input to models examining radiative forcing over this time period needed for input to climate models to evaluate their performance by comparison with observations. Projected future emissions are required as well as input to models providing projections of future climate change. Because of the need to represent aerosol emissions in models at locations and times for which measurements are not available, such inventories must be tied to the particular activities that produce those emissions, with the emissions calculated as a product of an emission factor (emission per activity) times the activity rate, the latter developed or projected as a function of time, economic growth, and the like.

A requirement of emissions inventories of particulate matter is that they provide emissions rates of size-distributed composition. Much of the present inventory of aerosols provides only mass emissions

(generally in support of achieving air quality requirements) but this is wholly inadequate to the task of determining climate influences of anthropogenic aerosols, given that aerosol optical and cloud nucleating properties depend on size distributed composition. Similarly, there is a requirement for emissions of aerosol precursor gases, of which a large component is thought, on the basis of recent work, to be biogenic organics, which interact with highly photochemically active urban plumes to produce secondary organic aerosol. Identification of precursor gases and of the pertinent chemical reactions is not firmly established, so emissions requirements will depend on identification of the pertinent precursor gases. Emissions inventories must be tied to underlying vegetation types including determination of dependence on controlling conditions, e.g., leaf area index, primary production, water stress, temperature, so that these inventories can be incorporated into global-scale models.

Aerosol production, transformation, and removal processes. We need to better understanding and model the processes of new particle formation, gas to particle conversion, and evolution of aerosol chemical and physical properties in the atmosphere based on concentrations of precursor gases and other dependences. This also includes in-cloud processes. There needs to be greater understanding of aerosol removal processes by wet and dry deposition.

Aerosol chemical transport modeling. Considering the other aspects that affect aerosol distributions, atmospheric transports in models can be tested by comparison with observations of long-lived species (e.g., Rind et al., 2007). Interhemispheric transports are strongly affected by the 'ageostrophic' circulations that are hard to detect directly, and which are generated by heat released from condensation of moisture associated with precipitation. Precipitation also functions as a primary removal mechanism for aerosols. Hence improving these processes requires improving precipitation fields – which also means improving observations of precipitation (including the vertical level of condensation) for comparison purposes. Convective precipitation and vertical transport are associated with the convective parameterization in models; its improvement, too, depends on observations and using appropriate scales in models, something that is not currently possible due to resource limitations. The 'way forward' for better aerosol transport and removal is contained in having better physical meteorological simulation capability in climate models.

Aerosol optical properties. Even were we to know the different aerosol component distributions perfectly, there would still be uncertainty concerning the aerosol optical properties (extinction coefficient, single scattering albedo, and asymmetry parameter or higher representation of the phase function) from size distributed aerosol properties. Observations have to be done locally as their generalizability in some cases is open to question; clearly, all 'organic' aerosols are not alike in terms of their reflectivity and absorption. The variation of aerosol properties with relative humidity is another parameterization models must use, and questions have arisen as to what shape it takes at high relative humidities (e.g., in the GFDL model). More observations of these factors would help modelers constrain their parameterizations and provide some degree of uniformity amongst the models.

Aerosol cloud nucleating properties. The interaction between aerosols and clouds is probably the biggest uncertainty of all climate forcing/feedback processes. As discussed in Chapter 3, the processes could well be very complicated, and are unlikely to be resolvable on the horizontal scales that are feasible to use in global climate models. This problem is usually handled by coarser-scale param-

eterizations, but observations of the fine-scale processes are also difficult to obtain, so it is not clear exactly what models should be parameterizing. We need to know the cloud nucleating properties for different aerosols and different size distributions (CCN concentration as function of supersaturation and any kinetic influences), which will require progress to take place simultaneously in observational and modeling capabilities.

What is true for the aerosol/cloud interaction is of course true for clouds themselves. Clouds represent the biggest uncertainty in understanding climate feedbacks and hence climate sensitivity. We need to demonstrate the capability of calculating cloud drop concentration for known (measured) updraft, humidity, and temperature conditions. As noted in Chapter 3, no improvement can be made in understanding the indirect effects of aerosols without better knowledge of cloud processes, and the ability of models to simulate clouds more realistically. Cloud resolving models, as noted in Chapter 3, are one possibility, as is the continual improvement in computing capability to allow the resolution of more appropriate scales. This latter approach, however, may take decades.

4.3.2. *Aerosol-climate modeling: the way forward*

The scientific community is poised to be able to develop a reliable representation of global and regional releases of primary aerosols throughout the time period of 1850-2050, and potentially to 2100. Emissions tasks that need to be accomplished include review and reconciliation of the extant estimates of historical trends of man-made emissions and incorporation of the best trends of open biomass burning that the science will presently allow. For further breakthroughs, the rather expensive task of testing sources in the field in developing countries would be valuable. The compilation of trends in natural-source emissions, though not so well developed, can be accomplished for some source types, and others can perhaps be held constant. In this way, it should be possible to develop a comprehensive dataset of all primary inputs of aerosols at 5- or 10- year intervals for the period 1850-2000 with a reasonable level of confidence. Such a dataset should be quickly tested within the aerosol components of climate models. We do not yet know what the effect of relatively high carbonaceous aerosol releases in the period 1850-1950 will have on the 20th century temperature reconstruction. The simulation of historical trends in secondary organic aerosol production is more difficult to accomplish and may require a special convocation of experts to design a way forward.

Climate change simulations need to be run for hundreds of years with coupled atmosphere-ocean models. The above discussion emphasizes that finer resolution is necessary to resolve the effects of aerosols and clouds, but long-term simulations and finer resolution compete for computer time. In addition, aerosol physics/chemistry is itself time-consuming, as multiple size-distributions for aerosols and multiple chemical interactions must be calculated; this too conflicts with the need for finer resolution and long-term simulations.

In the simulations that were done for IPCC (2007), aerosol properties and processes were highly simplified in GCMs. Since aerosol forcing had to be included in climate models to help produce realistic temperature changes, aerosols were just implemented as forcings. This was done basically by using 'offline' simulations to prescribe the aerosol forcings. However, this method does not allow any mutual interaction of the aerosol forcing with the meteorological variables, such as clouds, or precipitation.

A next step in aerosol-climate modeling is to have a simple representation of aerosols directly included in the climate models, incorporating the most important substances like sulfates, black and organic carbon, mineral dust and sea salt with its interactive sources and a simple scheme for sulfate chemistry. The size distribution might be described for each species and the aerosols assumed to be externally mixed. The number of aerosol particles that can nucleate to form cloud droplets can be treated as a simple autoconversion function, only considering external mixtures. Aerosol processes are in this representation highly simplified or neglected. Those kinds of models widely exist nowadays and are ready to be applied for long-term simulations, allowing first order aerosol climate feedbacks to be calculated.

The next generation of models will include various aerosol processes that allow for more realistic interactions (e.g., Ghan and Schwartz, 2007). These aerosol models will either describe aerosols in a sectional, modal or quadrature of moments scheme. Aerosol size distribution will be calculated rather than prescribed. The aerosol mixing state will be represented, so that particles forming by condensation will be capable of being internally mixed with primary particles and freshly nucleated particles. Hygroscopicity will be calculated depending on the chemical composition of a particle. Aerosol chemistry and size will determine the cloud activation and convective transport and removal will be linked to cloud microphysics. Aerosol composition, the inclusion of soluble material and aerosol water will be used to calculate the optical properties. Secondary aerosol formation will be explicitly calculated and determine the amount of organic carbon. Condensation and coagulation will determine aerosol size and mixing.

All these processes will require observations to understand them, and extensive computer time to simulate them. It is conceivable that off-line aerosol/chemistry models may incorporate many of them in the next decade, especially if the appropriate observations are obtainable. But it is unlikely that most of these can be included directly in GCMs on that time frame. More likely, the off-line aerosol/chemistry models could be used to calculate the difference these processes make in simulations, both for aerosols and radiative forcing, which might provide a zeroth-order estimate of the effect they would have in GCMs. This approach, however, would fail to provide much of the necessary information, for aerosol-climate interactions are highly interactive, and the interaction likely produces unique results. Furthermore, some of these interactions will likely change as climate does.

4.4. Concluding Remarks

Resolving the past and future aerosol effects on climate, both direct and indirect, is essential to gaining the requisite understanding of climate forcing necessary for informed decision making on CO_2 emissions and energy policy. In view of the multi-faceted nature of the scientific problem and the approaches to resolve it, a level of effort is required that is commensurate with the task. Extensive observational improvements will be necessary along with increased computational resources for the 'forward modeling' approach to produce more confident quantitative results. The continuing record of temperature and trace gas changes will also provide more data for the inverse approach to deduce the influence of aerosols (and clouds). Application of sufficient resources (including manpower) to this problem will be necessary to provide useful error bounds on aerosol forcing and thus climate sensitivity.

Finally, *aerosol-cloud interactions* continue to be an enormous challenge from both the observational and modeling perspectives, and progress is crucial to improving our ability to project climate change for various emission scenarios. The relatively short lifetimes of aerosol particles (order days), in addition to the even shorter timescales for cloud formation and dissipation (10s of minutes) make this a particularly difficult challenge. Moreover, the problem requires addressing an enormous range of spatial scales, from the microscale to the global scale. A methodology for integrating observations (in-situ and remote) and models at the range of relevant temporal/spatial scales is crucial if progress is to be made on this problem.

References

Anderson T., R. Charlson, N. Bellouin, O. Boucher, M. Chin, S. Christopher, J. Haywood, Y. Kaufman, S. Kinne, J. Ogren, L. Remer, T. Takemura, D. Tanré, O. Torres, C. Trepte, B. Wielicki, D. Winker, and H. Yu, 2005a.: An "A-Train" strategy for quantifying direct aerosol forcing of climate. *Bull. Am. Met. Soc.* 86:1795-1809.

Anderson T., Y. Wu, D. Chu, B. Schmid, J. Redemann, and O. Dubovik, 2005b: Testing the MODIS satellite retrieval of aerosol fine-mode fraction. *J. Geophys. Res.* 110: D18204, doi:10.1029/2005JD005978.

Bates T., et al., 2006: Aerosol direct radiative effects over the northwestern Atlantic, northwestern Pacific, and North Indian Oceans: estimates based on in-situ chemical and optical measurements and chemical transport modeling. *Atmos. Cehm. Phys.*, 6:1657-1732.

Bender F. A., H. Rodhe, R. J. Charlson, A. M. Ekman, N. Loeb, 2006: 22 views of the global albedo-comparison between 20 GCMs and two satellites. Tellus A 58(3): 320.

Collins W., P. Rasch, B. Eaton, B. Khattatov, J. Lamarque, and C. Zender, 2001: Simulating aerosols using a chemical transport model with assimilation of satellite aerosol retrievals: Methodology for INDOEX. *J. Geophys. Res.* 106:7313—7336.

Ghan, S. J. and S. E. Schwartz, 2007: Aerosol properties and processes. *Bull. Amer. Meteor. Soc.*, 88, 1059-1083.

Koch, D., G. A. Schmidt and C. V. Field, 2006: Sulfur, sea salt and radionuclide aerosols in GISS Model E. *J. Geophys. Res.*, 111, doi:10.1029/2004JD005550.

Mishchenko M., et al., 2007a: Accurate monitoring of terrestrial aerosols and total solar irradiance. *Bull. Amer. Meteorol. Soc.* 88:677-691.

Rind, D., J. Lerner, J. Jonas, and C. McLinden, 2007: The effects of resolution and model physics on tracer transports in the NASA Goddard Institute for Space Studies general circulation models. *J. Geophys. Res.*, 112, D09315, doi:10.1029/2006JD007476.

Schwartz S. E., 2004: Uncertainty requirements in radiative forcing of climate change. *J. Air Waste Management Assoc*. **54**, 1351-1359.

Yu H., R. Dickinson, M. Chin, Y. Kaufman, B. Holben, I. Geogdzhayev, and M. Mishchenko, 2003: Annual cycle of global distributions of aerosol optical depth from integration of MODIS retrievals and GOCART model simulations. *J. Geophys. Res.* 108:4128, doi:10.1029/2002JD002717.

U.S. Climate Change Science Program
1717 Pennsylvania Avenue, NW • Suite 250
Washington, DC 20006 USA
1-202-223-6262 (voice) • 1-202-223-3065 (fax)
http://www.climatescience.gov